

AD-A013 620

TEMPS (TRANSPORTABLE EMP SIMULATOR) FINAL REPORT.  
VOLUME I

H. Aslin, et al

Physics International Company

Prepared for:

Defense Nuclear Agency

August 1973

DISTRIBUTED BY:

**NTIS**

National Technical Information Service  
U. S. DEPARTMENT OF COMMERCE

237103

AD

①

FG

PIFR-372-D  
TEMPS FINAL REPORT

Volume I

by  
H. Aslin and R. Ryan

August 1973

Prepared for  
Harry Diamond Laboratories  
Washington, D.C. 20438  
Under Contract No. DAAK02-72-C-0059

Reprinted by  
NATIONAL TECHNICAL  
INFORMATION SERVICE  
U.S. Department of Commerce  
Springfield, VA 22151

Prepared by  
Physics International Company  
2700 Merced Street  
San Leandro, California 94577



AD A 013620

SECURITY CLASSIFICATION OF THIS PAGE (When Data Entered)

REPORT DOCUMENTATION PAGE		READ INSTRUCTIONS BEFORE COMPLETING FORM
1. REPORT NUMBER PIFR-372	2. GOVT ACCESSION NO.	3. RECIPIENT'S CATALOG NUMBER
4. TITLE (and Subtitle) TEMPS FINAL REPORT Volume I		5. TYPE OF REPORT & PERIOD COVERED DRAFT FINAL 9-1-71 through 10-16-72
		6. PERFORMING ORG. REPORT NUMBER PIFR-372 ✓
7. AUTHOR(s) H. Aslin and R. Ryan		8. CONTRACT OR GRANT NUMBER(s) DAAK02-72-C-0059
9. PERFORMING ORGANIZATION NAME AND ADDRESS Physics International Company 2700 Merced Street San Leandro, California 94577		10. PROGRAM ELEMENT, PROJECT, TASK AREA & WORK UNIT NUMBERS P0007
11. CONTROLLING OFFICE NAME AND ADDRESS Defense Nuclear Agency Washington, D.C. 20305		12. REPORT DATE August 1973
		13. NUMBER OF PAGES 234
14. MONITORING AGENCY NAME & ADDRESS (if different from Controlling Office) Harry Diamond Laboratories Washington, D.C. 20438		15. SECURITY CLASS. (of this report) Unclassified
		16a. DECLASSIFICATION/DOWNGRADING SCHEDULE
16. DISTRIBUTION STATEMENT (of this Report)  APPROVED FOR PUBLIC RELEASE; DISTRIBUTION UNLIMITED.		
17. DISTRIBUTION STATEMENT (of the abstract entered in Block 20, if different from Report)		
18. SUPPLEMENTARY NOTES		
19. KEY WORDS (Continue on reverse side if necessary and identify by block number)  Electromagnetic pulse Pulser system Pulse generator		
20. ABSTRACT (Continue on reverse side if necessary and identify by block number)  This report presents a description of the development, design, fabrication, and field testing of the TEMPS (Transportable EMP Simulator), a system conceived and specified by the Harry		

## DD Form 1473: Report Documentation Page

SECURITY CLASSIFICATION OF THIS PAGE (When Data Entered)

Diamond Laboratories (HDL), Laboratory 1000,\* and funded by the Defense Nuclear Agency (DNA).

The basic system is a simulator with the geometry of a cylinder parallel to the ground surface driven at its center by a high voltage capacitive pulser and terminated resistively at its ends to ground. The pulser and cylindrical antenna are supported by means of a dielectric support structure at elevations of up to 20 meters measured from the antenna/pulser centerline to ground.

Essentially, TEMPS has three individual subsystems: the pulse generator, the cylindrical antenna, and the support structure.

The pulse generated is a bilateral Marx generator-peaking capacitor circuit switched in series with the load impedance (the antenna) by means of a single, near uniform field, pressurized gas output switch. The pulser is contained within a biconical transmission line at the center of the cylindrical antenna. The biconical line guides line guides and launches the EM wave, produced by discharge of the pulser, from the small dimensions associated with the high voltage output switch to the large diameter (30 feet) cylindrical antenna.

A peaking capacitor circuit is employed to produce the fast rising load current that the Marxes cannot supply because of their stray series inductance.

Pulse generator capacity is 2.5 nF and produces a roughly double exponential output voltage pulse into the load impedance. Output pulse amplitude is greater than 6 MV and rises to this value in about 8 nsec (10 to 90 percent). Pulse decay time is approximately 300 nsec (e-fold). System electrical parameters are sufficient to produce a peak radiated electromagnetic field greater than 50 kV/m at a radial distance of 50 meters from the antenna.

The cylindrical antenna is a wire cage structure 30 feet in diameter and 1000 feet long. The antenna guides the lower frequency content of the EM wave from the source region as a rod to plane transmission line to the ends of the antenna, terminated to ground by way of resistors which match the characteristic impedance of the antenna viewed as a transmission line.

The antenna/pulser support structure is designed to be transportable, capable of being rapidly disassembled, transported and reassembled at a new location. The support structure is a

\* At the time that the request for proposal was issued (March 1971) this group reported administratively to the U. S. Army Mobility Equipment Research and Development Center, Fort Belvoir, Va.



*DD Form 1473: Report Documentation Page*

SECURITY CLASSIFICATION OF THIS PAGE (When Data Entered)

free standing guyed system to minimize site preparation and disturbance and it is fabricated from dielectric material as far as practical for high voltage insulation and for minimum disturbance of the EM fields produced by the system.

## ABSTRACT

This report presents a description of the development, design, fabrication, and field testing of the TEMPS (Transportable EMP Simulator), a system conceived and specified by the Harry Diamond Laboratories (HDL), Laboratory 1000,\* and funded by the Defense Nuclear Agency (DNA).

The basic system is a simulator with the geometry of a cylinder parallel to the ground surface driven at its center by a high voltage capacitive pulser and terminated resistively at its ends to ground. The pulser and cylindrical antenna are supported by means of a dielectric support structure at elevations of up to 20 meters measured from the antenna/pulser centerline to ground.

Essentially, TEMPS has three individual subsystems: the pulse generator, the cylindrical antenna, and the support structure.

The pulse generated is a bilateral Marx generator-peaking capacitor circuit switched in series with the load impedance (the antenna) by means of a single, near uniform field, pressurized gas output switch. The pulser is contained within a biconical transmission line at the center of the cylindrical antenna. The biconical line guides line guides and launches the EM wave,

---

\* At the time that the request for proposal was issued (March 1971) this group reported administratively to the U. S. Army Mobility Equipment Research and Development Center, Fort Belvoir, Va.

produced by discharge of the pulser, from the small dimensions associated with the high voltage output switch to the large diameter (30 feet) cylindrical antenna.

A peaking capacitor circuit is employed to produce the fast rising load current that the Marxes cannot supply because of their stray series inductance.

Pulse generator capacity is 2.5 nF and produces a roughly double exponential output voltage pulse into the load impedance. Output pulse amplitude is greater than 6 MV and rises to this value in about 8 nsec (10 to 90 percent). Pulse decay time is approximately 300 nsec (e-fold). System electrical parameters are sufficient to produce a peak radiated electromagnetic field greater than 50 kV/m at a radial distance of 50 meters from the antenna.

The cylindrical antenna is a wire cage structure 30 feet in diameter and 1000 feet long. The antenna guides the lower frequency content of the EM wave from the source region as a rod to plane transmission line to the ends of the antenna, terminated to ground by way of resistors which match the characteristic impedance of the antenna viewed as a transmission line.

The antenna/pulser support structure is designed to be transportable, capable of being rapidly disassembled, transported and reassembled at a new location. The support structure is a free standing guyed system to minimize site preparation and disturbance and it is fabricated from dielectric material as far as practical for high voltage insulation and for minimum disturbance of the EM fields produced by the system.

## CONTENTS

	<u>Page</u>
SECTION 1 INTRODUCTION	1
SECTION 2 BACKGROUND	3
SECTION 3 ANTENNA DESIGN	7
3.1 High Frequency Launcher	7
3.2 Late Time Antenna (LTA)	15
SECTION 4 ANTENNA MECHANICAL DESIGN	21
4.1 Overall Antenna System	21
4.2 Hoops	23
4.3 Wire Connections	23
4.4 Wires	24
4.5 Transition Section	24
4.6 Straight Sections	25
4.7 End Dome Assemblies	26
4.8 Tensioning	26
4.9 Grounding Resistors	27
4.10 Anchor Assemblies	27
4.11 End Dome Support Structure	28
SECTION 5 PULSER ELECTRICAL DESIGN	31
5.1 Marx Generator	33
5.2 Peaking Capacitor Design	84
5.3 Output Switch	107
5.4 TEMPS Trigger System	110
5.5 Primary Power System (Figure 52)	134
5.6 Command and Controls	136
SECTION 6 PULSER MECHANICAL DESIGN	145
6.1 End Assemblies	145
6.2 End Structures	145
6.3 Marx Cylinders	147
6.4 Support Cones	147
6.5 Outer Containment Cylinder	148

## Contents (cont.)

	<u>Page</u>
6.6 Bicones	149
6.7 Electrical Boxes	149
6.8 Equalizing and Monitoring Resistors	150
6.9 Output Shorting Assembly	150
6.10 Output Switch	150
6.11 Marx Generator Assemblies	151
6.12 Peaking Capacitors	161
6.13 Output Shorting Assembly	163
SECTION 7 SUPPORT STRUCTURE MECHANICAL DESIGN	165
7.1 Concrete Footings	165
7.2 Guy Line Anchors	167
7.3 Winch Bases	167
7.4 Support Columns	167
7.5 Wood Cross Beams	168
7.6 Brackets and Braces	169
7.7 Rigging	169
7.8 Winches	169
SECTION 8 TEMPS TESTING	171
8.1 Marx Inductance	171
8.2 Pulse Charge Circuit	172
8.3 TEMPS Half Generator Equivalent Circuit	178
8.4 Radiated Output Pulse Risetime	184
8.5 Radiated Pulse Peak Amplitude	194
8.6 Output Prepulse	204
8.7 Output Pulse Amplitude Jitter	206
8.8 TEMPS Timing Jitter	208
8.9 Output Switch Closure Jitter	213
8.10 Command Jitter	215
8.11 Marx Generator Self-Fire	217
REFERENCES	221

## ILLUSTRATIONS

<u>Figure</u>		<u>Page</u>
1	TEMPS Pulser Assembly	4
2	Biconical Transmission Line and Field Distribution	9
3	Radiated Field Magnitude	10
4	Path Length Difference	11
5	Simplified Cross-Sectional View of TEMPS High-Frequency Launcher	14
6	TEMPS Late Time Antenna	16
7	TEMPS Antenna System	22
8	Simplified TEMPS Circuit	32
9	Schematic of TEMPS Marx Resisistors	34
10	TEMPS Energy Storage Capacitor	36
11	Marx Rail Gap Switch	38
12	Charging Resistors	40
13	Six-Stage Marx (barriers installed)	47
14	Six-Stage Marx	48
15	Six-Stage Marx Circuit	49
16	Six-Stage Output Waveform	50
17	Thirty-Five-Stage Prototype Marx Generator	53
18	TEMPS Marx Test Electrical Circuit	54
19	Prototype Marx Trigger Circuit	56

## ILLUSTRATIONS (cont.)

<u>Figure</u>		<u>Page</u>
20	Comparison of Calculated and Measured Marx Short-Circuit Waveforms	57
21	TEMPS Marx Self-Break Voltage Versus Pressure	59
22	Voltage-Waveform Oscillation	61
23	Marx Timing Measurement Circuit	62
24	Marx Timing Photograph	63
25	Capacitor Rail Reversal	67
26	Calculated and Measured Marx Output Waveforms	71
27	Erection Jitter Versus Percentage of Self-Fire for Fixed Marx Charge Level of 45 kV/Stage	77
28	Marx Erection Delay Versus Percentage of Self-Fire for Fixed Marx Charge Voltage of 45 kV/Stage	78
29	Marx Erection Delay Versus Marx Charge Voltage for Fixed Percentage of Self-Fire (80 Percent)	79
30	Marx Erection Jitter Versus Marx Charge Voltage for Fixed Percentage of Self-Fire (80 Percent)	80
31	Marx Erection Delay Versus Marx Charge Voltage for Fixed Percentage of Self-Fire (80 Percent)	81
32	Marx Erection Jitter Versus Charge Voltage for Fixed Percentage of Self-Fire (80 Percent)	82
33	Idealized Peaking Capacitor Circuit	86
34	Peaking Capacitor Test Setup	97
35	Ten-Module Peaking Capacitor in Freon Enclosure	99
36	3.5 MV Peaking Capacitor	102
37	Peaking Capacitor Assembly	103
38	One-Sixth Scale Output Switch	108
41	Typical Applied Waveform	109

## ILLUSTRATIONS (cont.)

<u>Figure</u>		<u>Page</u>
42	Trigger System Block Diagram	111
43	Optical Transmitter/Receiver Unit	114
44	Low Voltage Trigger Amplifier Sub-Module	116
45	Low-Voltage Gap	117
46	Low-Voltage Gap (Side View)	118
47	High Level Trigger Amplifier Chain	124
48	Cable-Transformer Test	125
49	Block Diagram Symbols	130
50	Generation of Trigger Timing Signals	131
51	Interlock Function Generator	133
52	TEMPS Primary Power System	135
53	Command and Control Console Layout	138
54	Power and Firing Controls	140
55	Charge Voltage and Enclosure Gas Controls	142
56	Marx Gas and Output-Switch Pressure and Spacing Controls	144
57	TEMPS Pulser	146
58	Marx Generator Assembly	152
59	Marx Output Contact Connectors	154
60	Marx Rear Plate Assembly	155
61	Series Current Limiting Resistor	156
62	Storage Capacitor Adapter Bar	157
63	Marx Charging Connectors	158
64	Trigger Coupling Resistor	159



## ILLUSTRATIONS (cont.)

<u>Figure</u>		<u>Page</u>
65	Case-To-Case Coupling Resistor	160
66	Stage Insulators	162
67	The TEMPS Pulser and Antenna Support Structures	166
68	Simplified Electrical Circuit for Marx Inductance Measurements	173
69	Inductance Measurement, Calculated, and Measured Waveform	174
70	Simplified Equivalent Circuit--Marx/Peaking Capacitor	175
71	Peaking Capacitor Ringing Waveforms	176
72	Simplified Equivalent Circuit	178
73	Computed and Measured Peaking Capacitor Pulse Charge Waveforms (No Switch Closure)	179
74	TEMPS Output Voltage dc Charge	181
75	Peaking Capacitor Pulse Charge and Output Voltage Waveform (Near Optimum Output Switch Closure Time)	182
76	Peaking Capacitor Pulse Charge and Output Voltage Waveform (Output Switch Closure Delayed)	183
77	TEMPS Pulse Decay Time	185
78	Diagnostics Setup	186
79	Probe Position Relative to Pulser	187
80	Biconic Discontinuity	189
81	Typical Radiated Waveform (Early Time)	191
82	Radiated Waveform--Inflection on Pulse Rise	192
83	Direct and Ground Interacted EM Fields	195
84	Modified Biconical High-Frequency Transition	199

## ILLUSTRATIONS (cont.)

<u>Figure</u>		<u>Page</u>
85	Probe Position Relative to Pulser	200
86	Typical Radiated Waveform	203
87	TEMPS Trigger System Block Diagram	211
88	Relative Trigger System Jitter	214
89	Air Path rf Trigger Link	216

## TABLES

<u>Table</u>		<u>Page</u>
I	TEMPS Antenna Termination for 3-Meter Dome-To-Ground Clearance--All Heights	19
II	Summary of Marx Timing Test Results	74
III	Single Shot Breakdown--Water Graded	92
IV	Single Shot Breakdown--Glycol Graded	94
V	Trigger System Design Criteria	112
VI	Low-Voltage Rail Gap Test Results	122
VII	Relative Reflected Wave Arrival Time	188
VIII	Relative Reflected Wave Arrival Time	201
IX	TEMPS Peak Pulse Amplitude Jitter	209

## SECTION 1

### INTRODUCTION

This report is the final technical report describing the design, development, fabrication, and testing of the TEMPS (Transportable EMP Simulator) system which began with issuance of the TEMPS purchase description #DAAK02-72-C-0059, March 1, 1971. This purchase description was issued by the Electromagnetic Effects Branch of the U.S. Army Mobility Equipment Research and Development Center (USMERDC), Ft. Belvoir, Virginia.\*

Physics International Company's proposal for the design, development, fabrication, and testing of the TEMPS was submitted to the USMERDC in May of 1971. Much of the discussion contained herein is based on this proposal.

Work was begun on the TEMPS system in September of 1971 and the system was delivered to the Harry Diamond Laboratories (HDL), Lab 1000 at its Woodbridge, Virginia test site in late December 1972. The system was erected at Woodbridge for acceptance testing in January of 1973.

Section 2 of this report is a brief summary of the proposed TEMPS system design. Following this is a discussion of the detailed design, development, and fabrication of the major components which comprise TEMPS: Sections 3 through 7. Section 8

---

\*This group has since been administratively transferred to the HDL and is designated as Laboratory 1000.

PIFR-372

describes system performance based upon TEMPS testing at Camp Parks, California, located near the San Francisco Bay Area, and upon acceptance tests performed at Harry Diamond Laboratories' Woodbridge, Virginia test site.

## SECTION 2

### BACKGROUND

The TEMPS system is a synchronized bilateral Marx-generator-peaking-capacitor electrical circuit switched by means of a fast-charged, self-breaking, pressurized-gas output switch into the terminals of a dipole antenna supported horizontally over earth ground. The electromagnetic wave produced by discharge of the pulser into the antenna is guided to the 30-foot-diameter maximum dipole antenna by a 120-ohm-impedance biconical transmission line which forms the high frequency launcher portion of the antenna. Pulser components are contained within the biconical transmission line as illustrated in Figure 1.

The electromagnetic wave launched from the biconical transmission line is horizontally polarized, but, as a result of interaction of the initial EM wave with the nearby earth medium, the field distribution becomes essentially vertically polarized as the EM wave expands, i.e., each one-half of the dipole forms a rod-to-plane transmission line. Each end of the dipole antenna is resistively connected to ground to terminate the EM wave propagating on the antenna.

The pulser and antenna are supported by means of a dielectric structure (a) for insulation from the high voltages that are applied to the antenna to produce the requisite field strength and (b) to minimize perturbation of the electromagnetic fields launched from the system.

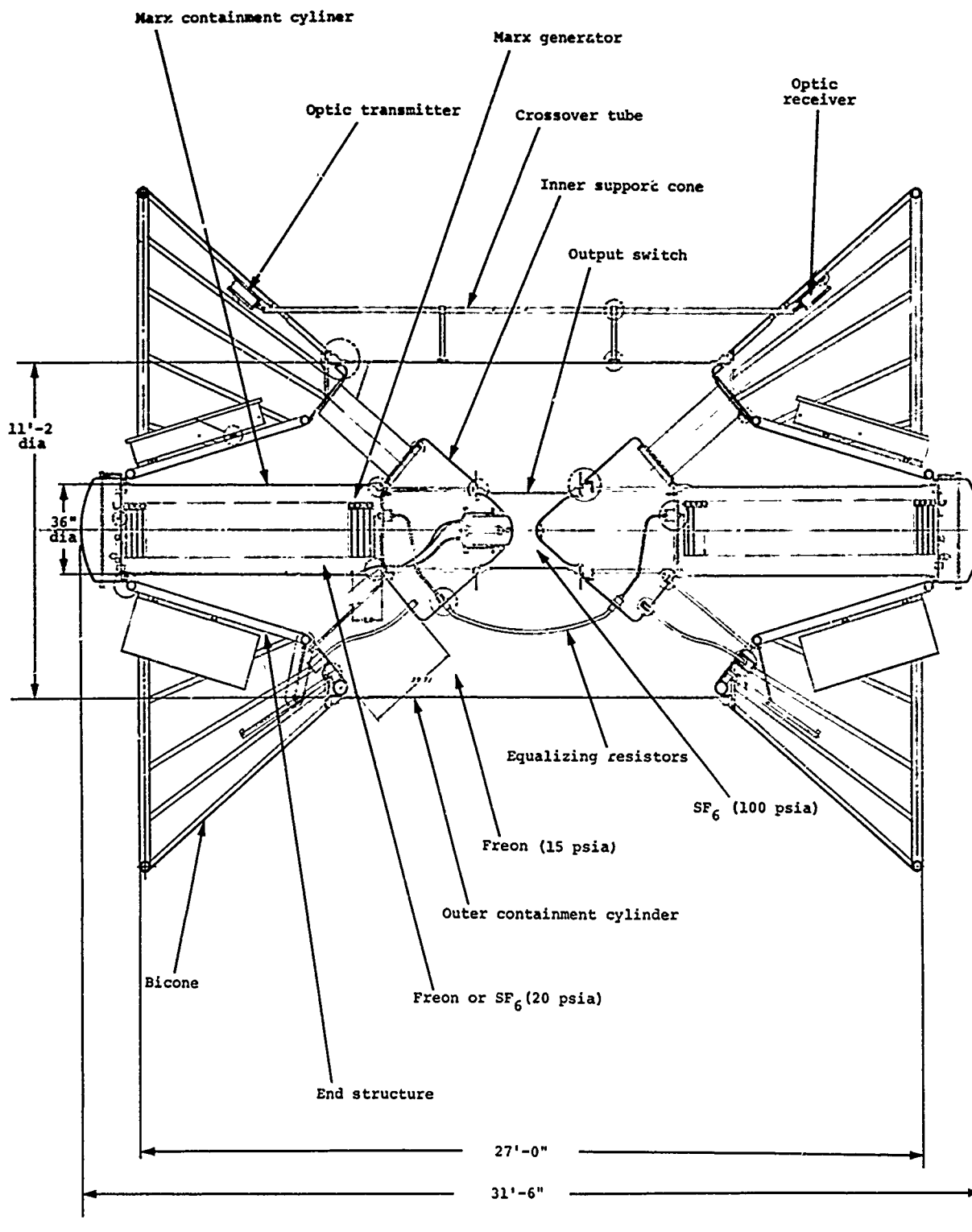


Figure 1 TEMPS pulser assembly.

The next section presents the design of the antenna and a description of the electromagnetic fields produced by the system.



## SECTION 3

### ANTENNA DESIGN

The design of the antenna may be conveniently divided into two parts: (a) the biconical-transmission-line high-frequency launcher and (b) the late-time antenna (LTA). Design of the high-frequency-launcher portion of the antenna was undertaken by Physics International (PI) using both analytical and experimental techniques. Design of the LTA and determination of the EM fields produced in the vicinity of the antenna was undertaken by Stanford Research Institute (SRI).

#### 3.1 HIGH FREQUENCY LAUNCHER

A biconical-transmission-line conducting structure forms the feed section of the dipole antenna at its center and guides the initial EM wave from small dimensions associated with the pulser output switch to the large-diameter (30-foot) cylindrical wire cage antenna. This choice is appropriate since the EM wave propagating in such a conducting geometry is spherical, and since EM field magnitudes and their distribution in space bounded by the conducting surfaces are known as functions of driving voltage applied to the antenna terminals at the apex of the biconical line. For a step voltage,  $V_0$ , from a zero impedance source applied to the biconical line, the electric and magnetic field magnitudes propagating in a line of infinite extent in free space are given by:

$$E(r, \theta) = \frac{60 V_o}{r z_k \sin \theta} \quad (3-1)$$

$$H(r, \theta) = \frac{E(r, \theta)}{120\pi} = \frac{V_o}{2\pi r z_k \sin \theta} \quad (3-2)$$

where  $r$  and  $\theta$  are position coordinates. From Figure 2,  $\theta \geq \theta_{hc}$  where  $\theta_{hc}$  is the cone half angle; and from Equations 3-1 and 3-2, the fields produced in a biconical line are azimuthally symmetric.

The proposed value of biconical line impedance for TEMPS was 120 ohms which corresponds to a cone half-angle of about 40.4 degrees. Thus, the peak field magnitudes, as a function of peak applied voltage for a position 50 meters radially from the bicone apex, directly broadside ( $\theta = \pi/2$ ) to the antenna, are given by:

$$E(50, \pi/2) = \frac{60 V_o}{50(120)} = 0.01 V_o \text{ V/meter} \quad (3-3)$$

$$H(50, \pi/2) = \frac{V_o}{2\pi(50)(120)} \approx 2.65 \times 10^{-5} V_o \text{ A/meter} \quad (3-4)$$

and are plotted in Figure 3.

From Figure 3, a minimum applied voltage of 6 MV is required to produce peak electric field magnitudes of 60 kV/m at a radial distance of 50 meters from the antenna on the equatorial plane.

As a practical matter, the extent of the biconical transmission line is limited to some maximum diameter,  $D$ , at which point the conducting geometry departs from biconical and may, for example, become cylindrical as illustrated in Figure 4. The

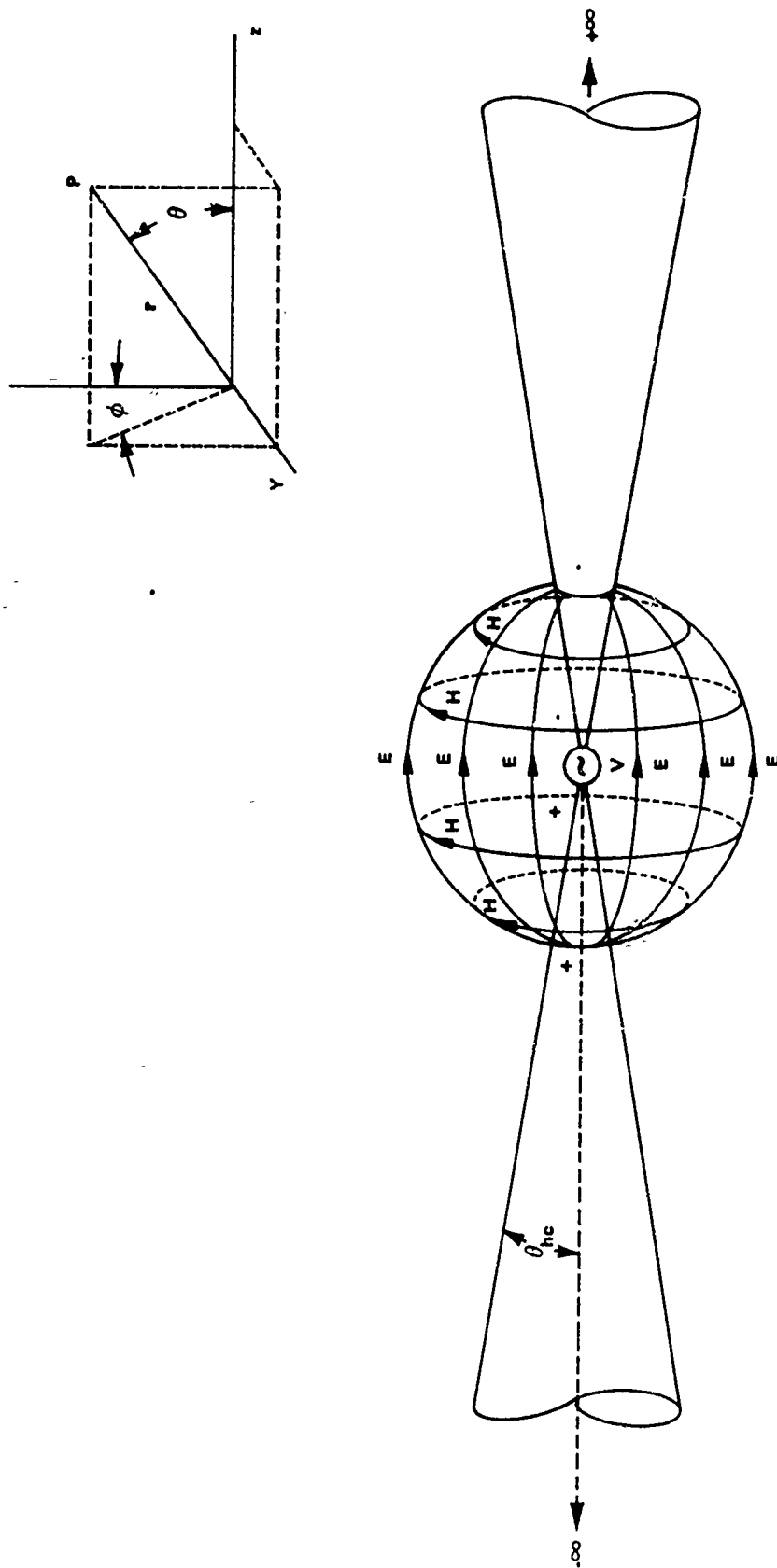


Figure 2 Biconical transmission line and field distribution.

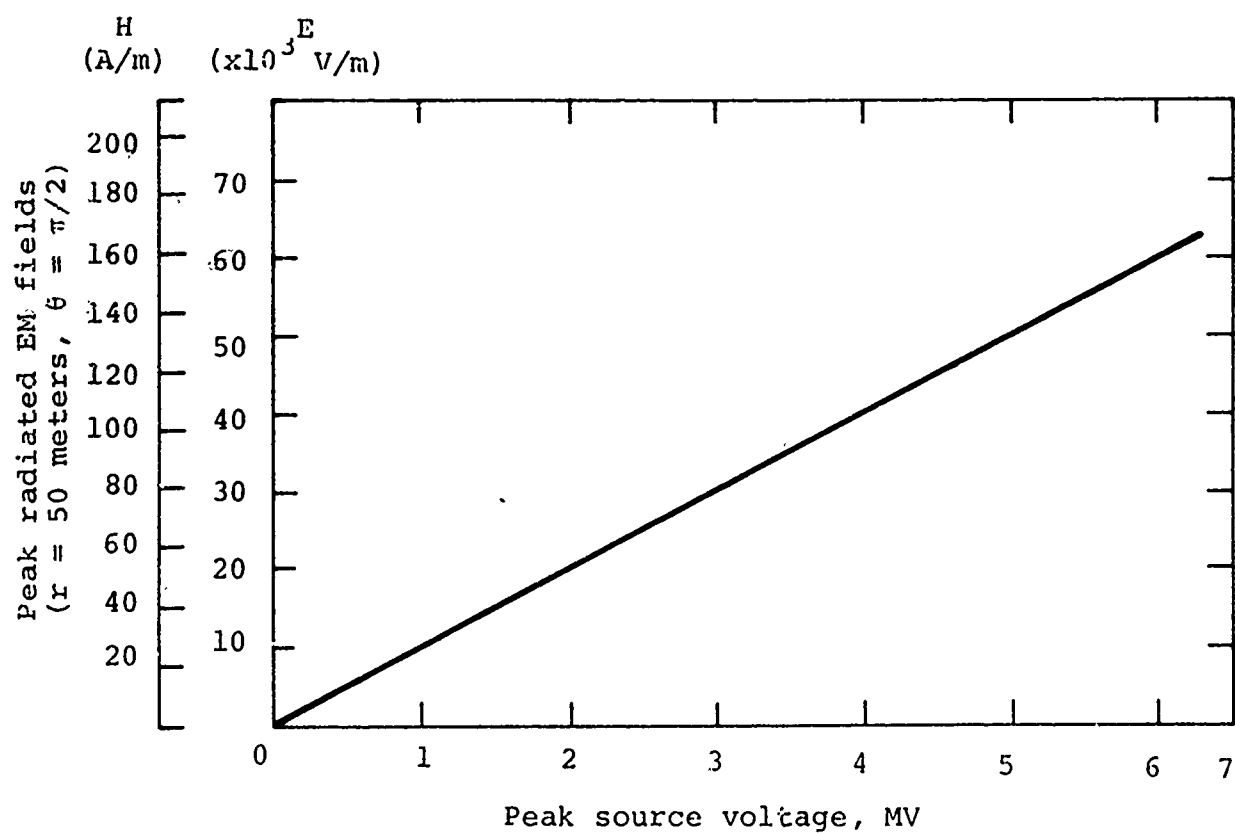


Figure 3 Radiated field magnitude ( $r = 50$  meters,  $\theta = \pi/2$ ).

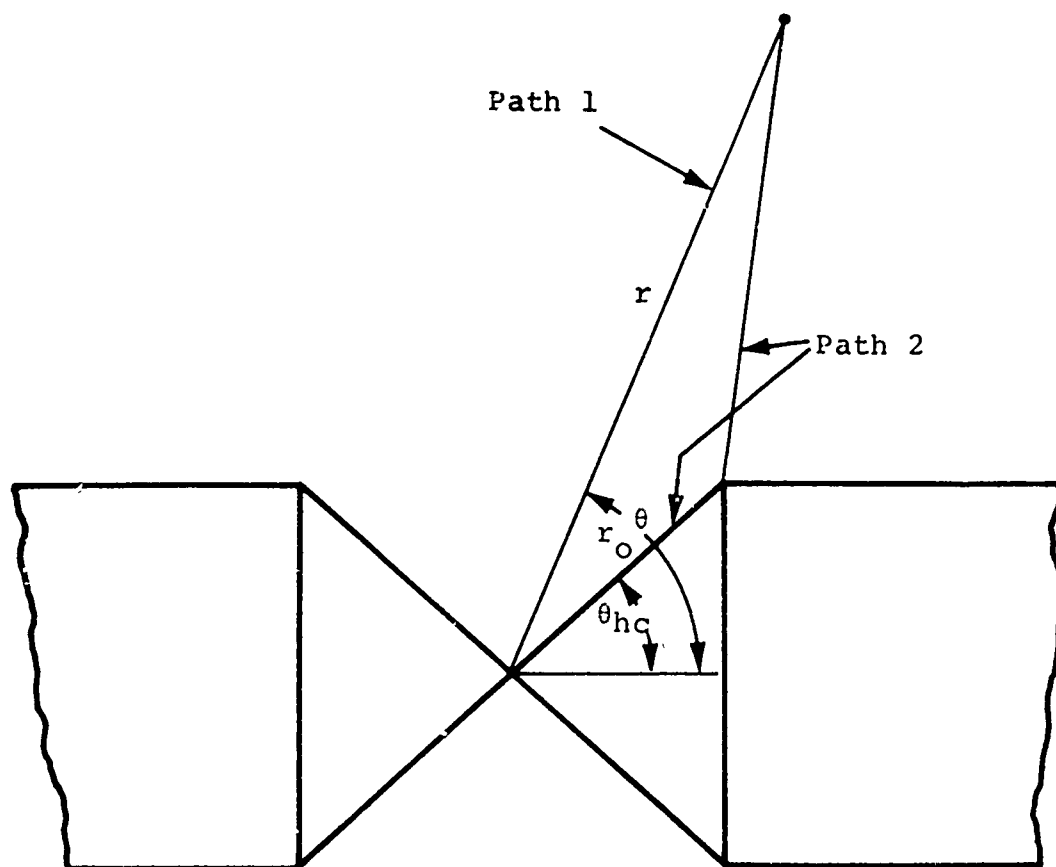


Figure 4 Path length difference.

discontinuity at the end of the bicone is a source of frequency-dependent wave reflections which interact with the initial wave such that, after interaction, field magnitudes and their distribution in space are no longer accurately described by Equations 3-1 and 3-2. This interaction is time-dependent and the time interval between arrival of the initial and reflected EM waves at any point in space can be determined by calculation of path length difference between the direct and reflected waves at an arbitrary point in space. This time interval  $\tau_c$  is called the cleartime. Simply defined, cleartime is that time during which the direct EM wave remains undistorted by wave reflections produced from discontinuities associated with a departure of the conducting geometry from a uniform-impedance biconical line. From Reference 1, cleartime  $\tau_c$  is given by

$$\tau_c = \frac{1}{c} \left[ r_o - r + \left( r_o^2 + r^2 - 2 r_o r \cos (\theta - \theta_{hc}) \right)^{\frac{1}{2}} \right] \quad (3-5)$$

If the observation point P is at a sufficiently long distance such that parallel direct and reflected rays may be approximately assumed, then cleartime becomes

$$\tau_c \approx \frac{r_o}{c} \left[ 1 - \cos (\theta - \theta_{hc}) \right] \quad (3-6)$$

In practice, the risetime of the applied voltage is not instantaneous but increases to maximum value in some time expressed most frequently as a 10 to 90 percent risetime. This assumes an exponential rise characteristic governed principally by stray inductance  $L_s$  in series with the initial load impedance and expressed by

$$\tau_R = \frac{L_S}{Z_k} \text{ sec (e-fold)}$$

or

$$\tau_R \text{ (10 to 90)} = 2.2 \frac{L_S}{Z_k} \text{ sec (10 to 90 percent)}$$

Thus, to radiate the peak field requires that the cleartime be sufficiently long compared with applied voltage risetime. The determination of antenna diameter is based upon this consideration.

Cleartime effects and related EM performance characteristics of the TEMPS high-frequency launcher were evaluated using scaled models to determine antenna design. Specific objectives of the modeling program and a description of the experimental results are described in References 2 and 3.

Based upon analytical and experimental results Physics International recommended that the originally proposed biconical transmission line impedance of 120 ohms be retained for the final design, and that the design of the feed sections take the form illustrated in Figure 5. The continuous conducting biconical line is carried to a diameter of 23 feet, at which point transition is made to a wire cage biconical line to reduce wind loading. In addition, wire cage bicone angle was reduced to about 20 degrees to smooth the transition from the 120-ohm bicone to the cylindrical LTA. A cylindrical wire cage antenna diameter greater than or equal to 25 feet was recommended by PI and in subsequent discussions between PI and HDL, a value of 30 feet was ultimately chosen.

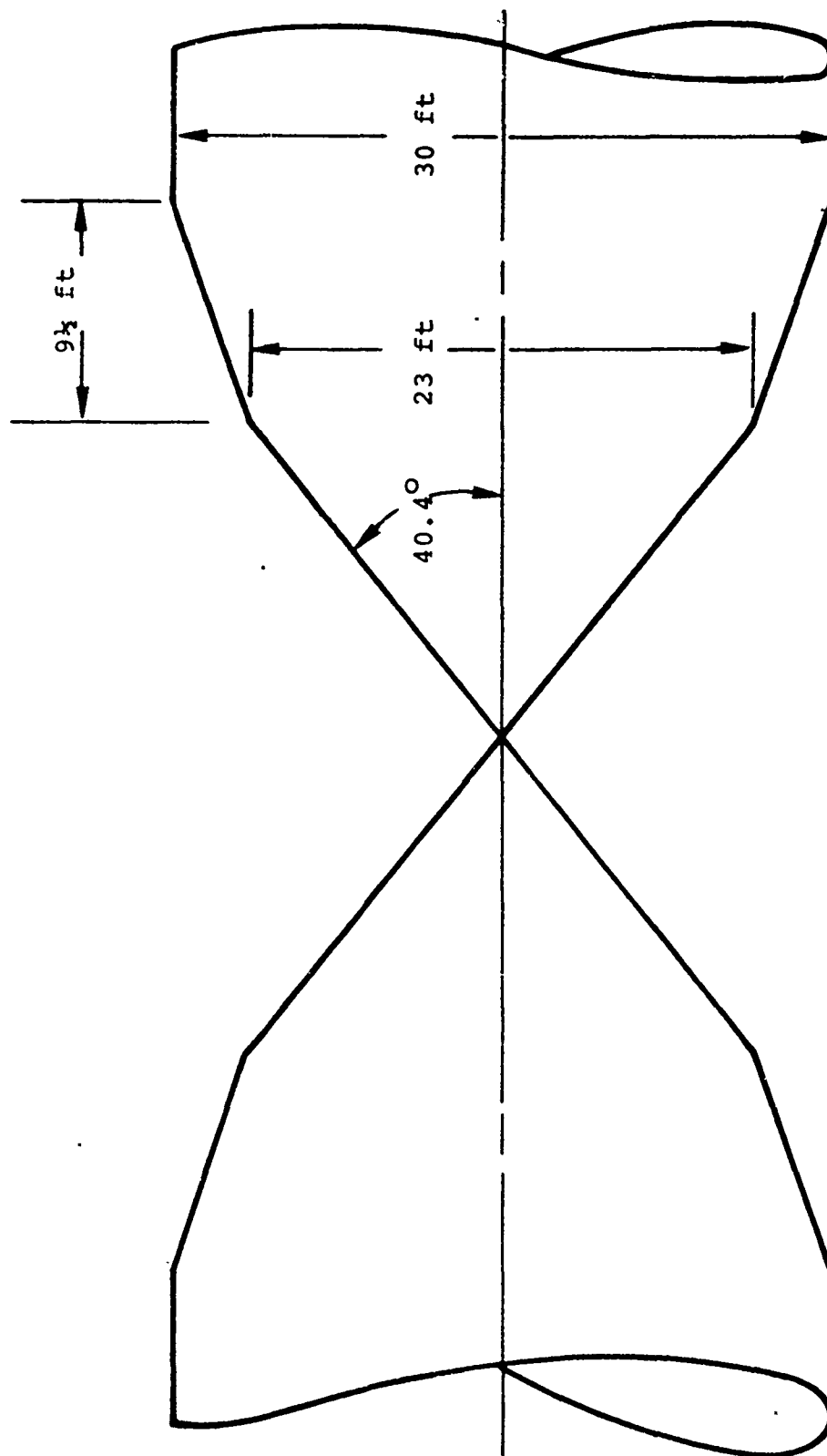


Figure 5 Simplified cross-sectional view of TEMPS high-frequency launcher.



### 3.2 LATE TIME ANTENNA (LTA)

Design of the LTA and its location with respect to ground, in conjunction with the pulser, determine the late-time EM pulse shape and distribution of fields in space. Overall antenna length was specified to be 300 meters by the Statement of Work, and pulse undershoot was to be less than 20 percent of the peak value.\* Moreover, the EM field produced by TEMPS was required to be as uniform as possible over a range of 100 meters measured parallel to the antenna at a horizontal distance 50 meters from the antenna.

Three design alternatives for the LTA were examined by Stanford Research Institute (SRI) in the course of their design investigation: (a) tapered conical LTA, unterminated, (b) constant impedance antenna, terminated to earth ground, and (c) resistively loaded dipole antenna, unterminated. These alternative designs are described in Appendix A.

Based upon the analytical and experimental work of SRI, PI and SRI recommended that the LTA antenna design take the form of a constant-impedance wire cage LTA, terminated to earth ground through matched resistive loads (Figure 6).

3.2.1 LTA Impedance. In late pulse times (for pulse times on the order of a double transit time from the antenna to ground, the LTA forms a rod-to-plane transmission line geometry, although strictly speaking, the conducting structure is a "transmission line" for pulse frequency content with radian wavelength on the order of the spacing of the antenna to ground or longer.

---

\* As assessed by measurement of the tangential component of magnetic field at the reference location, which is defined as a point on the ground plane 50 meters horizontal from the antenna centerline, directly broadside to the antenna at its center.

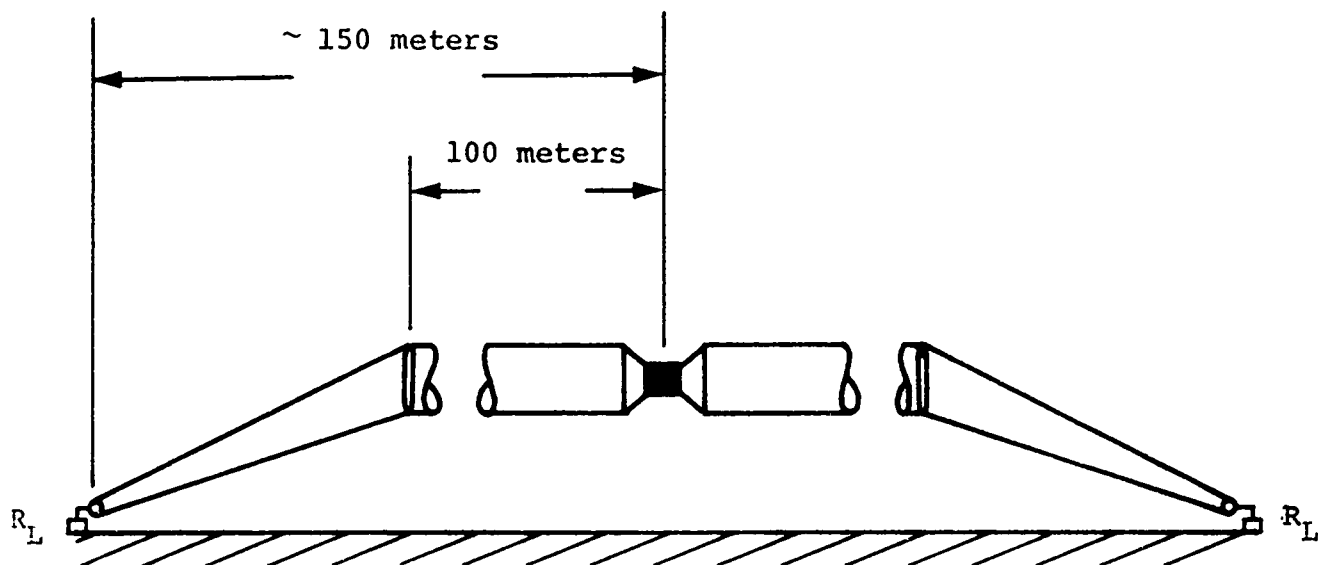


Figure 6 TEMPS late time antenna.

For a rod-to-plane line, line impedance is given by

$$Z_o = 60 \cosh^{-1} 2s/d$$

where  $s$  is the spacing measured from the antenna axis to ground and  $d$  is antenna diameter.

Assuming a continuous conducting LTA (as opposed to a wire cage), the impedance  $Z_o$  of each half of the antenna to ground for  $d = 30$  feet and  $s$  in the range of 10 to 20 meters varies from about 85 to 130 ohms, respectively. The pulser drives each half of the LTA in series; thus, late time pulser load impedance is in the range of 170 to 230 ohms for an antenna height of 10 to 20 meters respectively.

3.2.2 Wire Cage LTA. A wire cage LTA is utilized in TEMPS to reduce system weight and wind loading and thus eases system support structure design requirements.

From Reference 4, the effective diameter of a cylindrical wire cage conducting structure decreases with decreasing number of wires. The approximate relationship is

$$d_{\text{eff}} = d_{\text{cage}} \left( \frac{n d_{\text{wire}}}{d_{\text{cage}}} \right)^{1/n}$$

where  $n$  is the number of wires. Using this relationship, the effective diameter of the TEMPS LTA wire cage, and thus impedance, was determined as a function of the number of wires and the spacing of the antenna to ground and is reported in Reference 3. Based upon this analysis and on discussions with HDL, the design of the TEMPS LTA was agreed upon: a 30-foot-diameter constant-impedance wire cage antenna using 36 equally spaced 1/8-inch-

diameter wires. Since the use of wires decreases the effective diameter of the cylindrical antenna the total late time series impedance of the LTA increases from the previously determined values into values in the range of 186 to 274 ohms for associated antenna heights in the range of 10 to 20 meters.

3.2.3 Antenna Termination. Termination of the TEMPS antenna is effected by way of resistor strings, two at each end of the antenna, which are connected from the antenna end domes to earth ground. Connection to the earth medium is made by way of radial conductors buried at depths of about 2 feet, the number and length of radial conductors being dependent upon ground conductivity. This type of grounding technique was evaluated by SRI and is described in Appendix A in detail. Using this technique provides an effective ground termination with little disturbance to the site under test, an important consideration in some cases.

The ends of the TEMPS antenna wires terminate at 6-foot-diameter end domes which are spaced 3 meters from ground as measured from the bottom of the domes. This spacing provides the requisite voltage insulation in air for TEMPS at the highest output voltage. For this condition, SKI (Appendix A) has shown that a reasonably good termination impedance match, independent of antenna height, is achieved using the parameters listed in Table I.

TABLE I

TEMPS ANTENNA TERMINATION  
FOR 3-METER DOME-TO-GROUND CLEARANCE--ALL HEIGHTS

$\sigma$ (mho/meter)	Termination Resistance for Each End of the Antenna ( $\Omega$ )	Number of Radial Ground Conductors	Length of Radials (meter)
$10^{-2}$	112	3	4
$10^{-3}$	112	5	12
$10^{-4}$	69	8	20

3.2.4 Termination Resistors. Ideally, the distribution of termination resistors at the antenna ends should match the quasi-static field distribution at that location. In addition, for a step-incident EM wave at the antenna ends, the termination should include distributed series inductance to optimize the impedance match for the high-frequency spectral content, i.e., for frequencies with half wavelength on the order of or less than dome-to-ground spacing. However, the series inductance must not be too large or reflection of intermediate pulse frequency content will occur.

From Appendix A, the high-frequency content of the EM wave launched onto the TEMPS antenna is significantly degraded due to propagation of the wave over a lossy earth medium. For example, from Appendix A the calculated 0 to 90 percent pulse risetime at the end of the TEMPS antenna (half length 150 meters) assuming a step input pulse, for an antenna height of 8.5 meters and ground conductivity of  $10^{-2}$  mho/meter, is about 1.6  $\mu$ sec. The time to reach 50 percent amplitude in this case is 55 nsec, a significant degradation.

As the high-frequency content of the incident EM wave is decreased, stray inductance in series with the terminating resistance becomes of less concern and the number of parallel resistor strings that comprise the load may be reduced.

For TEMPS, two parallel resistor strings are used to terminate the EM wave at each end of the antenna. The nominal value of each resistor string is about 235 ohms using 120 1.96-ohm noninductive wire-wound resistors connected in series, 1.96 ohm being an off-the-shelf value for resistors of this type. Each string is divided into six sections containing 20 series resistors each. The resistors, which are epoxy potted in groups of five, are contained with acrylic tubes for protection from the environment. Fabricated in this way, the series sections may be varied in number to optimize the termination, depending upon ground conductivity.

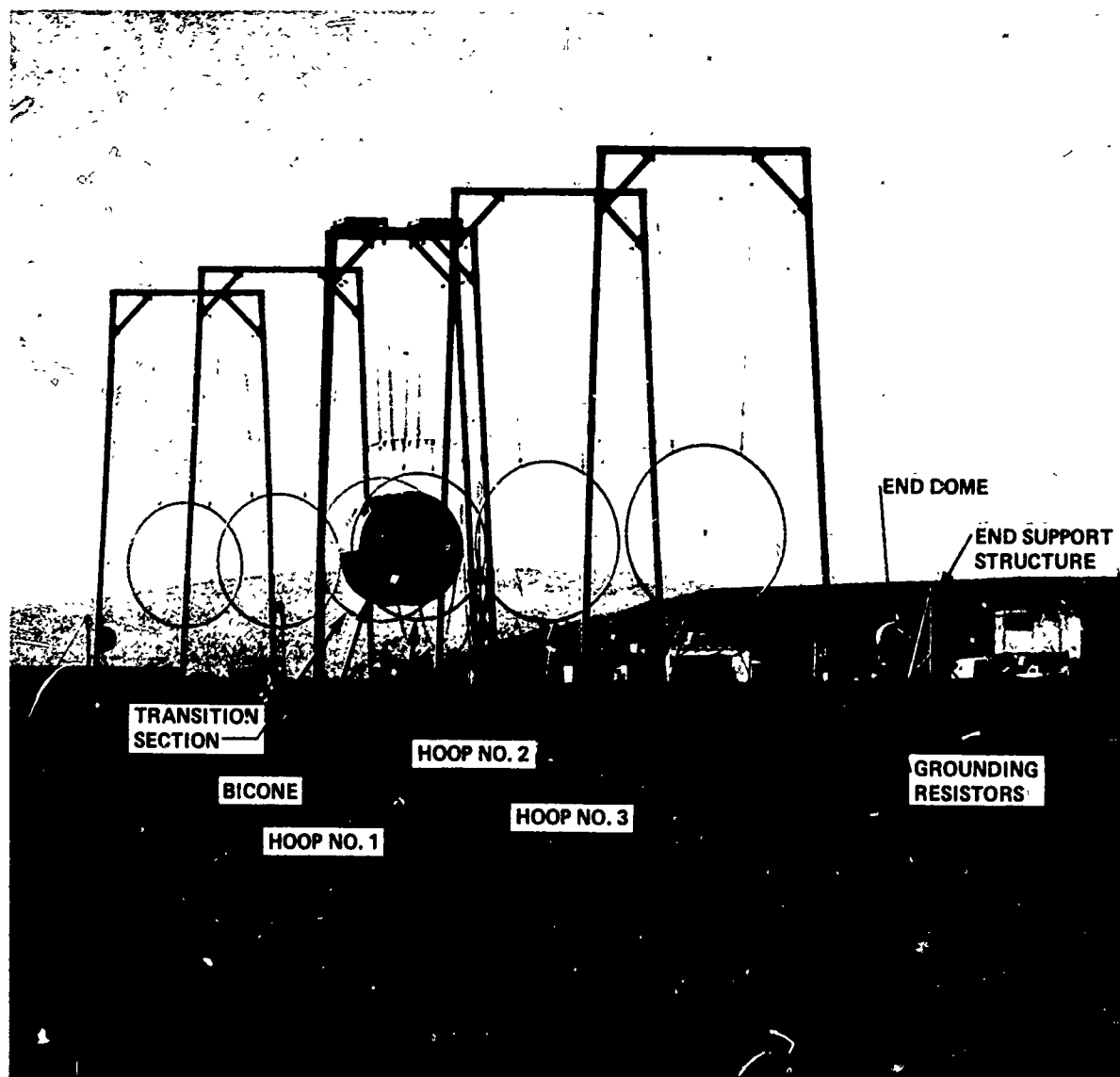
## SECTION 4

### ANTENNA MECHANICAL DESIGN

#### 4.1 OVERALL ANTENNA SYSTEM

The TEMPS antenna shown in Figure 7 is a dipole configuration emanating from the centrally located pulser. The antenna cage array consists of thirty-six 1/8-inch-diameter aircraft cables supported on three 30-foot-diameter hoops on each side of the pulser. From the outermost hoops the antenna wires taper down to the 6-foot diameter of the antenna end dome assemblies which include provision for adjusting the tension of individual wires. The end dome assemblies are connected with Dacron ropes to the end dome support structures located at each end of the antenna. Electric winches are mounted on the end structures to apply a preset level of tension to the ends of the antenna through spring tensioning devices equipped with limit switches. The ends of the antenna are terminated to ground by means of grounding resistor strings, each consisting of six modules, which connect the end assemblies to grounding anchor assemblies.

The design of the antenna corresponds to the primary operational configuration, which is 300 meters long (from end dome to end dome), with the system axis elevated at a height of 20 meters. The antenna can also be erected in optional configurations at intermediate heights down to 10 meters and/or shortened to either 200 or 100 meters by leaving out one or two 30-foot-diameter straight sections per side.



72-10-74-1

Figure 7 TEMPS antenna system.



All antenna wire hardware is compatible with the different antenna configurations. There are quick acting coupler connections and cable "quickie" connections which facilitate any antenna configuration changes.

#### 4.2 HOOPS

The 30-foot diameter of the antenna is formed by wires attached to aluminum hoops which are suspended from the support structures. There are three hoops on each side of the pulser spaced 47.6 meters apart. The hoops are made of 6 inch o.d. x 1/8-inch wall tubing rolled to 30 foot o.d., and each hoop is made up of four segments with welded circular connecting flanges that bolt together to form a full hoop. Each hoop can be disassembled into four segments for ease of transportability.

While the hoop design is self-supporting and hoops can be lifted from a single point, the loads imposed on the two no. 1 hoops (adjacent to pulser) and the two end hoops (furthest away from pulser) by the antenna wires would cause distortion of the circular hoops. Consequently, these four hoops incorporate eight spoke assembly wires connected to a central hub. The tension of the spoke wires is adjusted until they are just taut by means of the turnbuckles. Attachment and positioning of the antenna wires are accomplished by means of aluminum blocks welded on the outside diameter of the hoops.

#### 4.3 WIRE CONNECTIONS

Two basic connections are used. One type is a quick-acting coupling attaching to male connectors. These are used at the 23-foot-diameter bicone, the adjacent no. 1 hoops, and at the

disconnect blocks located at the outermost hoops. The construction of the quick-acting coupling accommodates both angular and swivel motion which minimize kinking, twisting, and fouling of antenna wires. The second wire connection, called a "quickie connection," is used to connect adjacent cable ends with swaged-on ball terminals.

#### 4.4 WIRES

The intermediate cables are nominally 140 feet long with double shank ball terminals and are 1/8 nominal diameter pre-formed aircraft cable of 7 x 7 construction, galvanized steel, impregnated and covered with black polypropylene.

All other wires are 1/8-inch-diameter bare stainless steel aircraft cable of 7 x 7 construction with the exception of end dome wires which are 7 x 19. Approximately 90 pounds of tension is applied to each wire to limit catenary sag to about 1 foot between hoops spaced 156 feet apart. A colored numbering and coding system is employed as defined on the antenna wire drawing to facilitate making the proper wire connections.

#### 4.5 TRANSITION SECTION

The transition section connecting the 23-foot diameter of the bicone to the adjacent 30-foot-diameter hoop of the wire cage late time antenna is comprised of 144 wires. The transition section effectively extends the bicone out from the 23-foot diameter to the 30-foot diameter of the straight cylindrical cage sections.

The transition wires are comprised of 36 cable assemblies, each with four 1/8-inch-diameter cables with two connectors at the bicone end and three connectors at the 30 foot hoop end forming a "W" shaped wire assembly. The resultant wire spacing around the bicone is 1.0 foot and around the 30 foot hoop is 1.3 feet. Connections to the bicone and 30 foot hoop are made by the quick-acting coupling with the male half of the connector screwed into small aluminum blocks welded to the hoops as indicated on the drawing.

#### 4.6 STRAIGHT SECTIONS

The balance of the antenna section is comprised of 36 wires and it is divided into three equal axial lengths of 156 feet each from the end of the transition section (no. 1 hoops) to the end dome assembly of the antenna.

The first two 156-foot lengths are the straight 30-foot-diameter cylindrical sections and last 156-foot length extends from the outermost hoop and tapers down to the end dome assembly.

Hoops no. 2 and 3 have 36 equally spaced aluminum blocks welded around the o.d. Short lengths of bare slide wires (approximately 14 feet long) are held captive by means of slotted retaining blocks and the swaged on double shank ball on each end of the wires. Thus, a limited length of cable is free to slide through the hoop retaining blocks, when coupled to the long lengths of adjoining cables: this allows individual cable tensioning at the end dome assemblies.

#### 4.7 END DOME ASSEMBLIES

The end dome assembly is a 6-foot-diameter semi-elliptical aluminum head with 36 winch assemblies and associated pulleys. The winch assemblies allow individual tension adjustments of the antenna wires. The winch pulley positions are controlled by an integral spring loaded pawl assembly. Adjustments can be manually accomplished through the wire cage with a special tool and a torque wrench.

Since the last 30-foot-diameter hoop (nearest the end dome) is subjected to antenna forces which tend to displace the hoop from the vertical position directly under the supporting structure, four fixed wires connect the hoop to the end dome assembly. These wires maintain the proper hoop position and also serve as base members for alignment and tensioning of the antenna.

#### 4.8 TENSIONING

The pulser to hoop wire attaches to both the bicone and hoops no. 1, and therefore establishes the positions of these hoops relative to the pulser bicones. All but the four fixed wires extend from hoops no. 1 through guides on hoops no. 2 and 3 to the end domes where they enter through a guide hole near the o.d., pass around a pulley, and then wind on the antenna winch assembly. In this manner adjustment at the antenna winches controls the individual tension of wires over the entire length of the antenna from the end of the transition to the end dome assembly. The tension of each wire is nominally 90 pounds to reduce the wire sag to approximately 1 foot between supports.

The four fixed control wires, spaced 90 degrees apart on the hoops, are attached to each hoop and thereby establish hoop spacing along the antenna axis. The control wires are attached to hoops no. 3 and are terminated in the end domes on winches as are the other wires. Thus, there are four control wires which allow for vertical attitude positioning of the outermost hoops by adjusting the four respective antenna winches on the end dome.

#### 4.9 GROUNDING RESISTORS

Ground connection at each end of the antenna is accomplished by dual strings of solid wire wound resistors which couple to the end domes and to grounding strips buried at each of the antenna. Each string is comprised of 6 resistor modules which consist of an acrylic enclosure tube, four resistor units, end connectors, gaskets, and retaining nuts. The resistor units are joined by threaded connections and the end connections are made with giant banana plugs. Grounding resistor modules are connected by means of stainless steel tubular braid and hose clamps. This method provides flexibility and electrical continuity as well as axial tensioning capability.

#### 4.10 ANCHOR ASSEMBLIES

Four grounding resistor anchor assemblies are used, two at each end dome assembly. The anchor plates are positioned and oriented in the ground in a radial pattern. Up to eight radial aluminum strips 3 inches wide by 0.050 inch thick by about 20 feet long, buried approximately 12 inches below ground level, are attached to the anchors with clamp bars. The anchor mast is

rotated about its centerline to align with the resistor string and then clamped in place. The elevation of the connector mast is aligned with the resistor string and then clamped with a single lock screw.

#### 4.11 END DOME SUPPORT STRUCTURE

Each of the two assemblies is located at the outermost position of the antenna; the support structures incorporate provisions for:

- Applying tension to the end dome
- Regulating and maintaining the applied tension load on the antenna
- Indicating visually tension level
- Adjusting the height of the end dome with respect to ground to obtain necessary voltage standoff distance
- Anchoring stabilizing ropes connected to the end domes

The end dome support structure is a triangulated structure which rests on three concrete blocks measuring 4 feet by 5 feet by 20 inches high. The vertical column is bolted to the concrete block and is supported and stabilized by four pipes called support and extender bars. The rear concrete blocks are connected by another support and extender bar. All such joints are made with single 3/4-inch-diameter bolts, washers, and nuts. The front concrete block supports the electric winch mounted on its base. The 5/16-inch-diameter preformed 7 x 19 stranded aircraft tensioning cable is rigged from the sheave bracket assembly to the single wire rope block on the tensioning device and

through the triple and double wire rope blocks in the manner shown. The sheave assembly can be attached at different vertical levels as may be necessary to establish the proper location of the end dome relative to ground level.

A pendant pushbutton station is provided to control the "UP" and "DOWN" mode of the winch operation. The limit switch assembly on the tensioning device controls the maximum tension which may be applied by the electrical winch operation in the "UP" mode. Care should be exercised to maintain approximately equal tensioning at the opposing end structures when tensioning the antenna.

## SECTION 5

### PULSER ELECTRICAL DESIGN

The pulser system proposed for TEMPS (Reference 1) is a bilateral-Marx generator peaking capacitor circuit. A bilateral design makes more effective use of the available volume within the bicones, but requires that the Marxes be well synchronized to produce the output EM wave. A peaking circuit is used to provide the initial fast-rising load current that the Marxes, because of their stray series inductance, cannot supply. A peaking circuit reduces system weight compared with a transfer capacitor circuit; the peaking capacitors store only the energy required to produce the fast risetime portion of the pulse, whereas a transfer capacitor, which is also a low-inductance fast-risetime component, stores the entire pulse energy.

A simplified electrical circuit of the TEMPS system is shown in Figure 8.  $C_g$  represents the erected series capacity of each Marx generator.  $L_s$  is the stray series inductance associated principally with the Marx generators.  $R_s$  is the sum of stray and lumped series resistance within the Marxes.  $R_{sh}$  is shunt resistance formed principally by the Marx generator spark gap triggering resistors.  $C_p$  is the peaking capacitor, and  $Z_a$  is the driven impedance associated with the antenna.



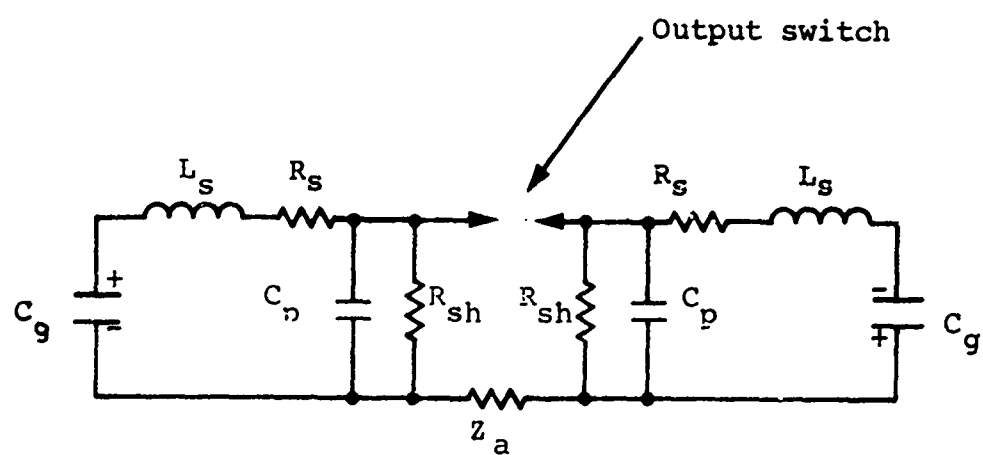


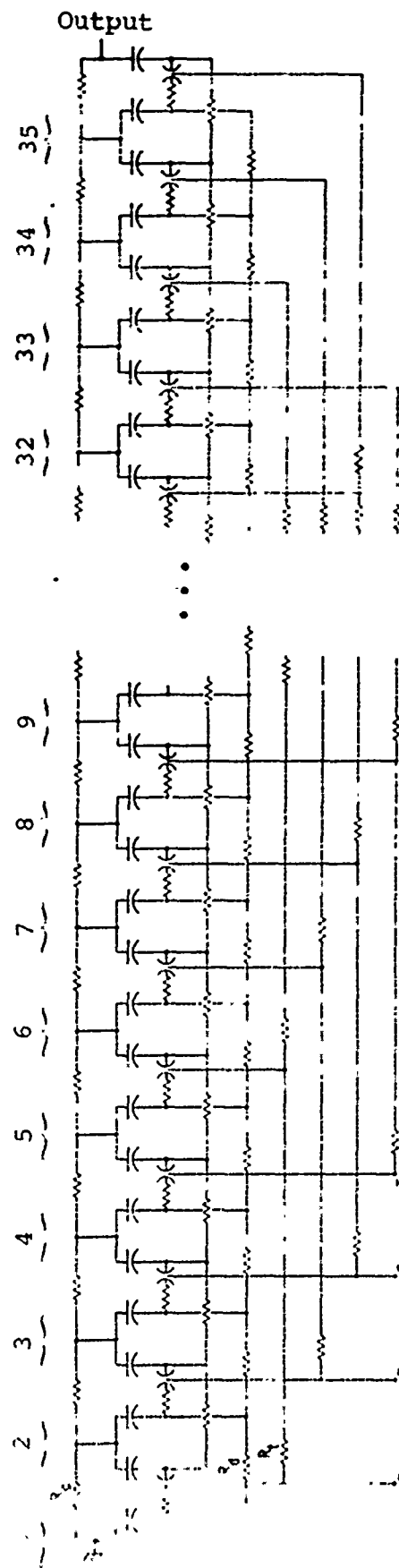
Figure 8 Simplified TEMPS circuit.

The sequence of electrical events leading to launch of an EM pulse is as follows: the Marx generator energy storage capacitor stages are dc charged in a time less than about 40 seconds to a voltage between about 35 kV and 100 kV, depending upon the desired output voltage. Upon completion of dc charging, the Marxes are synchronously erected by means of a fast trigger system which couples across the bicone by way of dielectric optical light-pipe system. Marx erection proceeds very rapidly. Erection is the process by which the Marx generator spark gaps are overvolted, usually sequentially, and broken down. Marx erection time, i.e., the time for all Marx gaps to close such that load current may begin to flow, is on the order of 150 nsec for the TEMPS 35 stage Marx generators. Once erected, the Marxes pulse charge their respective peaking capacitors in about 65 nsec to the required high voltage (in the range of 1 to 3 MV for each side of the system), at which time the output switch (Figure 8) closes, discharging the peaking capacitors and Marxes into the antenna. For TEMPS, this cycle may be repeated as often as once every 3 minutes.

A description of the basic electrical components which comprise the TEMPS system are the subjects of the following sections.

#### 5.1 MARX GENERATOR

Each Marx generator of the TEMPS system consists of 35 capacitor stages dc charged and triggered by way of resistor strings. The electrical circuit of each Marx is shown in Figure 9.



Stage capacity =  $0.175 \mu\text{F}$  at 100 kV

#### Resistors

1. Case-to-case,  $R_m = 20 \text{ kohms}$
2. Charging,  $R_c = 500 \text{ ohms}$
3. Triggering,  $R_t = 500 \text{ ohms}$ ,  $R_i = 250 \text{ ohms}$
4. Series,  $R_s = 0.3 \text{ ohms}$

Figure 9 Schematic of TEMPS Marx resistors.

Stages are connected in series by way of pressurized gas, rail electrode switches. The erected series capacity of each Marx is approximately 5 nF; thus, stage capacity is approximately 175 nF.

Marx output voltage into a high impedance load is  $nV_{dc}$  when  $n$  is the number of stages and  $V_{dc}$  is initial dc charge voltage. For TEMPS  $V_{dc}$  is 100 kV maximum and maximum Marx open-circuit output voltage is 3.5 MV, a total of 7 MV for the system.

5.1.1 Energy Storage Capacitors. An energy storage capacitor evaluation and selection program was initiated at the outset of the TEMPS program. Five energy storage capacitors with electrical characteristics compatible with TEMPS requirements were ordered from two manufacturers. Prototype capacitor specifications and the test plan for energy storage capacitor test and evaluation are attached to this report in Appendix B. Prototype energy storage capacitor pulse discharge test results and inductance and equivalent series resistance measurement results are also presented in Appendix B.

Based upon the results of prototype capacitor test and evaluation, the Condenser Products Corporation units were selected. A typical final design unit is shown in Figure 10.

5.1.2 Marx Switches. Pressurized gas, rail type Marx generator switches were proposed for the TEMPS system (Reference 1). This type of switch design is particularly well suited to the overall anticipated Marx physical configuration and energy storage capacitor design.



72-1-13

Figure 10 Energy storage capacitor.

At the outset of the TEMPS program, a prototype Marx switch test and evaluation effort was initiated. Switch design requirements and a description of prototype switch experimental test and evaluation results are presented in Appendix C to this report.

A final-design Marx switch is shown in Figure 11. The main electrodes are formed by a 11/16-inch-diameter brass rod about 13 inches long, shaped at their ends to reduce field enhancement. Electrodes are contained within an 18-inch-long acrylic plastic envelope; electrode separation is 1/2 inch. Each switch is equipped with a knife-edge midplane trigger electrode, and every switch is triggered to reduce Marx erection delay and jitter. During dc charge of the Marx generator stages (balanced charging with respect to ground), the midplane trigger electrodes are resistively connected to ground. For this condition, the sharp trigger electrode is physically situated on the appropriate equipotential surface, ideally, there is no enhancement at its edge. When triggered, however, the electrode is electrically displaced from its midplane position and the electric fields ending on the knife edge increase to very large values, breaking down the surrounding gas dielectric with subsequent arc closure to the nearby main electrodes.

The Marx switches are designed for use with two gas dielectrics, nitrogen and sulfur hexafluoride ( $\text{SF}_6$ ), to cover the requisite voltage range of the system. Switch self-breakdown voltage as a function of type of gas and gas pressure is presented in Appendix C.

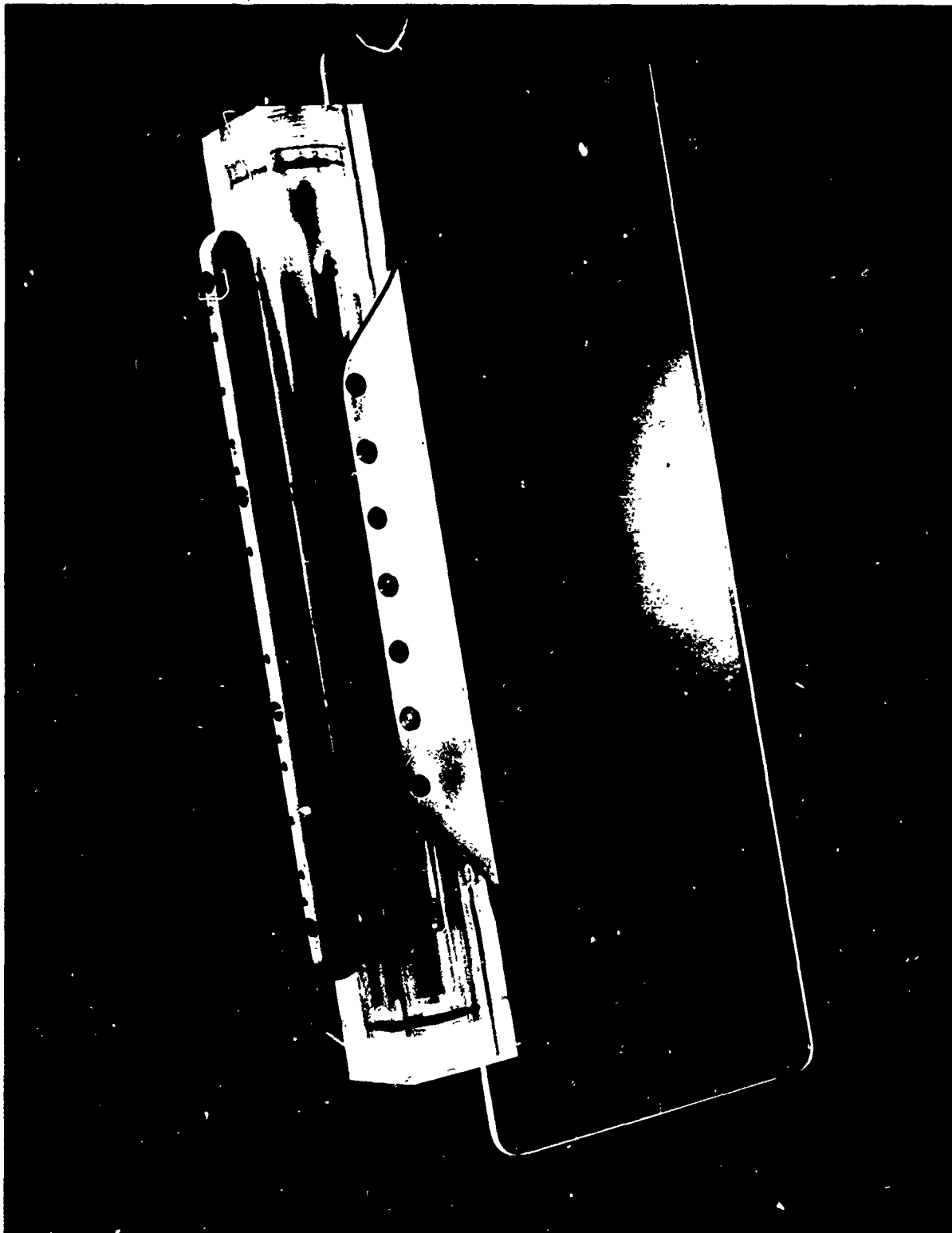


Figure 11 Marx rail gap switch.

72-4-19

In order to ensure more reliable operation of the TEMPS Marx generators, a Marx switch acceptance test procedure was established. This testing consists in mechanical inspection to ensure that the assembled switches are within allowable mechanical tolerances, followed by pulse discharge testing to ensure uniform electrical characteristics in terms of self-breakdown voltage and low self-fire scatter. Acceptance test procedures are described in Appendix D to this final report.

5.1.3 Marx Generator Charging, Triggering, and Current Limiting Resistors. Resistive components play an important role in Marx generator design and operation. The Marx energy storage capacitors are generally dc charged by way of resistor chains as shown in Figure 12. In addition, these resistors isolate adjacent stages during Marx erection and production of the high-voltage output pulse.

Marx spark gaps are triggered by way of coupling resistors. In this application, the resistors must combine low stray series inductance with high-voltage insulating properties.

Resistive components, for TEMPS, are also installed in series with the Marx stages to limit current reduce energy storage capacitor reversal in the event of a short circuit fault at the Marx output.

The electrical performance characteristics of liquid resistors, such as cupric sulfate solution, contained within plastic tubing are well known. Their ease of construction and proven reliability in a large number of high-voltage pulser systems would make them an attractive choice for TEMPS were it not for the temperature environment specified for the TEMPS system.



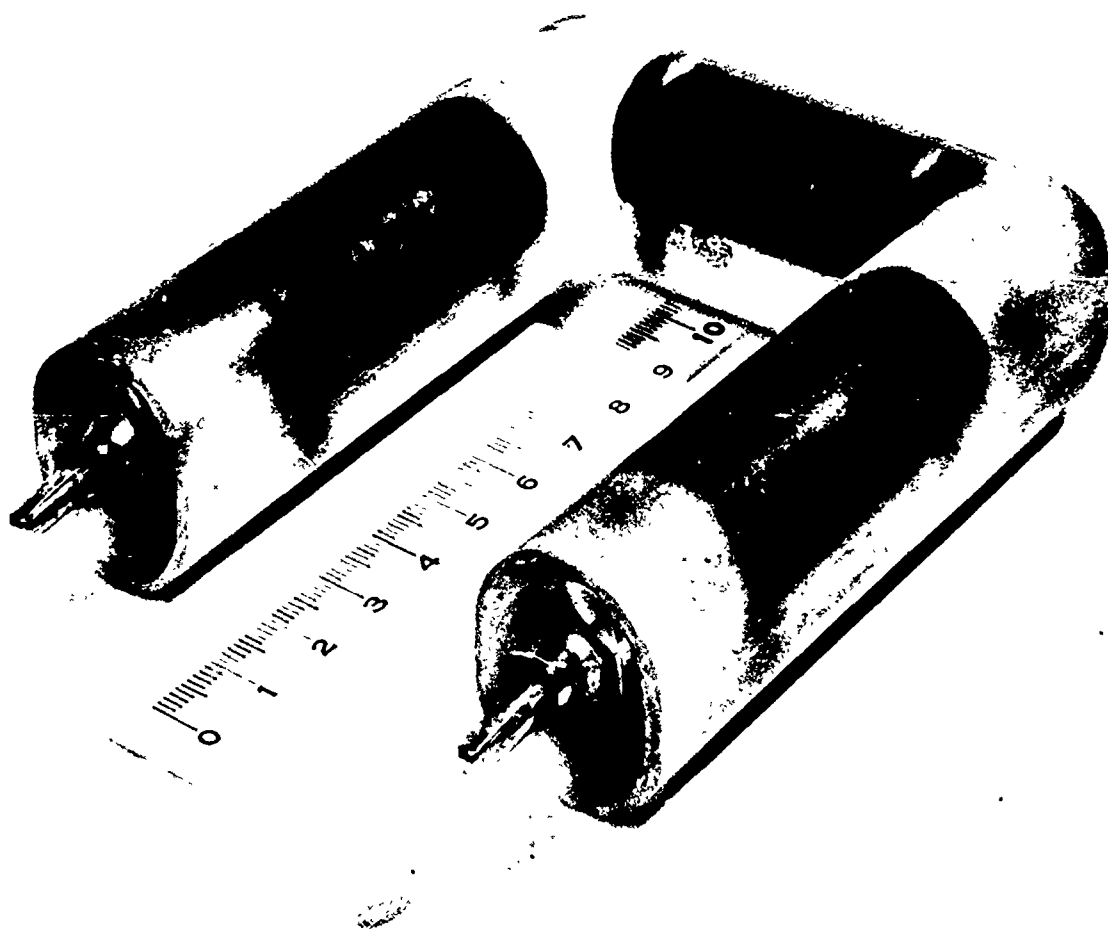


Figure 12 Charging resistors.

72-1-36

Thus, as proposed, work was initiated to investigate other resistive materials that would potentially combine the excellent electrical performance characteristics of cupric sulfate solutions with lower weight materials, non-susceptability to leakage, and nearly constant resistivity with temperature over the specified range.

An investigation of resistive materials was initiated at the outset of the TEMPS program. As a result of work performed at the Air Force Weapons Laboratory on solid resistors of the wire wound type (Appendix E), PI's investigation was quickly narrowed to consideration of commercially available low-inductance wire wound resistors.

The design of resistor assemblies for the TEMPS Marx generator, using Dale NS-10 low-inductance wire-wound resistors is discussed in the following paragraphs.

5.1.4 Marx Charging Resistors. Each Marx is dc charged by way of two series resistor strings (Figure 9). Resistor value is 500 ohms and each is a potted assembly consisting of five series-connected low-inductance Dale NS-10 wire-wound resistors potted in epoxy (similar to that shown in Figure 12).

The charging resistors form a shunt load across the erected Marx which for TEMPS is given approximately by

$$R_{sc} = \frac{n R_c}{2}$$

where  $R_{sc}$  is the equivalent shunt load resistance,  $n$  is the number of stages, and  $R_c$  is the value of each potted resistor assembly. For each TEMPS Marx,  $n = 35$  and  $R_c = 500$  ohms.

Therefore,

$$R_{sc} \approx \frac{n R_c}{2} = \frac{35 (500)}{2} = 8750 \text{ ohms}$$

The discharge time constant of an erected TEMPS Marx through its charging resistors is  $C_g R_{sc}$  and is about 44  $\mu\text{sec}$ , long compared with output pulse duration. This represents an insignificant energy loss mechanism.

5.1.5 Marx Triggering Resistors. Marx generator erection delay and timing jitter are reduced by triggering all of the Marx generator spark gap switches by way of trigger coupling resistor chains, and the electrical circuit is shown in Figure 9. An  $m = 4$  coupled Marx is used for TEMPS,  $m = 4$  coupling meaning that the midplane trigger electrode of the  $n$ th switch is coupled resistively to the  $n + m$ th switch where  $m = 4$ .

The trigger coupling resistors,  $R_T$ , like the charging resistors, are potted assemblies consisting of four series-connected low-inductance wire-wound resistors. Resistance of each potted assembly is 500 ohms.

The trigger resistor coupling chains also form a shunt load across the erected Marx. The equivalent shunt resistance  $R_{st}$  is given by

$$R_{st} \approx \frac{n}{m} R_T$$

where  $n$  is the total number of stages in each Marx; this assumes that the coupling chains are carried the entire length of a Marx, for TEMPS,  $n = 35$ ,  $m = 4$ , and  $R_T = 500$  ohms. Therefore,

$$R_{st} \frac{n}{m} R_T = \frac{35}{4^2} (500) \approx 1.1 \text{ k}\Omega$$

The decay time constant of an erected TEMPS Marx through  $R_{st}$  is approximately 5.5  $\mu\text{sec}$ , but this value is about a factor of 10 larger than output pulse decay time and thus does not seriously load the system.

5.1.6 Midpoint Coupling Resistors. Marx generator energy storage capacitors are balance dc charged which leaves the midpoint connections between capacitor halves at ground potential during charging. Resistors,  $R_m$ , connect capacitor midpoints together and ultimately to ground at the low-voltage end of the Marx.

This capacitor midpoint resistor chain performs two functions. First, these connections ensure that the capacitor midpoints are discharged to ground and are safe from a personnel hazard standpoint. Secondly, monitoring the current flowing in the midpoint chain is a useful technique for detecting a shorted Marx stage half capacitor and, to a lesser degree, an open charging resistor chain. Under normal conditions, almost no current flows in the midpoint connection chain since it is nominally at ground potential. However, if a half stage is short circuited (a defective capacitor) or the charging chain is open, then substantial current flows in the midpoint chain and can be detected and used to give a charging unbalance indication and system shutdown signal.

Midpoint connection resistors, like the charging and triggering, are potted assemblies consisting of four series-connected wire-wound resistors, except that total assembly resistance is 20  $\text{k}\Omega$  in this case.

The equivalent shunt load across the erected Marx due to midpoint coupling resistors is just the total series resistance of the chain or  $n R_m$ . This value is about 0.7 M $\Omega$  and is very large compared with charging and triggering resistor equivalent shunt resistance.

Marx generator resistor design and performance evaluation, including Marx erection delay and jitter measurements, were performed in the course of the Marx development which is the subject of the next section.

5.1.7 Marx Generator Testing. Based upon the system requirements, a preliminary design of the Marx was conceived and immediate experiments were performed to evaluate the two primary component designs: those of the switches and capacitors. Appendices B and C describe the experiments that resulted in the choice of capacitors and the acceptability of the Marx prototype switch design. A more detailed design of the various remaining components and hardware followed and a six-stage Marx utilizing the charging connectors, switch-couplers, current limiting resistors, etc. was constructed. The six-stage Marx test provided a starting point for what is referred to here as the Marx prototype testing.

Early in the testing, high-voltage insulation of the Marx was regarded as a primary objective. The ability to charge and erect the Marx at up to 20 percent above a normal full charge of 100 kV/stage was the goal of this phase of testing. Since the six-stage Marx was provided with a 20-ohm load and enclosed within a dielectric box capable of being filled with an insulating gas, it was well suited for this test. Stage-to-stage voltage, both during dc charging and erection for the six-stage Marx, was

the same as for a 35-stage Marx; therefore a valid prediction as to the performance of the 35-stage Marx could be derived from the six-stage test, including information about the acceptability of the wire-wound type resistors which were to be employed in the system. Breakdowns between stages did occur and the geometry was modified to correct this condition. A Marx geometry and component design was arrived at which was capable of being charged and erected to 20 percent above full specified operation voltage. Thus, the finalized version of the Marx design was ready to be extended to 35 stages.

The 35-stage Marx was assembled and fitted into a biconic section for testing purposes. A preliminary investigation of the inductance associated with a one-half Marx generator was immediately begun in order to confirm the peaking capacitor design which was dependent upon this value. The testing proceeded with the operation of the Marx at elevated voltages by using an  $\text{SF}_6$  gas insulation within the Marx containment vessel and Freon gas surrounding the load. Had there been the need, modifications of the components would have been made at this time. The remainder of the Marx test was devoted to analyzing the output waveform and empirically determining the optimum type of triggering and trigger coupling for the proper synchronization of the TEMPS pulser.

Throughout the testing of the 35-stage Marx, the self-fire behavior and prefire occurrence was evaluated since system specifications call for prefires occurring less than 1 percent of the time.

The successful performance of the Marx followed the release of the Marx components for manufacture and the ultimate construction of two additional Marxes.

Six-Stage Marx Test. The six-stage Marx test geometry is shown in Figures 13 and 14 consisting of six 0.175  $\mu\text{F}$  capacitors, six switches, and the associated Marx hardware. Schematically, the test circuit is shown in Figure 15. A  $\text{CuSO}_4$  resistive load of 20 ohms was used throughout this phase of testing to produce an output waveform as shown in Figure 16 with an e-folding decay time of 590 nsec. The expected output voltage into a high-impedance load would have been the number of charged stages ( $5\frac{1}{2}$ ) multiplied by the charge voltage per stage; however, the peak voltage measured across the load was clipped to approximately 80 percent of this value because of the inductance associated with the circuit.

This Marx was gas-insulated with either  $\text{SF}_6$  or Freon which was contained within the dielectric box surrounding the geometry.

To evaluate the high-voltage performance of the wire-wound resistors and components, the Marx was dc charged to a specified voltage which was monitored by an electrostatic voltmeter. The gas pressure was adjusted such that the self-break voltage corresponded to that level at which one intended to erect the Marx. This procedure was followed because no triggering source had been provided for this Marx. An oscilloscope, which was internally triggered by the output signal produced upon erection, recorded the output voltage and was used as a means of determining the type of breakdown occurring. If the scope did not trigger and a breakdown was heard from the geometry, a dc breakdown was presumed to be the cause of failure. A breakdown occurring during erection would not necessarily be observed on the waveform but the fact that a waveform was recorded and a breakdown seen or heard indicated that a transient-caused-break occurred during erection.

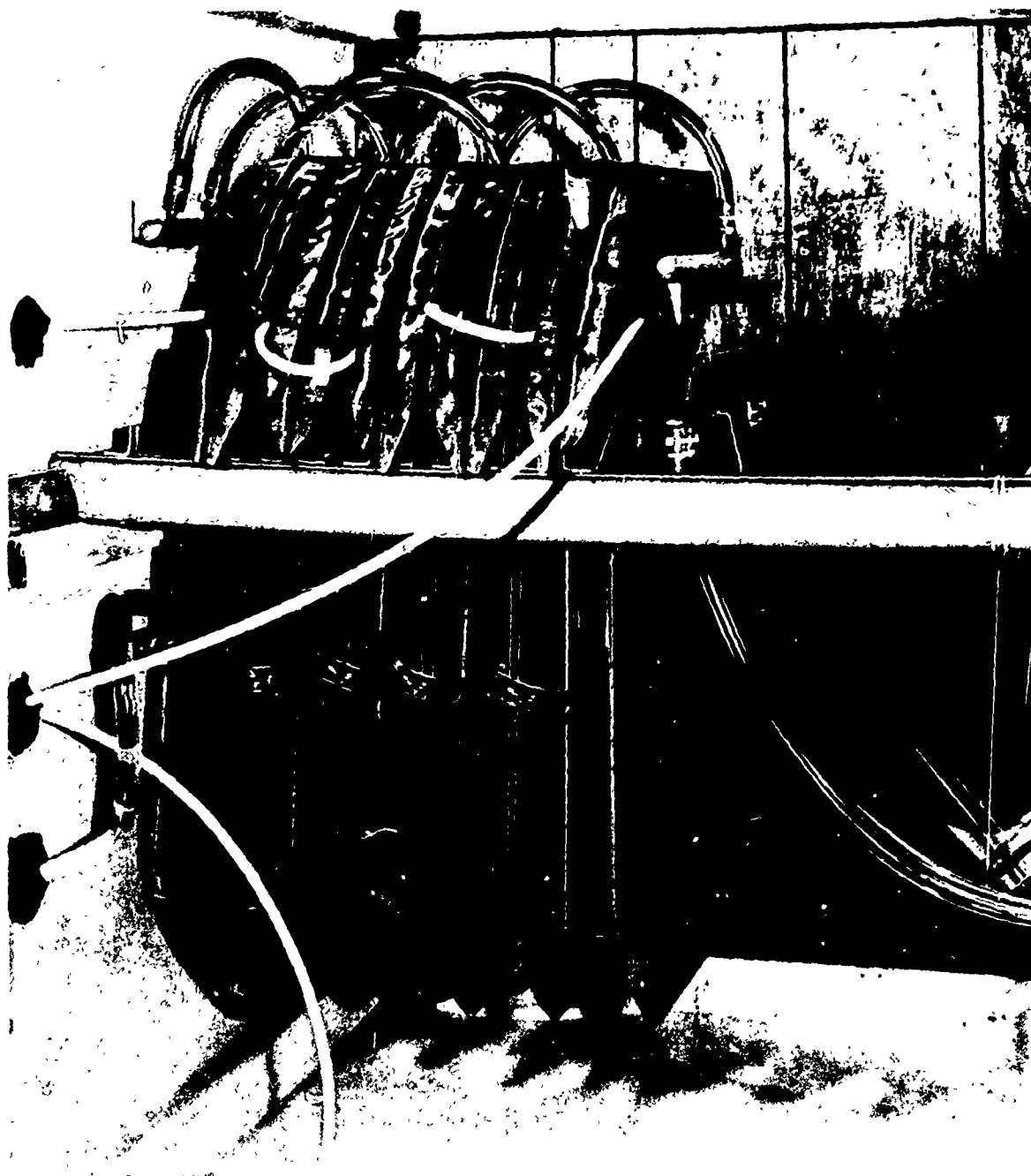


Figure 13 Six-stage Marx (barriers installed).



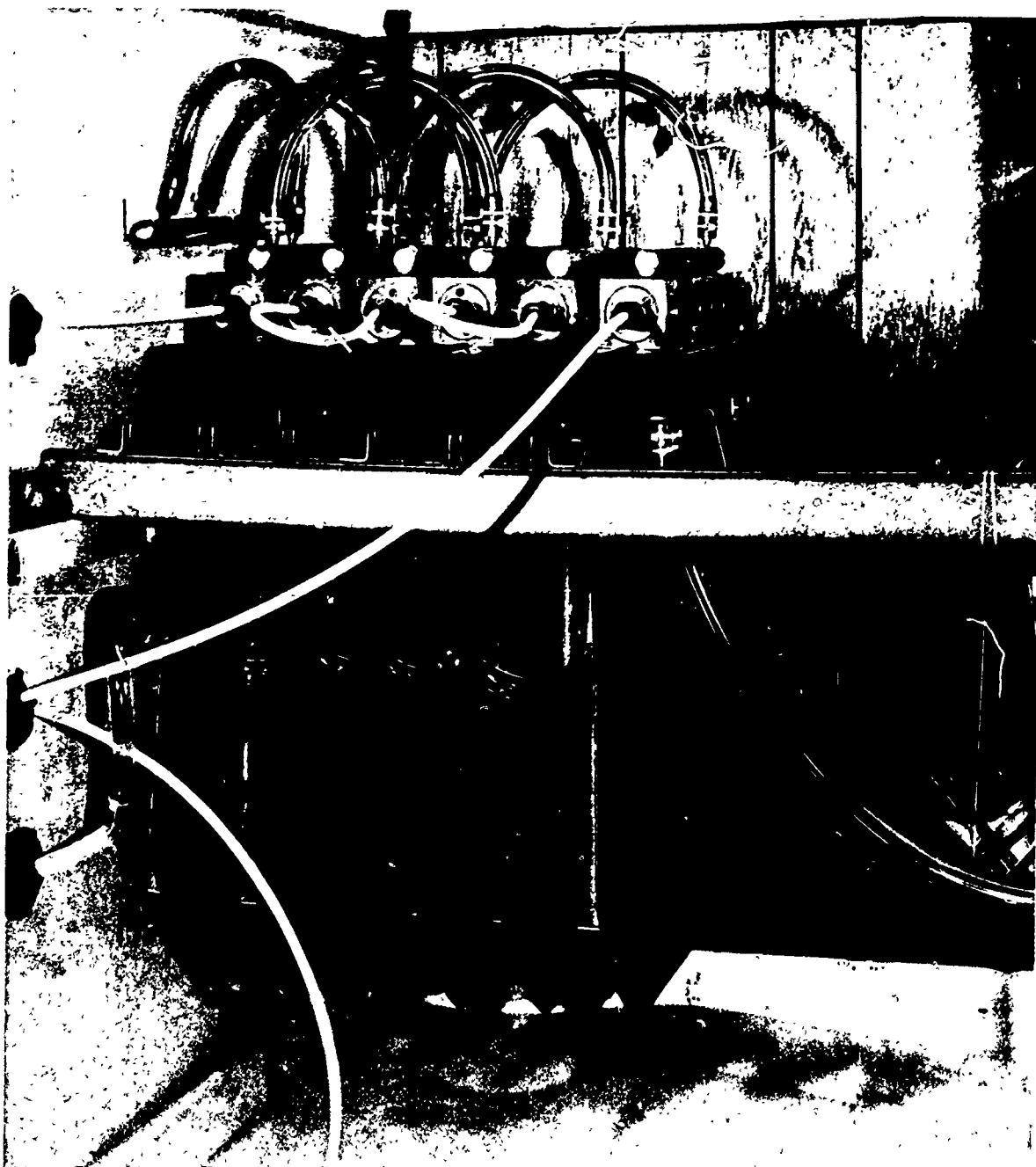
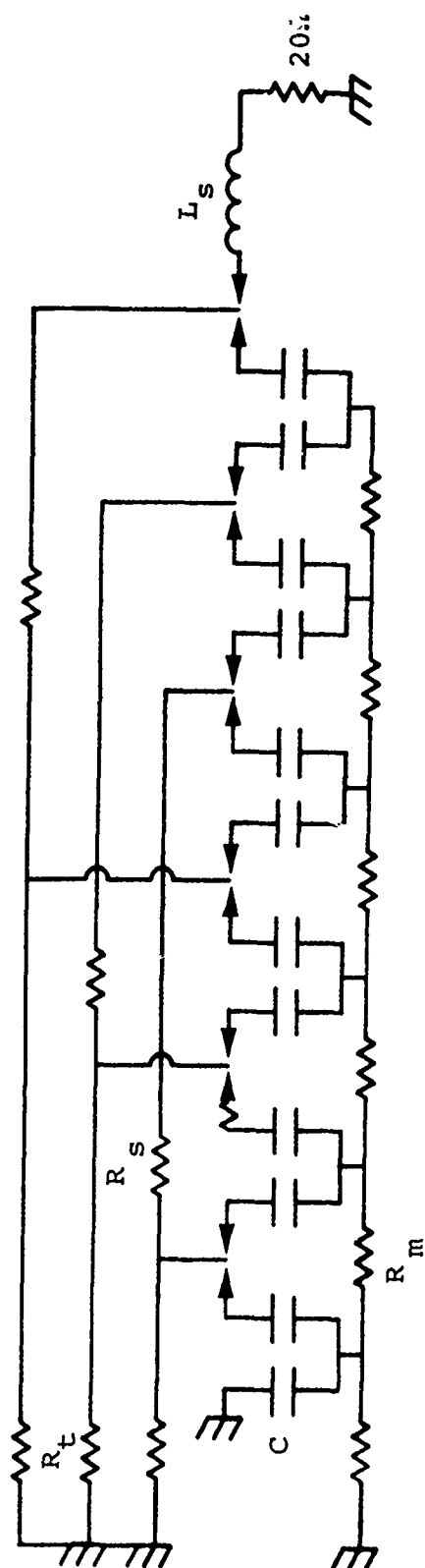


Figure 14 Six-stage Marx.



$C = 0.175 \mu\text{F}$

$L_s = \text{series stray inductance} \approx 500 \text{ nH}$

$R_s = \text{current limiting resistance (} 0.3\Omega \text{)}$

$R_t = \text{trigger coupling resistors, } 1200\Omega, m = 3$

$R_m = \text{case to case resistance, } 2000\Omega$

Simplified circuit (charging resistors omitted)

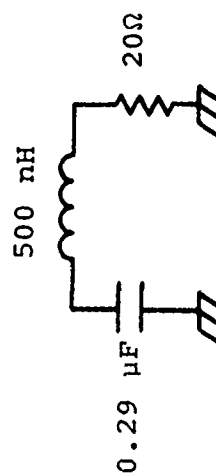


Figure 15 Six-stage Marx circuit.



$\text{CuSO}_4$  monitor atten. 673/1,

25/1 atten. at scope

10 V/division

100 nsec/division

$V_{\text{peak}} = 505 \text{ kV}$

Figure 16 Six-stage output waveform.

The voltage produced between stages was the indicated voltage during dc charging but as mentioned above only approximately 80 percent of this value, ignoring transients, was effectively applied between stages during erection, giving a somewhat less than valid test in regard to erection flashover. However, the intent of this procedure was to dc charge and erect the Marx at up to 20 percent over the normal operating full-voltage charge level. The result is (80 percent)  $\times$  (1.20) or 96 percent of the interstage voltage produced during an actual erection of the TEMPS pulser at peak voltage. Considering that the e-fold decay time of the output pulse is almost a factor of two greater than that produced by the TEMPS pulser, the results of the six-stage test could be extended and expected to reflect the performance of the TEMPS pulser in normal operation.

The voltage insulation evaluation involved operating the Marx at various levels and diagnosing the cause of each failure until a level of 120 kV/stage was achieved with successful erections.

The wire-wound resistors used in the Marx application were also tested during this phase. The erection voltages applied across each type of resistor were nearly those expected from the TEMPS pulser under the normal operating conditions but slightly decreased due to the clipping of the output pulse as described earlier. The mechanism associated with resistor failure is usually one of voltage stressing and interwinding flashover.

In every iteration above, the Marx stage/stage spacing was accurately controlled.

Thirty-Five Stage Testing. The 35-stage Marx was assembled consisting of 35 charged stages of 0.175 F each. The expected peak output is 3.5 MV into a high-impedance load ignoring any losses. The Marx is shown in Figure 17 and schematically in Figure 18. The Marx series current limiting resistors are each 0.3 ohm and placed at each switch location, giving a 10-ohm total series resistance distributed through the Marx. The charging resistors are  $\text{CuSO}_4$  which will be used throughout testing since the wire-wound types are not available. They are each 500 ohms and are constructed of 1/2-inch tygon tubing and are 12 feet long. The unexpected failure rate of the type of wire-wound resistors anticipated to be used necessitated this substitution. The case-to-case resistors are partly wire-wound and partly  $\text{CuSO}_4$  due to the unavailability of enough wire-wound resistors. Each unit is 2 k $\Omega$ . The trigger coupling resistors are  $m = 3$  and are 1200 ohms each. All but a few of the units are potted wire-wound resistors with the remainder being  $\text{CuSO}_4$ .

Each switch, prior to installation into the Marx, had undergone an acceptance test that placed fairly rigid requirements upon each switch. The procedure described in Appendix D was performed to minimize the prefire probability of the Marx.

The dummy load into which the Marx was erected was 110 ohms, comprised of eight 3-inch-i.d. x 44-inch-long  $\text{CuSO}_4$  resistors placed at each peaking capacitor location in the bicone section.

The circuit (Figure 18) showing the known parameters represents the circuit used throughout the testing.

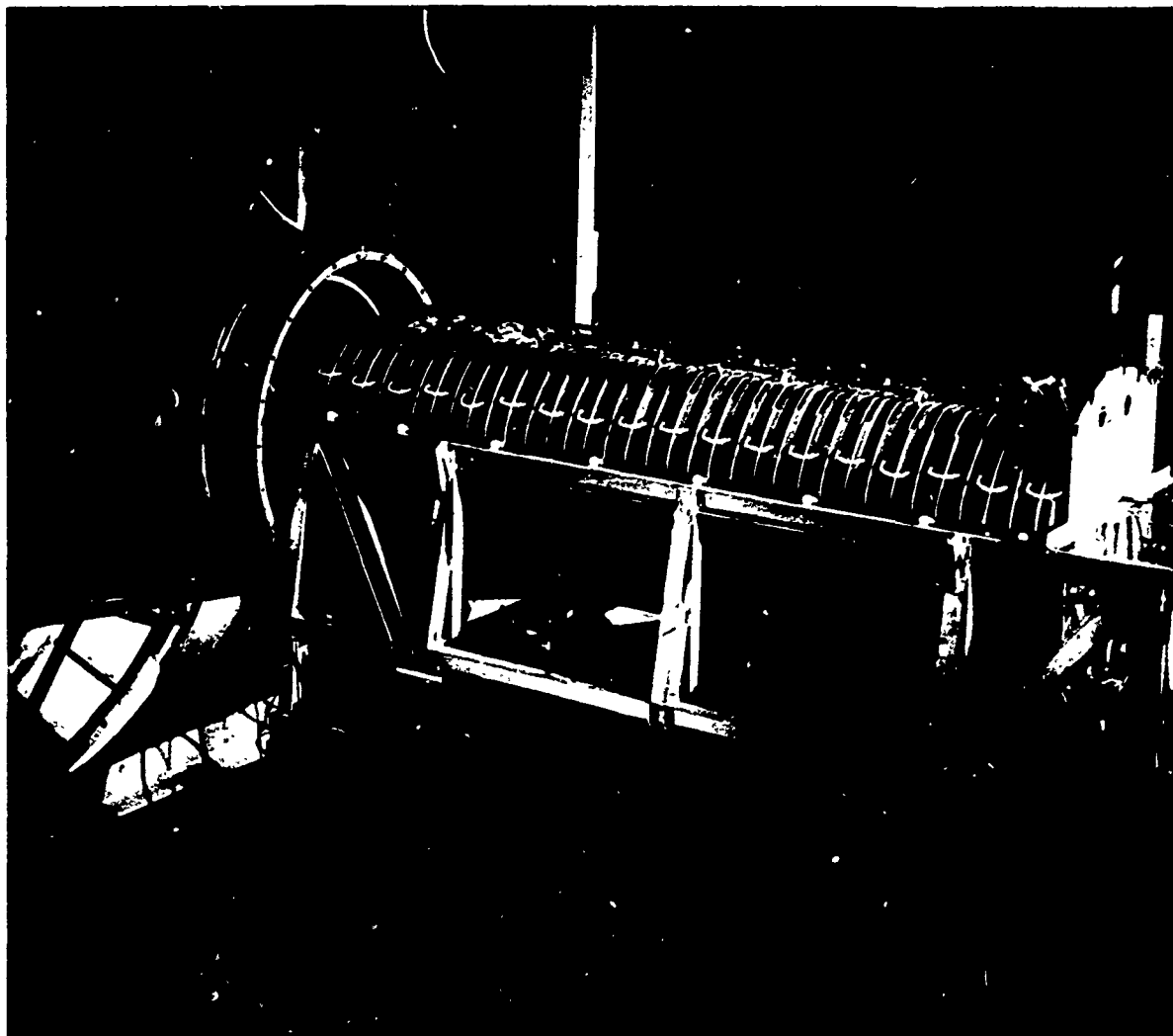


Figure 17 Thirty-five-stage prototype Marx generator.

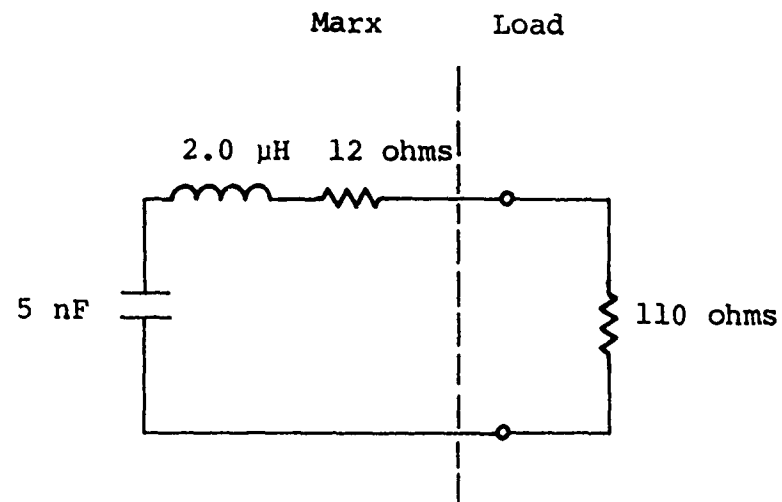


Figure 18 TEMPS Marx test electrical circuit.

The Marx was triggered by means of the circuit shown in Figure 19. A charged length of RG-218 was shorted at the switch end of the cable to launch a fast-rising pulse of equal magnitude and opposite polarity as that of the dc charge. Figure 19 also shows the trigger pulse waveform which has a 10 to 90 percent risetime of approximately 9.5 nsec. The primary trigger switch triggering generator is discussed in Reference 5.

The monitoring of the Marx output voltage was accomplished by the use of a  $\text{CuSO}_4$  resistive divider placed between the inner support cone and the ground plane. Its attenuation value was calibrated to be 1858/1. A current loop was placed in series with the Marx circuit and was located at the low-voltage end plate. From this loop, the i-dot signal was derived and integrated to obtain the output current waveform.

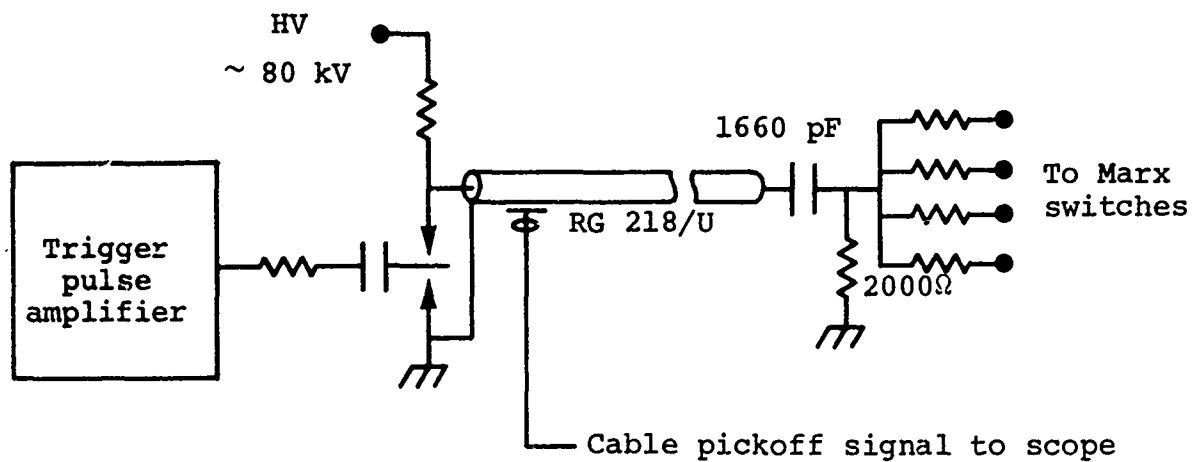
Timing measurements were accomplished with reference made to the launching of the trigger pulse down the trigger cable which coupled to the Marx. A capacitive cable pickoff was used to produce this timing reference pulse.

Initially prototype Marx testing was concerned with determining the exact Marx parameters of Figure 19.

The determination of the circuit inductance of Figure 19 involved short circuiting the dummy load of the bicone-Marx geometry by using eight 12-inch-wide strips of foil across each load resistor.

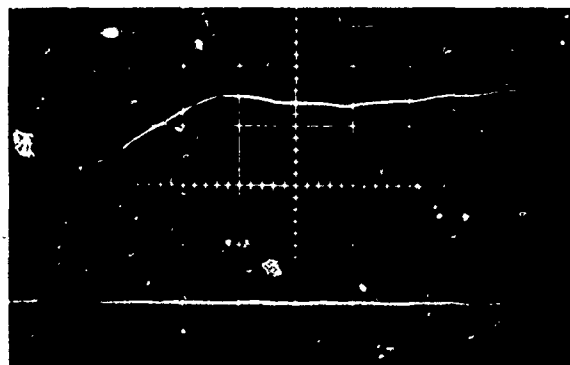
The Marx generator was charged to a low dc level and erected. The resulting ring frequency of the waveform associated with the underdamped circuit of Figure 20 was analyzed to yield a value of the inductance.





Trigger circuit

10 - 90%  
Risetime  $\approx$  9.5  
nsec

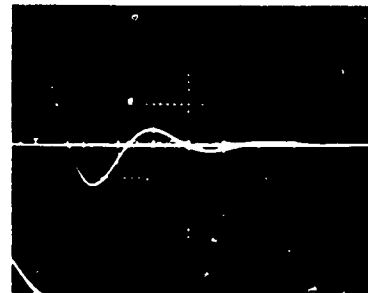
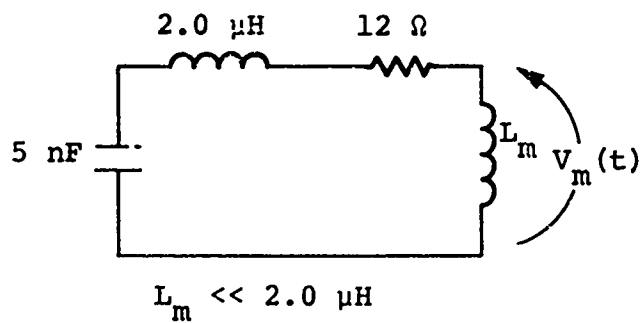


5 nsec/cm  
10 V/cm  
60 kV negative  
dc charge on  
trigger switch  
55 psig N<sub>2</sub>  
in switch<sup>2</sup>

Trigger pulse

Figure 19 Prototype Marx trigger circuit.

Circuit



i-dot 200 nsec/div.

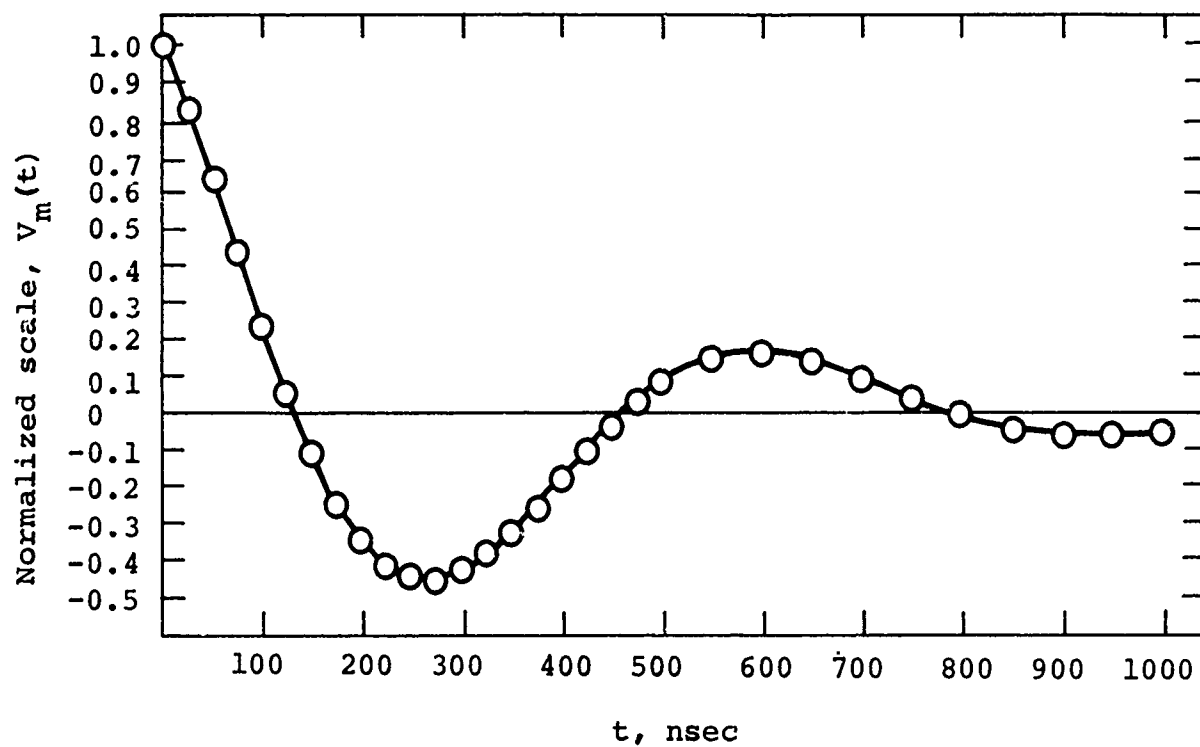


Figure 20 Comparison of calculated and measured Marx short circuit waveforms.

For an underdamped RLC circuit, the inductance associated with a circuit with negligible resistance is given by

$$L = \frac{T^2}{(2\pi)^2 C}$$

where T is the period of oscillation and C is the effective series capacity of the erected Marx.

The remainder of testing was performed with the 110-ohm load installed as in Figure 18.

A self-break voltage versus Marx switch pressure curve (Figure 21) was formulated and Marx operation proceeded at 80 percent of the self-fire level using either  $N_2$  or  $SF_6$ .

High-voltage testing of the Marx generator involved charging and erecting the Marx at increasing voltages, first using air within the Marx enclosure and then  $SF_6$  at atmospheric pressure. In both cases, Freon at atmospheric pressure insulated the output load section of the bicone test stand against voltage breakdown. A maximum charge voltage of 100 kV/stage was set and eventually reached. Peak output voltage was attempted in both Marx output polarities.

A chart recorder was used to indicate the actual charge voltage while oscilloscope pictures were taken of each output waveform. Essentially no timing measurements were taken at this time.

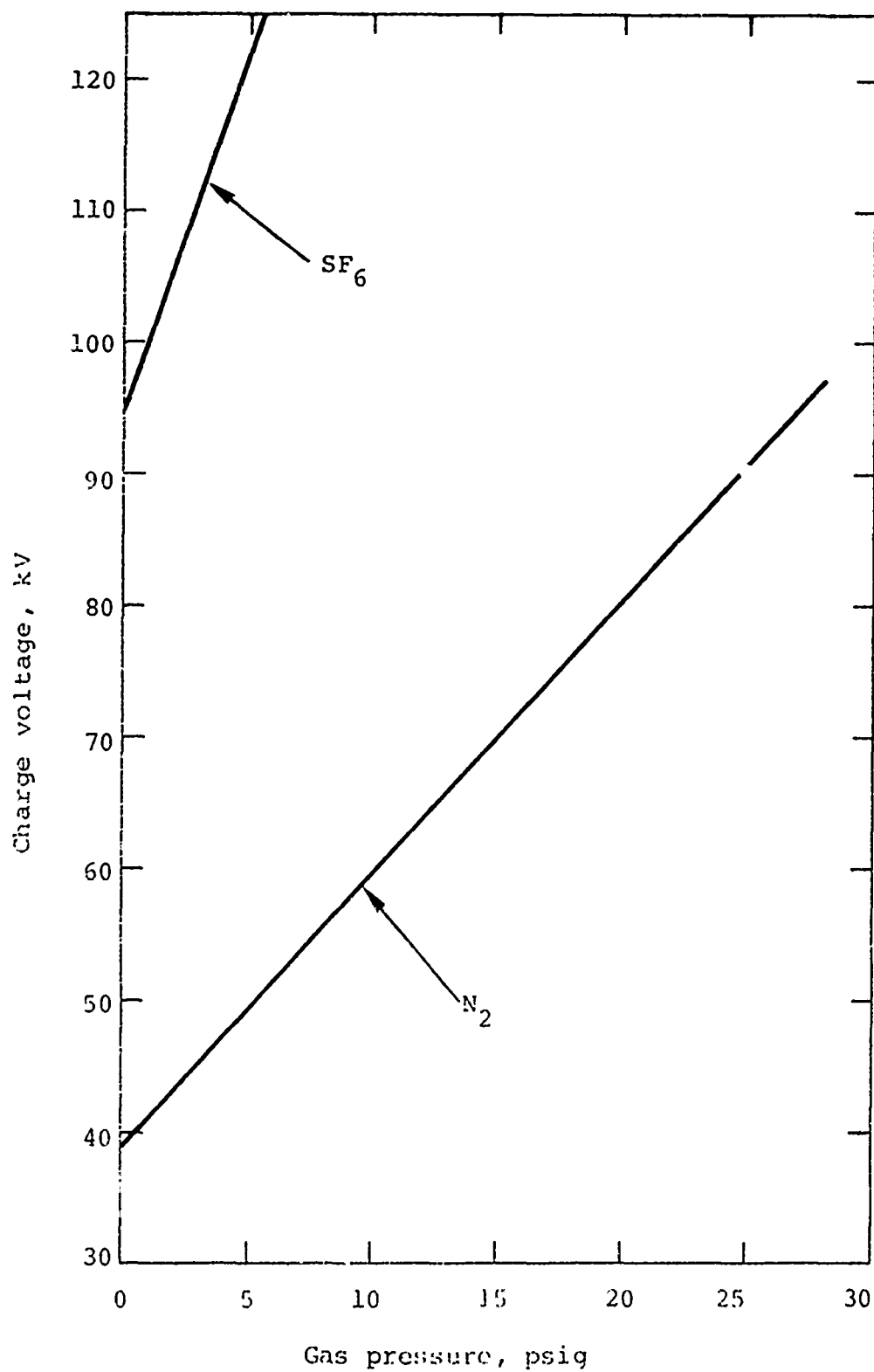
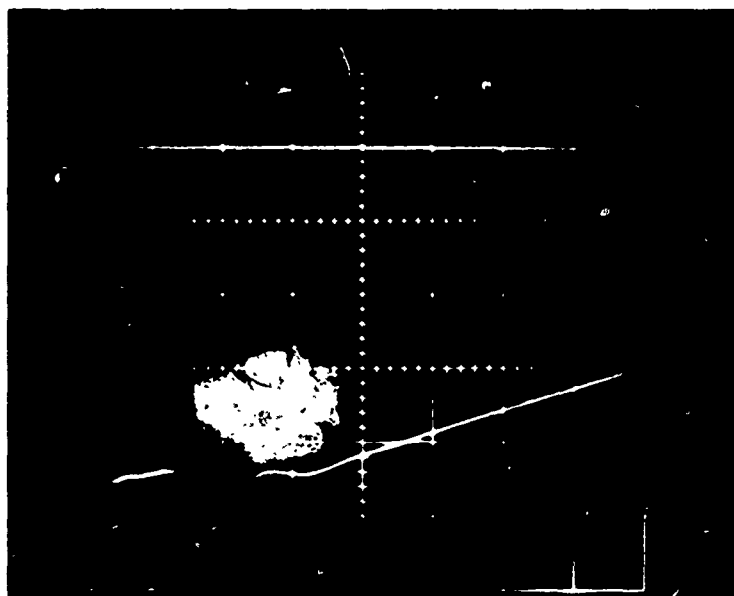


Figure 21 TEMPS Marx self-break voltage versus pressure (1.27-cm gap).

Although the full dc charge level was achieved, the open circuit peak voltage was clipped somewhat due to the circuit inductance as it was in the six-stage test. This and other factors produced a peak output voltage as measured across the 110-ohm load of approximately 78 percent of the open circuited voltage.

The Marx transmission line behavior was examined by varying the load resistance until it was sufficiently high to produce noticeable oscillation in the output waveform. A 250 ohm dummy load was used and produced the waveform shown in Figure 22. Analysis of this oscillation coupled with the Marx inductance measurements yielded the transmission line parameters of the Marx.

Marx timing measurements were made by using the circuit of Figure 23. The charged RG-218 cable was shorted at the trigger switch end, thus launching a pulse of equal and opposite polarity as that of the dc charge. As the pulse passes the capacitive pickoff situated approximately 4 feet from the switch, a signal is detected which triggers the oscilloscope after being delayed by an appropriate length of cable. Meanwhile, the trigger pulse arrives at the Marx, the Marx erects after some delay, and the output signal is recorded by the oscilloscope. Figure 24 shows a typical scope photograph; one trace shows the trigger pulse, which was used both for triggering and display, while the other trace is that of the Marx output with the scope still being triggered externally by the trigger pulse. The observed time difference between the two traces determines the Marx erection delay when account is taken of all circuit delays indicated in Figure 23.

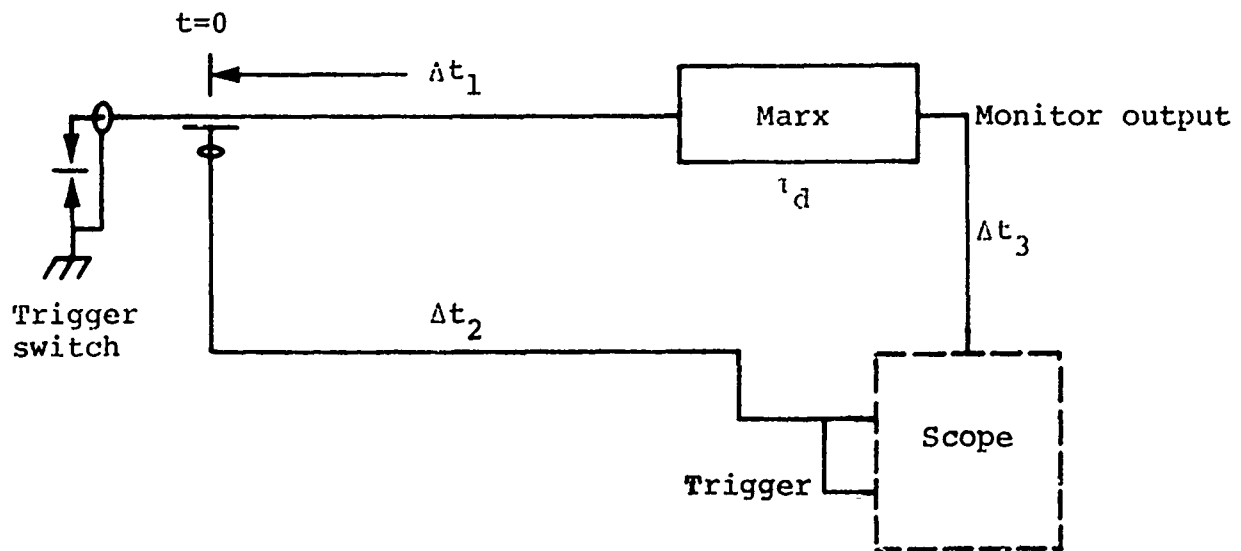


Horizontal:  
100 nsec/div.

Marx output voltage

$R_L \approx 250$  ohms

Figure 22 Marx output waveform with resistive load.



$\Delta t_1$  = trigger cable delay

$\tau_d$  = Marx erection delay

$\Delta t_3$  = monitor cable delay

$\Delta t_2$  = trigger pulse pickoff signal cable delay

Trigger pulse arrives at scope after time  $\Delta t_2$

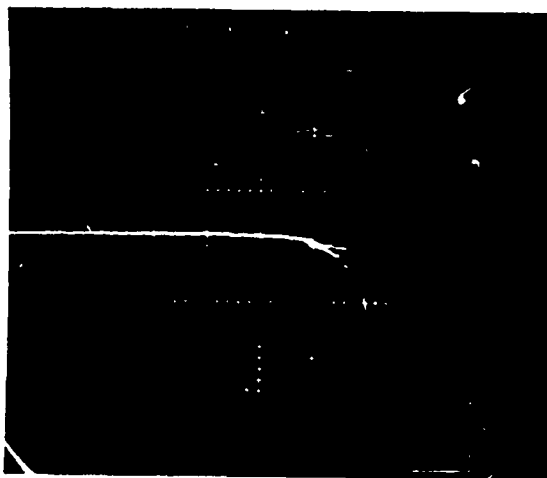
Marx output arrives after time  $\Delta t_1 + \tau_d + \Delta t_3$

The apparent time difference between the two signals is  $\Delta T$  measured in Figure 24.

$$\Delta T = \Delta t_1 + \tau_d + \Delta t_3 - \Delta t_2$$

$$\text{Marx delay } \tau_d = \Delta T - \Delta t_1 - \Delta t_3 + \Delta t_2$$

Figure 23 Marx timing measurement circuit.



50 nsec/division

Trigger pulse-top: 10/1  
2  $\mu$ /cm

Marx output-bottom: 5/1, 2/1  
20  $\mu$ /cm

Figure 24 Marx timing photograph.



Throughout the course of the Marx jitter and delay evaluation many changes were made. These changes involved going from the original  $m = 3$  type coupling to the  $m = 4$  coupling of Figure 15 or to some point in between which utilized a combination of  $m = 4$  and  $m = 3$  coupling as indicated in the test results. For each case, resistor values were varied from 1200 to 260 ohms to obtain the minimum jitter.

Initially the first and last Marx switches were untriggered. Deletion of those untriggered switches was accomplished by simply short circuiting each of these two switches and appropriately removing the necessary charge resistors. The associated jitter and excessive delay associated with the closure of the untriggered gaps was readily determined.

The Marx trigger amplitude and polarity were varied to obtain optimum timing synchronization of the Marx. The percentage of self-fire operation was varied at about the nominal 80 percent level while the charge level ranged between 33 kV/stage and 45 kV/stage. The chosen charge levels marked the extreme low-voltage end of the desired 3/1 Marx voltage range while the 45 kV/stage charge produced the highest possible output voltage that could be applied across the load in air.

A slight improvement in the Marx timing resulted in paralleling two RG-218 50-ohm cables to produce a 25-ohm effective trigger cable impedance. The result was to increase the voltage applied to the midplanes during triggering. The trigger pulse risetime was essentially unchanged from the single cable arrangement since the decrease of the cable impedance was counterbalanced by a comparable decrease in the inductance of the cable connections at the trigger output switch, thus causing the L/R risetime of the pulse to remain unchanged.

Two difficulties arose in the course of the testing that, in general, are common to any system using a significant number of spark gap type switches. These were the occurrences of pre-fires during charging and an increase in erection delay and jitter for low switch gas pressures. The potential seriousness of either problem appears as overvoltage stressing the peaking capacitor due to a prefire or poor synchronization of the two half generators.

A number of possible cures for the above were explored. A gap pressure of between 0 and 30 psig  $N_2$  and 0 and 10 psig  $SF_6$  would have provided the entire 3/1 voltage range of the Marx. This required a charge range between 33 kV/stage and 100 kV/stage. The work done at a charge level of 45 kV/stage using 7-3/4 #  $N_2$  showed the delay and jitter to be very satisfactory for proper Marx synchronization. A decrease in charge voltage to 40 kV and 33 kV/stage with the appropriate decrease in  $N_2$  pressure to 5.5 and 1 psig to remain at 80 percent of self-fire operation produced increased delay and jitter. Likewise, operation at elevated pressures above 15 to 20 psig produced a substantial number of prefires. The desirability of limiting the nitrogen gas pressure between 7 and 15 to 20 psig made necessary the testing of gases other than  $N_2$  or  $SF_6$  in order to maintain something close to the 3/1 continuous voltage range. An  $Ar/CO_2$  mixture was tested as was an  $SF_6/N_2$  mixture. Characteristic self-break voltage versus pressure curves were made for a 14 percent  $SF_6/N_2$  mixture, and 5 percent  $Ar/CO_2$  mixture. Jitter and delay measurements were taken for the 5 percent  $Ar/CO_2$  mixture and compared to those taken using pure  $N_2$ . Measurements were limited to 33 kV/stage charge, 40 kV/stage, and 45 kV/stage using either pure  $N_2$  or 5 percent  $Ar/CO_2$  mixture.

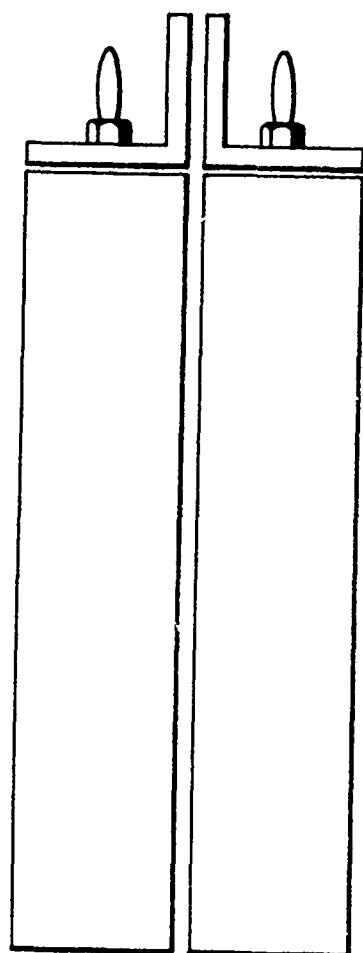
Throughout the entire test, prefires were evaluated and some diagnosis made.

Results: Six-Stage Marx. The primary failure mechanism causing the dc breakdowns occurring during charging of the six-stage Marx appeared to be the dielectric field enhancement due to the fiber capacitor rails. Surface tracking arcs were consistently found to have originated or terminated near the rail edges occurring at charge levels of 80 kV/stage or less. By placing a 1/8-inch polyethylene spacer insulator between the two 1/16-inch-thick stage-to-stage barriers, the dc breakdown charge level was raised to 100 kV/stage.

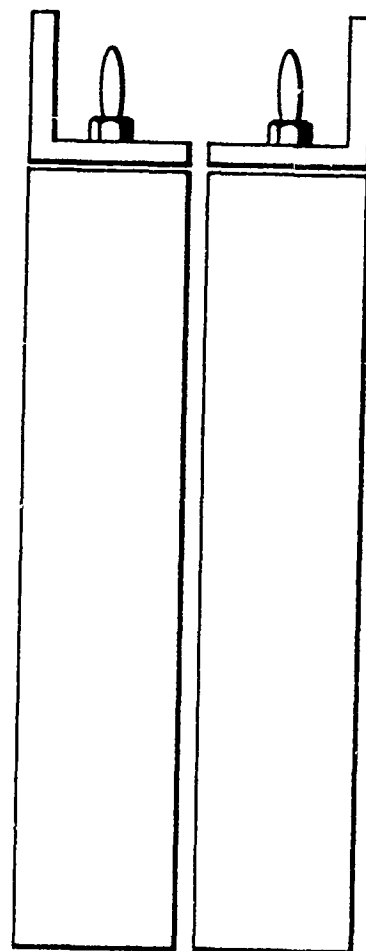
Stage-to-stage spacing was increased from 2.75 to 3 inches to both further lower the fields between adjacent switches and to provide sufficient spacing for the barriers to be easily slipped into place. DC charging up to 106 to 110 kV/stage was possible after the above modification.

The rounding of the capacitor rail edges produced another slight gain in the breakdown charge level. The most marked difference, however, was observed after reversing the capacitor rails as shown in Figure 25.

The fiber rails, by being reversed, became placed in a higher field region which ionized the gas layer to provide the corona self-shielding effect. Although the total spacing between conducting surfaces was the same before and after reversing the rails, the fields increased because of the presence of 3/8 inch of dielectric rather than the 1/4 inch that had existed before reversal between the conducting surfaces.



Original orientation  
of rails



Reversed orientation

Figure 25 Capacitor rail reversal.

DC charge levels of up to 120 kV/stage were reached without failure by employing the above change.

A slightly different condition exists during Marx erection. For short times, adjacent conductors of the Marx may be subjected to potential differences greater than the dc charge level due to transients developed during erection. Although SF<sub>6</sub> and Freon exhibit almost identical dc-insulating characteristics, the streamer growth produced by erection transients from highly stressed field regions of the Marx may be suppressed to a greater extent by the use of SF<sub>6</sub> rather than Freon. For this reason SF<sub>6</sub> was chosen to be the Marx enclosure insulating medium. Testing did show it to increase the erection voltage attainable without breakdowns by at least 10 percent; the six stage Marx could be charged and erected at up to 20 percent above the maximum charge voltage of 100 kV/stage with no flashover.

Incorporated into the six-stage test was a preliminary evaluation of the various types of resistors to be used in the TEMPS system. At least one of each type of potted resistor was installed into the Marx. One current limiting, four m = 3 potted resistors, and two case-to-case resistors were tested through the course of the insulation evaluation phase of testing. Periodically, usually after every iteration, each resistor was inspected and its value measured. The current limiting resistors consisted of 15 parallel NS-10, 4.5-ohm Dale wire-wound resistors potted in epoxy. Although the actual peak current of 50 kA was not achieved during testing, the effects of its geometrical shape on voltage breakdown was examined and no unfavorable effects found. The other two resistor applications also used NS-10 Dale resistors. The case/case application used four series-connected

500-ohm resistors while the  $m = 3$  used six NS-10, 200-ohm resistors. The NS-10 variety resistors have been shown in a number of in-house bench tests to be capable of being stressed to 50 kV/resistor under pulsed conditions. The six-stage test exposed the  $m = 3$  resistors to nearly 50 kV/resistor while the case-to-case resistors were only stressed to 25 kV/resistor. No failures occurred in either case and the indicated values remained within the 3 percent tolerance.

The charging resistors were chosen by their energy deposition capability. Three NHL-25 Dale resistors were used in place of five NS-10 types. Although the NHL-25 resistors were only subjected to approximately 33 kV/resistor, failure occurred in almost every unit tested. The failure mode was interwinding voltage arcing. NS-10 type resistors were chosen to replace the NHL-25 types for this application. The electrical stressing of the charging resistors will be nominally 20 kV/resistor, far below its capability of 50 kV.

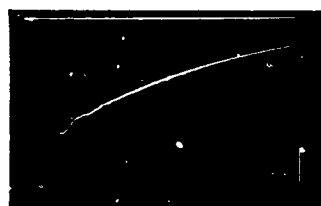
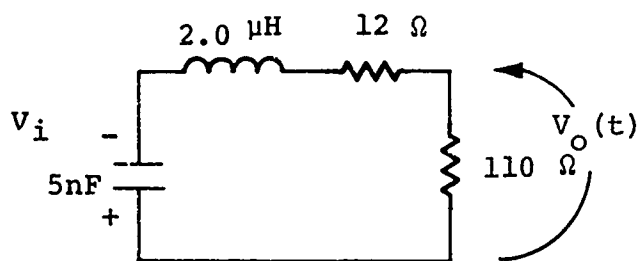
Thirty-Five Stage Marx. The discharging of the Marx generator into the circuit of Figure 20 produced the waveform also shown in Figure 20. Analysis of the oscillation period using the method of Reference 6 showed that the series inductance associated with the Marx generator bicone geometry was  $2.0 \mu\text{H} \pm 5$  percent or 57 nH/stage with an approximate series equivalent resistance of 12 ohms. Additional curve fittings comparing the calculated  $i$ -dot waveform to the measured waveform confirmed the above parameter values to be realistic and is also shown in Figure 20 with the equivalent circuit. Of the 12 ohms of series resistance, 10 ohms is due to the added series current-limiting resistance while the other 2 ohms result from the series capacitor resistance and arc-channel resistance.

The remainder of Marx testing, except where noted, proceeded using a 110-ohm dummy load.

The Marx generator could be erected at voltages up to 45 kV/stage without the need of any Freon gas within the load enclosure. Therefore, initially the self-break versus gas pressure curve was made for the voltage in this range and later extended as high-voltage testing progressed. The completed curve is shown in Figure 21 for  $\text{SF}_6$  and  $\text{N}_2$  gas. Also shown is the self-break voltage for a single switch, which differs by less than 3 percent. The 80 percent of self-break operating level is indicated by the dotted lines.

Operation within the range of 45 kV/stage to 70 kV/stage used Freon gas inside the load enclosure and air within the Marx enclosure. The purpose was to arbitrarily set a limit of 70 kV/stage charge voltage with air within the Marx enclosure. If the system could be erected without failure at this level, then an increase of 100 kV/stage using  $\text{SF}_6$  within the Marx enclosure would not be expected to precipitate breakdowns involving the Marx components. The results showed that the Marx could be erected at 70 kV/stage in both polarities without breakdown with air in the Marx enclosure. No attempts were made, however, at any higher level under these conditions.

The calculated waveform based upon the circuit of Figure 18 used throughout high-voltage testing is shown in Figure 26. Also shown is a comparison of the measured waveform. Both agree well and yield a 600 nsec e-folding pulse length measured from peak value. For these tests, output-pulse length was about a factor of two greater than that associated with the early-time impedance driven by the Marx in the TEMPS system. Although the



Marx output-voltage  
waveform--negative  
pulse  
Horizontal: 100 nsec/div.

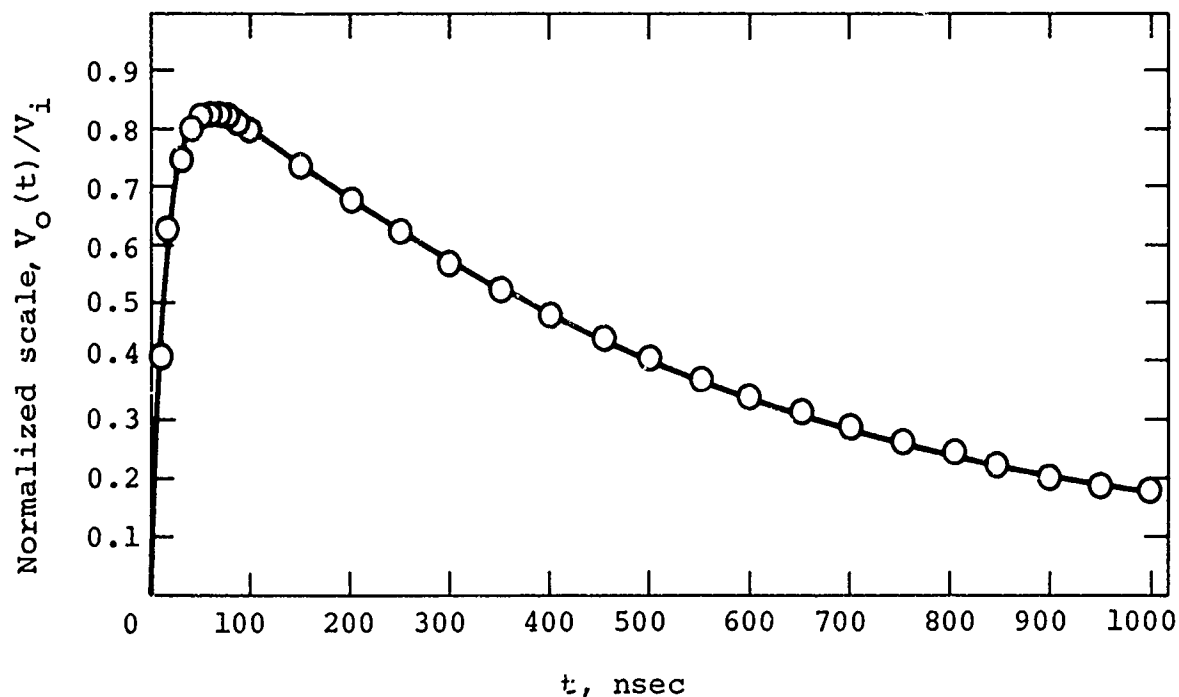


Figure 26 Calculated and measured Marx output waveforms.



expected peak voltage into a high-impedance load should be 35 stages times the charge voltage per stage, a number of losses make its measured peak to be approximately 78 percent of this value. The most obvious is the resistive voltage division between the 12 ohms of added series inductance in the Marx and the 110 ohm load. A 10 percent loss is associated with the division. In addition, the waveform of Figure 26 shows that the clipping of the peak due to the finite risetime accounts for an additional 7 percent loss. The remaining 5 percent loss is due to the charging of the stray shunt capacity during erection. The effective stray shunt capacity in the Marx circuit is approximately 200 pF.

At the maximum charge level of 100 kV/stage, 2.75 MV could be achieved. It is only with a peaking capacitor circuit that a full voltage test of the Marx can be performed.

The heavily damped oscillation that is seen just following the initial pulse rise in the measured waveform of Figure 26 is due to the transmission-line behavior of the Marx strays, distributed series stray inductance, and shunt capacity to ground. This is shown more clearly in Figure 22 where Marx load resistance was increased to about 250 ohms. Analysis of the oscillation in Figure 22, coupled with Marx inductance measurements, yielded the following results:

- a. Average stray series inductance per stage: 57 nH
- b. Average stray shunt capacity per stage: 13 pF
- c. Average impedance of the transmission line formed by the strays: 66 ohms
- d. One-way transit time: ~ 30 nsec

The nominal early-time load impedance driven by each Marx in TEMPS is about 66 ohms. Therefore, the transmission line formed by the Marx strays is nearly matched and no transmission-line oscillations will be observed on the output pulse.

High-voltage testing proceeded in 5 kV steps continuing at 70 kV/stage, using Freon gas in the load enclosure and atmospheric pressure  $\text{SF}_6$  gas within the Marx enclosure. Considering the capacitor specifications, maximum charge voltage was limited to 100 kV/stage. A peak amplitude of 2.75 MV was reached at this level.

No breakdowns occurred at voltages up to and including 100 kV/stage when the Marx output polarity was negative. A breakdown did occur at a charge level of 90-kV/stage, 2.4-MV output operating in the positive output mode. An arc occurred from the inner support cone output terminal towards the ground plane on the floor of the test enclosure. The presence of the ground plane raises the fields on the lower side of the inner support cone and thus is not representative of the TEMPS system.

The results of the Marx timing measurements are best summarized in Table II. The results are confined, however, to charge voltages less than 45 kV/stage and trigger voltages of 90 kV or less.

Many resistive trigger coupling schemes were tried until 500-ohm  $m = 4$  coupling with a 250-ohm input resistor with all 35 switches triggered was found suitable. Optimum trigger voltage with this type of coupling was found to be 80 kV with no further improvement in jitter and with an increase in trigger voltage. The two bilateral Marx generators, operating in opposite output polarities, must have separate trigger sources of opposite polarities. The trigger pulse must have the opposite polarity from the Marx output to obtain acceptably low jitter.

TABLE II

## SUMMARY OF MARX TIMING TEST RESULTS

Note: All iterations taken at 80 percent of self-break voltage of Marx at 7-3/14 N<sub>2</sub> and a charge level of 45 kV/stage. Initial input trigger resistors were in all cases 300 ohms each.

Coupling Type	Resistance (ohms)	Extent of Coupling (Switch Nos)	Marx Output	Trigger Pulse	Delay (nsec)	Jitter (nsec)
1. M = 3	260	2 - 11	negative	-70 kV	239	20.3
M = 3	600	11 - 29				
M = 3	1200	29 - 35				
2. M = 3	260	2 - 11	positive	+70 kV	224	24.2
M = 3	600	11 - 29				
M = 3	1200	29 - 35				
3. M = 4	500	2 - 23	negative	+70 kV	180	21.2
M = 4	700	23 - 29				
M = 3	1200	29 - 35				
4. M = 4	500	2 - 23	negative	+80 kV	183	11.6
M = 4	700	23 - 29				
M = 3	1200	29 - 35				
5. M = 4	500	2 - 23	negative	+80 kV	185	12.1
M = 4	700	23 - 29				
M = 4	1200	29 - 35				
6. M = 4	500	2 - 23	negative	+90 kV	182	15.7
M = 4	700	23 - 29				
M = 3	1200	29 - 35				
7. M = 4	500	2 - 28	negative	+80 kV	184	10.4
M = 3	300	28 - 35				
8. M = 4	500	2 - 28	negative	+80 kV	180	6.7
M = 3	300	28 - 35				
9. M = 4	500	2 - 28	negative	+80 kV	166	5.85
ground end untriggered switch deleted from circuit.						
10. M = 4	500	2 - 28	negative	+80 kV	170	4.0
M = 3	300	28 - 35				
both untriggered switched deleted from circuit.						
11. M = 3	400	2 - 35	negative	+80 kV	188	8.8
both untriggered switches deleted.						
12. M = 3	400	2 - 35	negative	+80 kV	192	8.8
both untriggered switches deleted.						

TABLE II (cont.)

Initial input triggering resistors changed to 250 ohms and all 35 switches triggered.

Coupling Type	Resistance (ohms)	Extent of Coupling (Switch No.)	Marx Output	Trigger Pulse	Delay (nsec)	Jitter (nsec)
13. m = 4	500	1-35	negative	+80	146	3.6
14. m = 4	500	1-35	negative	+80	160	3.76
15. m = 4	500	1-35	negative	+80	170	6.24
run at 75% of self-break voltage of Marx						
16. m = 4	500	1-35	negative	+90	155	5.4
17. m = 4	500	1-35	negative	+90	170	5.4
run at 75% of self-break voltage of Marx						

Double trigger cables installed on switches below.

18. m = 4	500	1-35	negative	+80	160	2.98
19. m = 4	500	1-35	negative	+80	162	3.7
20. m = 4	500	1-35	negative	+80	150	2.64
21. m = 4	500	1-35	negative	+80	198	6.36
charge level at 33 kV/stage with 1 psig N <sub>2</sub>						
22. m = 4	500	1-35	negative	+80	395	7.2
charge level 33.5 kV/stage with 7.5 psig Ar/CO <sub>2</sub>						
23. m = 4	500	1-35	negative	+80	385	10.3
charge level at 34 kV with 7.5 psig Ar/CO <sub>2</sub>						
24. m = 4	500	1-35	negative	+80	290	11.4
charge level at 45 kV with 16 psig Ar/CO <sub>2</sub>						
25. m = 4	500	1-35	negative	+80	148	3.6
charge level at 45 kV with 7-3/4 psig N <sub>2</sub>						
26. m = 4	500	1-35	negative	+80	140	3.3
run at 90% of self-break voltage of Marx						
charge level 45 kV/stage with 5.5 psig N <sub>2</sub>						
27. m = 4	500	1-35	negative	+80	395	6.3
charge level 33 kV/stage with 7.5 psig Ar/CO <sub>2</sub>						
28. m = 4	500	1-35	negative	+80	285	8.6
charge level 45 kV/stage with 16 psig Ar/CO <sub>2</sub>						
29. m = 4	500	1-35	negative	+80	147	5
charge level 40 kV/stage with 5.5 psig N <sub>2</sub>						

The effect of the percentage of self-fire operation upon delay and jitter is shown in Figures 27 and 28. Eighty-percent operation appears to yield acceptably low jitter and delay while self-fire appears to be no problem at this level in most cases.

The effect of charge voltage for fixed percentage of self-fire is shown in Figures 29 through 32 where a  $N_2$  and 5 percent  $Ar/CO_2$  mixture has been tested. The gas mixture, because of its triggerability, appears unsuitable for the TEMPS application. At pressures and charge voltages of 7.5 to 16 psig and 33 to 45 kV/stage, the erection characteristics show slow risetimes and unacceptably long delay and high erection jitter. Using  $N_2$ , the charging voltage range lower limit tends to be 40 kV/stage. Below this level, jitter becomes too great for proper Marx synchronization. Further tests are planned to use a  $N_2$ , Ar mixture. Such a mixture would be likely to have good nitrogen-like erection quantities while the argon doping would lower the self-break voltage level of such a gas. If lower Marx switch pressures are to blame for poor jitter at the low charge voltage, then the use of such a mixture would solve this problem. Unfortunately, the  $Ar/CO_2$  mixture showed no such trend.

Earlier an  $SF_6/N_2$  mixture had been tried for different reasons. Higher switch gap pressures ( $> 15$  psig) tend to produce higher prefire occurrence and the use of an intermediate gas to limit the maximum gas pressure to approximately 17 psig could alleviate this problem. Unfortunately, at the time of testing, many self-fires occurred. Although apparently occurring more for the 14 percent  $SF_6/N_2$  than for pure  $N_2$ , the prefire frequency was abnormally high for both gases. The testing was immediately terminated in the belief that the gas mixture was unacceptable. Since that time, it was observed that when the Marx remains

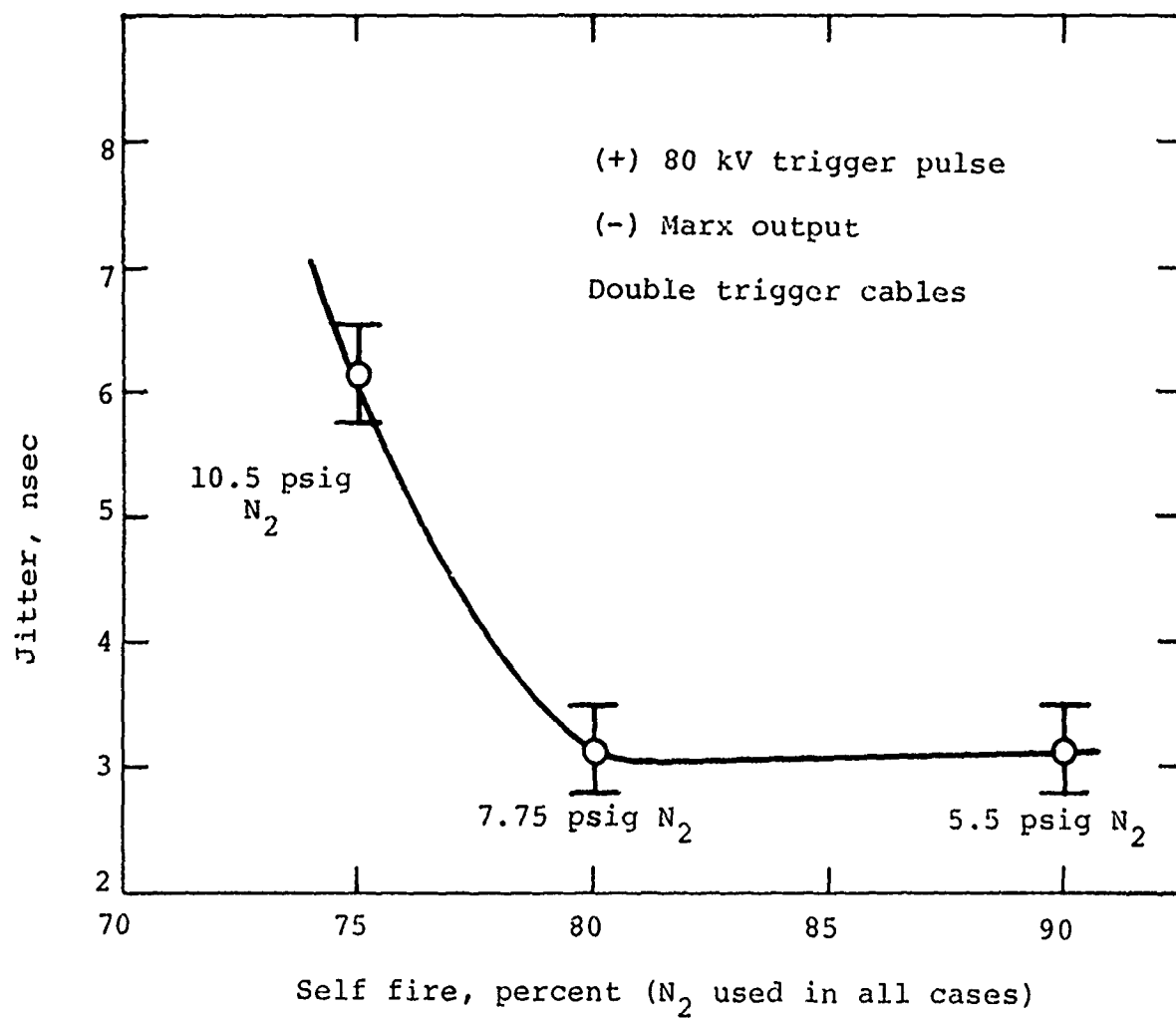


Figure 27 Erection jitter versus percentage of self-fire for fixed Marx charge level of 45 kV/stage.

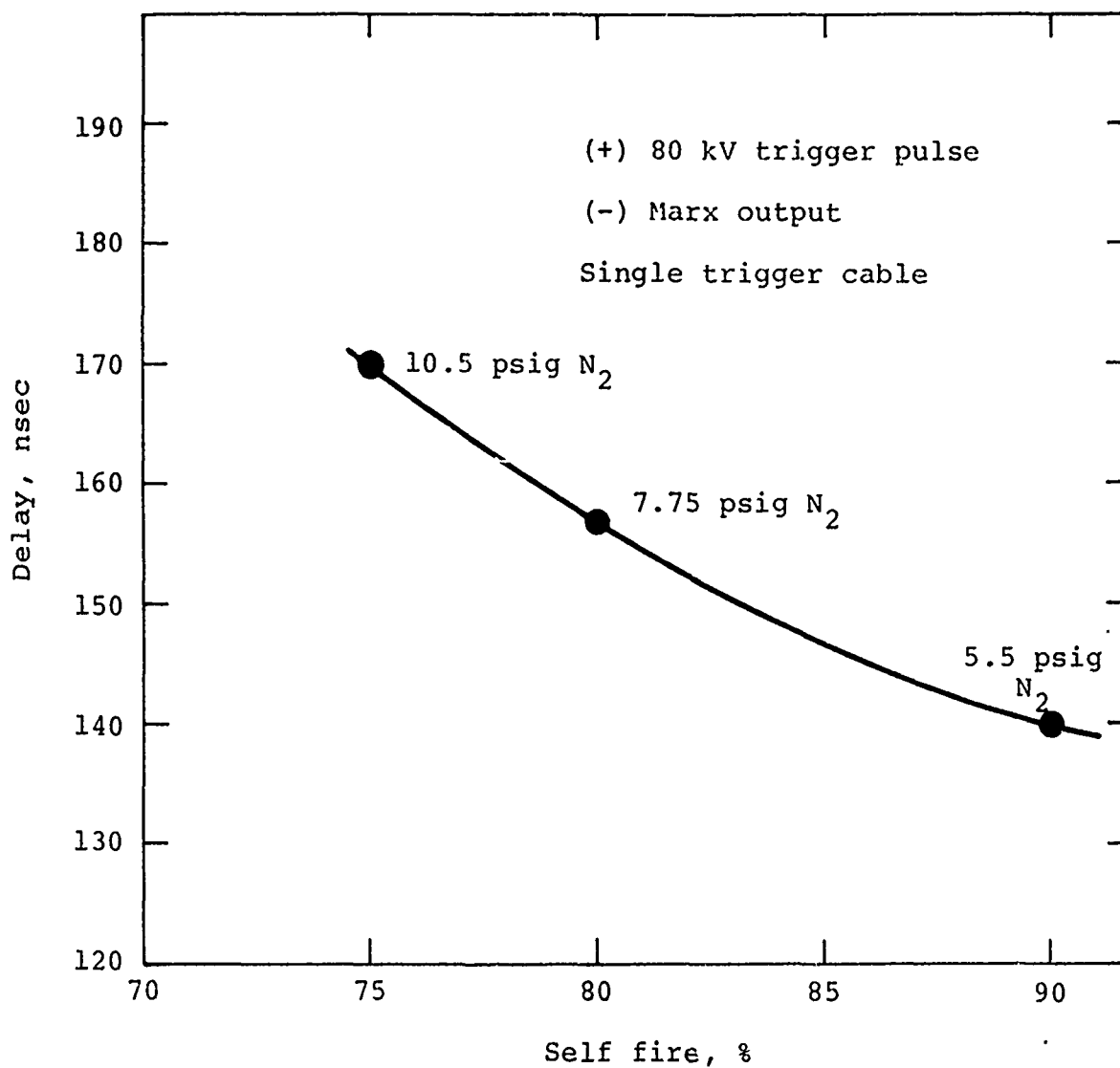


Figure 28 Marx erection delay versus percentage of self-fire for fixed Marx charge voltage of 45 kV/stage.

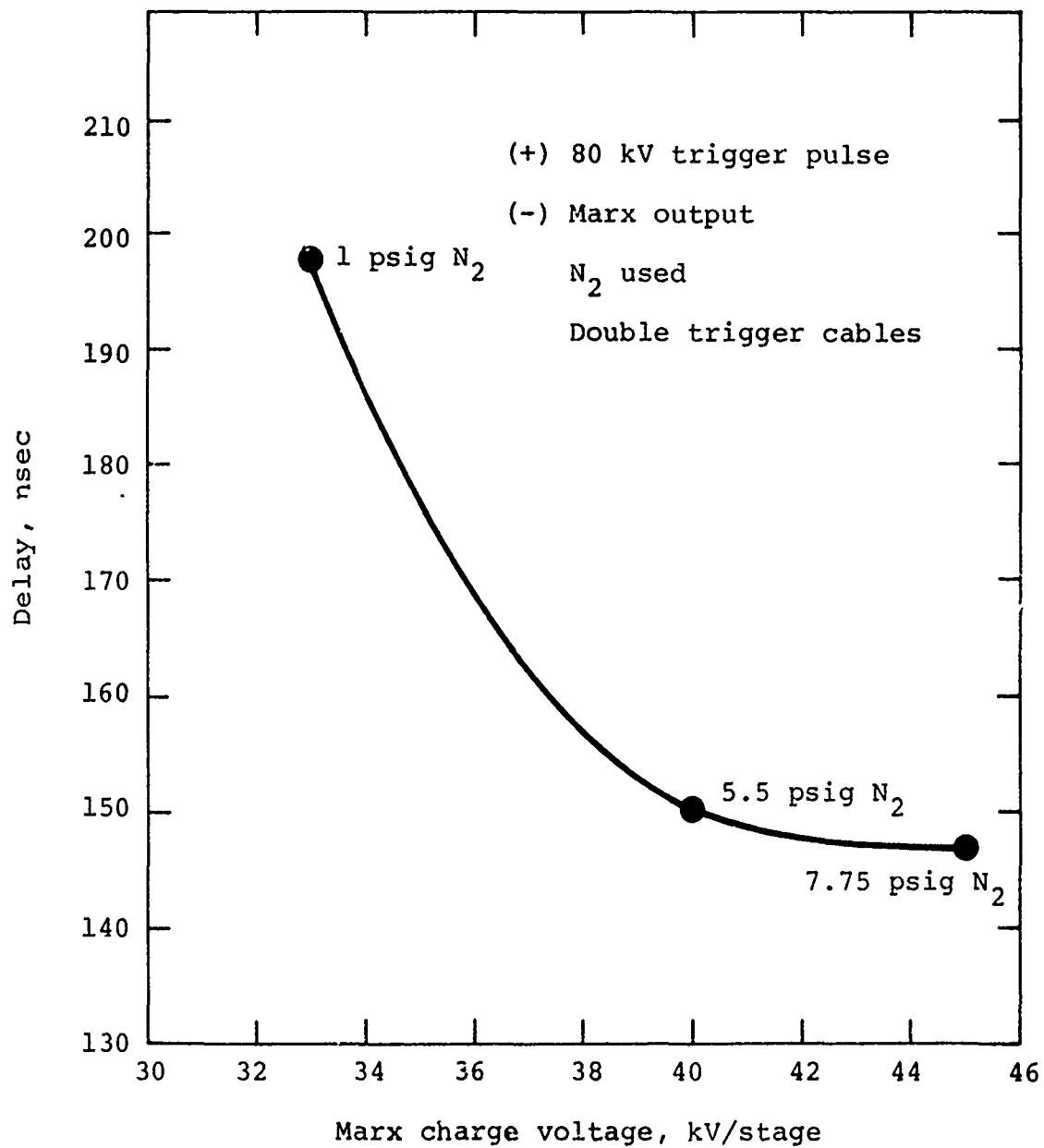


Figure 29 Marx erection delay versus Marx charge voltage for fixed percentage of self-fire (80 percent).



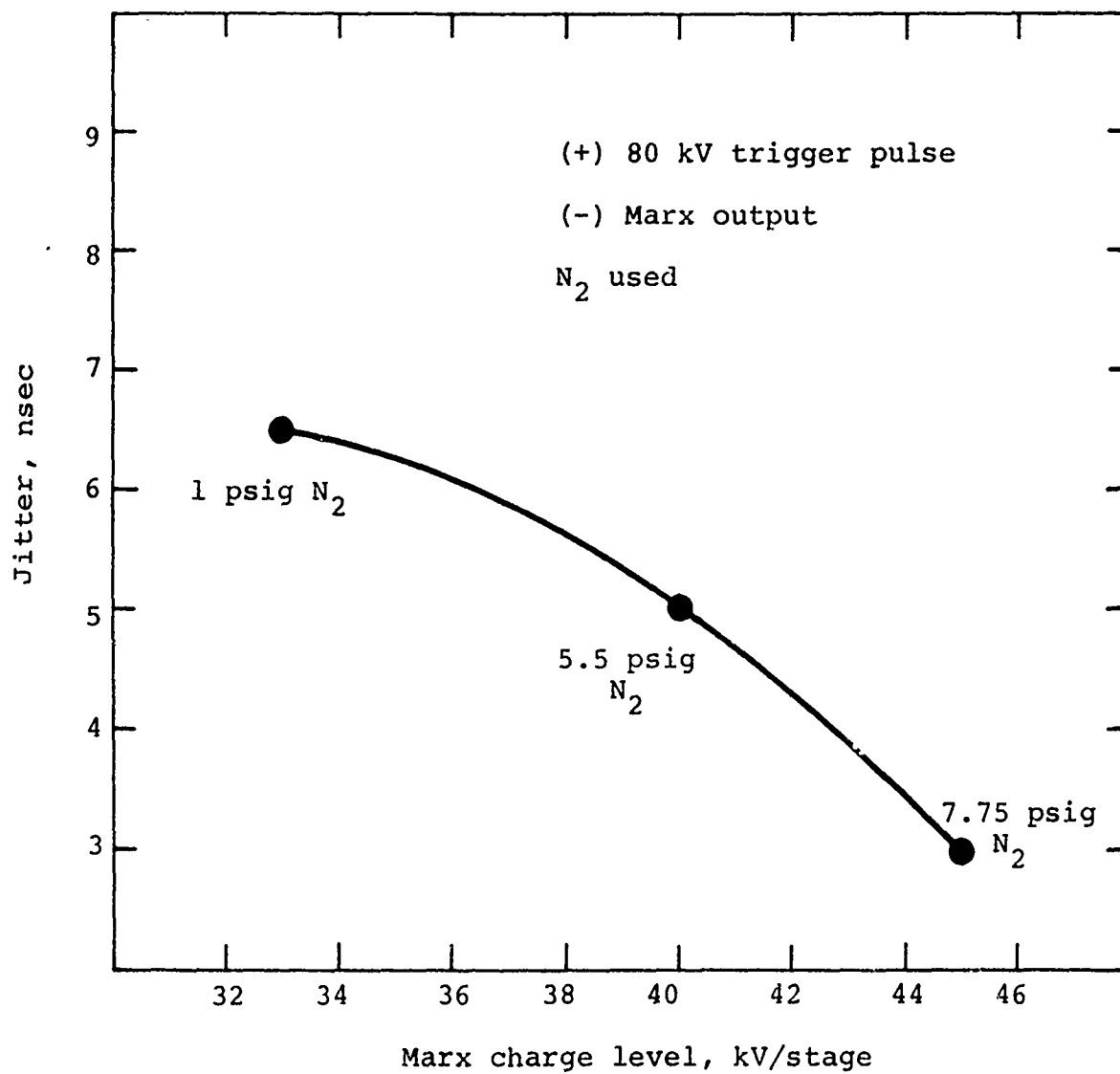


Figure 30 Marx erection jitter versus Marx charge voltage for fixed percentage of self-fire (80 percent).

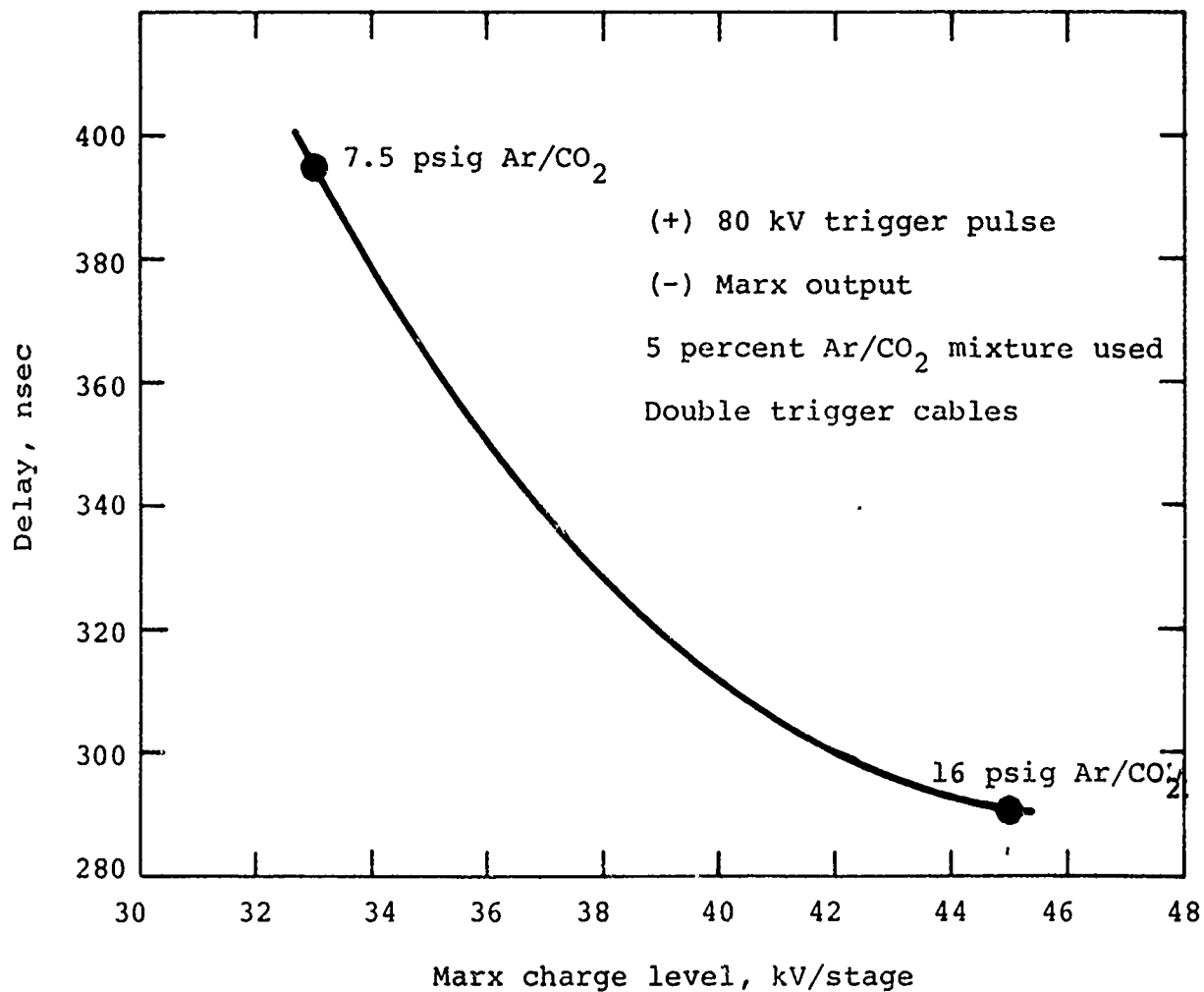


Figure 31 Marx erection delay versus Marx charge voltage for fixed percentage of self-fire (80 percent).

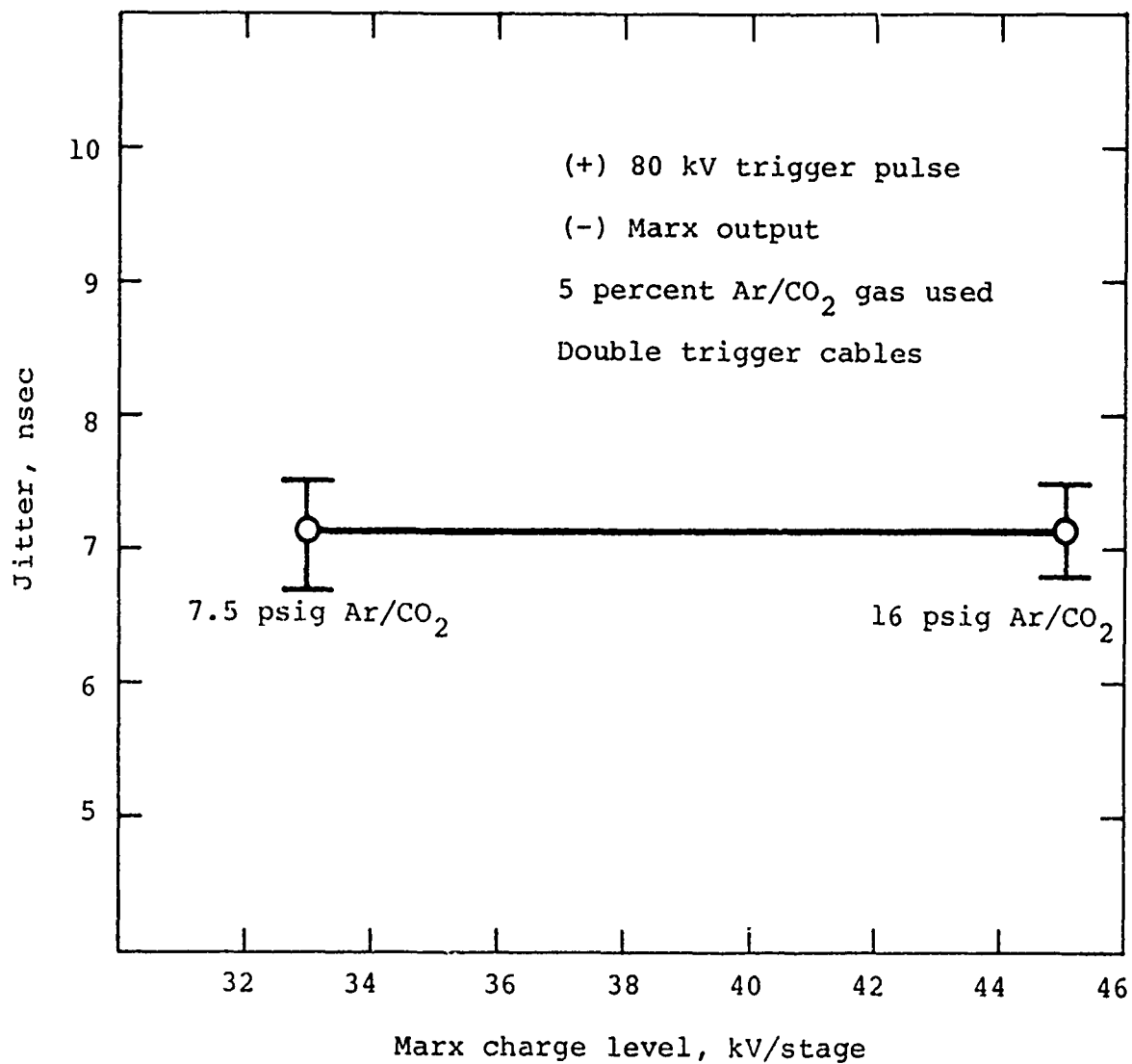


Figure 32 Marx erection jitter versus charge voltage for fixed percentage of self-fire (80 percent).

unused for two weeks or longer, the switches appear to develop hair-like projections, possibly corrosion, that must be burned off. The standard initial startup procedure now adopted calls for erecting the Marx at approximately 45 kV/stage into its load impedance in both polarities for at least 20 shots in both polarities. After such a procedure, the self-fire frequency decreases to its normal levels which, over hundreds of shots, has been found to be less than 1 percent at a level of 45 kV/stage and about 10 psig  $N_2$ . As mentioned previously, the self-fire frequency increases rapidly to 4 to 5 percent at pressures above 15 to 20 psig  $N_2$ . In all cases, the self-fire frequencies are quoted for operation at 80 percent of mean self-fire.

Conclusion. The results of the preliminary Marx testing indicate that the general design of the Marx is satisfactory. All parameters that are essential to the Marx operation and which required manufacturing were determined as a result of Marx testing.

The finalized Marx generator utilizes 500-ohm  $m = 4$  coupling throughout with 250-ohm input trigger resistors. Charge resistors are 500 ohms each, case-to-case 20 k $\Omega$ , and the series current limiting remain 0.3  $\Omega$ /stage. All resistor applications use Dale NS-10 type resistors. Thirty-five stages are used, each with its own triggered spark gap. In all, 35 triggered switches are employed; all other components remain unchanged from the preliminary Marx design. The finalized schematic is shown in Figure 9.

The use of  $N_2$  or  $SF_6$  is anticipated although further tests involving Ar/ $N_2$  and  $N_2/SF_6$  mixtures will be made at Camp Parks. The ultimate goal of testing other gases will be to limit gas pressure to 5 to 10 psig, to minimize self-fire probability, and to yield an acceptable timing jitter over the entire 1.16 to 3.5 MV output voltage range.

Erection jitter and delay are expected to be further reduced using a capacitive rather than resistive load that clamps the Marx output to ground during erection, thus speeding Marx erection and reducing jitter. This effect was examined in the course of TEMPS testing at Camp Parks and is described in Section 8 of this report.

## 5.2 PEAKING CAPACITOR DESIGN

5.2.1 Operation. Peaking capacitors supply the initial load current that the Marxes, because of their stray series inductance, cannot supply. Peaking capacitors must satisfy the low inductance requirements that the Marxes cannot meet and several other design criteria.

First, the wave impedance must be low, since a fraction of the output pulse will be developed across the peaking capacitor and not radiated. It can be shown that the early signal radiated by the system is reduced by the peaking capacitors as if the system impedance were the characteristic impedance of the bicone structure and the wave impedance of the peaking capacitors in series.

Second, the peaking capacitors must be physically small, so that they fit close to the output switch. Achieving low wave impedance, as required, suggests the need for a large circumference, entailing a large area of the bicone that must be charged to the switch potential before the switch closes. The charge that this requires flows through the antenna and generates a prepulse\* that is, in general, proportional to the capacity enclosed by the peaking capacitors.

---

\* Stated slightly differently, prepulse arises as a result of stray capacity across the output switch which couples a fraction of peaking capacitor pulse charge current into the load impedance before output switch closure (Appendix G of Reference 1).

Third, peaking capacitor weight must be held within reasonable bounds to facilitate handling of the overall system.

For the simplified circuit of Figure 33, it can be shown (Reference 7) that for the limiting case, where the Marx capacitance can be replaced by ideal voltage source, the correct value of peaking capacity,  $C_p$ , is

$$C_p = \frac{L}{R_L^2}$$

and that if the output switch  $S_2$  is closed at  $\omega t = \pi/2$ , where  $\omega$  is the resonant angular frequency of the series combination of  $L$  and  $C_p$ , a step output is produced across  $R_L$ . Assessment of circuit operation reveals that the current  $i(t)$  at  $t = \pi/2\omega$  is just that required to produce  $V$  volts across  $R_L$  where  $V$  is ideal source voltage.

Where the Marx capacitance has a finite value and where an exponential decay is required, the analysis is valid as long as the ratio of Marx capacitance to peaking capacitance is large ( $> 10$ ). For smaller ratios, slightly different values of  $C_p$  and  $t$  are required, but the desired output waveform can be attained with ratios as small as three or four to one (Reference 8).

The original anticipated value of Marx stray series inductance (each Marx) was about  $4.5 \mu\text{H}$ , thus implying a theoretical peaking capacitor value

$$C_p = \frac{L}{Z_L^2} = \frac{4.5 \mu\text{H}}{60^2} = 1.25 \text{ nF}$$

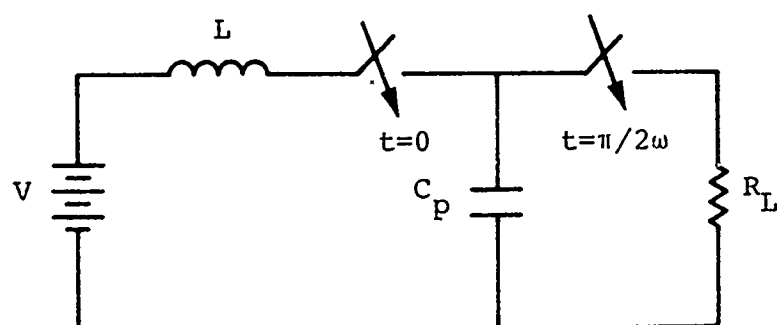


Figure 33 Idealized peaking capacitor circuit.

Using these values, a computer circuit analysis program was used to evaluate circuit performance. Peaker value and output switch closure time were permitted to vary from the theoretical values and were adjusted to yield an output waveform most nearly a pure single exponential decay into a constant load impedance. Analysis results (Reference 9) yielded an actual peaking capacitor value of 1.0 nF and switching time equal to about 1.13 times  $\tau/4$  where  $\tau/4$  is the nominal theoretical output switch closure time.

The proposed peaking capacitor design was one first suggested to us by J. C. Martin, AWRE, Aldermaston, England. This technique is one whereby the region between the main conducting surfaces that define the capacitor electrodes is separated by stacking relatively thin pads of high-electrical-strength solid plastic material separated by relatively thick conducting electrodes. The resulting subdivision tends to force a more uniform distribution of electric field between the conducting surfaces to which the capacitor is attached. Energy density is increased by the use of the electrically strong solid dielectric material, and this insulation extends beyond the edges of the interspersed electrodes, thereby allowing the high electric fields between electrodes to decrease with increasing radial distance and approach a value that can be safely withstood in the gas dielectric that surrounds the capacitor.

The design development of the TEMPS peaking capacitors, which form a continuation of the biconical transmission line surfaces to which they mate (Figure 1), is the subject of the next section.



5.2.2 Peaking Capacitor Development. As discussed in the proposal (Reference 1), the peaking capacitor for each TEMPS half-generator consists of eight parallel peaker modules. Each module in turn consists of 35-series sections using relatively thin pads of solid dielectric material separated by relatively thick conducting electrodes. The maximum design voltage for each peaker section is 100 kV which yields 3.5-MV maximum design voltage for the peaking capacitor modules that comprise each half-generator.

The principal design problem associated with use of the solid dielectric material is the grading technique that must be employed to reduce the electric fields from the high value within the solid dielectric material between the conducting electrodes to a low enough value at the gas/plastic peaker interface to be safely withstood in gas without flashover.

Solid dielectric, gas-graded designs, as discussed in the proposal, rely on corona currents to transfer charges to plastic film layers and thus relieve fields in the ambient gas without forming sparks or streamers that can induce breakdown between the electrodes. Although the design is most attractive from a weight standpoint, preliminary tests have not been encouraging with respect to breakdown. An in-house, single-module testing program completed before the program start date for TEMPS (Appendix F) showed that breakdown at the gas-graded edges of various configurations occurred at below the maximum design stress level of 2.0 MV/cm for solid dielectric TEMPS modules. The average breakdown field for nine iterations of various configurations of Mylar and polypropylene films was only 1.5 MV/cm, with the best configuration attaining a maximum strength of 2.0 MV/cm. These results tend to eliminate gas-grading as a viable alternative.

Solid-dielectric, liquid-graded designs utilize high dielectric constant liquids in conjunction with increasingly thicker sections of plastic at the capacitor edges to grade the electric field magnitude from its maximum value within the main body of dielectric to a low value at the plastic-Freon interface (outside surface of stack). High dielectric constant liquids are used to ensure that the electric field appears primarily in the plastic, which is electrically stronger. These designs may be subdivided into two categories based upon how the total thickness of dielectric is attained, i.e., whether it is composed of all solid sheets or built up from several layers of thin sheets.

A prototype module using a single sheet of standard grade, non-oriented polypropylene extruded to a thickness of 0.020 inch was embedded in an ambient water medium and tested as part of the program initiated on 21 September. The results, presented in Appendix G of this final report, were that the breakdown field strength of three such samples was around 1.3 MV/cm. The poor breakdown strength can be attributed to one or more of several phenomena. First, as is well documented from the experience of capacitor manufacturers, multilayer thin-film dielectrics are inherently electrically stronger than equivalent volumes composed of thicker sheets. The problems of producing sections of solid dielectrics without manufacturing defects become more severe as the thickness of sections increases. Other factors such as quality control and statistical considerations should be noted, but perhaps one of the most important is the question of molecular orientation, which is discussed in the following paragraphs.

The tests, using single stacks of twenty 0.001-inch-thick sheets of balanced, bi-axially oriented capacitor grade polypropylene, reported in Appendix G indicated a breakdown field in excess of 2.0 MV/cm. Subsequent to the maximum voltage tests, similar samples were tested for reliability by subjecting them to over 1000 shots at the maximum design stress level of 2.0 MV/cm. No failures occurred during these tests, but gradual degradation of the polypropylene surface from dendriting was observed at the electrode edges. This was felt to be a phenomenon associated with the prototype edge-grading geometry and was subsequently investigated and solved. The solution of this particular problem is discussed in a following paragraph.

The fact that balanced oriented polypropylene was used in these tests unquestionably contributed to their success over the single-sheet tests. Balanced orientation results when the film is distended equally along two mutually perpendicular areas during the manufacturing process. Comparisons of the breakdown characteristic for both oriented and nonoriented polypropylene subjected to both ac and dc high voltage have been reported by the manufacturer--Hercules, Incorporated. The results show the oriented films are intrinsically stronger.

The production of balanced, biaxially oriented polypropylene films thicker than 0.00125 inch is beyond manufacturing capability although the advantages in terms of simplified peaking capacitor assembly using thicker material was obvious. Thus, the possibility of bonding thin sheets together with retention of the excellent insulating properties of the thin material was explored, but, unfortunately, without success.

5.2.3 Surface Dendrites. As described in Appendix G, dendriting of the polypropylene material at or near the edges of the dielectric film was observed. Electrostatic field plots of the test configuration at the electrode edge were made, taking into account the dielectric boundary between the solid dielectric material and ambient liquid grading material. The plots revealed the presence of relatively high fields at the triple point boundary between the polyethylene ring, the polypropylene pad, and the liquid medium; fields were high enough to break down the liquid. This problem was alleviated by moving the triple point boundary radially outwards (see Appendix G).

5.2.4 Single-Shot Breakdown Measurements. Having effectively solved the dendriting problem described above, the test facility described in Appendix G was upgraded by doubling the available voltage. This was achieved by marxing two 0.2- $\mu$ F 100-kV energy storage capacitors. The test setup in other respects remained the same as described in Appendix G.

Single-shot breakdown measurements were first performed using deionized, degassed water as the grading medium. Table III summarizes the test results.

From Table III, the majority of breakdowns occurred within the body or, more accurately, within the uniformly stressed area of plastic rather than at the edge. The implication here is that body breakdown is indicative of the "intrinsic" electrical strength of the plastic material for the volume tested.

TABLE III

## SINGLE SHOT BREAKDOWN--WATER GRADED

Dielectric Material: EK 500 polypropylene, 20 sheets, 0.020 inch total thickness. Stacked and assembled under de-ionized and de-gassed water to exclude air.

Electrodes: Aluminum, 14.7 inches in diameter, edge radius, 1/4 inch, volume of stressed plastic = 56 cm<sup>3</sup>

<u>Sample No.</u>	<u>Breakdown Field (MV/cm)</u>	<u>Breakdown Location</u>	<u>Comments</u>
1	~ 3.45	body	
2	~ 3.90	body	
3	3.54	edge	
4	3.80	edge	
5	3.54	edge	Wetting agent added to H <sub>2</sub> O
6	4.04	body	Wetting agent added to H <sub>2</sub> O
7	3.32	body	
8	3.70	body	
9	<u>3.70</u>	body	
Mean = 3.67 MV/cm			

A wetting agent was added to the water for test samples 4 and 5 (Table III) to eliminate air bubbles which otherwise adhere tenaciously to the plastic film. The technique was helpful in terms of bubble removal, but its use was discontinued because of the unknowns associated with its effect upon breakdown field strength.

The mean breakdown field strength for these tests was 3.67 MV/cm. The breakdown field strength of an equal volume of Mylar (Reference 10) is about 2.85 MV/cm, and thus EK 500 polypropylene in thin sheets is substantially stronger than Mylar which has previously been considered the strongest sheet plastic material.

Single-shot breakdown measurements were also conducted with ethylene glycol rather than water as the grading medium using the same test setup. These results are summarized in Table IV.

A comparison of Tables III and IV indicates substantially greater breakdown field strength using glycol instead of water. The increased strength over water was at first surprising, since the polypropylene is the dominant material with respect to breakdown. There appear to be two basic explanations. The most important factor in increasing the strength stems from the assembly technique; it is easier, in practice, to assemble a module under ethylene glycol without trapping significant amounts of air between polypropylene sheets. The other factor is that trapped layers of glycol can effectively decrease the stress in the polypropylene as a result of its lower dielectric constant compared with water. This effect is minimal; even if equal thicknesses of glycol and polypropylene were in the

TABLE IV  
SINGLE SHOT BREAKDOWN--GLYCOL GRADED

Dielectric Material: EK 500 polypropylene, 20 sheets, 0.020 inch total thickness. Stacked and assembled under de-ionized and de-gassed ethylene glycol to exclude air.

Electrodes: Aluminum, 14.7 inches in diameter, edge radius 1/4 inch, volume of stressed plastic = 56 cm<sup>3</sup>

<u>Sample No.</u>	<u>Breakdown Field (MV/cm)</u>	<u>Location</u>	<u>Comments</u>
1	4.18	body	Breakdown 1/4 inch inside of start of radius at edge
2	4.48	body	Breakdown 1/2 inch inside of start of radius at edge
3	4.40	body	Breakdown 1/2 inch inside of start of radius at edge
4	4.52*	body	Breakdown started 1/2 to 3/4 inch in from start of radius at edge
5	4.43	body	Two breakdown locations: one 1-1/2 inches in from start of radius, the second 2 inches in
6	3.85	edge	May have been due to dirt in glycol

\* This shot prior to breakdown shot. Breakdown shot photo missed.

TABLE IV  
SINGLE SHOT BREAKDOWN--GLYCOL GRADED (ccnt.)

<u>Sample No.</u>	<u>Breakdown Field (MV/cm)</u>	<u>Location</u>	<u>Comments</u>
7	4.53	body	Broke down 2-1/2 inches in from start of radius at edge
8	4.57	body	Broke down 1/2 inch in from start of radius at edge
9	5.07	No breakdown	
10	4.48	body	Broke down 1/8 inch in from start of radius at edge
11	4.12	body	Broke down close to radius at edge
12	<u>4.55</u>	body	Broke down 2-1/2 inches from start of radius at edge

Mean breakdown  
field strength = 4.43 MV/cm



assembly, the glycol could decrease the stress in the polypropylene by only 5 percent. The average breakdown strength would still be almost 20 percent higher than it was with water.

In summary, testing during this period did show that the primary design is more than adequate. Also, the success with ethylene glycol seems to indicate that it should be utilized in the final design. The benefits of using it go beyond improving performance. It eliminates the freezing problem encountered with water. It also seems to minimize the probability of edge failures because its lower dielectric constant tends to enhance the sharp corners of dielectric boundaries less.

5.2.5 Life Testing. The prototype design for solid-dielectric liquid-graded peaking capacitor sections described in Appendix G was used to construct a test configuration consisting of two series sections, thereby doubling the volume of stressed plastic material. Life testing began by repeatedly stressing the assembly such that the main dielectric (polypropylene) mean field was about 2.0 MV/cm, the same as for the previous single module tests. A failure occurred at about 1000 shots. Several subsequent modifications to edge-grading design were effected (Appendix G) until the fatigue breakdown at 2.0 MV/cm was essentially eliminated for reasonable lifetimes. One module survived 5000 shots with no failures at this level; another survived 8000. In both cases the test series was terminated for inspection purposes.

Life testing continued with the assembly and testing of ten series sections. A test facility was constructed expressly for this testing and Figure 34 illustrates the experimental



Figure 34 Peaking capacitor test setup.

apparatus. At the far left is seen the 1-MV, 12-stage Marx generator in its Freon enclosure. The 4-inch galvanized output conductor extends from the corona shield atop a Marx to a set of four parallel  $\text{CuSO}_4$  load resistors in series with a field-enhanced pressurized  $\text{SF}_6$  switch. From there, it continues to a Freon enclosure containing the ten-module peaking capacitor which is shown in more detail in Figure 35.

When testing began, the peaking capacitor consisted of 10 solid aluminum electrodes, ten 20-layer stacks of 0.001-inch polypropylene and ten polypropylene rings, eight of which were the injection molded type designed for the final pulser. The stack was clamped between two end plates using 7/8 inch nylon rods.

When voltage was first applied to the 10 module stack, an interface flashover occurred about 1.5  $\mu\text{sec}$  after initiation of a pulse with an approximate 650-kV peak output. The maximum peak voltage for full-scale peaking capacitors is 3.5 MV over a 1-meter interface distance so that, notwithstanding edge effects, the mean field in Freon should not exceed 35 kV/cm. It follows that the scaled-design voltage is 100 kV/module, or 1.0 MV for the 10-module prototype; so the flashover occurred 28 percent low.

The 1.0-MV level was reached after modifying the external geometry. The 7/8-inch rod diameter was decreased to provide a 1/8-inch space between the peaking capacitor stack and the rod surface. Two pulses at the 1.0-MV level induced another flashover in the vicinity of a rod. Performance was improved slightly by moving the rods 1 inch from the peaker surface, but in the interest of time it was decided that a five module test configuration should be investigated further.

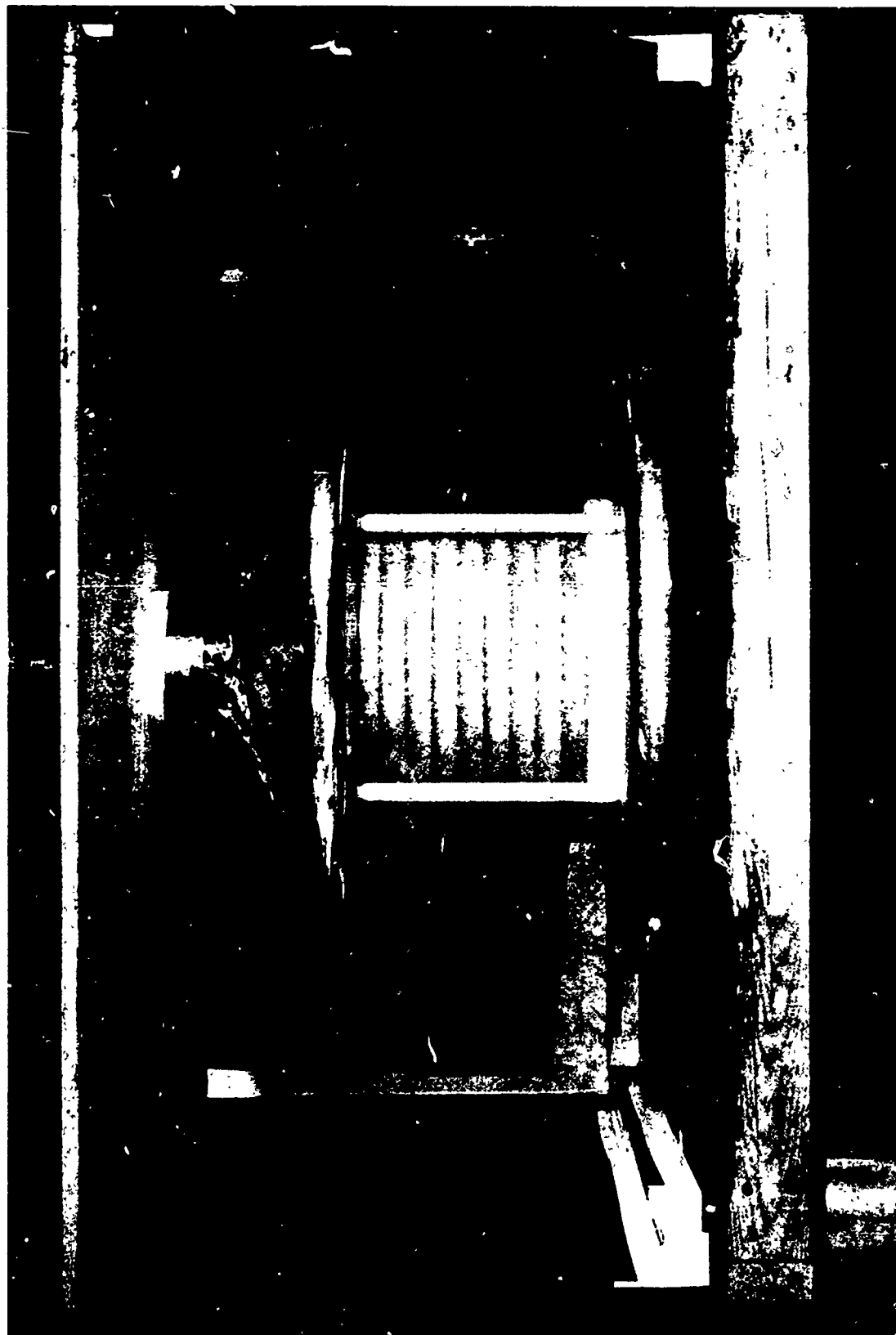


Figure 35 Ten-module peaking capacitor in Freon enclosure.

A peaker was assembled using five electrodes and rings with four 25-layer stacks of the 0.001-inch polypropylene. The elimination of one set of polypropylene disks removed an inherent asymmetry at one end of the assembly, which was considered contributory to eliminating the interface problem. This assembly successfully withstood over 50-kV/cm mean field in Freon before it flashed. The flashover occurred 450 nsec after initiation of the pulse. Another five-module stack was assembled and the rods moved radially inward to determine the effect of their proximity to the peaker interface. This assembly tracked at 45 kV/cm after approximately 450 nsec.

A preliminary conclusion resulting from 10-module tests was that the interface flashover problem was influenced by the end geometry and condition of the interface. There was a correlation between surface flashover level and the amount of residual moisture on the interface.

Regarding leaks, it was determined that the polypropylene ring design possessed an annular chamber outside the main O-ring seal. This chamber tended to trap the grading liquid during assembly, and caused a troublesome "weeping" at the junction of each module. It was found that the problem was substantially eliminated when small bleed notches are placed in each ring. These notches introduce no electrical problem and allowed easy detection of O-ring leaks in the full-scale peakers.

In addition to the notches cut in the rings, a volume-compensating reservoir consisting of an acrylic cylinder fitted with a sealed acrylic piston was attached to one peaking capacitor endplate. When expansion or contraction of the polypropylene

rings occurs as a result of ambient temperature variations, the reservoir acts to prevent excess pressure buildup inside the peaking capacitor assembly and thus minimizes leaks. Different O-rings were also used to create a more positive seal.

With these modifications, testing resumed and over 1500 shots were fired at or above the design stress level of approximately 100 kV per module. The interface was kept clean and free of moisture and no failures occurred.

5.2.6 Final Peaking Capacitor Design. A prototype peaking capacitor module fitted with a volume compensater at one end is illustrated in Figure 36. It became apparent during fabrication of the prototype peaker that assembly of such a design was complex. Furthermore, since each section of the design was sealed by means of O-rings, the likelihood of maintaining an adequate seal during assembly and handling was questionable. Therefore, an alternative design, but one that retained the basic electrical design, was initiated.

The modified design consisted basically of enclosing all the peaking capacitor sections within an epoxy fiberglass tube. Polypropylene ring design was simplified by elimination of individual O-ring seals and reduction of ring outside diameter to yield an overall peaker diameter equal to that of the previous design. The modified design is illustrated in Figure 37.

The first series of tests for a six series section modified peaker design was conducted (five full modules with two halves at either end) using 36 layers of 0.001-inch polypropylene film in each section. The test objectives were fourfold: (1) to

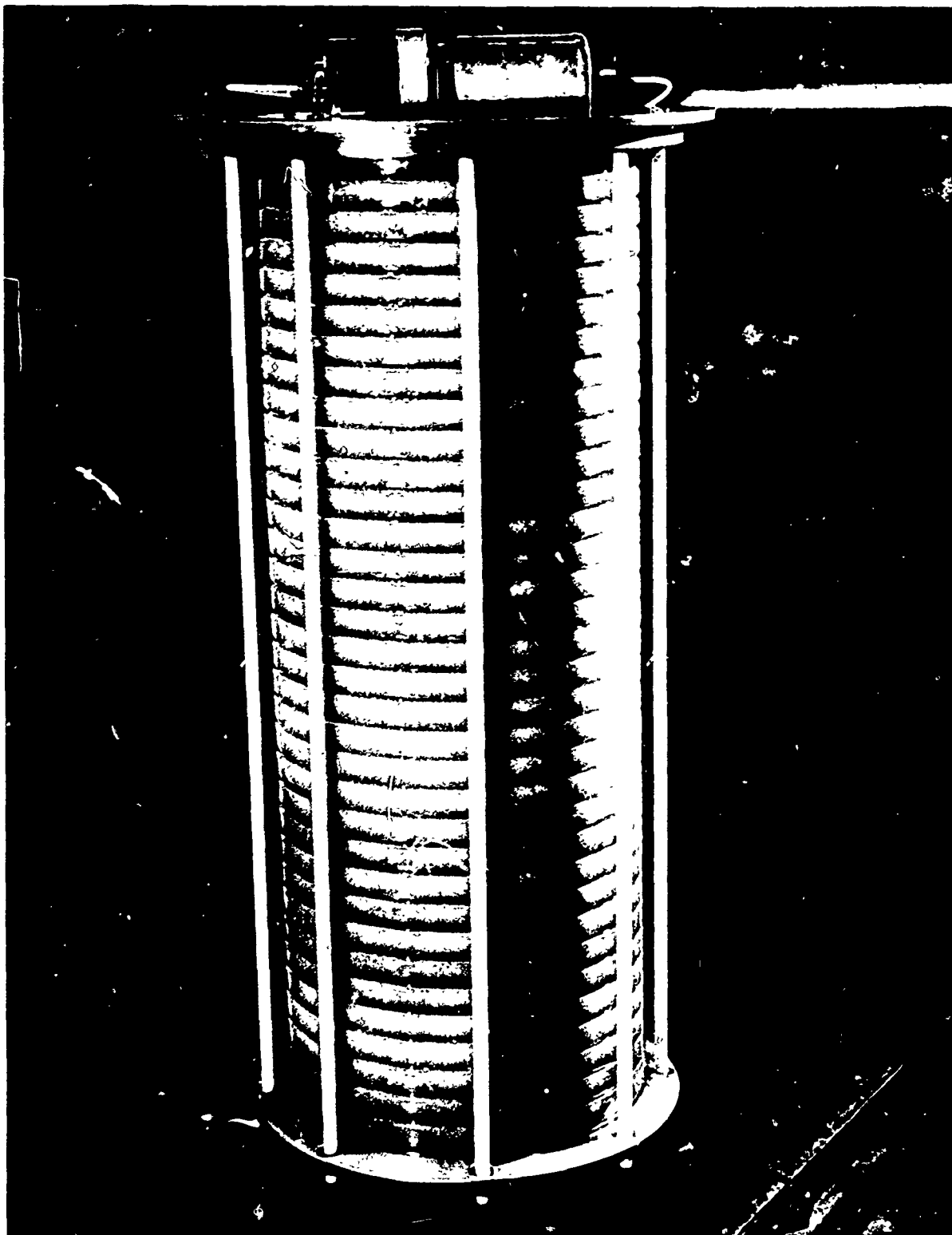


Figure 36 3.5 MV peaking capacitor.

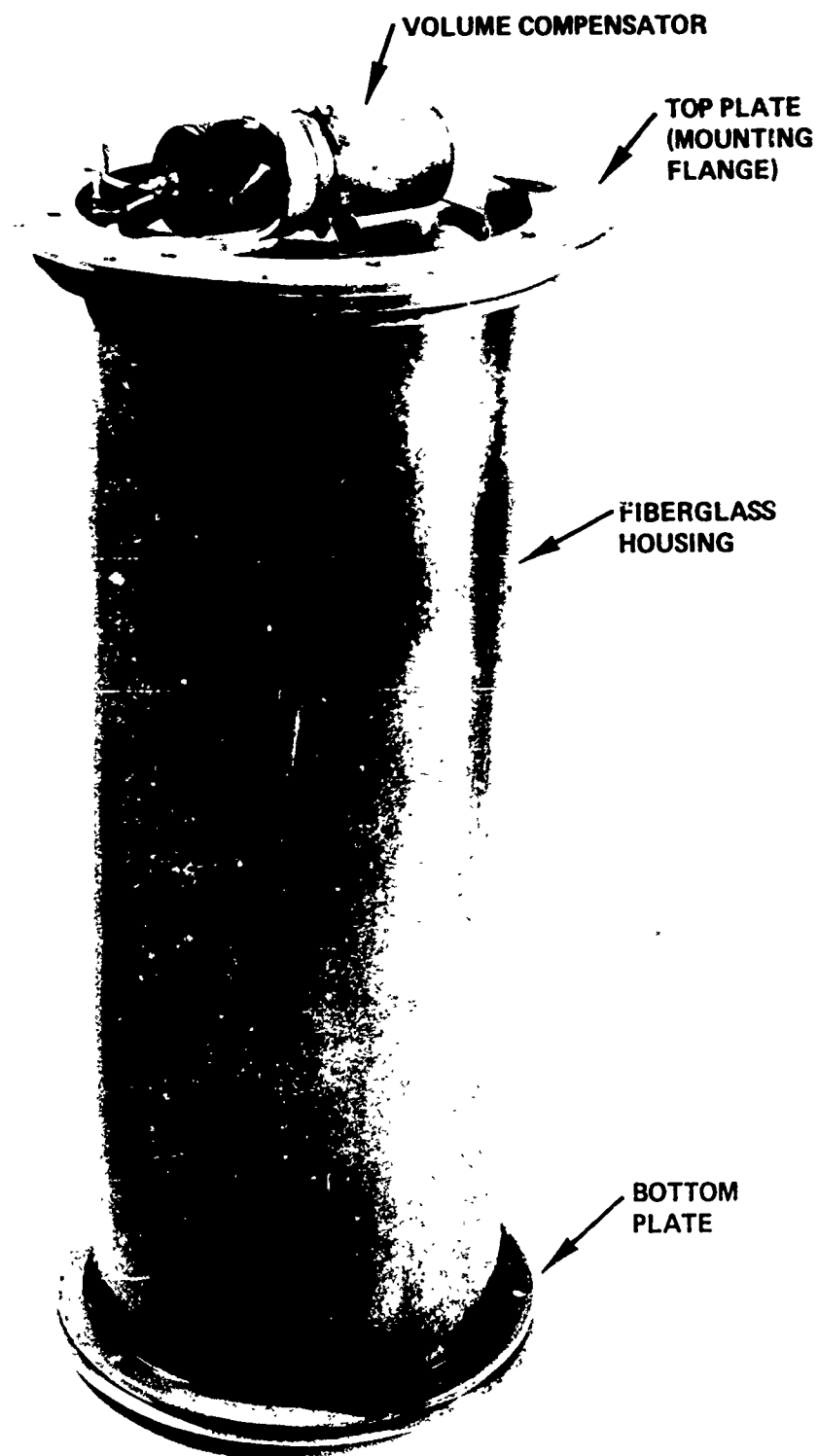


Figure 37 Peaking capacitor assembly.

72-7-59



determine design integrity with regard to interface flashover under conditions of repeated stress at the maximum design voltage; (2) to evaluate low stress reliability of the primary energy-storage medium under these conditions; (3) to measure the maximum stress to which the envelope may be subjected without tracking; and (4) to determine the damage sustained if tracking does occur.

The assembly was subjected to a voltage waveform which rose to approximately 700 kV in about 250 nsec, then e-folded with a slight initial oscillation in about 3.3  $\mu$ sec for 5000 shots. No flashovers occurred and no sign of envelope degradation was present.

The peak voltage across the assembly was then gradually raised until the test apparatus maximum of approximately 1.2 MV was attained without failure. This subjected the envelope to a mean stress of 56 kV/cm in its Freon environment, a value which is 60 percent greater than the mean stress it will see at maximum voltage in the operating system.

Part of the Freon was then removed from the test fixture to deliberately induce interface flashover to evaluate the extent of resulting damage. After the tracking had occurred, the assembly was removed and inspected. Damage was found to be minimal. No serious internal damage was sustained despite the fact that the arc channel did succeed in traveling through the fiberglass envelope at a glue joint securing the flange at one end.

A second test assembly was prepared using 20 layers of polypropylene rather than 36 in each section. This raised the mean field in the main dielectric from 1.3 MV/cm to 2.3 MV/cm for 700 kV total peak voltage across the stack. This assembly was also subjected to 5000 shots, after which it was disassembled and inspected. It was found that one of the end modules (consisting of 10 layers of polypropylene) had sustained arc damage; however, the damage was apparently confined to this region without affecting the rest of the assembly. It is not known at which point during the 5000-shot series the module failed but, judging from the minimal thermal damage present, the failure is assumed to have occurred near the end of testing.

These tests provided high confidence in the modified peaker design.

5.2.7 Peaking Capacitor Final Design. The final design peaking capacitor from a physical standpoint is that shown in Figure 37 as discussed in the previous section. This design combines mechanical ruggedness with good electrical characteristics in terms of freedom from external flashover; i.e. the design is electrically "clean."

The peaking capacitor design value was established early in the TEMPS program based upon conservative estimates of Marx inductance. This was necessary in view of the long lead time associated with fabricated peaker electrodes.

Based upon an estimated Marx inductance of 4.5  $\mu\text{H}$  (each half system), the theoretical peaking capacitor value is given by

$$C_p = \frac{L}{Z^2} = \frac{4.5 \times 10^{-6}}{60^2} = 1.25 \text{ nF}$$

For a system which produces an exponentially decaying pulse, Reference 9 indicates that the actual peaking capacitor value  $C'_p$  is the series combination of the theoretical value in series with the generator capacity. For TEMPS,  $C'_g$  (half generator capacity) is 5 nF. Thus,

$$C'_p = \frac{C'_g C_p}{C'_g + C_p} = \frac{(5 \times 10^{-9})(1.25 \times 10^{-9})}{5 \times 10^{-9} + 1.25 \times 10^{-9}} = 1 \text{ nF}$$

The capacity of each peaking capacitor module is therefore one eighth this value, or 125 pF.

Primarily by virtue of the low-inductance energy storage capacitor design, the final value of Marx inductance was about 2.15  $\mu$ F which implies a peaking capacitor value equal to about 533 pF, substantially less than the planned value. To partially compensate for the lower Marx inductance, the number of EK 500 polypropylene sheets within each section of the peaking capacitors was increased to 32, yielding an individual module capacitance of about 100 pF but with decreased stress level in the polypropylene material. The final stress value for 3.5 MV is 1.30 MV/cm which, based upon EK 500 breakdown measurements, is very conservative. The final number of peaking capacitor series sections is 33: 32 full sections, with 2 half sections, one at each end of each module to preserve symmetry.

### 5.3 OUTPUT SWITCH

A high-pressure gas-insulated near-uniform-field, self-breaking output switch was proposed for TEMPS. Its design and projected performance is described in Reference 1.

A one-sixth scale of the TEMPS output switch was fabricated for testing and is shown in Figure 38. The primary objective of initial switch testing was to determine interface flashover voltage commensurate with scaled projected operating conditions.

For this testing, the switch was installed in the "dump" circuit of the peaking-capacitor test setup (Figure 34). A simplified electrical circuit of the test is shown in Figure 39.

In operation, the test bed Marx generator is fired and charges the peaking capacitor on a nearly  $1-\cos \omega t$  waveform (Figure 40). This voltage waveform also appears across the switch being tested. Before peak voltage is reached on the first half cycle of the waveform, the switch self-breaks, discharging both the Marx and the peaking capacitor through the load resistance  $R_L$ . Control over switch breakdown voltage is achieved by gas-pressure adjustment of the switch. For this testing,  $\text{SF}_6$  gas was used in the pressure range of 15 to 100 psig. Gap spacing was 2 cm.

Voltages as high as about 950 kV were successfully withstood over the switch envelope and no interface breakdowns occurred. A typical voltage waveform is shown in Figure 41.



Figure 38 One-sixth scale output switch.

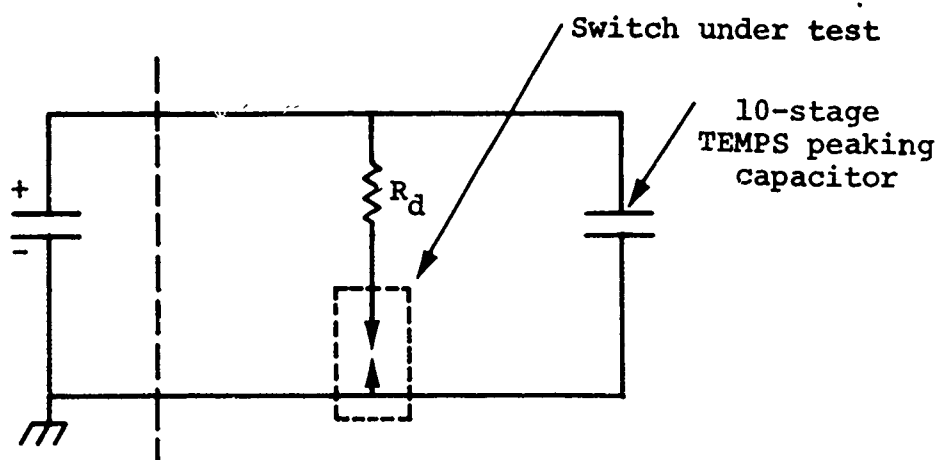


Figure 39 Electrical circuit for switch testing.

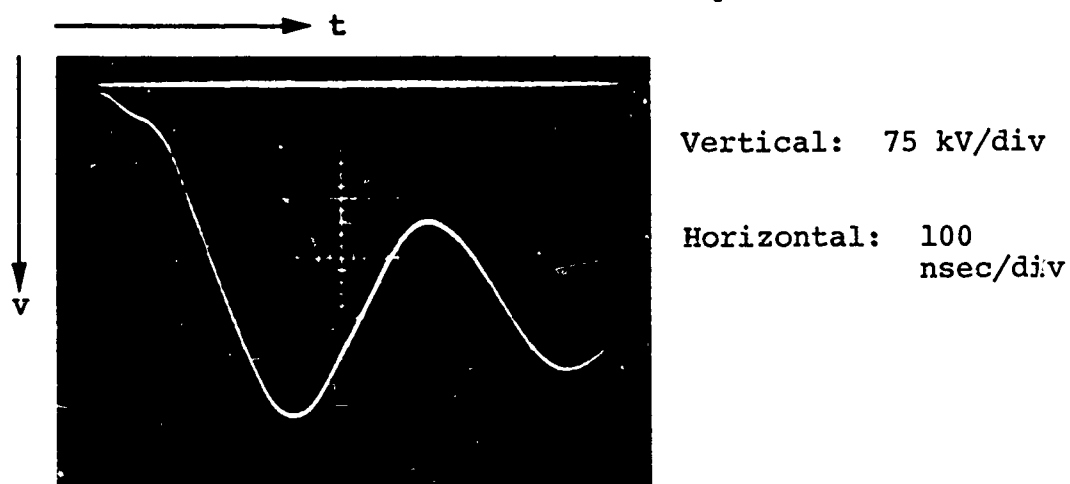
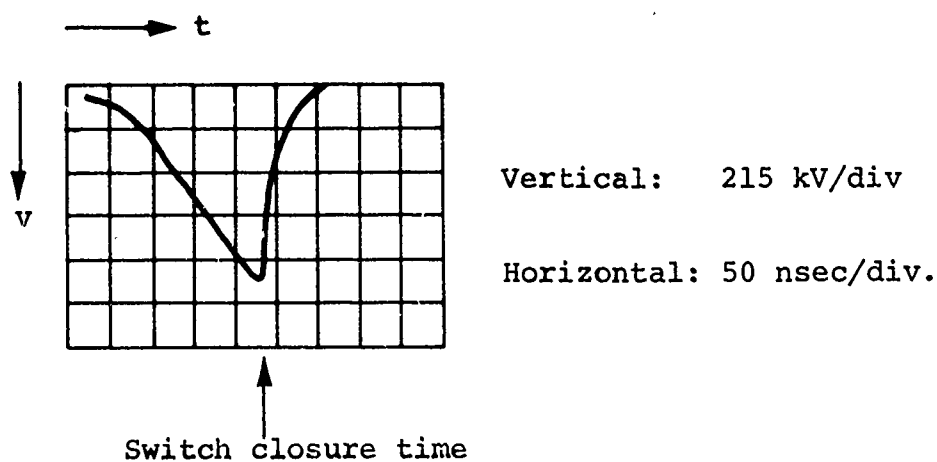
Figure 40  $1 - \cos \omega t$  waveform.

Figure 41 Typical applied waveform.

The voltage waveform applied to the TEMPS output switch will also be a  $1-\cos \omega t$  waveform, and will rise to switch closure voltage in about 65 nsec. In comparison, risetime of the voltage across the one-sixth-scale switch being tested was about 200 nsec and is therefore an overtest in terms of the duration of applied voltage.

#### 5.4 TEMPS TRIGGER SYSTEM

Since TEMPS is a bilateral pulser, synchronized operation of the half generators is required to ensure reproducible output waveforms and to prevent half generator peaking capacitor overvoltage. Design of the proposed trigger system is presented in Reference 1 and the system block diagram is shown in Figure 42.

Two separate trigger amplifier chains are required that are isolated by the full system output voltage. These each receive low-level input triggers and ultimately provide high-level triggers at their respective Marx switches.

The trigger system performance requirements were discussed in Reference 1. There it was shown that the rms jitter in the erection time of each Marx must be  $\leq 4.3$  nsec in order to limit peaking capacitor overvoltage to  $\leq 10$  percent in 95 percent of the shots. As a result of reduced Marx inductance, the peaking capacitor charging time is somewhat less than that originally estimated. This in turn required an improved trigger system jitter. Accordingly, the objective of a  $\lesssim 3.5$  nsec jitter was adopted as the primary goal of the trigger system.

The design criteria are summarized in Table V.

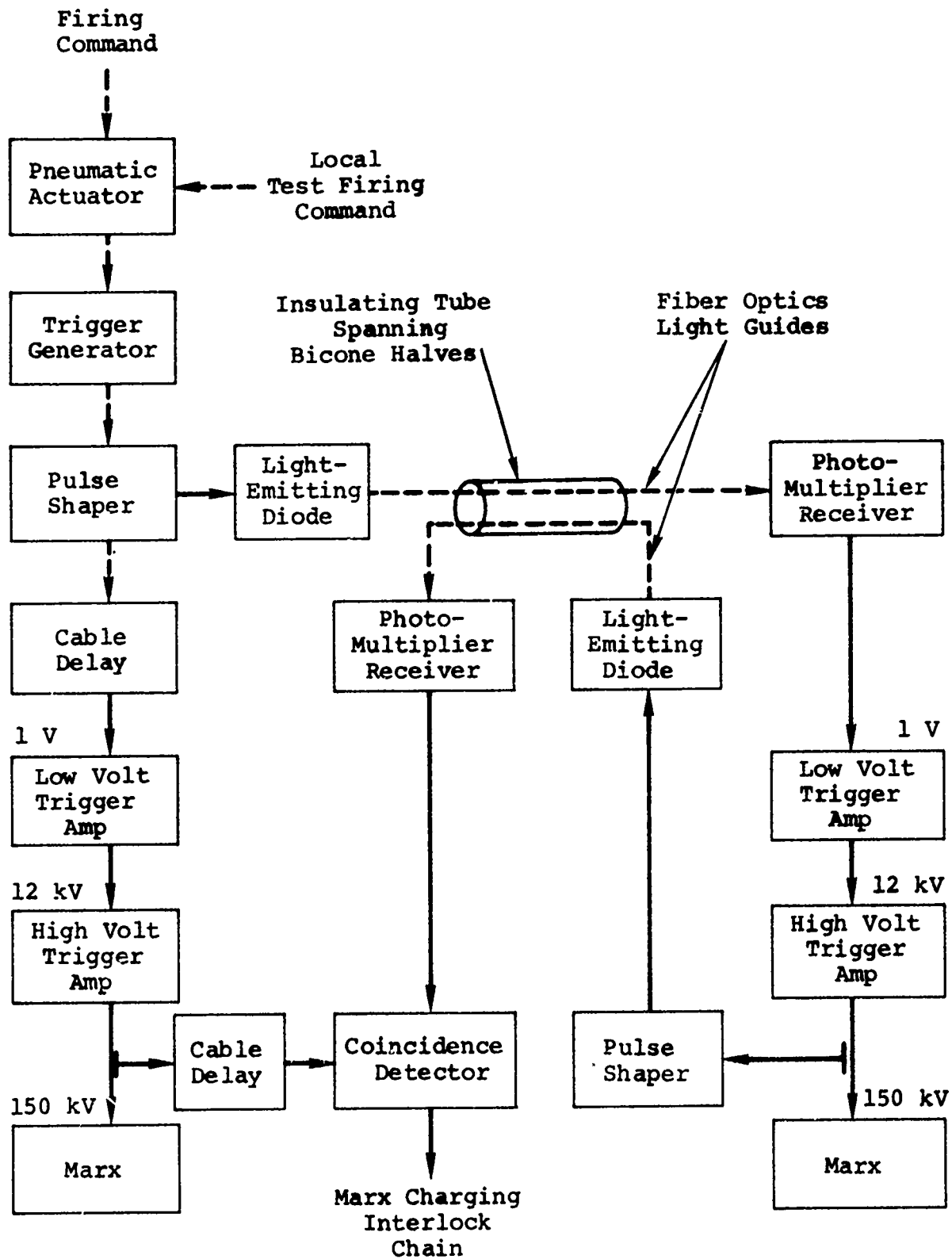


Figure 42 Trigger system block diagram.



TABLE V  
TRIGGER SYSTEM DESIGN CRITERIA

## ELECTRICAL PERFORMANCE

Voltage isolation between two amplifier chains	$> 6 \text{ MV}$
Low-level input trigger amplitude	$\geq 1 \text{ V}$
Low-level input trigger risetime	$\leq 10 \text{ nsec}$
High-level Marx trigger amplitude	$\geq 120 \text{ kV}$
High-level Marx trigger risetime	$\leq 5 \text{ nsec}$
Jitter (low-level input to Marx erection)	$\lesssim 3.5 \text{ nsec rms}$
Maintenance cycle; shots between gap adjustments	$\geq 5000 \text{ shots}$
Trigger delay tracking between two amplifier chains	$\leq 2 \text{ nsec}$

## FUNCTIONAL PERFORMANCE

Proper trigger system performance to be checked before each charging cycle.

Prefire detection and indication circuitry to be provided.

Monitors and controls permitting easy local checkout and troubleshooting to be provided.

The trigger system is shown in Figure 42. The major functional blocks are the low-voltage trigger amplifiers, high-voltage trigger amplifiers, and the optical pulse distribution system. Other required system elements include primary power, test and command controls, and monitoring and interlocking functions. The latter elements interface strongly with the general command and control system.

5.4.1 Optical Pulse Distribution. A breadboard optical pulse distribution system was assembled and tested and test results are reported in Reference 11. Its performance is more than adequate for the TEMPS requirement. This system consists of an avalanche transistor pulsing a semiconductor light-emitting diode, a 20-foot length of an inexpensive 1/8-inch-diameter fiber optics bundle, and an RCA type 931 photomultiplier tube. A signal of 1 to 2 volts was produced by the photomultiplier receiver at a 100-ohm impedance level, and adequately triggers the low-level amplifier. The risetime of this pulse was  $< 3$  nsec, ensuring jitter-free triggering of the low-level amplifier input stage. The overall jitter referred to the driver transistor output was  $< 1$  nsec rms, essentially immeasurable. Since the driver transistor stage can easily be made to operate with a jitter of  $< 1$  nsec, the entire optical distribution system contributes negligible jitter to the overall trigger system.

Two optical transmitter/receiver units were fabricated for TEMPS that incorporate the circuitry described above. These are shown in Figure 43. Each has a light-emitting diode transmitter and a photomultiplier receiver. A short length of fiber optics light guide is shown positioned in one of the custom connectors. The transmitter input trigger requirement is 1 volt; the receiver output signal is typically several volts. In order to minimize

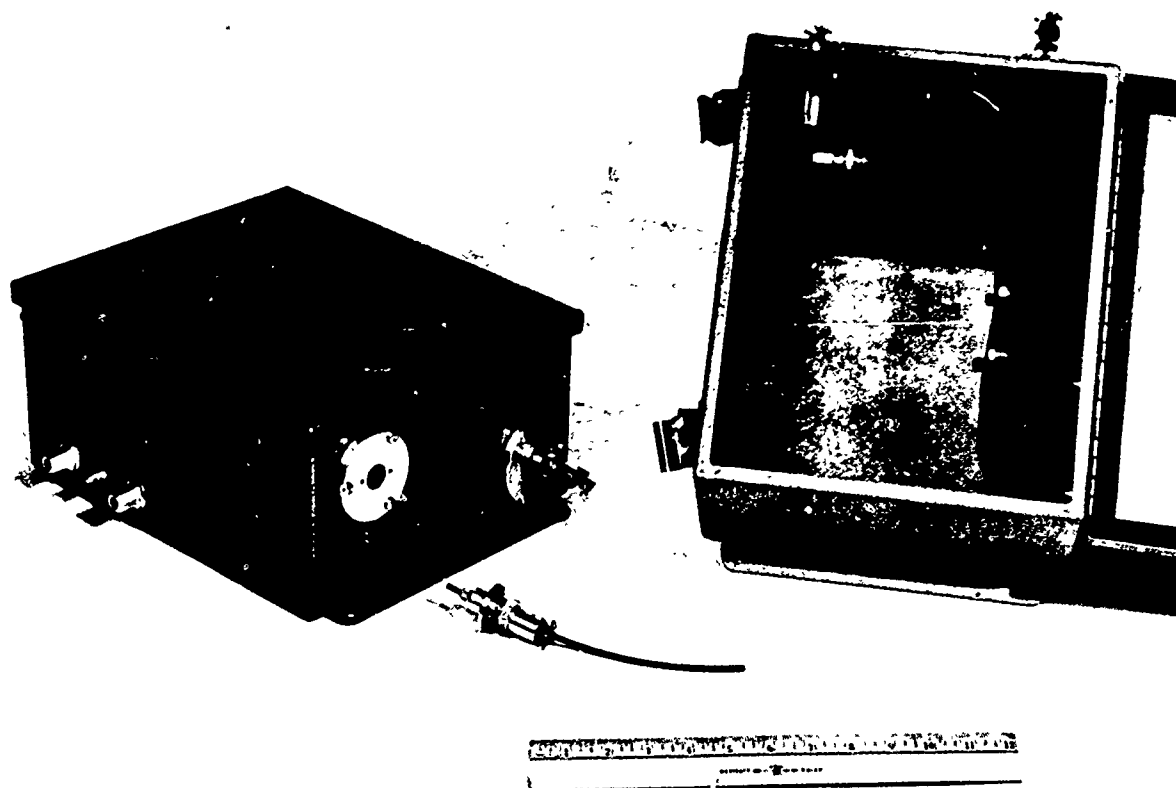


Figure 43 Optical transmitter/receiver unit.

attenuation and risetime degradation caused by the fiber optics, these units are physically located as close as possible to the ends of the insulating tube that spans the bicone halves and carries the fiber optics (Figure 1). Since they are exposed to ambient weather, they are ruggedly constructed and sealed against dust, moisture, and RFI. Extra space has been provided in the event that additional optical channels are required in the future.

5.4.2 Low-Level Trigger Amplifier (Figure 44). These modules consist of a low-inductance, generally coaxial arrangement of three amplifier stages: one avalanche transistor and two planar triode stages, the last in a grounded grid configuration. This module accepts a 1 volt trigger and produces a 10 kV, 16 to 18 ampere output pulse to trigger a switch gap. For a typical load capacitance of 10 pF or less, a 1.5 to 2 kV/nsec voltage rate of rise can be produced at the gap trigger electrode. The jitter of this amplifier module, from 1 volt input to the gap trigger electrode, is significantly less than 0.5 nsec rms, provided the input pulse shape is reasonably consistent from shot to shot.

The principal source of jitter in the low-level amplifiers is the switch gap triggered by the modules just discussed. A short ( $\approx 3$  inch) rail gap was designed that permitted an experimental determination of the optimum gap configuration and its operating characteristics.

The experimental rail gap had 3-inch-long brass main electrodes and a 3-inch-long sharpened tungsten alloy trigger "blade" (Figures 45 and 46). Self-fire voltage versus pressure was measured over both air and nitrogen pressure ranges of 15 to 70 psig. For these studies, main-electrode spacing was varied from

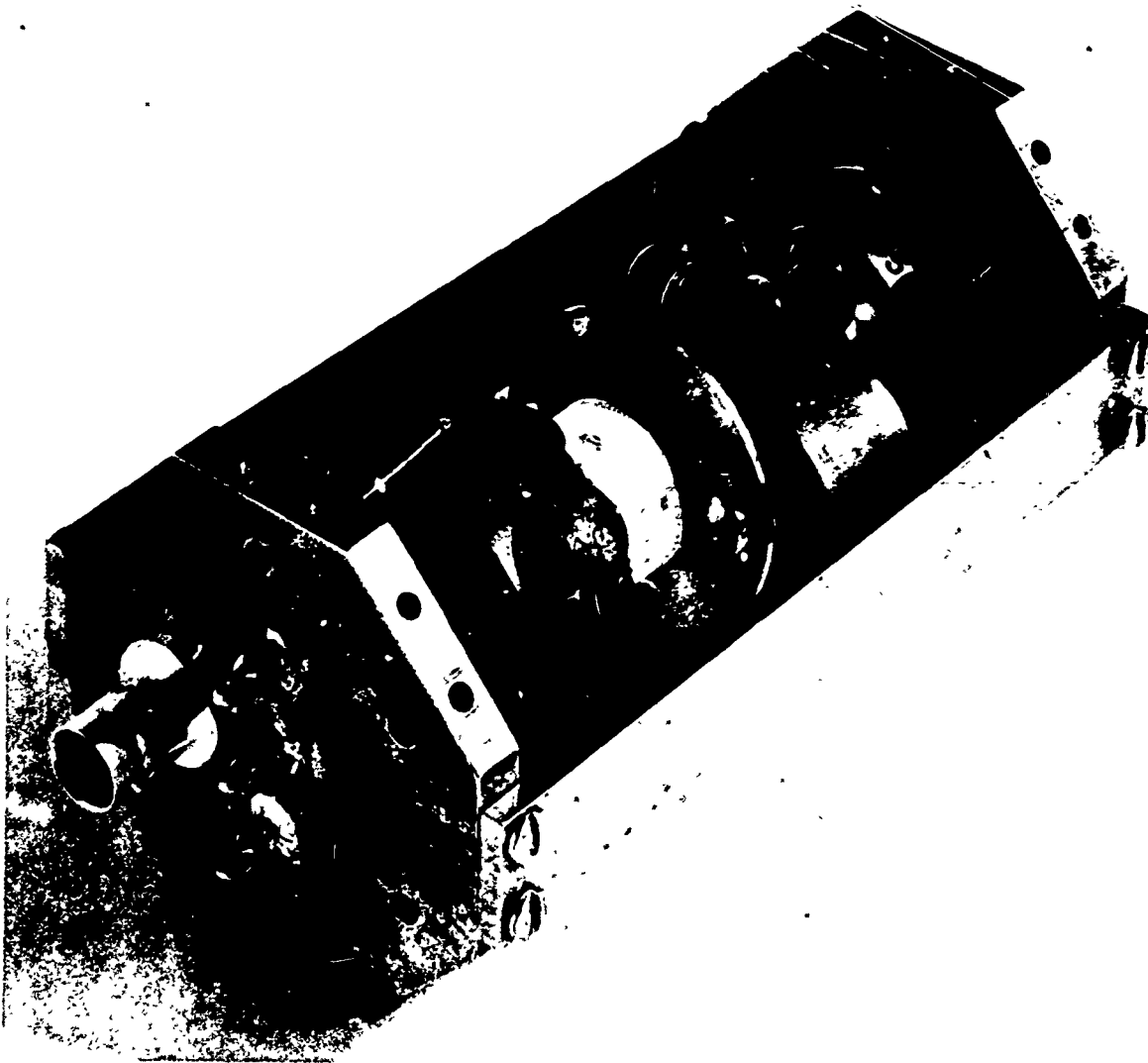


Figure 44 Low-voltage trigger amplifier sub-module.

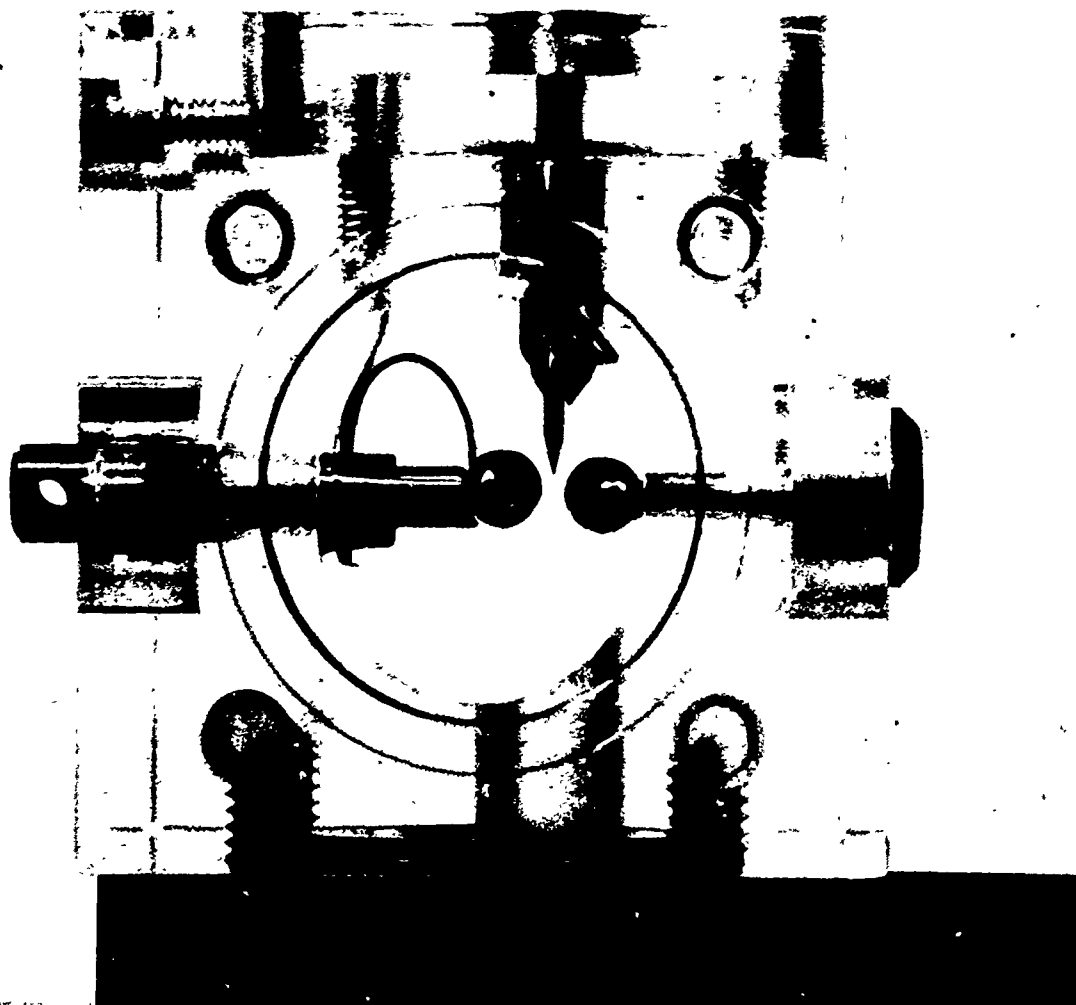


Figure 45 Low-voltage gap.

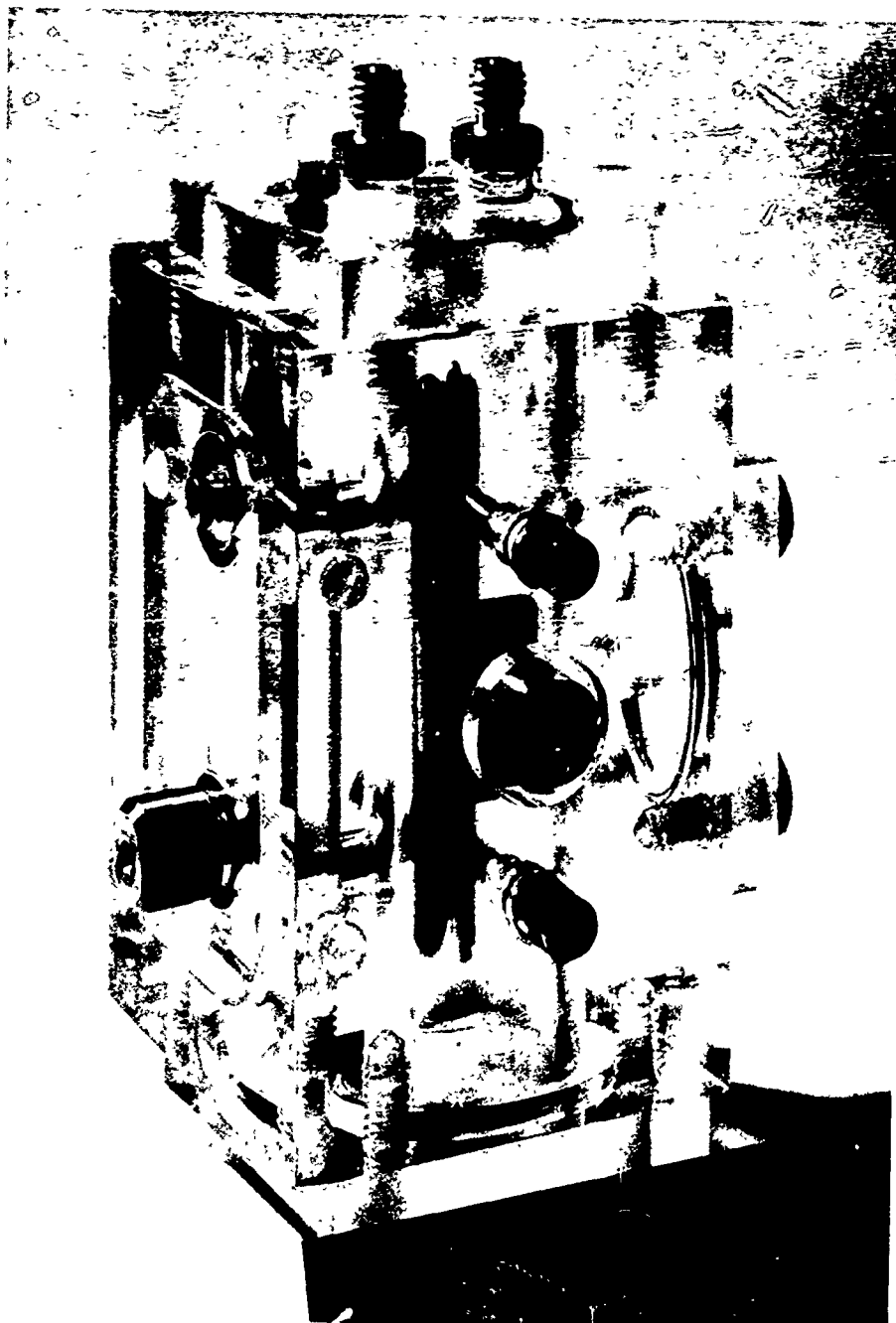


Figure 46 Low-voltage gap (side view).

47 to 81 mil and the spacing between the trigger electrode and one main electrode was held constant. Two values were chosen for this latter constant spacing: 30 and 45 mil. Two other parameters were measured for each different electrode spacing: total trigger-electrode capacitance and the trigger-electrode bias voltage that resulted in the maximum self-fire voltage. The latter agreed well with the optimum bias voltage expected from simple geometrical consideration. Also it was found to be non-critical. For a V/2 geometrical arrangement, the trigger bias voltage could be varied from about 44 to 56 percent of the main-gap voltage without significantly affecting the self-fire voltage. The effect of such a variation on jitter was not investigated.

For jitter testing, the gap was connected to short circuit two dc-charged 50-ohm cables when triggered by the planar triode-amplifier module. The entire arrangement was chosen to closely simulate the general mounting geometry and stray inductance and capacitance to be expected in the final version of the trigger amplifier. Total trigger electrode capacitance included not only the gap capacitance, but all strays and the triode-plate capacitance with filament power off.

The input trigger to the triode module was supplied by a mercury-reed pulser. Its amplitude and risetime were about 1.5 volts and  $< 1$  nsec, respectively, as measured when connected to the avalanche-transistor input stage.

A capacitive pickoff located on one of the input cables provided the output signal; a portion of the input trigger pulse provided the reference-trigger pulse. These were mixed and displayed on a Tektronix 454 scope in such a manner that the



absolute delay between the amplifier input and output signals could be determined and was unaffected by scope triggering jitter. The jitter values quoted below are thus the rms variations in absolute delay between the 1.5-volt input to the amplifier and the output signal.

For jitter measurements, a V/2 arrangement with a 45-mil main-electrode spacing was chosen. This afforded a near-minimum value of total trigger-electrode capacitance (approximately 13.5 pF), permitting fastest trigger risetime and a self-fire voltage near maximum. Our intent was to study other electrode configurations (e.g., V/3 to V/5). The V/2 configuration proved more than satisfactory for the TEMPS requirement; so the other studies were not performed, in the interest of meeting schedule and minimizing development costs.

A pulsed ultra-violet lamp was incorporated in initial tests but it did not operate properly. Before it could be repaired, promising gap performance was demonstrated. Therefore, all subsequent testing was carried out without the ultra-violet lamp. Very good performance was obtained without it in the present gap geometry.

From the method of measuring delay on the scope photos, the uncertainty or maximum probable error in any rms jitter determination was estimated to be about  $\pm 0.15$  nsec. A jitter series usually comprised 10 shots. The delay was measured between a consistent point on the reference-trigger pulse and a fixed amplitude point on the leading edge of the output pulse, generally taken at about the 80 percent of peak-amplitude point.

The better gap and cable charging polarity from the standpoint of jitter proved to be positive. However, since the trigger electrode breaks to the output electrode first (rather than the grounded electrode), a prepulse of typically 25 to 30 percent amplitude and few nanosecond duration appears on the output waveform. The second half of the gap then breaks down after a delay of  $< 5$  nsec. (These ratios and values could conceivably be improved in other gap configurations.) Following the full-gap breakdown, the risetime of the output signal was typically about 2.5 nsec, as measured on the scope. Since the scope has a basic 2.4-nsec risetime limitation, the actual risetime is approximately 1 nsec.

Better results were obtained with nitrogen rather than air from the standpoint of waveshape, risetime, and jitter. Operation at 70 percent of self-fire voltage appeared to yield slightly better risetimes and jitter values than corresponding data for 80 percent of self-fire at the same gap voltage.

All power supplies had regulated ac-line inputs. The output triode (Y-518) had a 9.8-kV plate voltage and delivered a peak gap trigger voltage of approximately 9.3 kV. The nitrogen and air supplies were "dry" bottled gas of laboratory quality. A dryer cartridge was also always used at the pressure regulator output. The gap was initially pressure tested to 70 psig.

The jitter from the 1.5-volt input to the gap trigger electrode was not accurately measured but was determined to be  $\leq 0.3$ -nsec peak-to-peak. This implies that the majority of the measured overall jitter does indeed originate in the gap. The jitter measurements are summarized in Table VI.

TABLE VI  
LOW-VOLTAGE RAIL GAP TEST RESULTS

Gas	V <sub>Gap</sub> , (kV)	Percent of Self-fire	Pressure (psig)	Mean Delay (nsec) ( $\pm 1.0$ nsec)	Delay Deviation, Maximum Spread, (nsec)	Jitter, rms, nsec, ( $\pm 0.15$ nsec)
N <sub>2</sub>	+16.4	80	30	23	1.9	0.59
N <sub>2</sub>	+16.4	70	41	26	1.6	0.47
N <sub>2</sub>	+19.6	80	44	27	1.5	0.49
N <sub>2</sub>	+19.6	70	53	27	1.3	0.48
N <sub>2</sub>	-21.0	70	53	28	4.0	1.17
Air	+15.4	80	30	22	3.3	~ 1.2
Air	+19.6	80	57	27	2.3	0.78

One attempt was made to fire the gap at the 28 kV, 70 psig N<sub>2</sub>, 80 percent of self-fire level. A capacitor failed on this shot and the gap tests were discontinued. However, the scope photo indicated that the overall delay was reduced by about 4 nsec from the previous 27-nsec figure. This indicates that it is likely that subnanosecond jitter is possible at gap voltages significantly higher than 20 kV, even though the trigger voltage is only ~ 9.3 kV. Since the 20-kV performance is already very satisfactory for TEMPS, this area of investigation was carried no further. Future arrangements may justify further study.

Several other observations are worth mentioning.

- No prefires occurred during testing.
- From shot to shot, the location of the gap arc moved randomly about along the rail electrodes, which means that erosion of the electrodes will occur rather uniformly along their lengths. Also, this variable arc location can account for a total jitter spread of about 0.3 nsec.

- After approximately 1000 shots, the sharpened tungsten-alloy trigger blade shows no evidence of erosion.
- The rate of rise of gap trigger voltage is estimated to be  $\geq 1$  kV/nsec.

The final design trigger system rail switches are similar to the experimental gap except that they will have fixed-space main electrodes. The trigger-electrode position is adjustable however.

5.4.3 High-Level Trigger Amplifier. This is a two-stage cable transformer that triggers a high level gap. This in turn shorts the dc-charged Marx trigger cables, producing a pulsed voltage in excess of 120 kV at the Marx switch trigger electrodes, initiating Marx erection. This entire arrangement is shown schematically in Figure 47.

The optimum voltage levels and number of cable transformer stages was determined experimentally, and experimental results are discussed in the following paragraphs.

Ferrite Core/Cable Transformer Tests. In this testing, two charged cables were shorted by the low-voltage gap arranged in a cable-transformer configuration (Figure 48). The cables were cut so they had equal lengths of outer conductor braid. The purpose

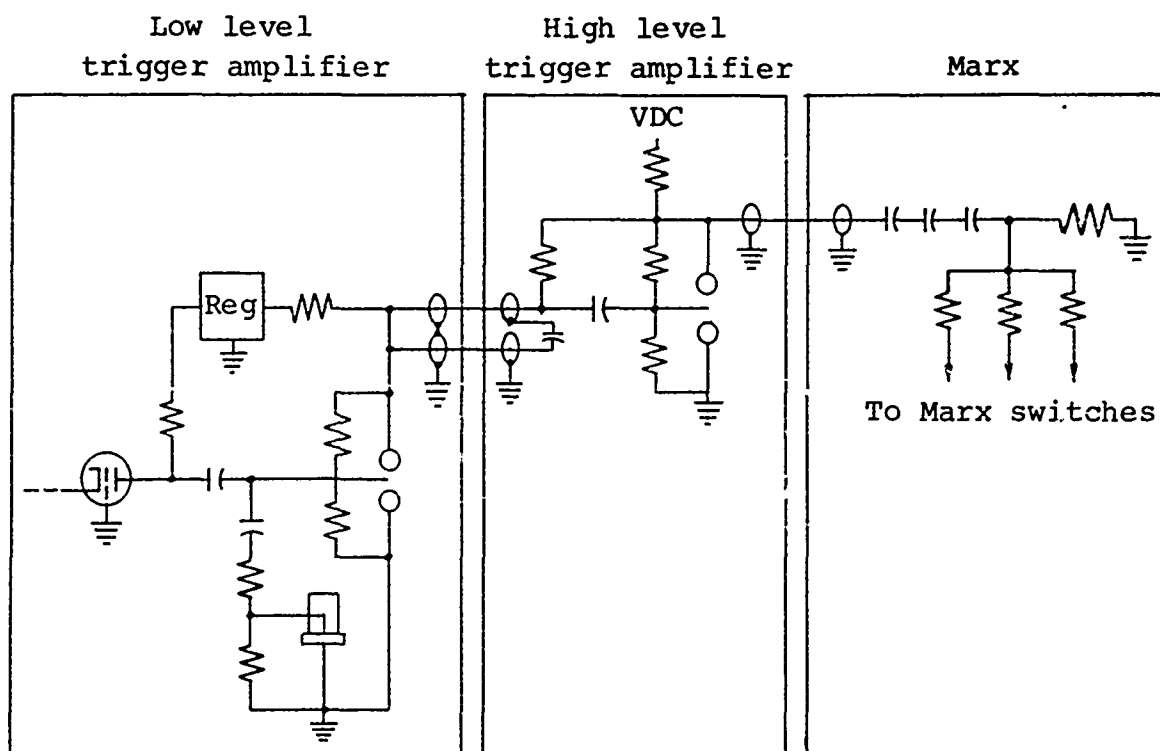
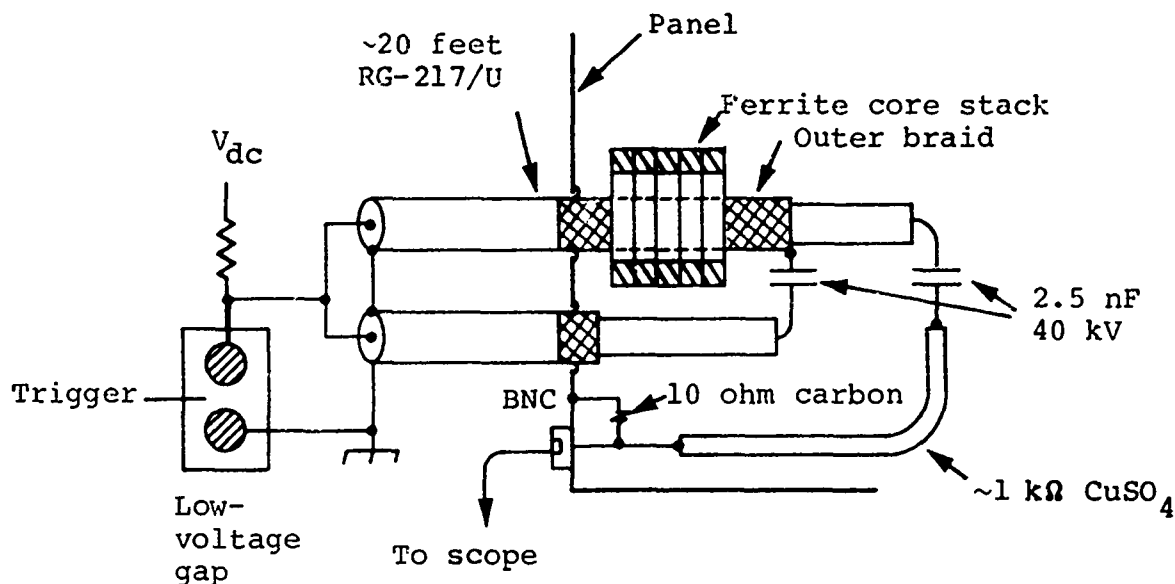


Figure 47 High level trigger amplifier chain.

was to measure how closely the output peak amplitude approximates the theoretical output (i.e., four times  $V_{dc}$ ), and to investigate risetime, waveshape, and other waveform details.



(Outer braids of both cables are grounded at the panel)

Figure 48 Cable-transformer test.

The monitor had a copper-sulfate resistor and carbon resistor in a voltage-divider arrangement, which is recognized as not being ideal. However, energies are low,  $\text{CuSO}_4$  heating effects are negligible, and the voltage across the carbon resistor is only a few hundred volts. The error due to the carbon resistor voltage coefficient is therefore  $< 4$  percent (assuming zero temperature coefficient for the  $\text{CuSO}_4$ ). Additionally, the divider was calibrated at a 10-kV level by discharging a 2.5-nF capacitor into it.

Three test shots were fired at  $V_{dc}$  amplitudes of 9, 16.4, and 19.6 kV. Even allowing for a 4 percent error, it was shown that a transformer efficiency of  $\gtrsim 75$  percent could be achieved. Moreover, the risetime was in the 5- to 10-nsec range.

This means that a 60- to 65-kV pulse is available for triggering the high-level gap that shorts the dc-charged Marx trigger cables. Since its voltage is only 60 to 75 kV, jitter of  $\approx 1$  nsec can be achieved in that gap. Also, the packaging of the ferrite cores allows the two input cables to be closely coiled or arranged in any desired manner without requiring specific layouts or spacings.

While the above high-level triggering scheme has been used before with success (in SIEGE II), it has a disadvantage associated with the lifetime of the Marx trigger cable. Both the dc-charging and possible Marx erection "kickback" transients contribute to reducing the cable lifetime. However, by selecting one of the larger standard coaxial cables (e.g., RG-220/U), reasonable lifetime can be obtained. A distinct advantage of this scheme is the fact that the condition of the trigger cable (whether or not it is shorted) can be easily checked by a simple dc voltage monitoring circuit. In TEMPS, this cable condition check is incorporated in the Marx charging interlock chain. If either Marx trigger cable is shorted, Marx charging will be inhibited.

A small trigger Marx was experimentally investigated as a backup high-level trigger amplifier. This Marx had three stages, used 2.5-nF 40-kV barium titanate capacitors, and directly fed a 50 $\Omega$  cable and termination. Its output was monitored by a fast

(< 1 nsec response) capacitive pickoff on the output cable. With the direct cable feed (i.e., no self-breaking output switch was employed) an erection risetime of about 10 nsec was observed. Charging voltages from 28 to 40 kV were applied. Both  $N_2$  and  $SF_6$  gas at 10 to 30 psig pressure were studied. Only the "lowest" gap was triggered by discharging a cable initially charged to 10 kV into a V/3 gap trigger electrode. The other two gaps were self-breaking, nearly uniform field types. All gaps and capacitors were in a common gas environment. The effect of ultraviolet light coupling between gaps was also studied.

Output voltages in the 70 to 95 kV range were observed. It was demonstrated that over a series of 20 shots taken 30 seconds apart, a peak-to-peak variation in delay of about 3.5 nsec was possible, implying subnanosecond rms jitter. Ultraviolet coupling between gaps (in some cases only between certain gaps) was shown to markedly reduce jitter; however, there were factors in the experimental setup that made it difficult to obtain good consistency and repeatability in the results. This amplifier had been intended to feed an uncharged Marx trigger cable, thereby maximizing that cable's life. But the desirability of continually checking the trigger cable condition, coupled with an interest in keeping development costs to a minimum, resulted in the decision to relegate the trigger Marx to a backup status.

Trigger System Controls, Monitoring, and Interlocking. To more adequately ensure that the trigger system is operating properly, the following operational checks were incorporated into the system:

- As part of the ARM function prior to every Marx charging, the trigger system is automatically test-fired and checked for proper operation and synchronization of the two Marx triggers. Any malfunction will inhibit Marx charging and require corrective maintenance.



- DC-charged Marx trigger cables are employed in the system. If either of these becomes shorted during Marx charging, the shot will be aborted and further charging prevented.
- Controls, monitors, and indicators are provided locally at each half bicone to permit rapid independent checkout or troubleshooting of that trigger system.
- As an operational diagnostic, circuitry is provided to detect a premature Marx erection (self-fire), to determine which Marx self-fire, and to indicate this information to observers at ground level.

In the interest of reliability, there was a strong desire to keep the trigger system design simple. Also, because it is necessarily a part of a high-voltage pulsed system, it is wise to minimize the usage of low-level semiconductor devices. However, at least one of the above stated objectives, the trigger synchronization or coincidence check, required circuitry capable of few nanosecond resolution. This could only be reasonably accomplished by fast semiconductor circuitry. Circuitry and packaging techniques were therefore provided that ensure the reliability of such devices. Careful attention was given to such areas as power supply bypassing or filtering, nested containers or compartmented chassis, and RFI gasketing in designing the system.

The circuitry associated with the other objectives stated above were somewhat less sensitive and/or slower than that associated with the trigger coincidence check. Therefore, the use of semiconductor elements for all necessary, fast, low-level circuitry seemed warranted and was incorporated into the system.

In the following discussion and figures, it will be convenient to use the nomenclature and shorthand symbols of electronic logic elements. Figure 49 defines those to be used here as well as some other block diagram symbols. In the logic circuitry discussed, "one-shots" with appropriate timing periods are used instead of "flip-flops" to eliminate the need for reset pulses.

Regarding the controls and timing, one half-bicone is called the master, or No. 1 side, while the other is the slave, or No. 2 side. All ground-linked controls are connected with the No. 1 side. It is also convenient to place the trigger detection and interlocking circuitry at the No. 1 side.

A portion of the trigger system shown in Figure B-3. Reference 12 is redrawn in Figure 50 in block logic form. This shows the method of producing the four basic signals needed for system monitoring and interlocking. These are:

- $A_1$  - No. 1 Marx trigger signal
- $B_1$  - No. 1 Marx monitor signal
- $A_2$  - No. 2 Marx trigger signal generated at No. 1 side
- $B_2$  - No. 2 Marx monitor signal generated at No. 1 side

Note that either the  $A_2'$  or  $B_2'$  will trigger the LED on the No. 2 side. These result in the appropriate  $A_2$  or  $B_2$  signal being generated at the No. 1 side according to whether or not the Command Fire one-shot has been triggered. In other words, if a signal arrives at the No. 1 P-M without the Command Fire one-shot having been triggered, it must have been caused by a No. 2 prefire as detected by the No. 2 Marx monitor. Therefore,


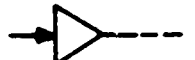



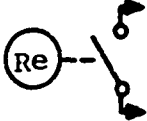

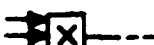
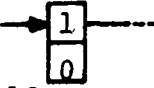
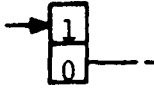
<u>Symbol</u>	<u>Meaning</u>
	Fixed time delay (e.g., cable)
	Amplifier or pulse shaper
	Capacitive pickoff on coaxial cable
	Photomultiplier tube
	Light emitting diode
	Relay
	"Or" circuit; output obtained if either or both inputs are present
	"And" circuit; output only obtained if all inputs are present
	Triggered 10 μsec "one-shot"; producing output dc gate only while timing
	Triggered 10 μsec "one-shot"; producing output dc gate only when not timing

Figure 49 Block diagram symbols.

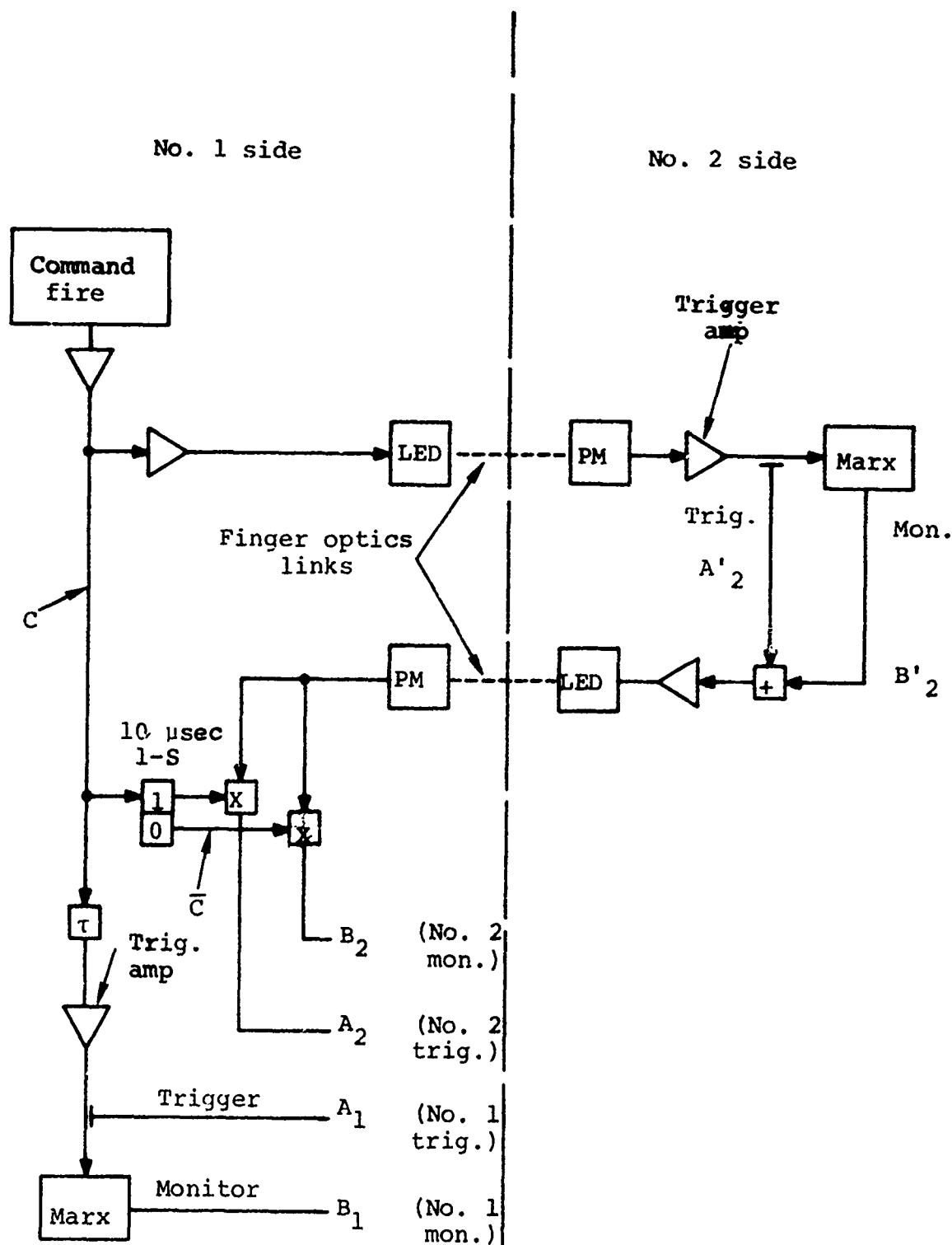


Figure 50 Generation of trigger timing signals.

the dc gating provided by the one-shot permits the  $B_2$  signal to be generated and not  $A_2$ . Conversely, following a command firing, the  $A_2'$  signal will be generated before the  $B_2'$  signal, resulting in the  $A_2$  signal being produced at the No. 1 side. The  $B_2$  signal generated later is of no consequence since the No. 2 LED driver circuitry is designed so that it cannot be retriggered before a long delay ( $\approx 10$  msec).

The four basic timing signals are processed to accomplish the trigger coincidence and prefire detection functions. The Marx-charging permissive is obtained after the system is test-fired during the ARM cycle only if the  $A_1$  and  $A_2$  signals are properly synchronized (within an established time "window" set by the coincidence circuit) and if the dc-charged trigger cables are not shorted.

Figure 51 illustrates the self-fire detection circuit. During normal firing, C precedes  $B_1$  and  $B_2$ . This inhibits the  $\bar{C}$  input to the circuit, preventing any output self-fire indication. If, say, No. 2 Marx self-fires,  $B_2$  will arrive before  $\bar{C}$  is removed, triggering the lower one-shot. This energizes the relay which causes the proper indication to be generated. The  $B_2$  signal also locks out the  $B_1$  output circuit. This prevents a double, ambiguous output indication in the event that the No. 2 self-fire causes the No. 1 Marx to erect. In the unlikely event that the two Marxes independently self-fire within 10 to 20 nsec of each other, the circuit time constants may result in an ambiguous double output indication. Note, however, that a self-fire is still definitely indicated; the only information not available is the identity of the first Marx to self-fire.

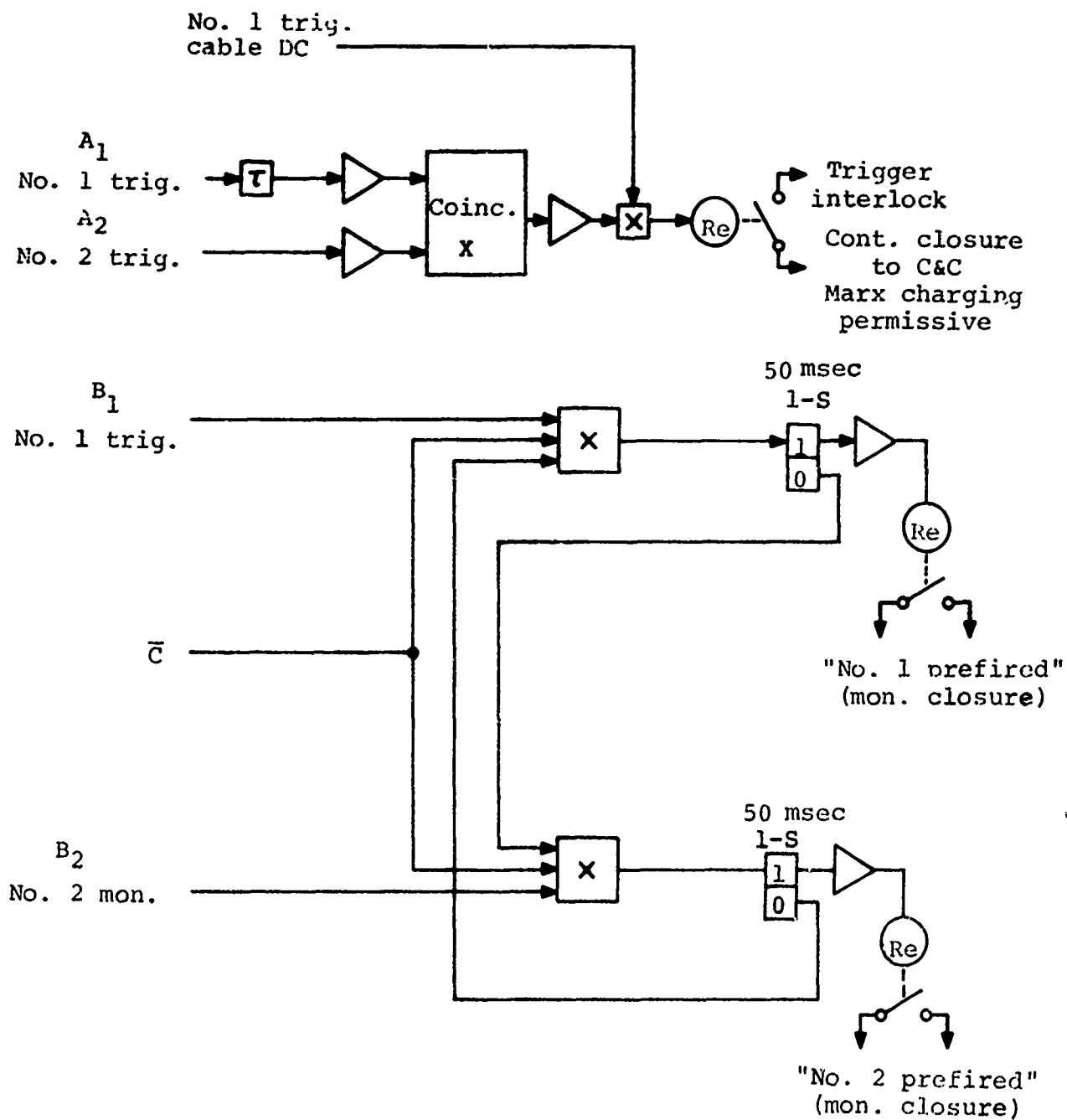


Figure 51 Interlock function generator

## 5.5 PRIMARY POWER SYSTEM (Figure 52)

To enhance the operation and maintenance of the TEMPS system, a continuous-charge primary power system is utilized.

5.5.1 Approach. A motor located within the C&C van drives a hydraulic pump. Oil is pumped at high pressure and low flow through nylon hydraulic lines to hydraulic motors located in the pulser. The hydraulic motors continuously charge on board 24-volt aircraft-type lead and batteries. The batteries supply the peak power demand during Marx charging.

5.5.2 Description. The charging system is similar to that used in the aircraft industry. It will be a 26-volt system with integral rectifiers and a voltage and current regulator. There are two batteries in each side of TEMPS, one for the trigger and control system and one for the Marx-charging supply. The voltage of the battery used to charge the Marx will sag during the short charging time. To prevent the voltage on the trigger-system battery from sagging at the same time, the batteries are isolated by diodes.

The charging-system power is 26 volts at 27 amperes or 700 watts average, which is more than sufficient power to keep the batteries at full charge even when the pulser is used at maximum duty.

The hydraulic lines are nylon reinforced with dacron and have a burst pressure of 8000 psi. Preliminary design calculations used a maximum pressure of 1000 psi and less than 2½ gal/min to each side for rated generator charging. The efficiency of the system is about 50 to 60 percent. The prime mover is a 5 horsepower electric motor.

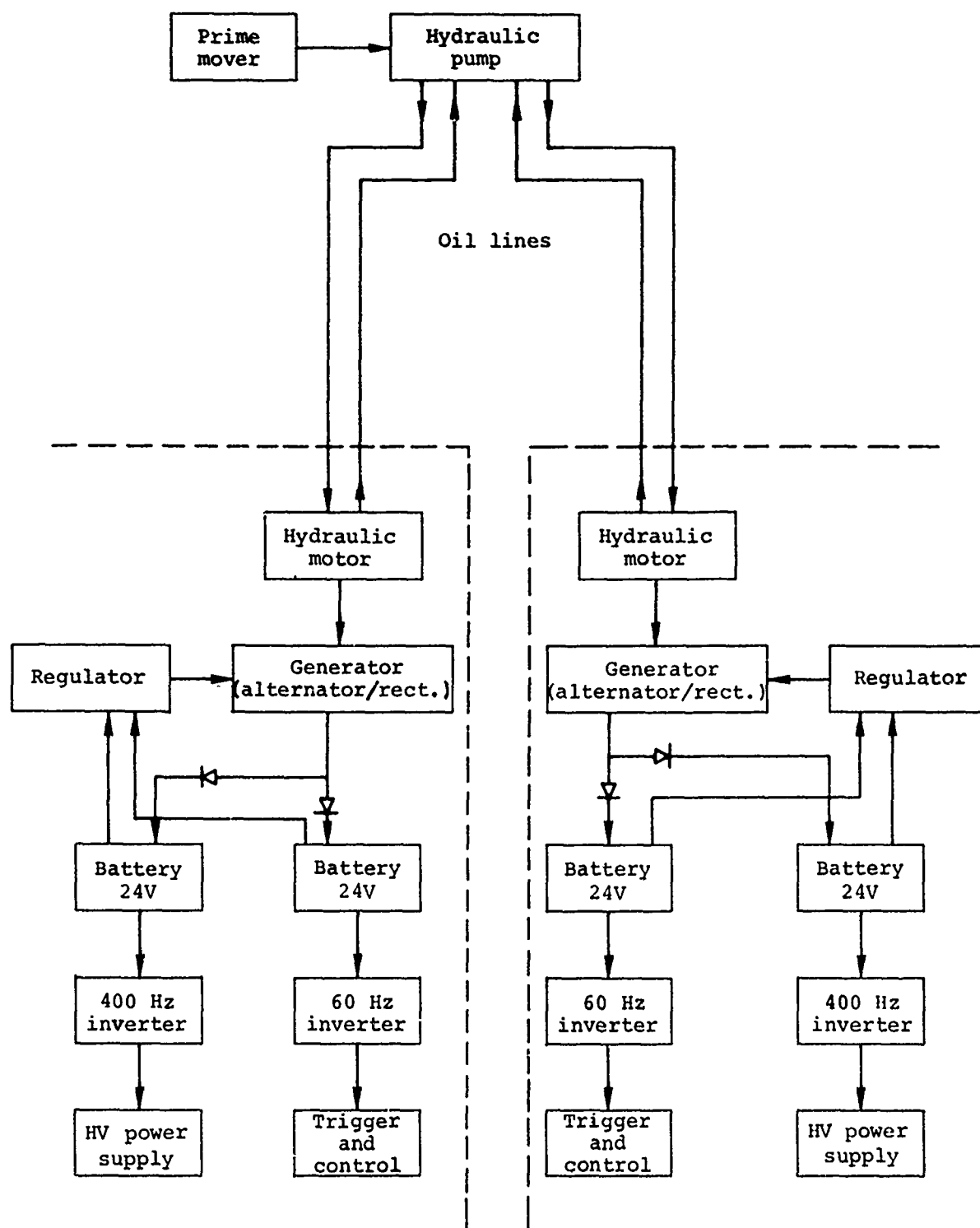


Figure 52 TEMPS primary power system.



## 5.6 COMMAND AND CONTROLS

### 5.6.1 Design Criteria.

- a. The operating controls must be high voltage and isolated from the pulser so that there can be no hard wires.
- b. Each Marx and associated controls must be isolated from the other.
- c. The system must also be lightweight, rugged, simple, and reliable.

5.6.2 Design Approach. The control functions are connected by pneumatic lines operated at pressures less than 60 psi. The air-operated components, such as solenoid-operated air valve, air-operated switches, electro-pneumatic transducers, and pneumatic rotary actuators are readily available catalog items. These are rugged, reliable components used for industrial control processes.

5.6.3 System Design. The control console, located in the C&C trailer, has all the controls necessary for normal operation of the TEMPS system. Located within the trailer is an air compressor to provide dry filtered air for the controls. A vacuum pump is also included so that the gas in the Marx spark gaps and output switch can easily be removed when necessary. The compressor, vacuum pump, control relays, warning lights, and warning horns will use 120-volt, 60-Hz line power, supplied either commercially or by a motor-generator set.

The controls on-board the pulser are air-operated where possible to conserve on-board power. The design is fail-safe, so that, if an air line should break, the pulser cannot be operated.

The control console is a U-shaped design with a visibility of more than 180 degrees through windows to the front and sides. The console panel arrangement is shown in Figure 53. All full panels are utilized, and one of the smaller corner panels will probably be used for the intercom and area speaker system controls. A full length rack is provided to the left rear of the control console for additional controls that might be required by HDL.

Using Figure 53 as a reference for position, the function of individual control panels will be described in the following paragraphs.

#### 5.6.4 Power Controls (Figure 54a).

##### Sequence of Operations

- a. Turn on the following circuit breakers:
  - a. Control
  - b. Interlock and warning
- b. Hydraulic power is turned on at the power unit in rear of trailer; the HYDRAULIC POWER OK lights come on.
- c. Air pressure is turned on at the compressor unit in rear of trailer. The AIR light comes on and the AIR gauge shows regulated pressure (60 psig).
- d. When vacuum is desired, turn on VAC PUMP breaker. VACUUM gauge will show vacuum in inches of mercury.
- e. INTLK lights come on when the air circuits are closed.

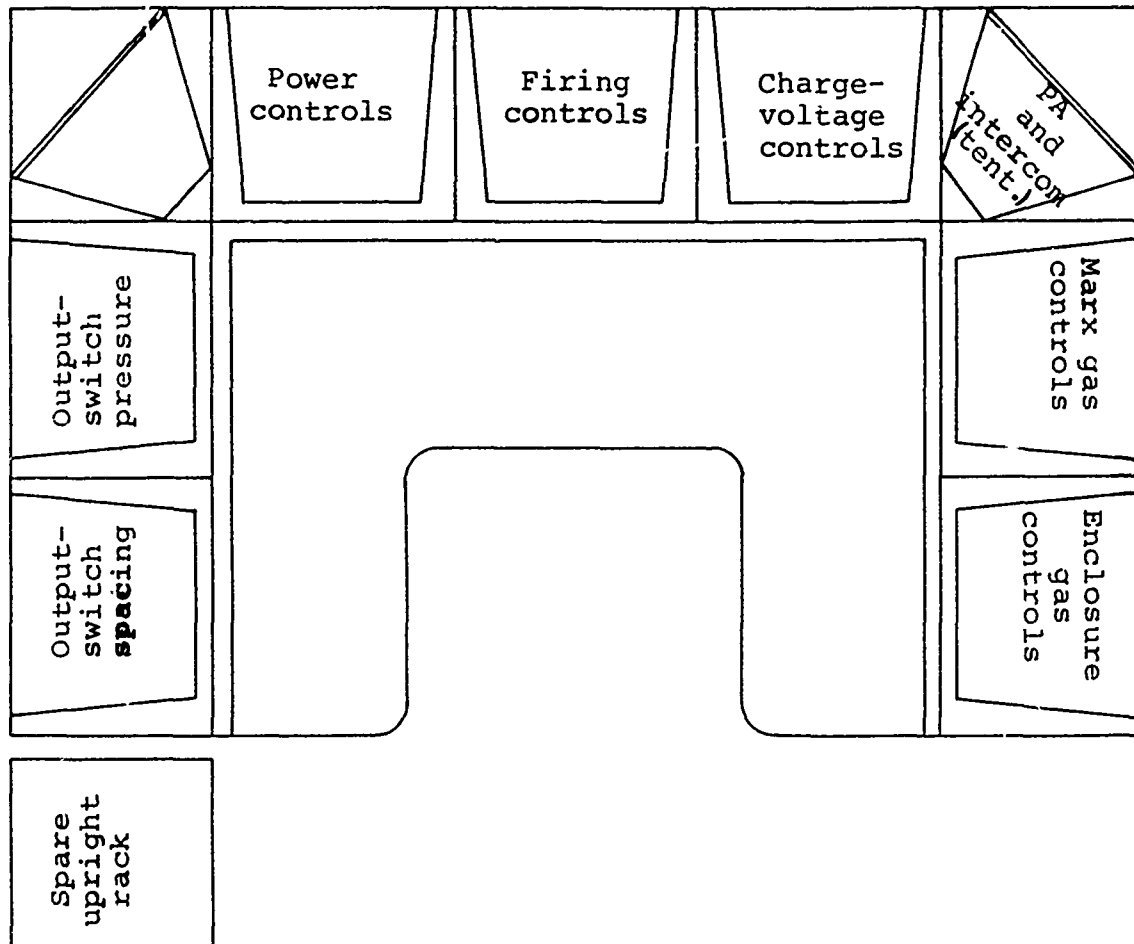


Figure 53 Command and control console layout.

### 5.6.5 Firing Controls (Figure 54b).

#### Sequence of Operations

- a. When interlock chain on the power panel is made up, the POWER indicator on the control panel turns green.
- b. PULSER POWER key is turned and POWER indicator changes from green to white. Area warning lights turn on. After a few seconds, the power lights for sides 1 and 2 come on white. One minute later, the ARM light comes on green.
- c. ARM key is turned and the ARM light turns from green to amber. (If either key is turned before its light is green, there is no response; neither light will turn green unless its key is off.)
- d. If all interlocks in the pulser are made up, the trigger system automatically goes through its checkout. When checkout is completed, the ARMED light for that side comes on amber. When both ARMED lights are on, the CHARGE light comes on green.
- e. When CHARGE button is depressed, it changes from green to amber, and warning horns come on. After charge is complete for either side, its CHARGE COMPLETE light comes on amber, and a stop charge signal is sent to the other side, which will stop charging when this signal reaches it or when it reaches its set point, whichever occurs first. The second side then sends down a signal turning on its CHARGE COMPLETE light.
- f. When both CHARGE COMPLETE lights are on, the FIRE button lights green and the fire circuit is enabled. FIRE button is pressed and it turns amber. This must be done before the maximum-charge-time timer times out; when the pneumatic fire signal reaches the pulser, it is triggered. After 20 seconds, to allow residual voltage to be read on the Marxes, the ABORT indicator turns from red to amber, the dump switches in the high-voltage power supplies close, and pneumatic signals are sent down from the pulser that turns off the ARMED lights, the CHARGED lights, and the warning horn.

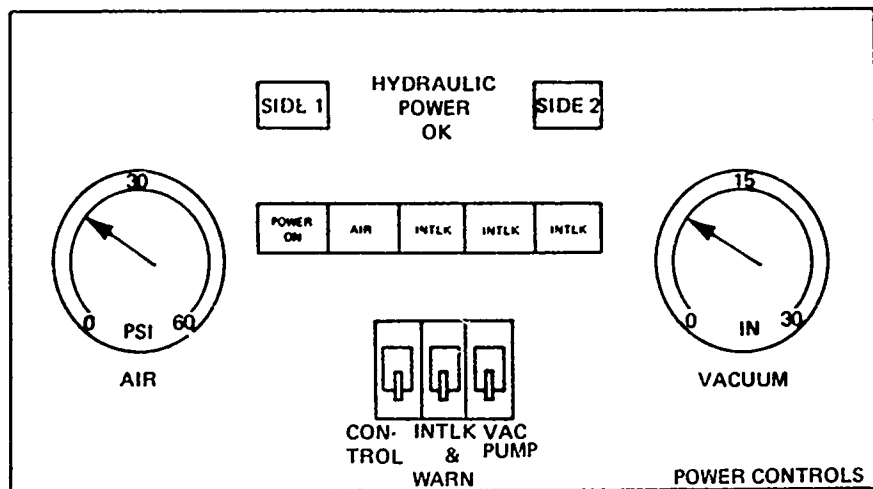


Figure 54a Power and firing controls.

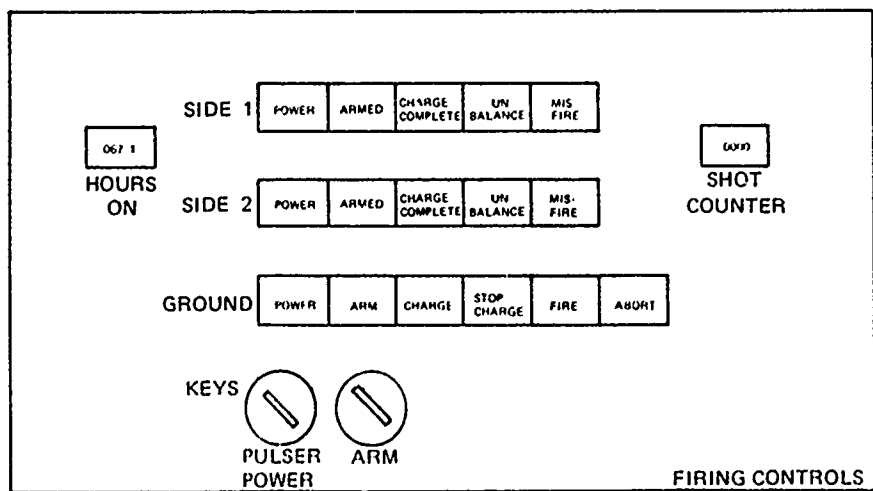


Figure 54b Power and firing controls.

g. ABORT button comes on red when the ARM key is turned on. It can now be pressed at any time, which causes it to turn amber and initiates abort. Abort is also initiated by opening any interlock in the pulser, by a two-minute limit on the time between arming and starting charge, by a limit on maximum charge time, by an unbalanced voltage or current in the pulser, or by a misfire. After an abort, the ARM and ABORT buttons remain amber and the UNBALANCE and MISFIRE indicators maintain state (either on, red, or off) until the ARM key is turned off.

h. UNBALANCE: Should an unbalanced voltage or current occur in one Marx, that Marx is aborted immediately and a pneumatic signal is set to the control panel, lighting an UNBALANCE light and activating the abort circuit. The ABORT indicator changes from red to amber and a pneumatic signal is sent to the other Marx, aborting it. The UNBALANCE light stays on until the ARM key is turned off.

i. MISFIRE: Should a prefire or late firing occur, the sequence is the same as for unbalance except that the appropriate MISFIRE indicator is lighted.

j. The HOURS ON timer records the time that the PULSER POWER is on.

k. The SHOT COUNTER records number of firings, including aborts, if charging has been started.

5.6.6 Charge Voltage Controls (Figure 55). This panel has two pressure regulators and gauges for producing pneumatic signals for setting the desired charge voltages. It also has two gauges for reading pneumatic signals indicating the charge voltage present.

5.6.7 Enclosure Gas Controls (Figure 55). This panel has valves and flow meters for controlling flow of Freon to the outer enclosure and of  $SF_6$  to the Marx enclosures. It also has pressure gauges and selector valves for reading pressures in the enclosures.

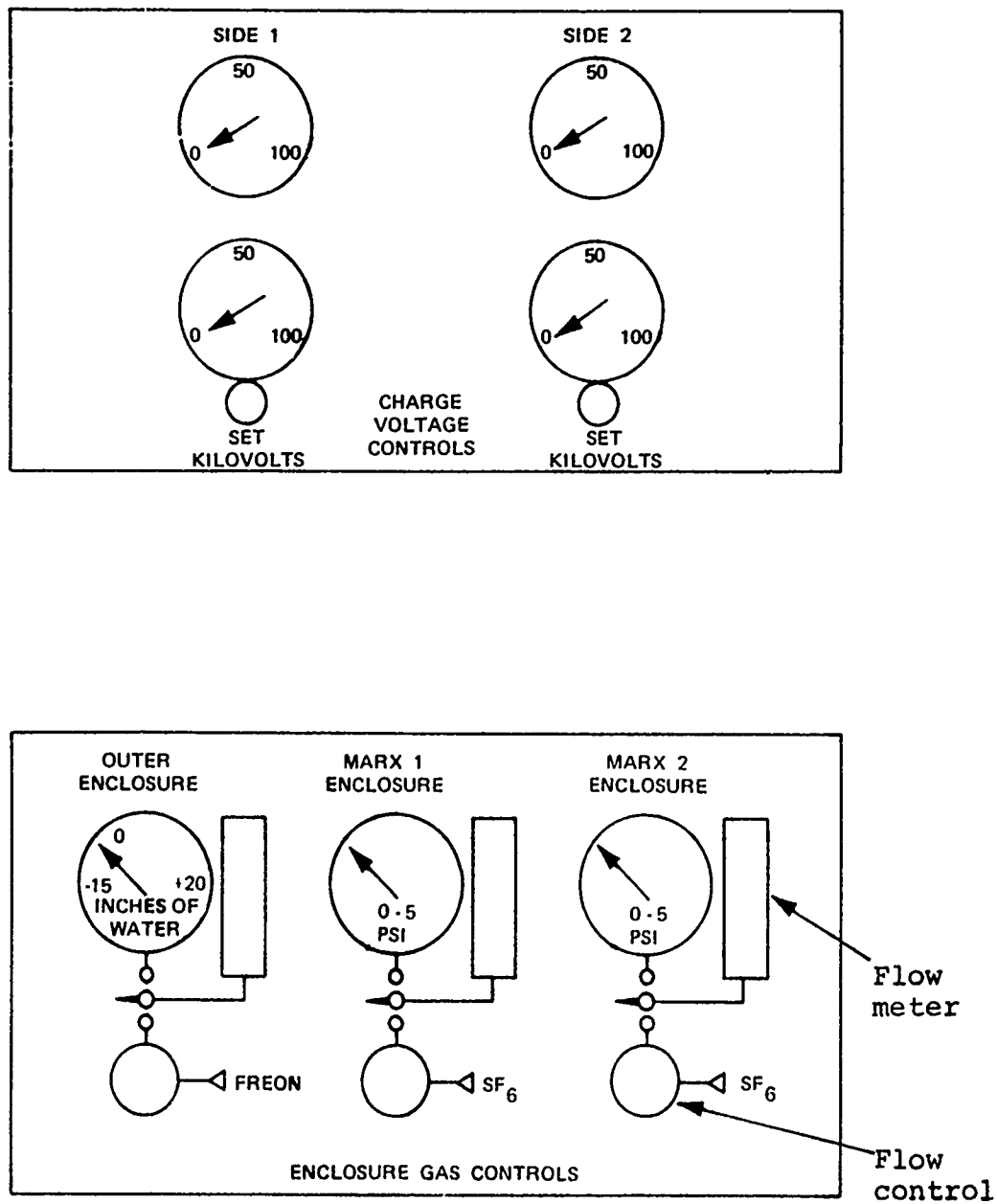


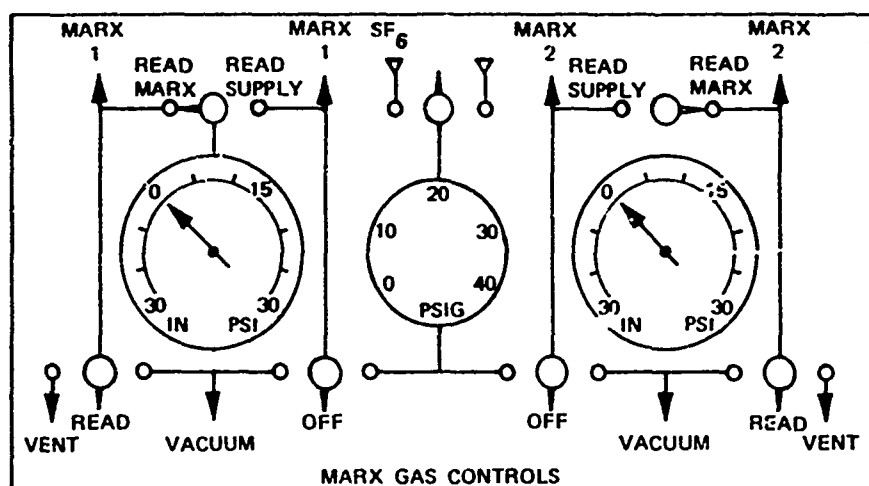
Figure 55 Charge voltage and enclosure gas controls.

5.6.8 Marx Switch Gas Controls (Figure 56). A valve selects  $\text{SF}_6$  or  $\text{N}_2$  from supply lines and directs it to a dial-type regulator for setting the desired pressure. Input lines to each Marx can be switched to either the regulated pressure or to the vacuum pump. Return lines from each Marx can be switched to a vent to atmosphere or to the vacuum pump, or they can be blocked. A compound gauge for each Marx can be switched to either the input or return line.

5.6.9 Output Switch Pressure (Figure 56). A valve selects  $\text{SF}_6$  or  $\text{N}_2$  from supply lines and directs it to a dial-tube regulator for setting the desired pressure. A single line to the output switch can be switched to either the regulated pressure or to a vent, or it can be blocked. The vent can be switched to either atmosphere or to the vacuum pump. A compound gauge is connected to the single line.

5.6.10 Output Switch Spacing (Figure 56). Hydraulic controls for adjusting and measuring the output-switch gap spacing are mounted on this panel, along with an instruction plaque for their operation.





ADJUSTABLE STOP  
SET AT 100 PSI

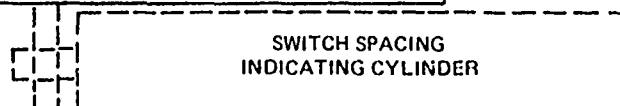
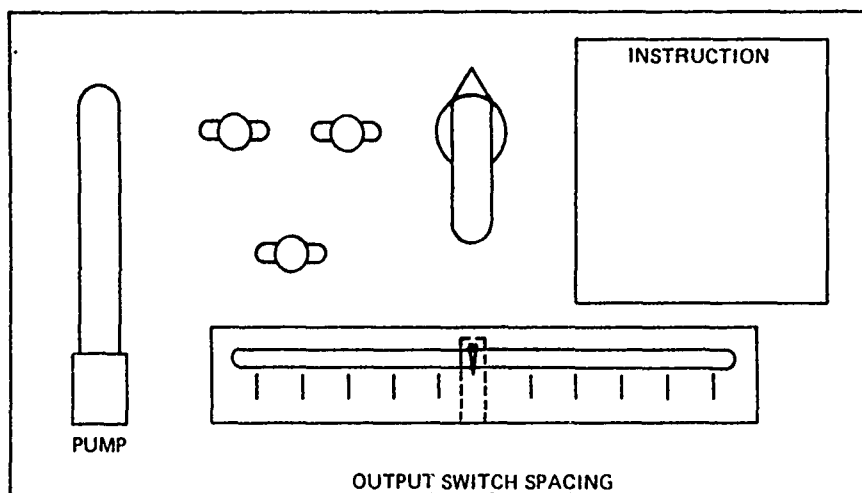
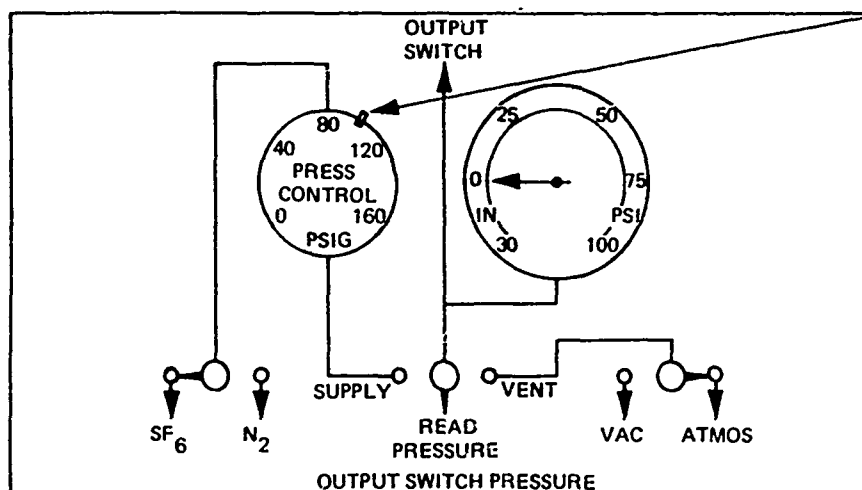


Figure 56 Marx gas and output-switch pressure and spacing controls.

## SECTION 6

### PULSER MECHANICAL DESIGN

#### 6.1 END ASSEMBLIES

The TEMPS pulser configuration is shown in Figures 1 and 57. It consists of two opposed pulse generator subassemblies, designated side 1 and side 2 assemblies, which are structurally coupled together by a fiberglass outer containment cylinder and are electrically coupled by a central output switch. Each side assembly contains all the basic elements of a pulse generator (i.e., a Marx generator assembly, peaking capacitors with associated power supply, controls, and triggering system). They differ in that the output switch is hard-mounted on the side 1 assembly while the side 2 assembly is fitted with a spring loaded plate which bears against the mating end face of the output switch to achieve electrical contact.

#### 6.2 END STRUCTURES

The end structure is a rather complex aluminum, hat-shaped weldment which is about 8-1/2 feet long and extends from a 42-inch diameter to the 11-foot, 2-inch diameter of the outer containment cylinder in two conical sections. The 42-inch-diameter end includes a hinged, dome-end closure and incorporates an internal flange which supports the Marx containment cylinder. The adjoining conical section is constructed of a

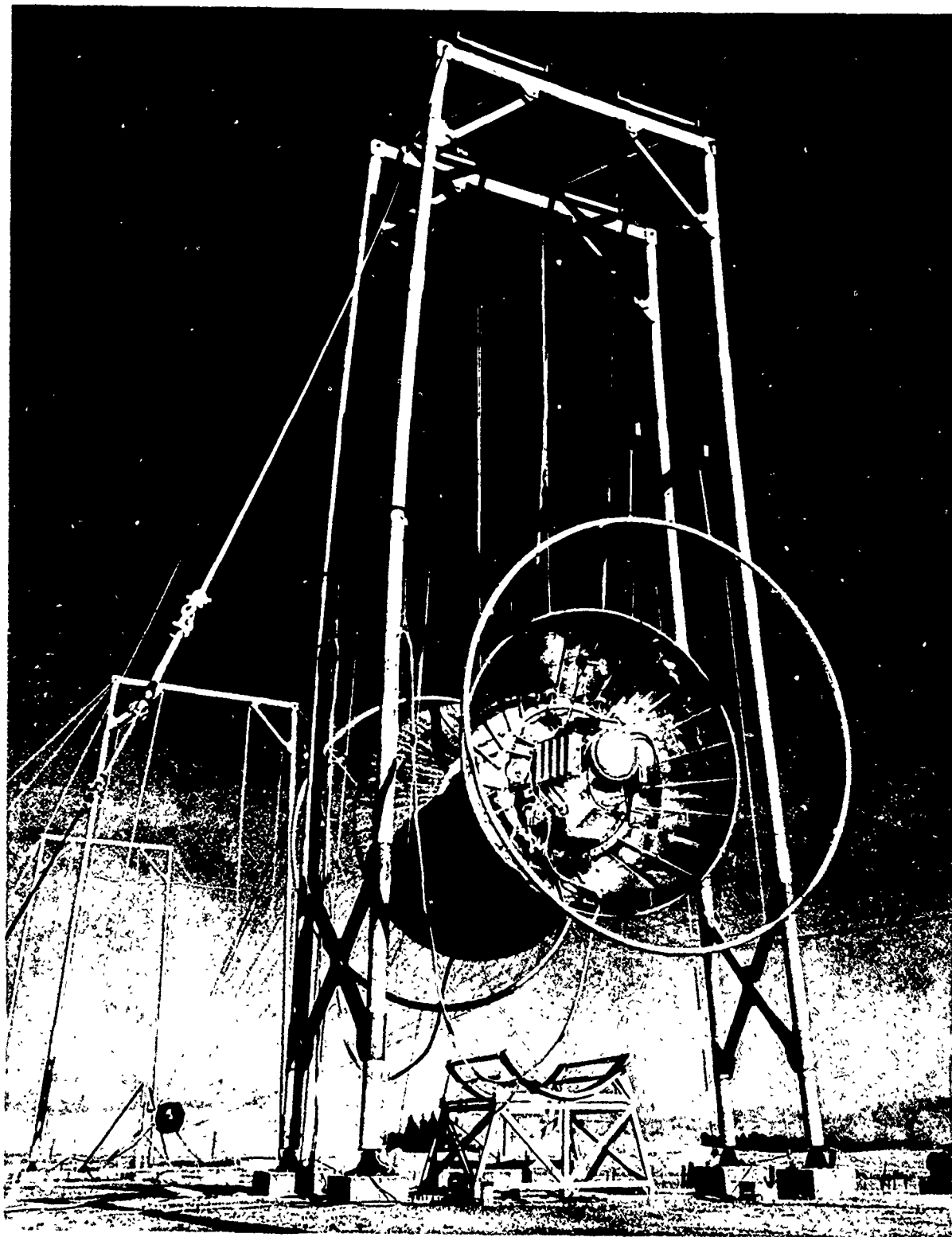


Figure 57 TEMPS pulser.

72-9-4-2

light aluminum tubular frame internally covered by 1/16-inch aluminum sheet. The adjacent larger conical section is covered by 3/16-inch aluminum which incorporates eight peaking capacitor mounting flanges and is joined to an 11-foot aluminum rollup made of 6-inch aluminum tubing. A short cylindrical skirt section joins the rollup to a 12-foot o.d. flange which mates with the outer containment cylinder on one side, and the bicone on the opposite side. The end structures also include provision for lifting the pulser (two support points per end structure) and for mounting the electrical enclosures and other subassemblies.

### 6.3 MARX CYLINDERS

The Marx containment cylinder is a 3-foot i.d. filament wound epoxy-fiberglass vessel approximately 9 feet long with an external flange on the mounting end and an internal flange on the opposite end. Gusseted support shelves, approximately 4 inches wide, made of G-10 grade fiberglass are bonded to the i.d. of the cylinder and run the length of the cylinder to support the Marx generator. The Marx cylinders mount on the internal flange of the end structure with a 1-1/4-inch-thick aluminum spacer ring sandwiched between flanges to obtain final stack-up dimensions for the pulser half assemblies. A 1/4-inch-thick aluminum backup ring bears on the outboard face of the fiberglass flange to distribute mounting bolt loads.

### 6.4 SUPPORT CONES

The inner support cones are octagonal shaped cone pieces constructed of 3/32-inch-thick aluminum with flanges on each end.

The support cones attach to the end of the Marx containment cylinders and include eight openings fitted with special finger stock which mate with the bottom peaking capacitor end plates. The output switch assembly bolts directly on the end of one of the inner support cones (side 1) and extends to the opposing inner support cone (side 2) where electrical contact is achieved by a spring-loaded face plate retained in the cone. Eight 1-1/2-inch-diameter nylon tie rods connect each inner support cone to the adjacent end structure to provide added structural rigidity and limited deflections of the otherwise cantilevered subassemblies. Closure of the Marx containment volume is completed by 30-inch-diameter aluminum end plates which bolt on the face of adjoining inner support cone flanges and include O-ring seals.

#### 6.5 OUTER CONTAINMENT CYLINDER

The outer containment cylinder is an epoxy-fiberglass cylinder, 11-foot, 2-1/2-inch i.d. by 14 feet long with integral flanges on each end. Aluminum rings with blind threaded holes are built into the flanges to provide additional strength and to grade electrical fields at the interface with the end structures and bicones. The metal rings face against 1-inch-thick fiberglass flanges which are integrally formed with the adjacent 5/8-inch-thick cylinder wall; the 5/8-inch wall extends 2 feet from each flange and then transitions to the 1/4-inch wall thickness forming the balance of the cylinder. There are approximately 18 layers of fiberglass per 1/4-inch thickness bonded with epoxy resin to produce biaxial yield strengths of at least 35,000 psi. Sealing of the flange joints between the outer containment and the two end structures is effected by 3/8-inch O-rings.

## 6.6 BICONES

The pulser bicones are constructed of a light tubular welded frame with 12-foot o.d. flanges, 1 inch thick, which bolt to the end structures. The bicones extend from the 12-foot diameter of the end structure to a 23-foot diameter with an included half angle of 40.5 degrees and are covered by 0.050-inch-thick aluminum skin which is riveted to the welded framework. The bicones are made in four matched quadrant sections which bolt together and can be easily disassembled for transport. Two 10-inch-diameter openings are provided in the top of each bicone for passage of the pulser lifting straps which are shackled to the end structure. A third opening on the bicone "TDC" is provided for the 2-inch fiberglass crossover tube which runs from bicone to bicone and contains communication lines between pulser ends. Intermediate supports for the 18.5-foot-long crossover tube are provided at 6-foot intervals by vertical fiberglass standpipes attached to the top of the outer containment cylinder.

## 6.7 ELECTRICAL BOXES

There are four aluminum electrical equipment enclosure boxes which mount on the exterior of each end structure of the pulser. These boxes contain primary power alternator and batteries, trigger system components, high voltage equipment, and system controls. The enclosures on each side of the pulser are coupled together with on-board electrical cables and are controlled through pneumatic lines which are routed with other hydraulic and gas lines to a common junction block mounted on each end of the pulser. Quick disconnect couplings are used to

connect 250-foot-long umbilical tube bundles from the Command and Control trailer to the pulser junction blocks. The two umbilical tube bundles are supported on the support structure and the pulser bicones.

#### 6.8 EQUALIZING AND MONITORING RESISTORS

The pulser is equipped with a pair of copper sulphate resistors which span across the output switch from inner support cone to inner support cone. These resistors are roughly 1 inch in diameter by 6 feet long and are electrically coupled to the output end of the two Marx generators to ensure equalization of dc charge voltage between pulser halves. In addition, similar resistors, approximately 3-1/2 feet long, are provided which span from each inner support cone to the adjacent end structure to monitor the voltage across peaking capacitors.

#### 6.9 OUTPUT SHORTING ASSEMBLY

Protection against pulser misfiring is also incorporated into the TEMPS pulser design by virtue of output shorting assemblies which act as electrical shorting paths from the support cones to the end structures. These devices are pneumatically operated cylinders which mount on the end structure and are extended to nearly touch the inner support cones during pulser charging. The cylinder rods retract within the two-second-period immediately preceding firing.

#### 6.10 OUTPUT SWITCH

TEMPS employs a self-closing, gas pressurized, near uniform field output switch that is located in the center of the pulser.

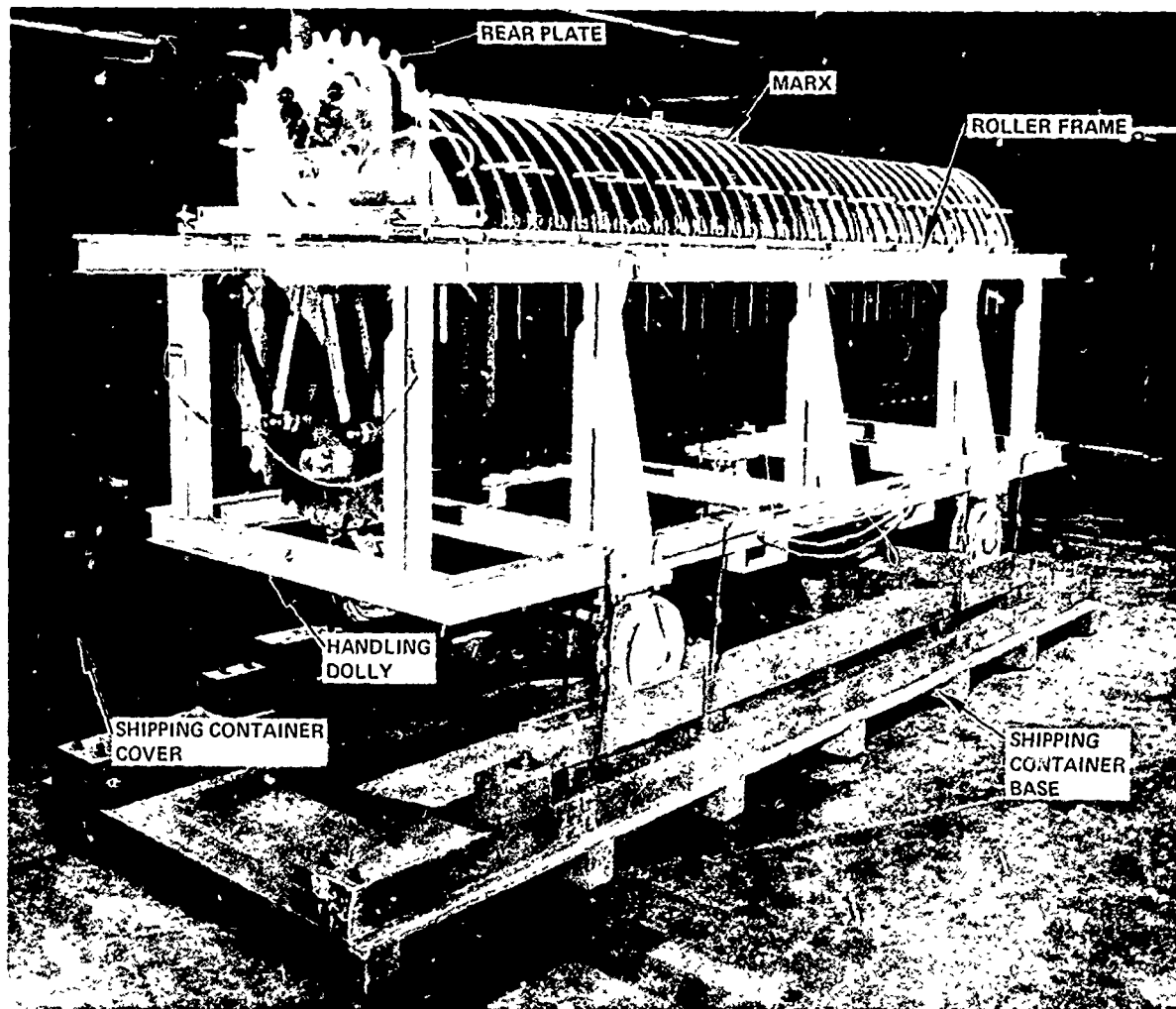
The output switch consists of a filament wound epoxy-fiberglass housing 30 inches in diameter by 43½ inches long with aluminum end domes and stainless steel electrodes. One electrode is fixed while the opposing electrode is hydraulically adjustable to vary the gap from 1.3 cm to 25 cm. The switch is designed for working pressures of up to 100 psig as well as a full vacuum. The overall length of the output switch is 45 inches and except for the two 4-foot-diameter flanges at each end of the housing the maximum diameter is 38 inches at the flanges. The weight of the fully assembled switch is 470 pounds.

Remote adjustment of the switch gap is effected by means of a master cylinder, assembled inside the output switch, and a slave cylinder and hand pump mounted on the TEMPS control console. When the cylinders are coupled together by two 1/2-inch hydraulic lines and the system is properly bled, adjustment is made by manually operating the hand pump to force the fluid into the master cylinder; the resultant return fluid from the master cylinder is introduced into the slave cylinder thereby resulting in identical movement of the cylinder rods so that electrode position is accurately tracked for remote indication at the control console.

#### 6.11 MARX GENERATOR ASSEMBLIES

The TEMPS Marx generator, shown in Figure 58 on the handling dolly, weighs approximately 1 ton and is 34 inches in diameter by 111 inches long. The 3.5-MV Marx contains 35 stages of energy storage capacitors with associated rail gap switches, resistors, insulators, and hardware to form a complete unit. Two such Marx generators are employed in the pulser.





72-11-47

Figure 58 Marx generator assembly.

The Marx generator is assembled to a light fiberglass frame equipped with rollers spaced along either side of the frame. The roller frame assembly requires the additional support of the rails provided on the handling dolly or those built into the Marx containment cylinders in the pulser. Transfer of the Marx generator from the handling dolly to the pulser is accomplished by aligning the dolly rails to the housing rails, and rolling the Marx inside the housing. Five spring loaded contacts shown in Figure 59, automatically couple the output end of the Marx to the pulser when fully inserted in the housing as shown in Figure 60. The exposed rear plate of the Marx fastens to the pulser to lock the Marx in position and form a uniform current return path. The rear plate also provides a convenient mounting surface for trigger circuitry, charging resistor connections, case coupling connections, and switch gap gas connections.

Each of the 35 stages of the Marx generator is comprised of the following components:

- (1) Energy storage capacitors, Figure 10.
- (2) Rail gap switch, Figure 11.
- (3) Series current limiting resistor, Figure 61.
- (4) Storage capacitor adapter bar, Figure 62.
- (5) Charging connectors, Figure 63.
- (6) Potted resistors:
  - (a) Trigger coupling resistor, Figure 64.
  - (b) Charging resistors, Figure 12.
  - (c) Case-to-case coupling resistor, Figure 65.

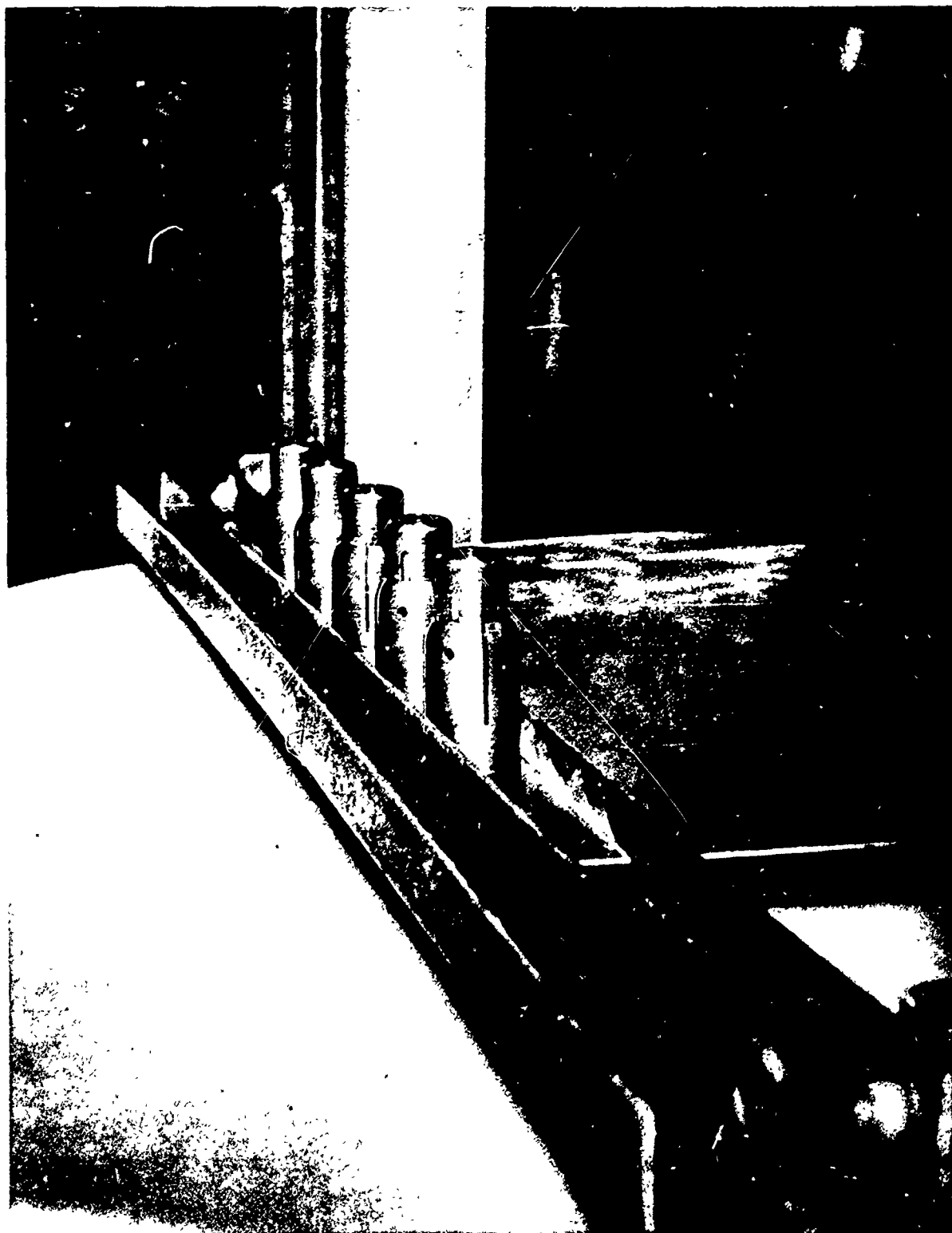
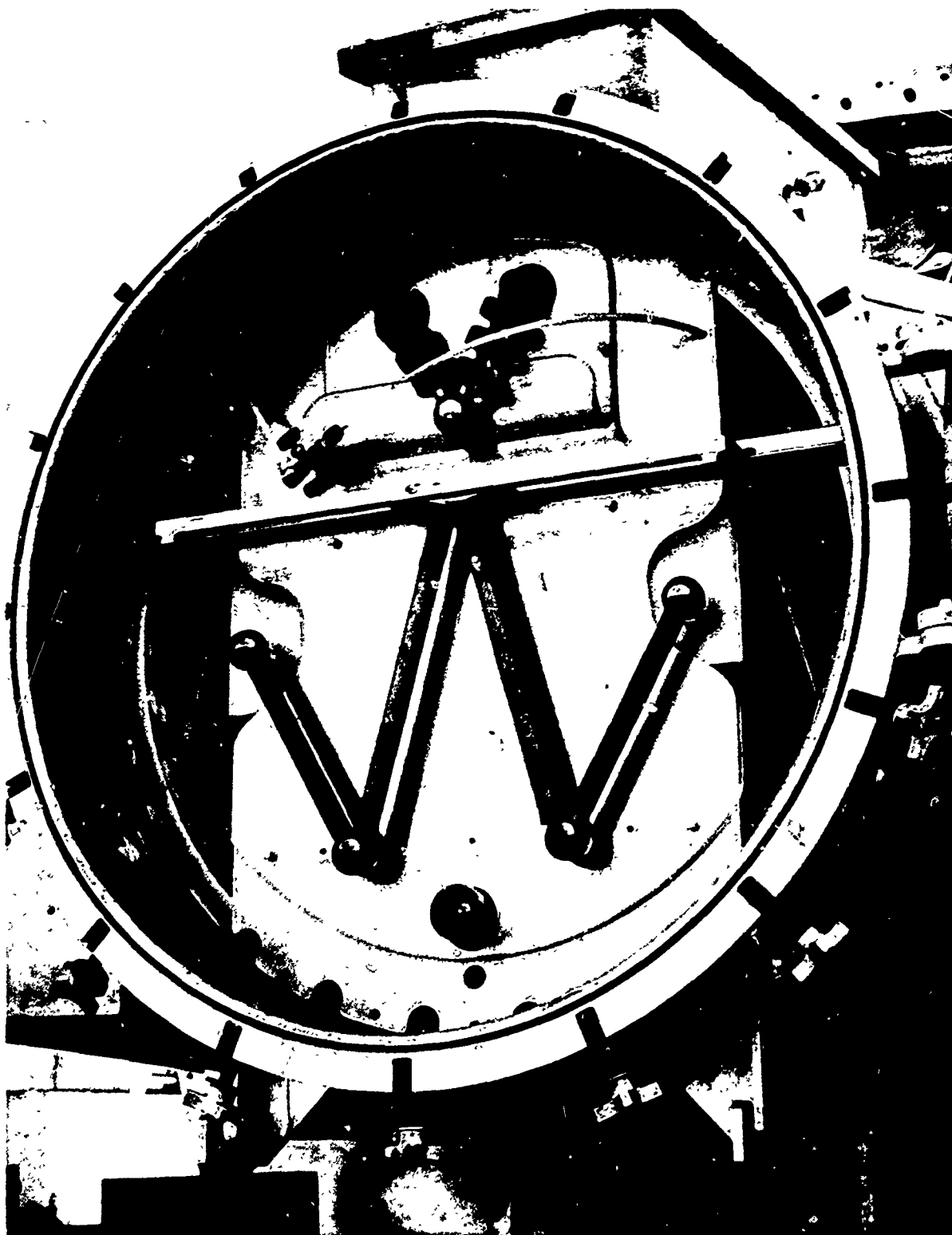


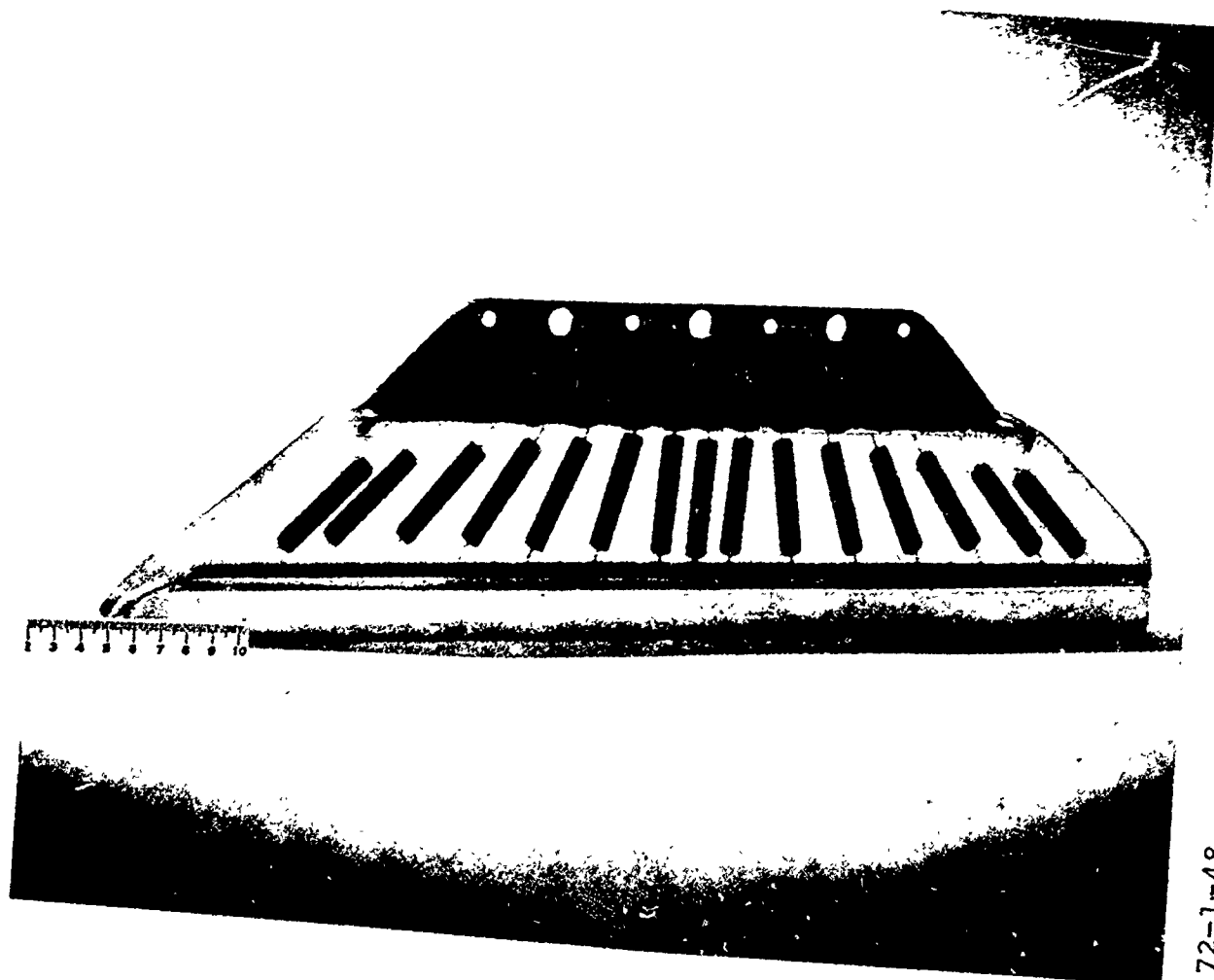
Figure 59 Marx output contact connectors.

72-4-15



72-8-27-2

Figure 60 Marx rear plate assembly.



72-1-48

Figure 61 Series current limiting resistor.

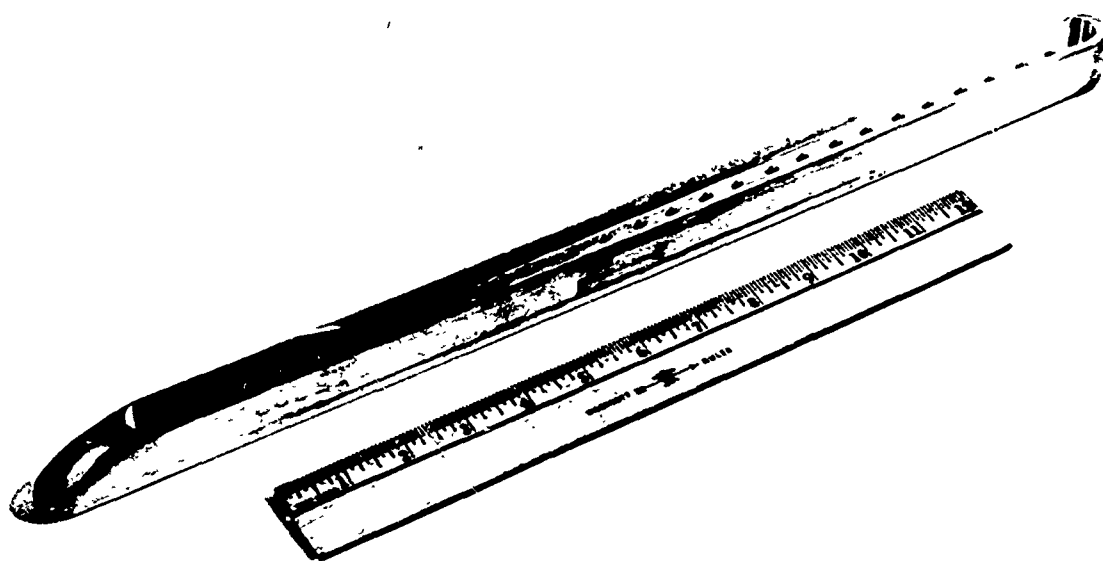
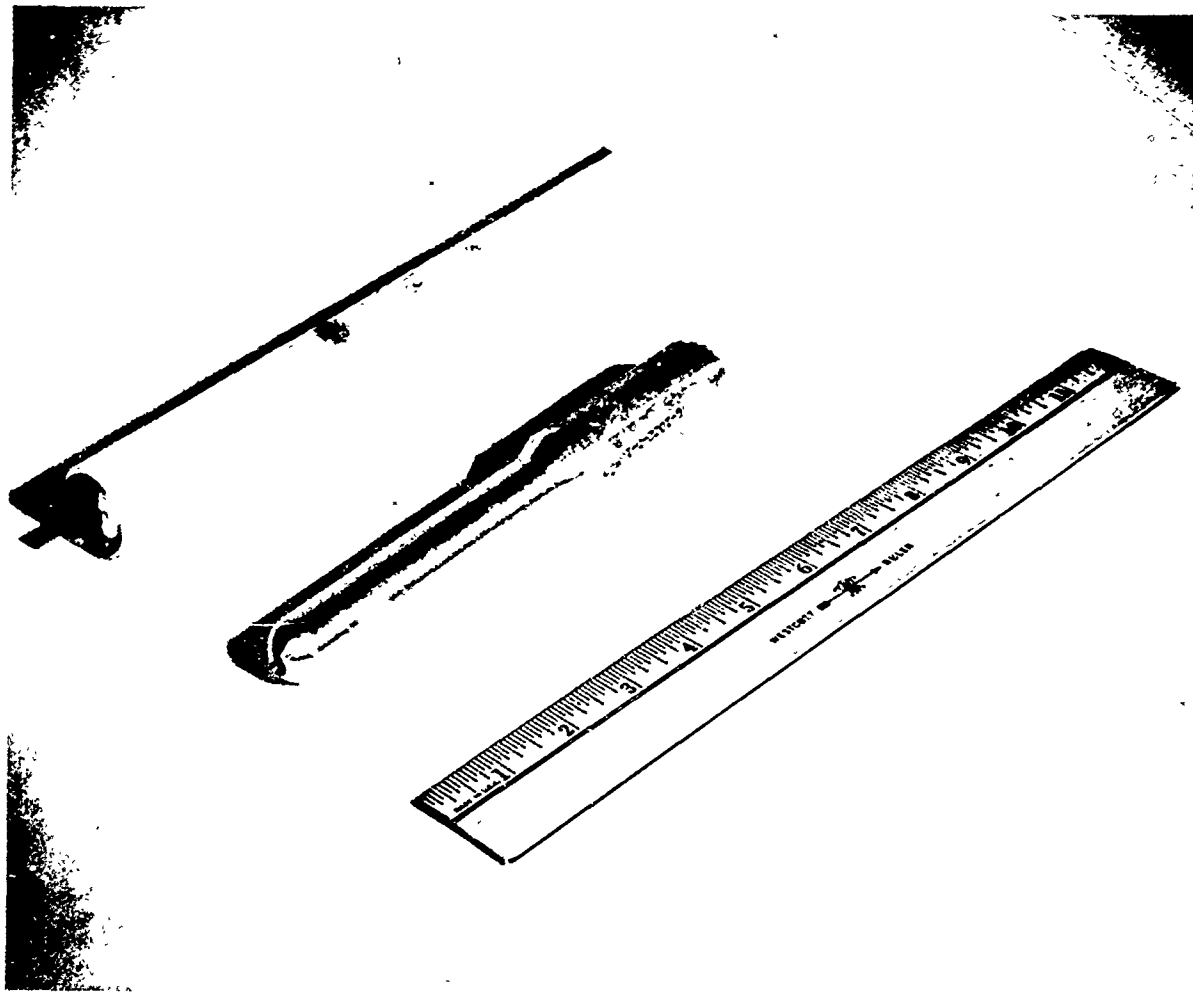


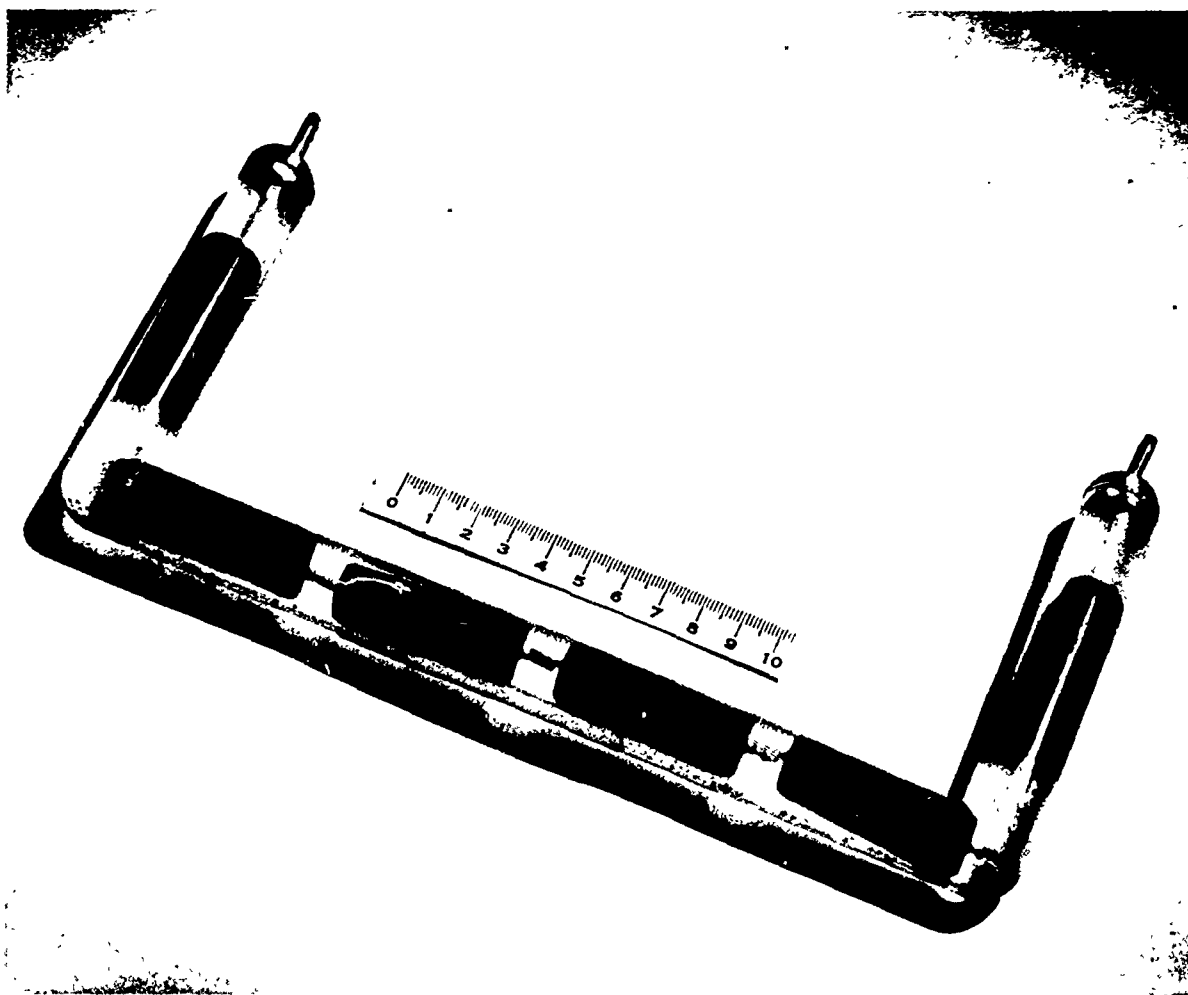
Figure 62 Storage capacitor adapter bar.

72-4-11



72-4-12

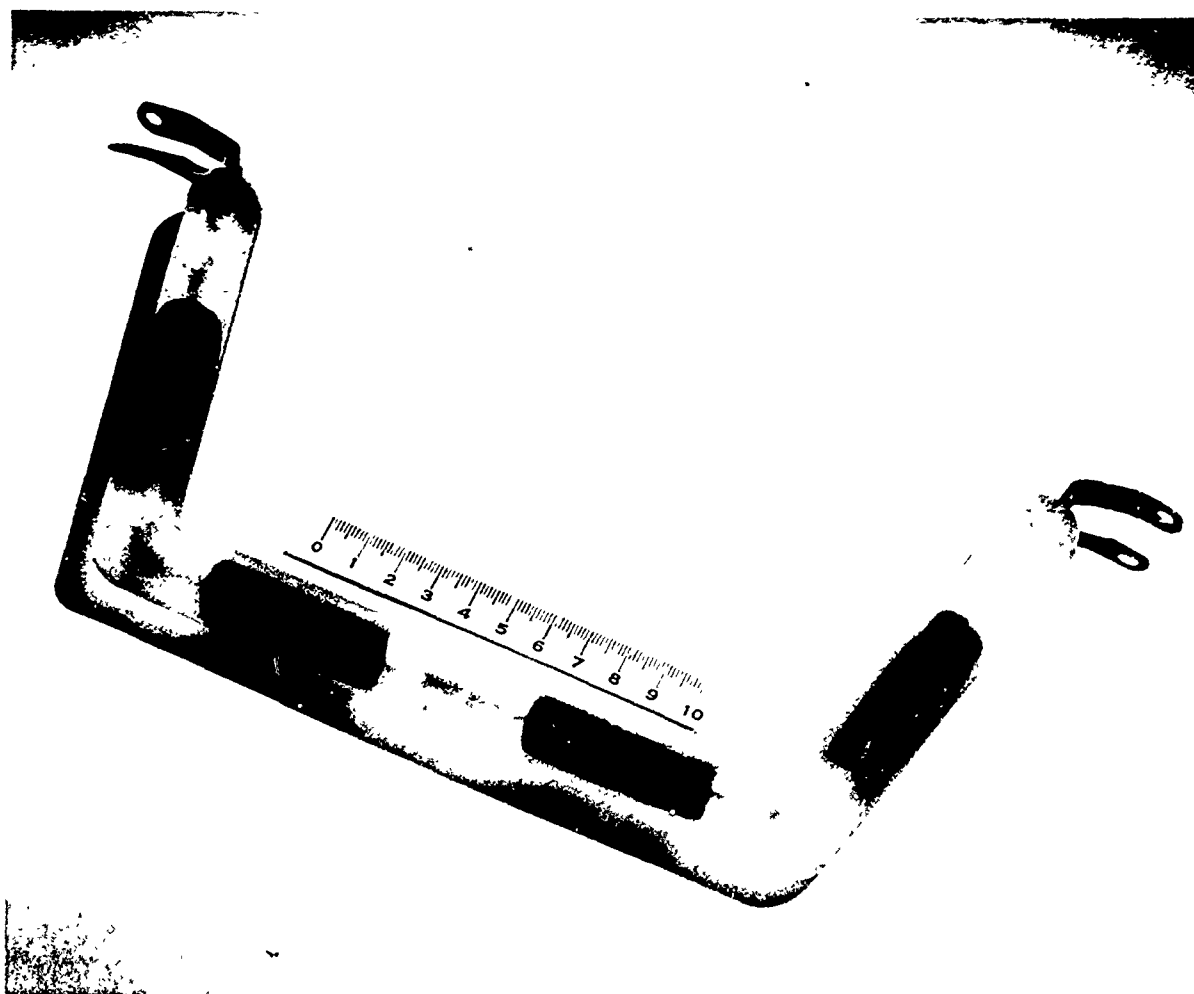
Figure 63 Marx charging connectors.



72-2-2

Figure 64 Trigger coupling resistor.





72-2-3

Figure 65 Case-to-case coupling resistor.

(7) High voltage barriers (Figure 66):

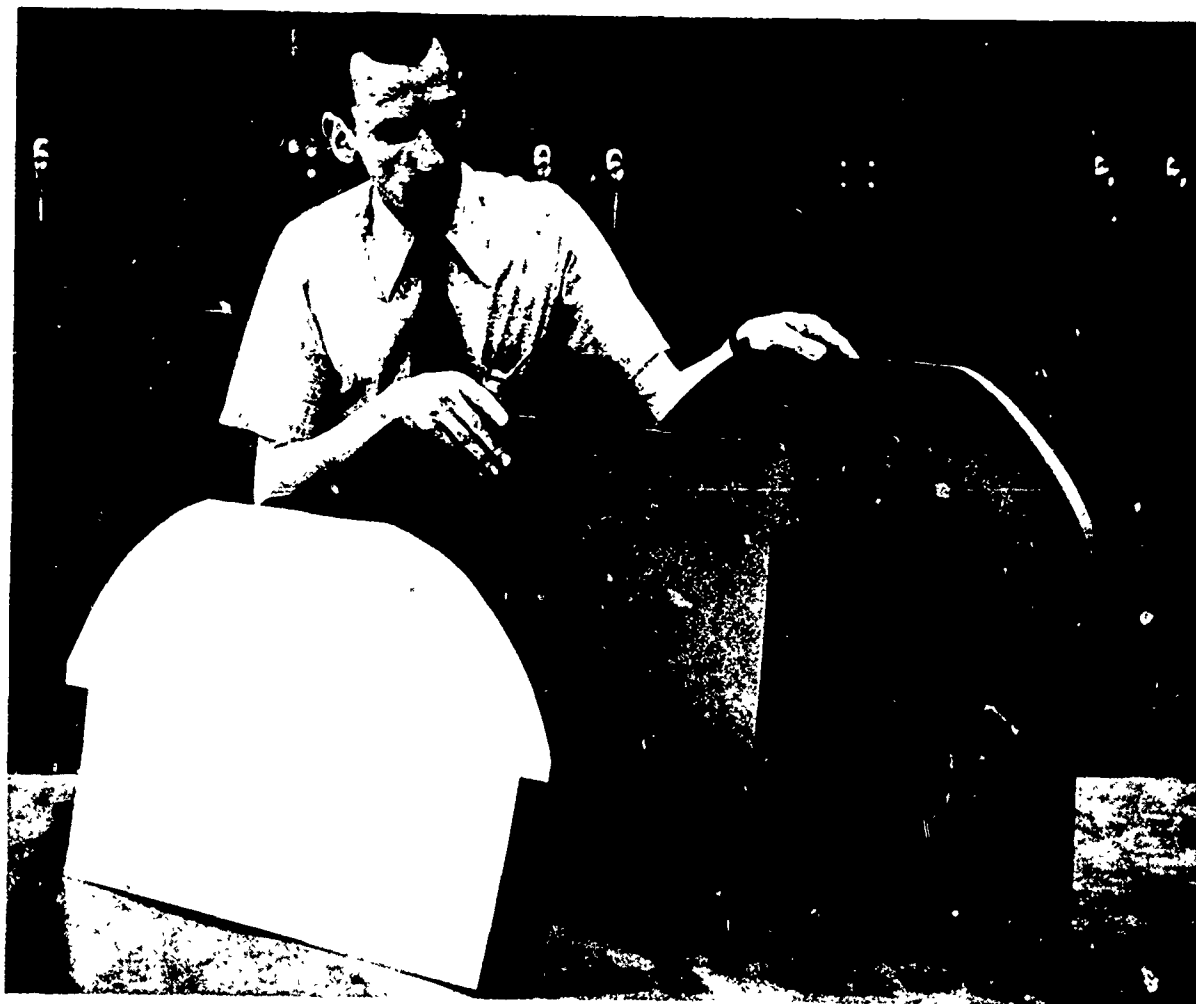
- (a) Stage insulator; insulator on right.
- (b) Interstage insulator; insulator on left.
- (c) Switch coupling insulator; insulator in center.

The energy storage capacitors are attached to the roller frame assembly which rests on the handling dolly rails; the above components are then added to build up the Marx stage by stage.

Two probes are attached to the high voltage end of each Marx which serve as an interface for resistively coupling the charging string of both Marx generators within the pulser. The probes engage in a spring loaded receptacle in the inner support cone which connects to a pair of equalizing resistors suspended across the output switch. Thus, the charging string of the two Marxes is resistively coupled to ensure equalization during charging. The trigger input resistors, initial case-to-case resistor, and the initial charge resistors are connected to the first few low voltage stages of the Marx assemblies.

#### 6.12 PEAKING CAPACITORS

The TEMPS pulser houses 16 peaking capacitor modules. Eight of these modules are installed, in a conical orientation, between the support structures and inner support cones of each half of the pulser. The peaking capacitors supply the early-time fast-rising output load current that the Marx generators, because of their stray series inductance, cannot supply.



72-4-13

Figure 66 Stage insulators.

The TEMPS peaking capacitor, shown in Figure 37, weighs 186 pounds, with an overall length of 40 inches and a 15-1/2-inch nominal diameter. The capacitor is comprised of a stack of lightweight honeycomb reinforced stainless steel electrodes, separated by multilayered polypropylene disks. The stack of electrodes is surrounded by polyethylene gradient rings which form an intermediate cylinder between the o.d. of the electrodes and the i.d. of the fiberglass outer housing. The housing incorporates fiberglass flanges which bolt to the top and bottom capacitor plates with O-ring seals to form a leak tight unit. The entire peaking capacitor is assembled under a glycol-water solution which completely fills all voids in the assembled capacitor. A volume compensator device mounts on the top plate and is connected to the capacitor interior to accommodate volumetric fluid changes due to ambient temperature fluctuations.

#### 6.13 OUTPUT SHORTING ASSEMBLY

The output shorting assembly is a device that shorts across the peaking capacitors to protect against fault conditions during system charging. Each of the two pulser sides is equipped with a pneumatically operated shorting rod mounted on the end structures with separate actuator assemblies. The shorting rods are extended across the peaking capacitors from the pulser end structures to inner support cones during the charging sequence and are withdrawn immediately prior to the fire command.

The pneumatic cylinders are double acting cylinders with a 1-1/2-inch bore and a 1/2-inch-diameter rod which has a 39-1/4-inch working stroke. The rod end of the cylinder is fitted with a special split contact ring which conducts electrical energy

from the rod to the pulser end structure. The rod end is equipped with a ball electrode which comes within 1/8-inch of touching the inner support cone when the rod is extended. The cylinder also incorporates limit switches for remote indication of rod position, i.e., fully extended or fully retracted.

The cylinders are operated from pneumatic control units also mounted on the pulser end structures adjacent to the cylinders. The control units include two small accumulators, supplied from pulser control air, and actuating valves which are integrated into the command and control system logic.

## SECTION 7

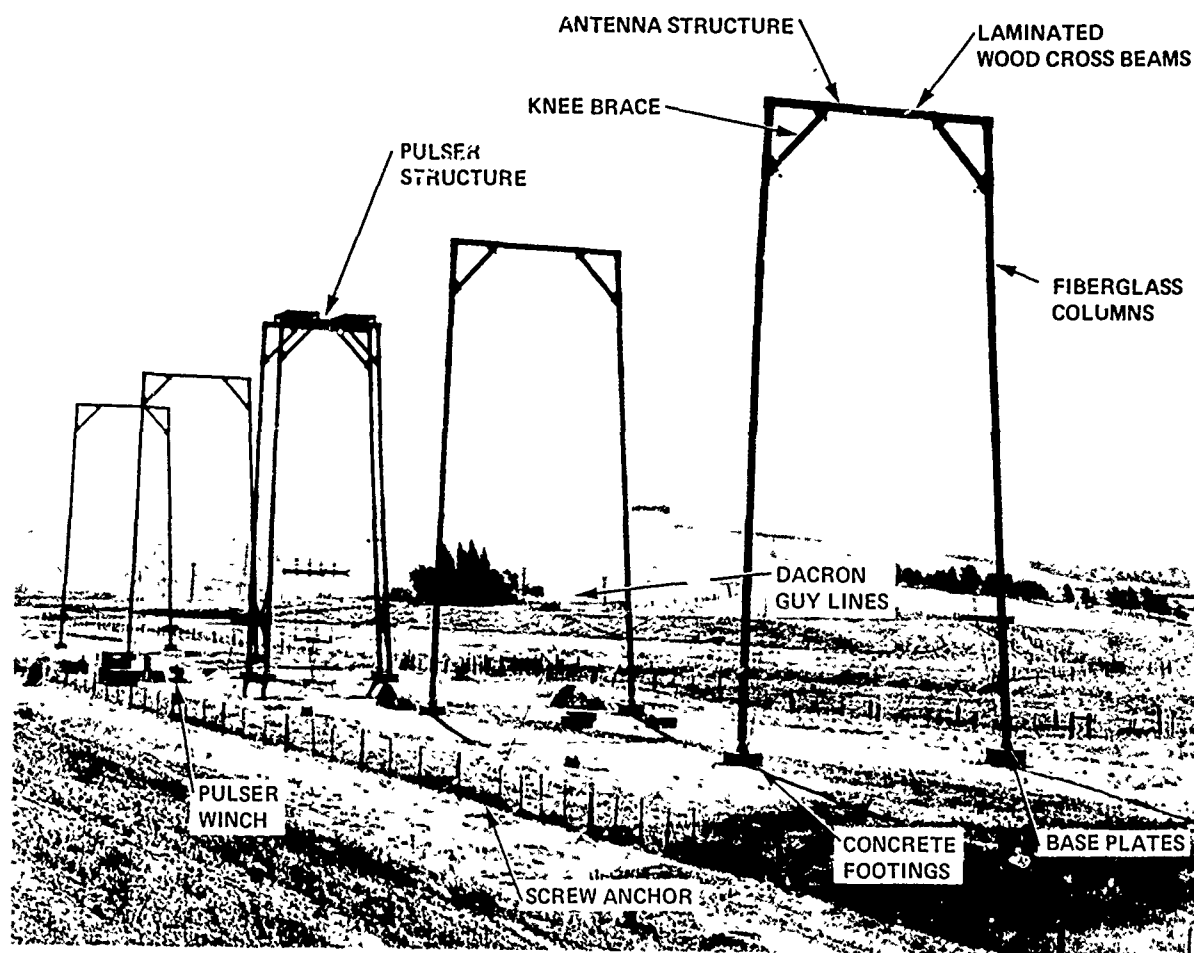
### SUPPORT STRUCTURE MECHANICAL DESIGN

The TEMPS pulser and antenna support structures, shown in Figure 67, are fabricated from dielectric materials as far as practical. The pulser support is a four leg A-frame type, designed as a free standing structure. Guy lines are provided to limit deflections and stresses from wind loads. The antenna supports (four units) are two leg A-frame type. The individual antenna structures are guyed at four points to maintain the vertical position and resist wind loads.

The pulser and antenna supports are assembled on the ground with the bases of the columns pinned to a concrete footing. The pulser and antenna lift lines and all guy lines are attached at ground level. The structures are then lifted to the vertical position by a crane and guy lines are anchored to the ground.

#### 7.1 CONCRETE FOOTINGS

The concrete footing for a typical structure column is 5 feet long, 4 feet wide, and 20 inches deep, and weighs approximately 3250 pounds. Eight 3/4-inch-diameter anchor bolts secure the column base bracket to the footing. The footing not only distributes the column weight but also acts as a counter-weight against the structure overturning during high winds. Lifting eyes have been provided in each block so that it can be relocated if desired.



72-8-5

Figure 67 The TEMPS pulser and antenna support structures.

## 7.2 GUY LINE ANCHORS

Two types of guy line anchors can be used depending on soil conditions and site restrictions:

(a) Concrete blocks, 4 feet long, 4 feet wide, and 3 feet thick, weighing approximately 7,200 pounds, are used where soil conditions or site restrictions do not permit the use of a screw type anchors. The blocks have lifting eyes for moving and a center eye for attaching the guy line.

(b) Where the earth shear loading force is high enough and site restrictions permit digging holes, a screw type anchor can be used. This type of anchor is used by utility companies in guying telephone and power poles. An eye is provided on the end of the anchor rod to secure the guy line. A hole 3 to 4 feet deep, 10 inches in diameter, is dug, the anchor set in place, and the hole backfilled with earth or concrete.

## 7.3 WINCH BASES

The pulser and antenna lift winches are set on reinforced concrete bases. The concrete slab provides a mounting base and also acts as ballast for the winch. The pulser winch bases are necessarily larger and heavier due to the lifting loads involved.

## 7.4 SUPPORT COLUMNS

A typical support column is made up of four pipe sections which are filament wound epoxy-fiberglass structures 24 feet long, 14 inches in i.d. with 1/2-inch walls. The section has a male and female end, except the bases, which have a female coupling on each end. When assembled, the sections form a



column 90 feet long. Bolts are used at the joints to preclude any separation during the erection sequence. Lag bolts are used to fasten the top section to the wood beam. The 90-foot-long columns weigh approximately 1840 pounds with each section averaging 460 pounds.

A knee brace is provided at the top of each column and diagonal cross-bracing on the bottom sections is provided for the pulser support structure. These braces are pinned to a fiberglass bracket which is bolted to the column. Integral shoulders are provided on the columns to locate and keep the brackets in position.

#### 7.5 WOOD CROSS BEAMS

The fiberglass columns are tied together at the top by a laminated-wood cross beam. The beams used on the pulser support structure are 18 inches deep by 9 inches wide. The antenna structure beams are 14 inches deep by 9 inches wide. The beams are fabricated by laminating 2-inch-thick Douglas fir with a resorcinol room temperature setting resin.

The beams are secured to the fiberglass columns by an extension on each end of the beam. The extension is also a laminated section that is bonded to the beam and machined so that it fits into the column. As an added safety feature lag bolts are inserted through the fiberglass pipe wall into the wood extensions.

## 7.6 BRACKETS AND BRACES

Knee braces and diagonal bracing at the base of the pulser support structure are secured to the columns and wood beams with non-metallic brackets. These brackets are of a polyester-chopped fiberglass composition. Where bearing surfaces require flat plates an "extren" plate is bonded to the bracket. Steel bolts are used to fasten the brackets to the wood beams. A steel pin is then used to hold the knee brace to the brackets.

## 7.7 RIGGING

Standard off-the-shelf pulley blocks and lines are utilized to raise the pulser and antenna to the operating height. The lift lines and guy lines are a double braided polyester (Dacron) fiber. This material provides a line that is non-rotational, torque free, and has less elongation and more strength than conventional twisted products.

The guy lines are equipped with a turnbuckle and cable termination at ground level. This arrangement permits measuring the amount of load on the line with a handheld tensiometer and the adjustment of this load with the turnbuckle.

## 7.8 WINCHES

Six winching units, two pulser winches, and four antenna winches are required to raise and lower the system. The winches are electrically operated and are complete with a base frame, motor starter, and pendant control station. A limit switch is provided to control the operating height so that the same elevation can be repeated for a long test series that may require more than one day to complete.

The winches are equipped with double drums. The pulser winches are capable of 2000 pounds pull and holding and lowering capacity of 4000 pounds. The antenna winches are capable of 200 pounds pull and holding and lowering capacity of 400 pounds. The line speed on the pulser drums is approximately 30 ft/min.

## SECTION 8

### TEMPS TESTING

This section of the final report presents the results of TEMPS field testing performed both at Camp Parks, located in the San Francisco Bay Area, and at HDL's Woodbridge, Virginia test site. Electrical testing of the system at Camp Parks began in mid-August 1972 and was completed at the end of the first week in November. The system was then packed, shipped, and installed at Woodbridge, Virginia in January of 1973.

Electrical testing at Camp Parks began with testing of each one-half generator separately followed by operation of the system as a whole. Specific objectives for one-half generator testing were (a) to determine the actual circuit characterization of each half generator for comparison and to form the basis for analysis of full system operation, (b) to determine Marx generator time delay and jitter under actual load conditions, (c) to provide the basis for assessment of system operating characteristics including reliability and to modify the system if required.

#### 8.1 MARX INDUCTANCE

Electrical testing of the half systems began with measurement of stray-series Marx-generator inductance. This was accomplished by short circuiting each Marx at its output. Wide strips of thin copper sheet were installed from the inner support cones to the bicones on each side of the system.

Each Marx was then dc charged to about 15 kV and erected into these short circuits. Cupric-sulfate resistive-divider monitors permanently installed between the inner support cones and the bicones (in parallel with the peaking capacitors) recorded the resulting oscillatory waveform with the aid of an oscilloscope. A simplified electrical circuit for inductance measurements is shown in Figure 68.

Marx-inductance measurements yielded a value of stray-series inductance equal to  $2.17 \mu\text{H} \pm 5$  percent and series resistance equal to about 13 ohms. These values were the same for both Marxes and are in good agreement with values determined previously during Marx testing at Physics International (Reference 6). A typical "ringing" waveform is shown in Figure 69 in comparison with a calculated waveform.

## 8.2 PULSE CHARGE CIRCUIT

Following Marx-inductance measurements, each Marx generator was charged to about 20 kV dc and erected into the peaking capacitors to determine the effective peaking-capacitor capacity during pulse charge. Output switch spacing and pressure were increased to preclude switch closure, thus yielding an oscillatory voltage versus time waveform across the peaking capacitors. The simplified equivalent electrical circuit for these measurements is shown in Figure 70.

Typical resulting waveforms using the resistive divider voltage monitors permanently installed within the system are shown in Figure 71 for two oscilloscope sweep speeds: 100 nsec/division and 500 nsec/division. Analysis of the waveforms of Figure 71 using the previously measured value of Marx inductance yields an effective load capacity of about 1 nF. Of this value, about 800 pF (eight parallel peaker modules) are associated with the peaking capacitors themselves; the remaining capacity is

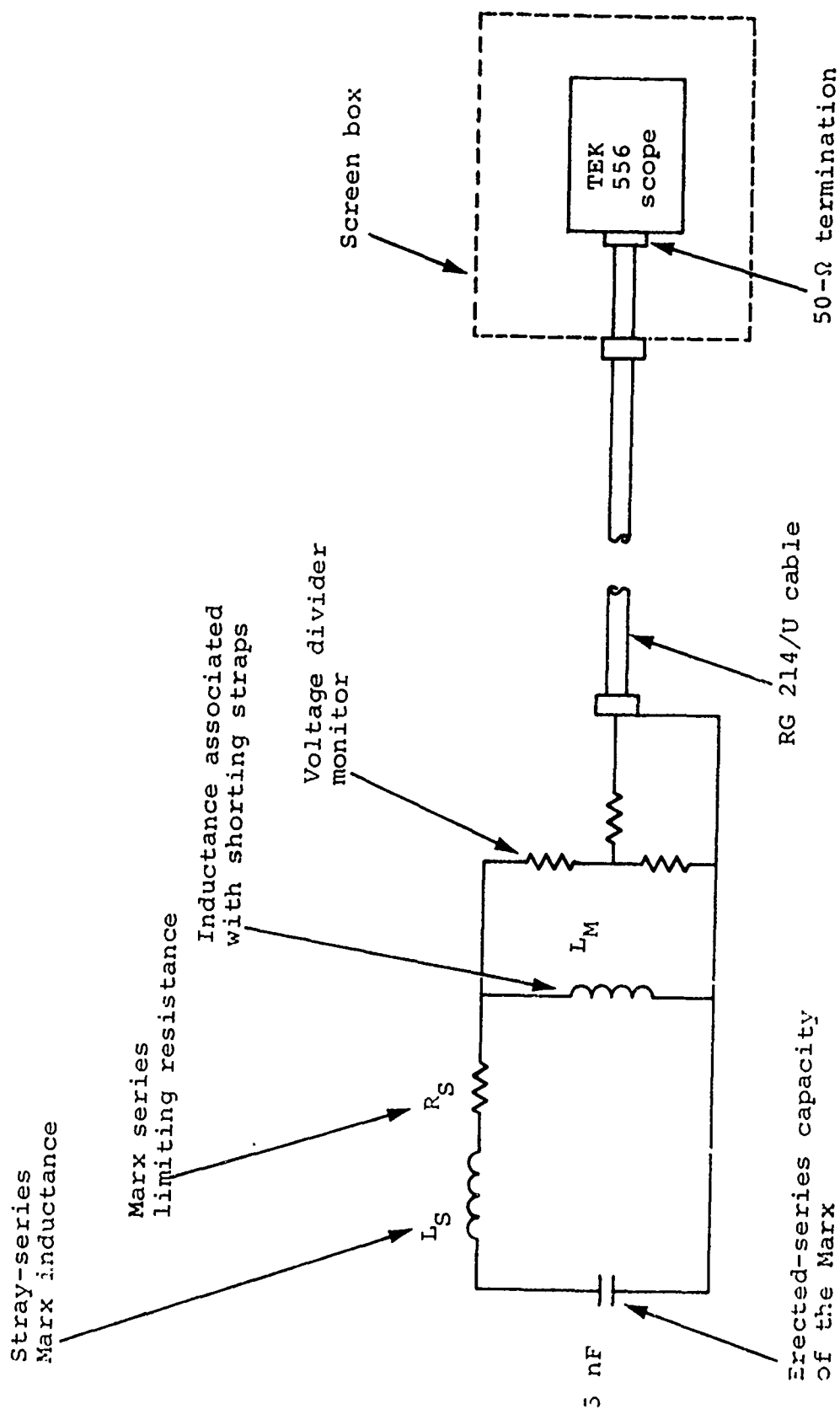


Figure 68 Simplified electrical circuit for Marx inductance measurements.

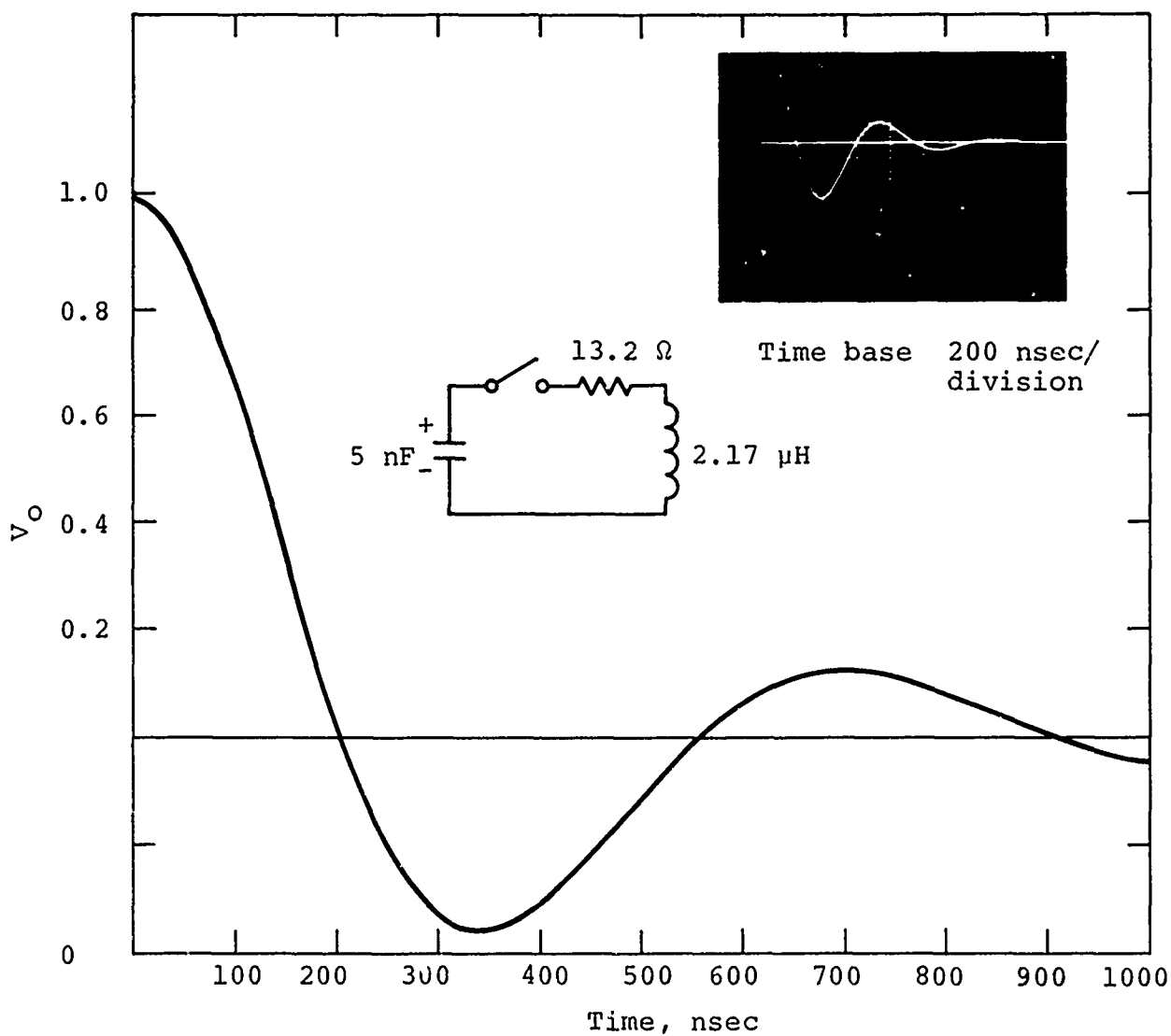


Figure 63 Inductance measurement, calculated, and measured waveform.

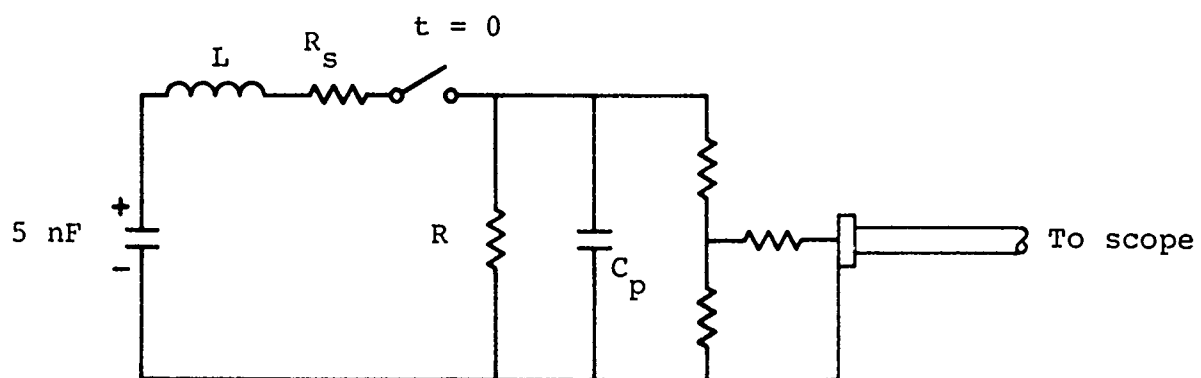
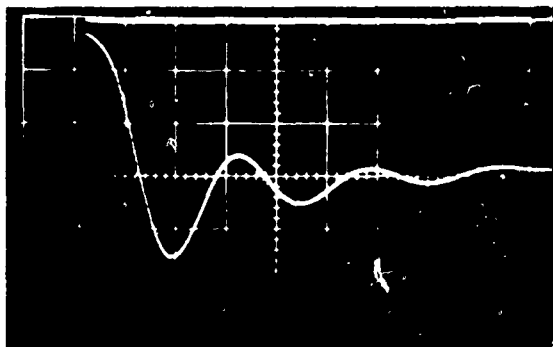
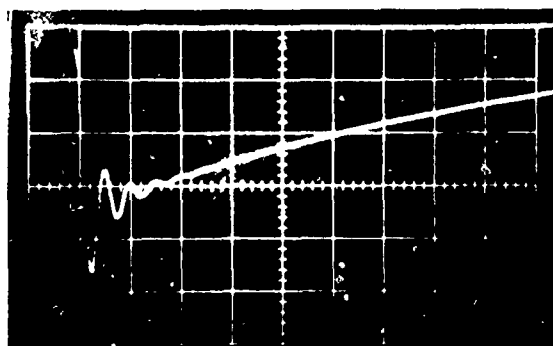


Figure 70 Simplified equivalent circuit--Marx/peaking capacitor.





100 nsec/division



500 nsec/division

Figure 71 Peaking capacitor ringing waveforms.

associated with the effective Marx stray capacity and stray capacity across the output switch. Total stray capacity from each Marx to its current return-path conductor was previously determined to be about 600 pF (Reference 6 ). Thus, the effective capacity that is charged in parallel with the peaking capacitors is one-third this value, or approximately 200 pF. The output switch is estimated to be about 40 pF. Thus, total capacity is about 1.05 nF and is in good agreement with the computed value based upon analysis of the waveforms shown in Figure 71.

The beginning of the voltage waveform measured across the peaking capacitors and shown in Figure 71 depart from a  $(1 - \cos \omega t)$  waveform during the very first part of the trace. This is due to the fact that the Marx is operated at low dc-charge levels and thus Marx erection proceeds relatively slowly. Thus, the Marx erection characteristics are superimposed on the actual lumped equivalent circuit waveform in the first 100 nsec or so of the trace.

The late time, essentially exponential decay of the waveform shown in Figure 71 is due to shunt resistance associated with the resistive voltage-divider monitor and the Marx charging and trigger resistors. Marx shunt resistance is dominated by the trigger coupling resistors and is about 1.1 k $\Omega$ . Monitor resistance for the waveforms shown in Figure 71 is about 2.8 k $\Omega$ . Total shunt resistance is therefore about 790 ohms. In terms of overall waveform decay time, total capacity is the parallel combination of Marx capacity and the effective value of the peaking capacitor. This value is about 6.0 nF. Thus, the calculated waveform decay time given by

$$\tau_d = RC$$

$$\text{is } \tau_d = 790 (6 \text{ nF}) = 4.74 \text{ } \mu\text{sec}$$

and is in fortuitous agreement with the measured value from Figure 71 of 4.70  $\mu\text{sec}$ .

## 8.3 TEMPS HALF GENERATOR EQUIVALENT CIRCUIT

Based upon the Marx inductance and peaking capacitor capacity measurements described in the previous paragraphs, a simplified equivalent circuit for each TEMPS half generator was developed and is shown in Figure 73.

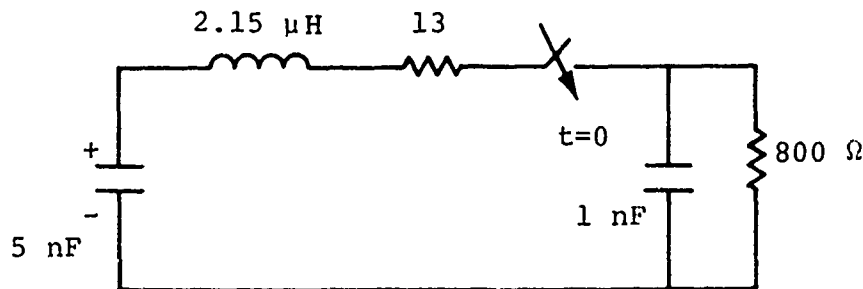


Figure 72 Simplified equivalent circuit.

The series resistance in Figure 72 is the sum of lumped and stray resistance. Lumped resistance is 10.5 ohms and is equally distributed within each stage of each Marx (0.3 ohm/stage). Of the balance of the resistance, about 1.5 ohms is associated with the energy storage capacitors and the remainder with capacitor connections and the spark gaps themselves.

The computed peaking capacitor pulse charge waveform (no output switch closure) is illustrated in Figure 73. Overlaid with it is a measured waveform scaled from a peaking capacitor monitor photograph. Agreement between computed and measured waveforms is good. The actual period of oscillation appears to be slightly less than the computed value, but the difference is not dramatic.

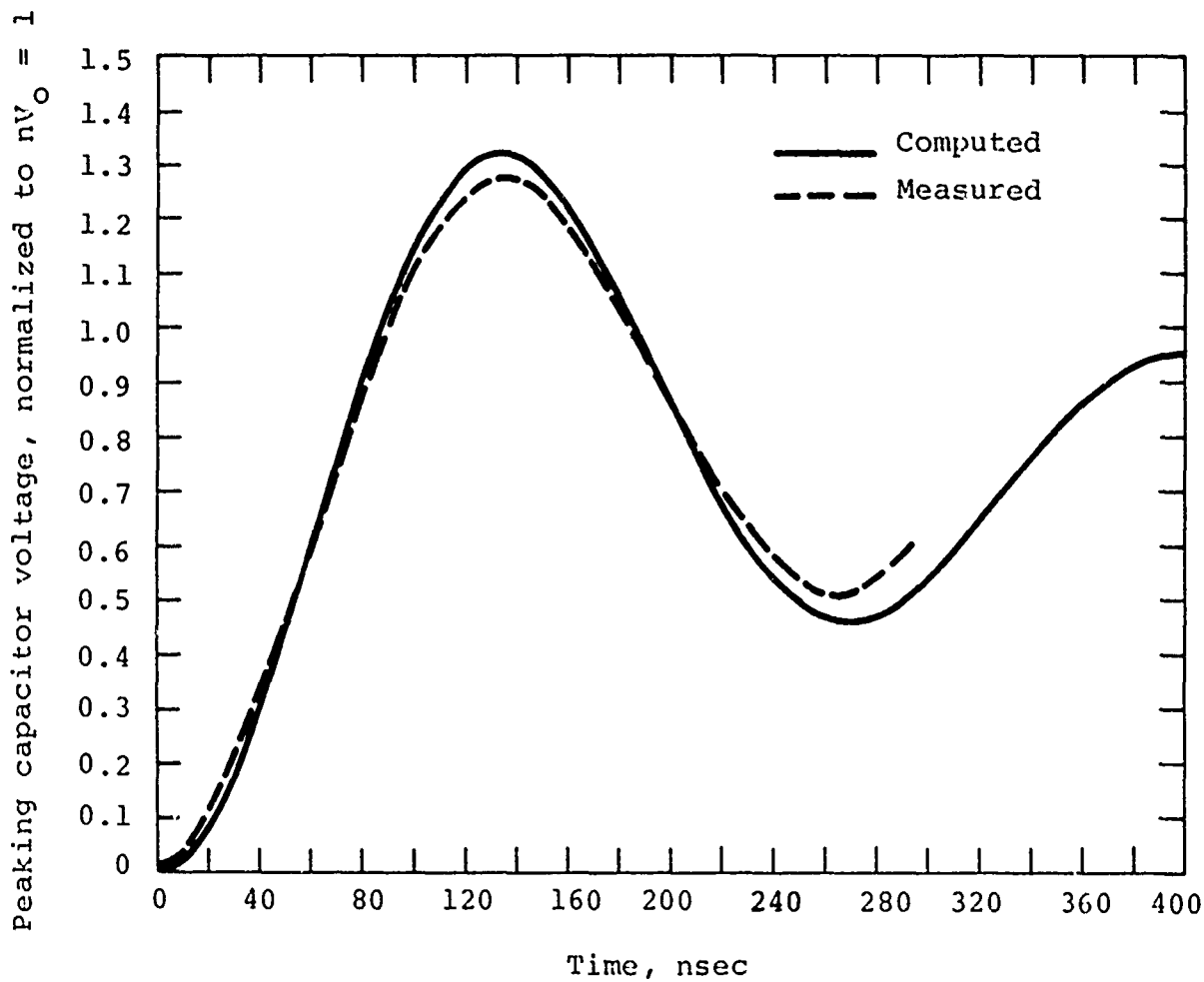


Figure 73 Computed and measured peaking capacitor pulse charge waveforms (no switch closure).

For an ideal peaking capacitor circuit, output switch closure at  $t_c = \pi/2\omega$  satisfies one of two conditions for production of a step output pulse (the second condition is  $C_p = L/R_L^2$ ). For the computed waveform this time  $t_c$  is about 66 nsec. However, based upon Reference 9, for a circuit where the ideal voltage source is replaced by a capacitor, output switch closure time is allowed to exceed the nominal time to produce an output waveform more closely approximating a single exponential decay into a constant load impedance. For TEMPS, Reference 9, this time is about 1.13 times the nominal time or about 75 nsec. The normalized value of peaking capacitor voltage corresponding to this time is about 0.85 (Figure 73). Thus, production of the optimum output waveform, with output voltage amplitude equal to  $V_{out}$  requires that the Marxes be charged to  $V_{dc}$  where

$$V_{dc} = \frac{V_{out}}{2n(0.85)}$$

and where  $n$  is the number of stages in each Marx ( $n = 35$ ). This relationship is plotted in Figure 74.

It is emphasized, however, that peak output voltage may exceed the value given by the above expression by delaying output switch closure, but at the expense of an output waveform that tends to be peaked in early times. This is illustrated in Figure 75 and 76 for two sets of peaking capacitor pulse charge and output voltage waveforms (full system operation). In Figure 75, dc charge level was 70 kV dc and output-switch closure voltage was adjusted to about 4.1 MV which nearly satisfies the expression for optimum output waveform, i.e.

$$V_{out} = V_{dc} 2n(0.85) = 4.17 \text{ MV}$$

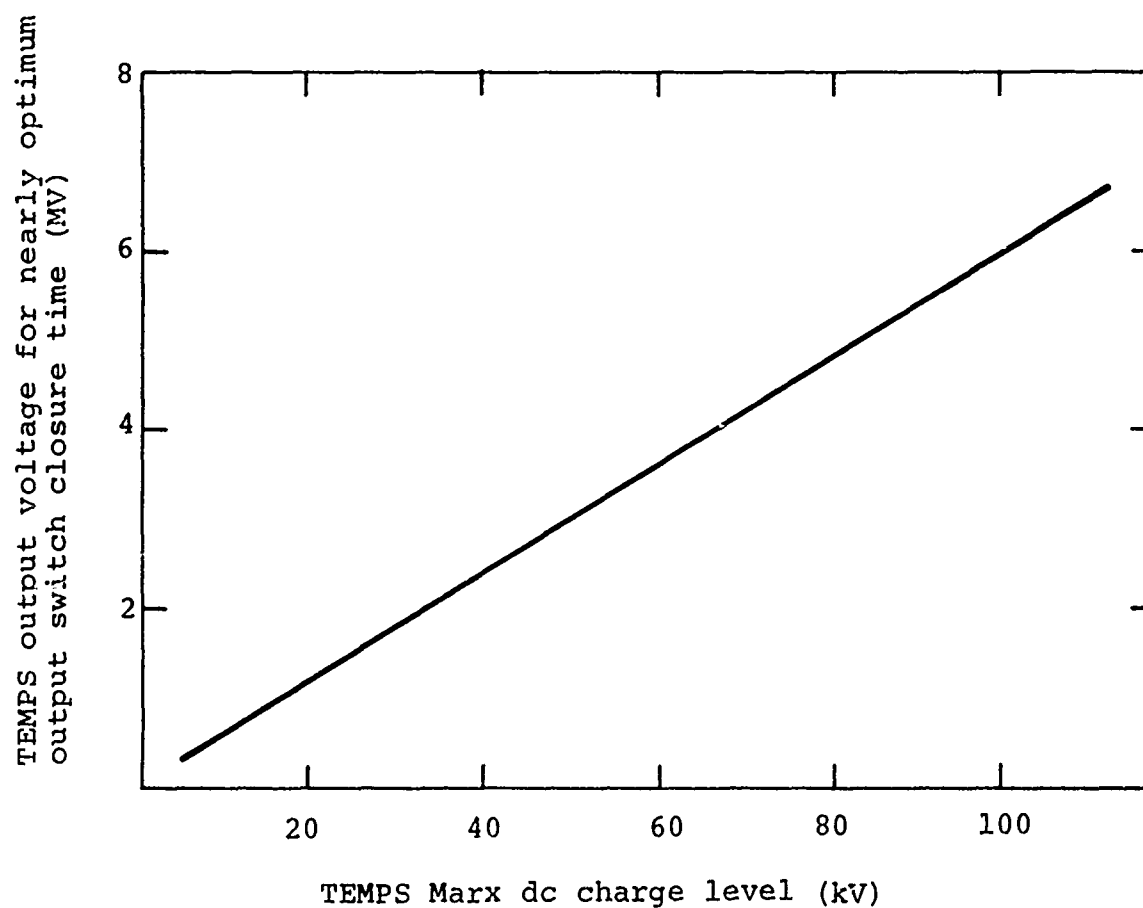


Figure 74 TEMPS output voltage versus dc charge.

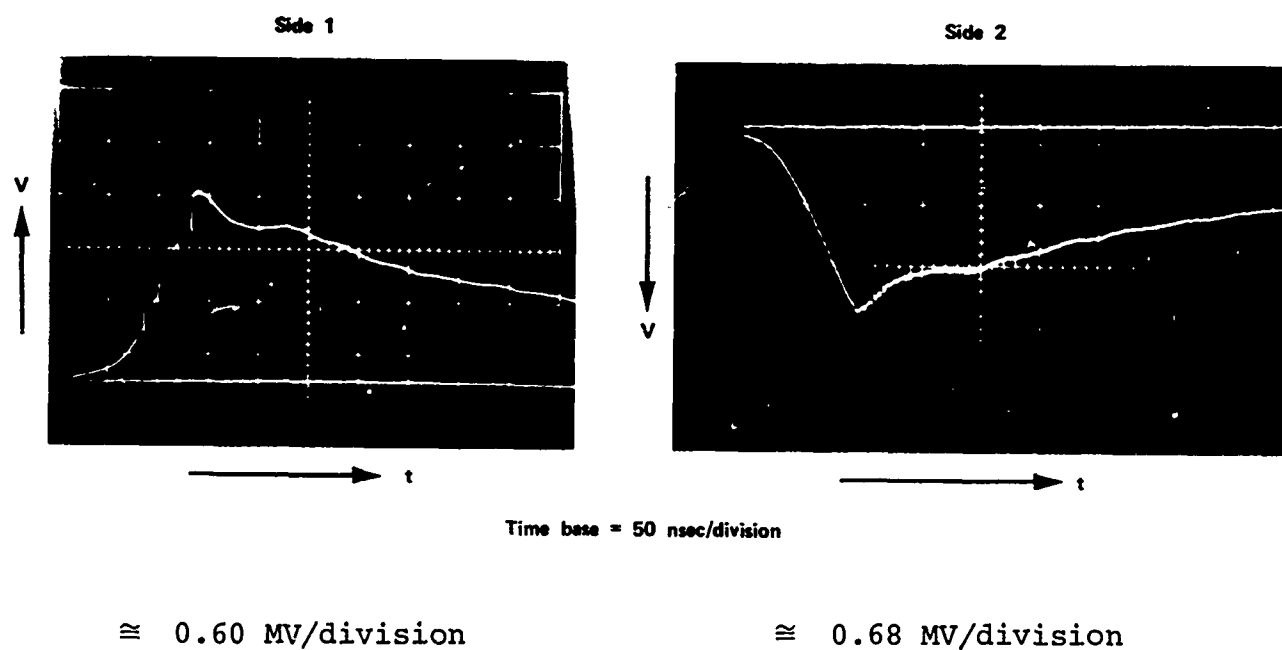
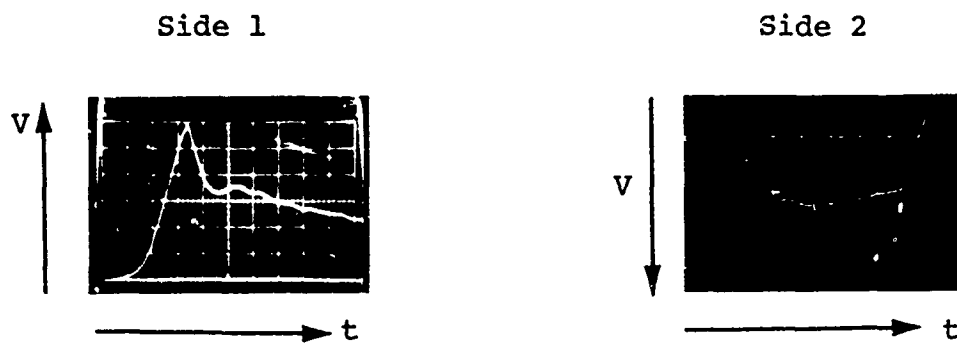


Figure 75 Peaking capacitor pulse charge and output voltage waveform (near optimum output switch closure time).



Time base = 50 nsec/division

Figure 76 Peaking capacitor pulse charge and output voltage waveform (output switch closure delayed).

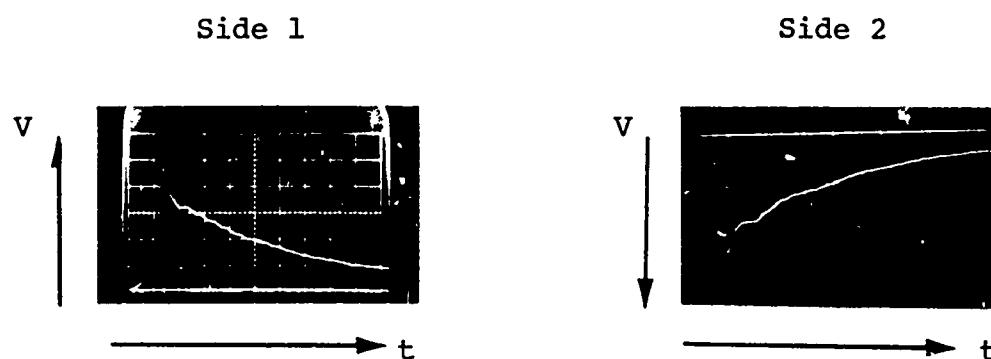


In the second example, Figure 76, the dc charge level was 40 kV dc, but output switch closure was delayed and produced a peak output voltage equal to about 2.72 MV whereas near optimum waveform conditions required an output voltage equal to about 2.38 MV. This is a rather extreme example, but in comparison with Figure 75 the waveform is noticeably peaked.

Overall pulse decay time for TEMPS is illustrated in Figure 77 (peaking capacitor pulse charge and output voltage waveforms). In this case, output switch closure is delayed slightly beyond that associated with an optimum output waveform ( $V_{out} = 5.13$  MV,  $V_{dc} = 83$  kV and  $V_{out\ optimum} = 4.94$  MV), and the waveform is slightly peaked as a result. The equivalent e-folding decay time (the average of side 1 and 2) is about 570 nsec. Antenna terminating resistance for the above measurement was approximately 235 ohms. This value in conjunction with the generator capacity yields a calculated RC decay time of about 590 nsec, in close agreement with the measured value.

#### 8.4 RADIATED OUTPUT PULSE RISETIME

Radiated output pulse risetime measurements were performed in the course of Camp Parks testing. A simplified schematic diagram of the pulse monitoring system is shown in Figure 78. MGL-2A probe position relative to the pulser is illustrated in Figure 79. The probe was supported on a wooden stand located on the equatorial plane of the pulser. Table VII in conjunction with Figure 80 summarizes reflected wave arrival times for the probe position associated with joints and discontinuities in the biconical-transmission-line high frequency launcher relative to initial EM wave arrival time at the probe.



Time base = 100 nsec/division

$$V_{out} = 5.13 \text{ MV}$$

$$V_{dc} = 83 \text{ kV}$$

Figure 77 TEMPS pulse decay time.

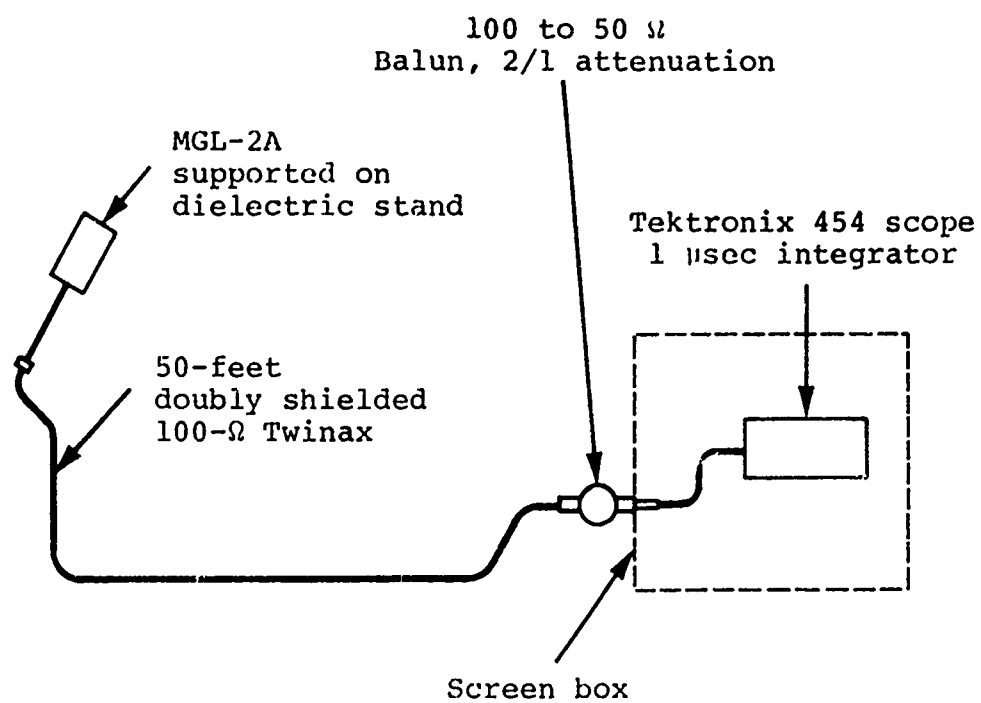


Figure 78 Diagnostics setup.

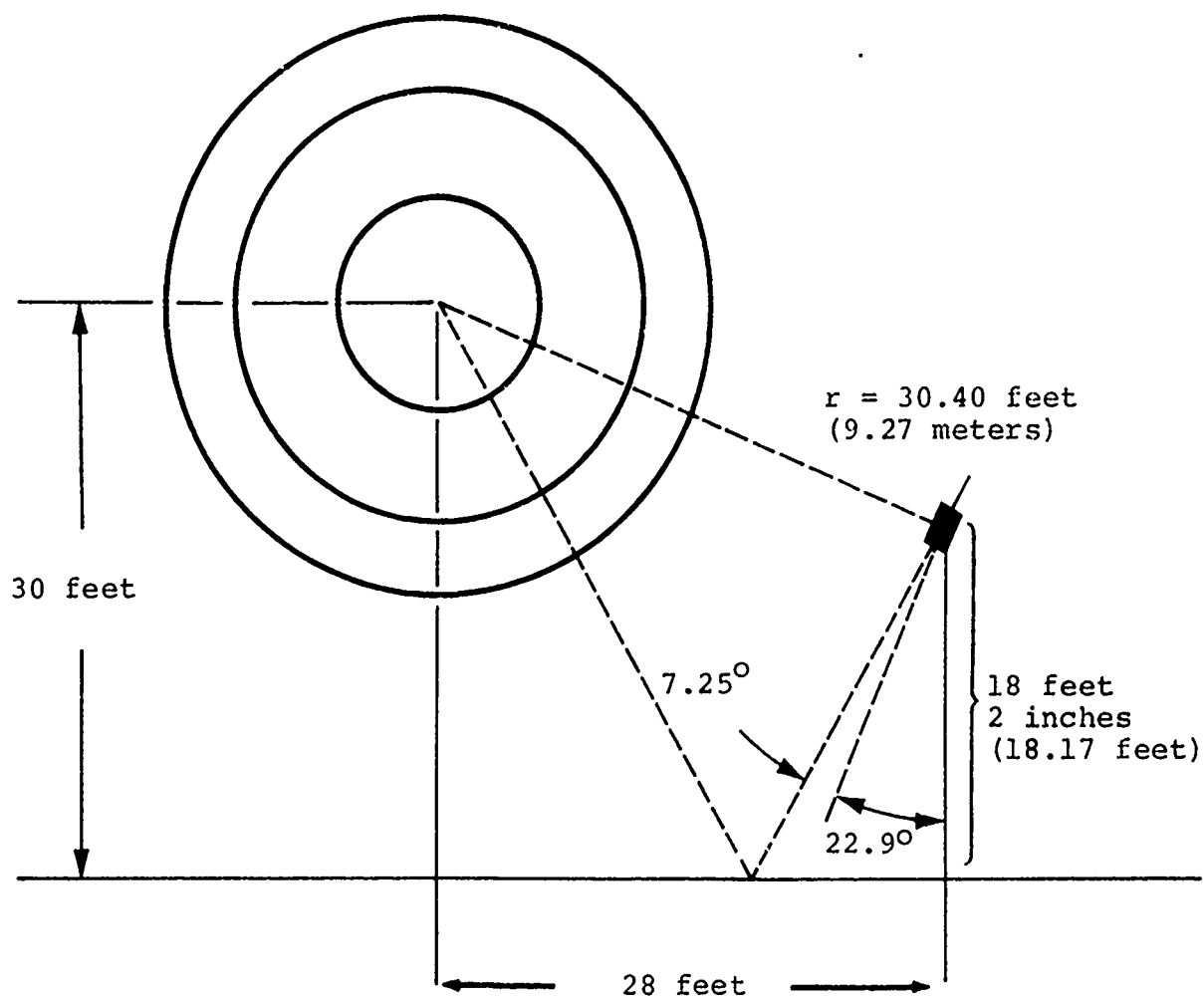


Figure 79 Probe position relative to pulser.

TABLE VII

## RELATIVE REFLECTED WAVE ARRIVAL TIME

(Probe Position: 28 feet horizontal on centerline,  
18 foot 2 inch high pulser antenna; 30 foot centerline)

<u>Location</u>	<u>Source of Reflected Wave</u>	<u>Relative Arrival Time</u> (nsec)
(Figure 80)	Ground reflection	25.3
A	Dielectric cylinder/bicone joint (also end of peakers)	2.3
B	End of 23-foot-diameter continuous conducting bicone	6.0
C	End of bicone transition (start of cylindrical wire cage)	18.7

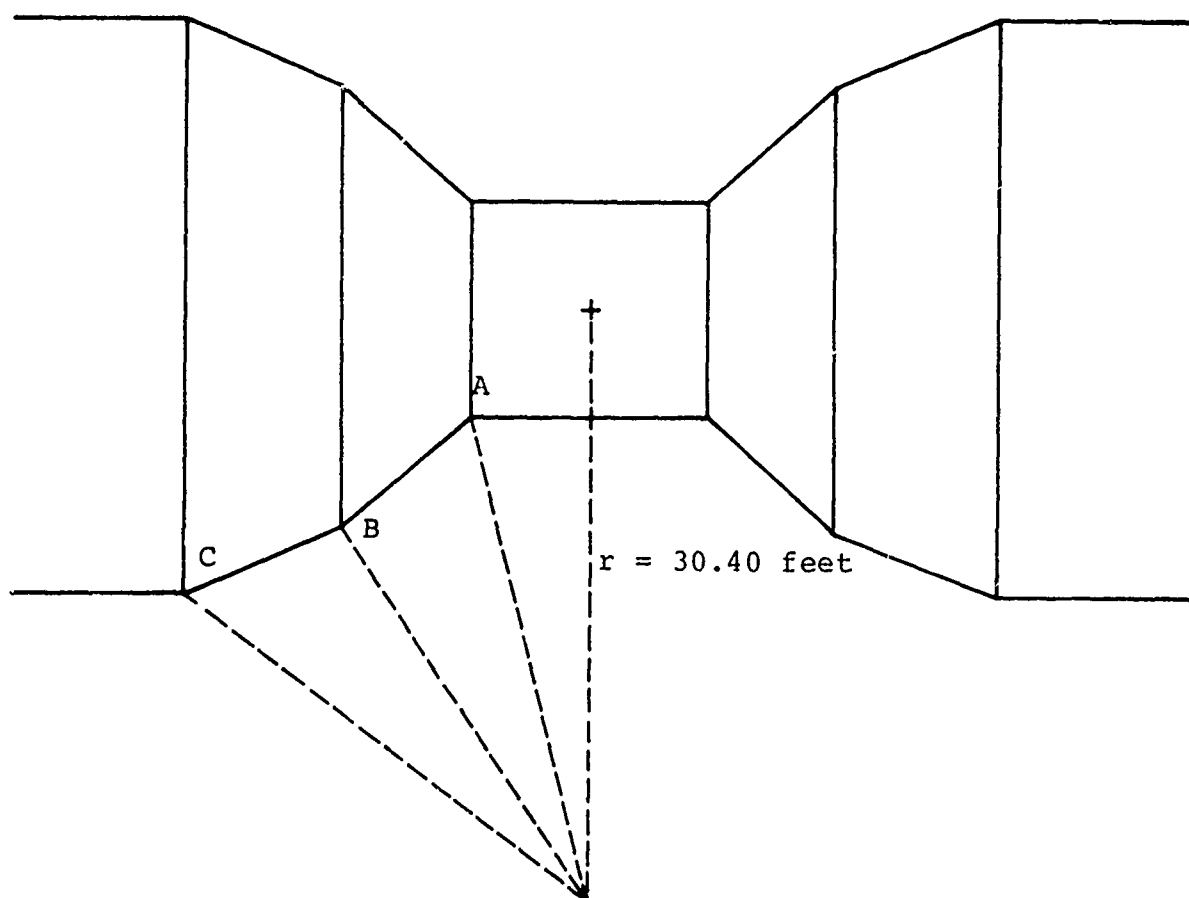


Figure 80 Biconic discontinuity.

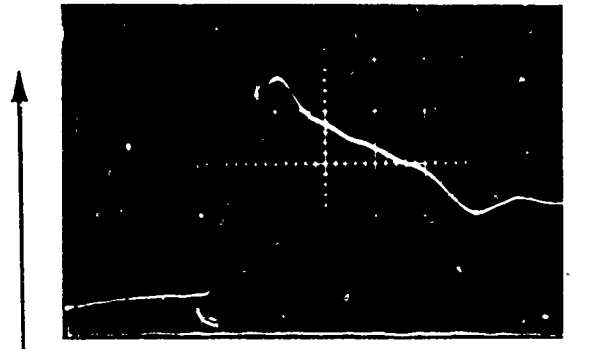
A typical early time radiated waveform recorded by the previously described monitoring system is illustrated in Figure 81. Output pulse risetime is approximately 8.5 nsec (10 to 90 percent).<sup>\*</sup> Risetime to peak value measured from the beginning of the fast risetime part of the pulse is about 12 nsec when corrected for recording system response. This value is well within the 19 nsec overall cleartime associated with the bicone transition to cylindrical wire cage antenna joint for the previously described probe and pulser/antenna position (Table VII).

Calculated output risetime for the conditions under which the waveform of Figure 81 was made, based upon output switch inductance and resistive phase of arc formation effects, Reference 1, is less than 4 nsec (10 to 90 percent), assuming a roughly exponential pulse front. However, the measured risetime is more than a factor of two greater than the estimated value. Thus, it is apparent that pulse risetime is controlled by other considerations. This effect is illustrated rather more dramatically in Figure 82, a waveform similar to that shown in Figure 81 except at lower output voltage and reduced gap spacing. (The pulse monitoring system position relative to the pulser is similar, but not identical to that used to record the waveform shown in Figure 81). In Figure 82, an inflection on the fast-rising pulse front is clearly seen and the initial slope of the fast-rising front is substantially greater than the average value. From the photograph, the 10 to 90 percent risetime is about 8.5 nsec. Folding in the response of the recording system

---

\* Risetime is measured between the 10 percent and 90 percent points on the pulse front where the fast front is extrapolated on the steepest slope back through the baseline to define the 10 percent point in the presence of prepulse. Risetime is corrected for recording system frequency response which is about 5 nsec 10 to 90 percent.

1 V/division



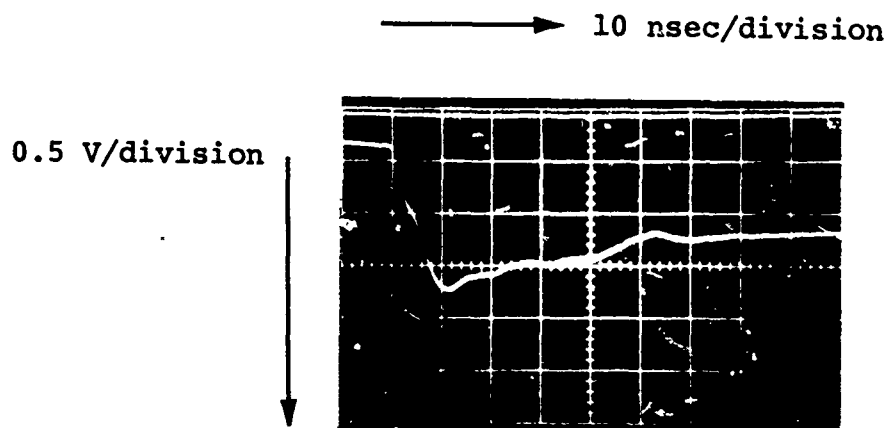
10 nsec/division

Integrated  $\dot{B}$  signal

Probe	{	MGL-2A, $A_{\text{eff}} = 0.01 \text{ m}^2$
		Tektronix 454 scope--add mode
		Integrators: 1 $\mu\text{sec}$ time constant
Pulser	{	$V_{\text{dc}} = 60 \text{ kV}$
		$V_{\text{out}} = 3.5 \text{ MV} \pm 5 \text{ percent}$
		Output switch gap spacing, gas type,
		and pressure: 12 cm, 50 psig $\text{N}_2$

Figure 81 Typical radiated waveform (early time).





Integrated  $\dot{B}$  signal

Probe	{	$MGL-2A, A_{eff} = 0.01 \text{ m}^2$ Balun attenuation: $\approx 2.0/1$ Integrators: $1 \mu\text{sec}$ time constant
Pulser	{	$V_{dc} = 45 \text{ kV}$ $V_{out} = 2.5 \text{ MV} \pm 5 \text{ percent}$ Output switch gap spacing, gas type, and pressure, 6 cm, 50 psig $N_2$

Figure 82 Radiated waveform--inflection on pulse rise.

reduces this value to about 7.0 nsec--the true output risetime for the described conditions. If, however, the pulse rise continued on the initial fast front, then the risetime as recorded would be about 5.5 nsec 10 to 90 percent. Correcting this value for monitoring system response would thus yield a true risetime between 1 and 2 nsec (10 to 90 percent), and this range of values is consistent with the estimated performance of the output switch for a 6-cm gap spacing.

The presence of the inflection (Figure 82) suggests that a discontinuity within the biconical high frequency launcher, and the subsequent EM wave reflections associated with the discontinuity acts to control system output risetime. The most probable discontinuity exists at the point where the peaking capacitors are electrically connected to the biconical transmission line surface just inside the 11.5-foot-diameter epoxy fiberglass containment vessel. Spacing between adjacent peakers at this point is greatest and thus the discontinuity the largest. From Table VII, the cleartime for this discontinuity and for the described probe position is about 2.3 nsec. Again correcting for recording system response, the inflection occurs approximately at this time. Thus, it is highly likely that the discontinuity at the output end of the peakers controls overall output pulse risetime. Subsequent measurements with a higher frequency response recording system (Tektronics 485 scope) tend to confirm this conclusion.

Implications with regard to system performance as a result of increased pulse risetime are discussed in the following section.

## 8.5 RADIATED PULSE PEAK AMPLITUDE

The radiated waveform illustrated in Figure 81 is representative of TEMPS performance during initial operation at Camp Parks. The measured peak output voltage in this instance is  $3.5 \text{ MV} \pm 5 \text{ percent}$  and corresponds very closely to optimum output switch closure voltage in terms of output waveform shape. Integrated signal peak amplitude is  $4.9 \text{ volts} \pm 3 \text{ percent}$  which corresponds, for the probe parameters and position, to a peak B field of 0.49 meter Tesla. The associated magnetic field intensity is 390 A/m. Assuming a singly propagating EM wave, the electric field peak amplitude is 147 kV/m. However, the peak values of H and E need to be corrected slightly since the prepulse at the point in time corresponding to peak amplitude is the ground interacted value.

As illustrated in Figure 83, the ground interacted magnetic field intensity reduces the value of incident magnetic field. Referring to Table VII and Figure 80, the ground reflected wave arrival time is approximately 25 nsec after direct wave arrival time. Prepulse amplitude corresponding in time to 25 nsec prior to peak pulse amplitude is very nearly the peak prepulse amplitude. Thus, the peak prepulse amplitude is used for the remainder of the correction calculation. The path length traversed by the reflected prepulse magnetic field intensity is greater than the direct path. Thus,  $H_{\text{ref}}$  is

$$H_{\text{ref}} = \frac{s_i}{s_r} H_{\text{inc}}$$

where  $s_r$  and  $s_i$  are reflected and direct incident path lengths respectively. For the described conditions,  $s_i/s_r \cong 0.546$ , and thus

$$H_{\text{ref}} = 0.546 H_{\text{inc}}$$

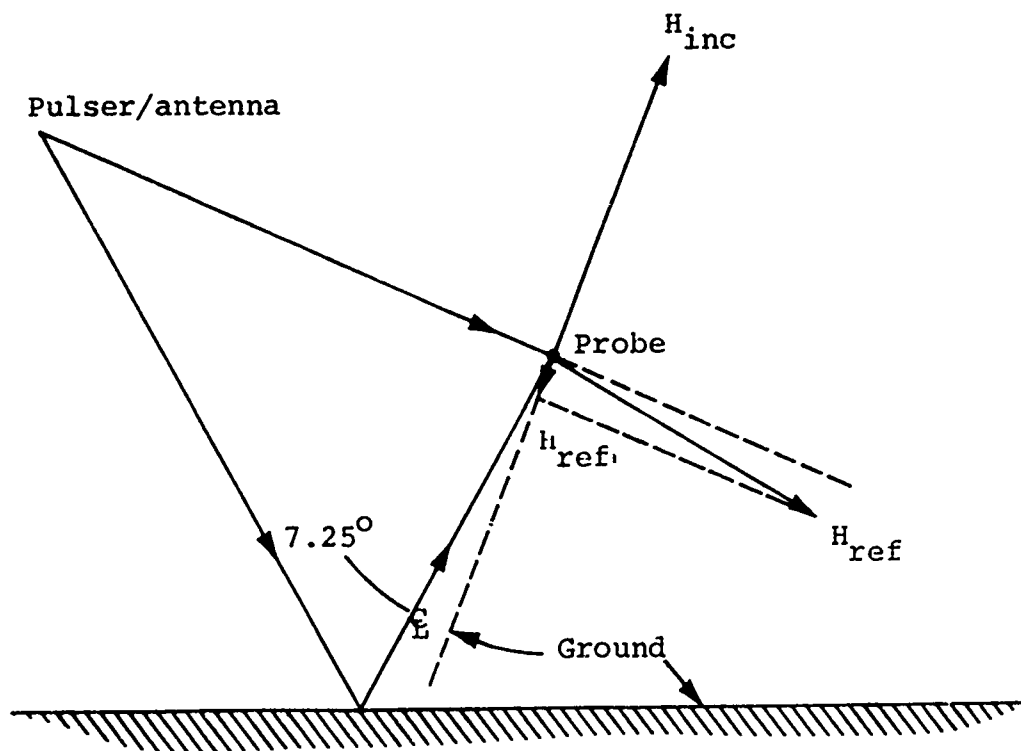


Figure 83 Direct and ground interacted EM fields.

From Figure 83 a small component of  $H_{ref}$  is in the direction of  $H_{inc}$  and this component  $H_{ref_y}$  is given by

$$H_{ref_y} = H_{ref} \sin \phi = 0.546 H_{inc} \sin \phi$$

$$H_{ref_y} = 0.126 H_{ref} = -0.069 H_{inc}$$

Therefore, the ground reflected prepulse amplitude reduces the direct prepulse amplitude by about 7 percent. From previous measurements, the free field prepulse amplitude is about 16 percent of peak radiated output signal amplitude for the condition where the output switch is closed at voltage  $V_{out} = 0.85$  (2 nV<sub>dc</sub>) on the pulse charge waveform. Thus, the overall effect for the situation under consideration is a reduction of peak radiated signal amplitude by about 7 percent of 16 percent or 1 percent, a small correction in this instance. To summarize, the corrected peak radiated H and E fields corresponding to the waveform photograph of Figure 81 are 394 A/m and 149 kV/m respectively.

A second necessary correction is associated with the response of the recording system which is about 5 nsec (10 to 90 percent). Due to the response of the recording system, the observed pulse risetime is slightly greater than the actual value and this in conjunction with the radiated pulse decay time decreases the actual peak field slightly. This correction is about 2 percent and thus the true values of peak H and E fields are more nearly 402 A/m and 152 kV/m respectively. The probable error associated with these values is about 5.5 percent and arises from two principal sources. First, the accuracy of the recording system: 1 percent for the probe, 2 percent for the integrators, and 3 percent

for the scope. These combine in quadrature to yield a probable error of 3.7 percent. The second principal source of error is associated with the radial distance of the probe from the pulser. This value is taken to be about 4 percent. Combining this value in quadrature with recording system inaccuracy yields the previously stated overall accuracy of about 5.5 percent (rms).

These values are compared with the theoretical calculated values given by

$$E_{pk} = \frac{60 V_{out}}{r Z_k}$$

$$H_{pk} = \frac{V_{out}}{2 \pi r Z_k}$$

where  $V_{out}$  is peak output voltage,  $r$  is radial distance to the observation location (on the equatorial plane), and  $Z_k$  is biconical transmission line impedance. For the specified conditions, these values are 501 A/m and 189 kV/m and the corrected measured values are about 20 percent less than these.

One source of the apparent reduction of output signal amplitude, compared with the theoretical value apart from recording system response considerations, was suggested in the previous paragraph, and is attributable to the decay of the radiated EMP waveform in conjunction with the finite pulse risetime. The average initial decay of the waveform, correcting for integrator time constant, is about 100 nsec (e-fold) and results in about a 10 percent reduction of radiated peak signal for a pulse risetime of about 8.5 nsec (10 to 90 percent).

Thus, if the radiated output pulse rose instantaneously to peak value, output pulse amplitude would agree within about 10 percent with the calculated values, and this difference is close to the extreme of the sum of probable error in the measurements, i.e. the sum of errors associated with radiated field measurements and with the output voltage measurement upon which the theoretical fields are based.

However, a second potential source of radiated field loss which may account for the remaining 10 percent discrepancy is associated with the cleartime of the continuous conducting biconical-transmission-line high-frequency launcher. At the end of this section of line, transition is not only made to wire, but there is also a change in angle (Figure 80). Both considerations tend to increase the effective impedance of the launcher and thus reduce the radiated field. Examination of radiated pulse waveform photographs reveals no obvious perturbation due to cleartime, but in view of the somewhat slower output risetime than originally anticipated, the biconical high frequency launcher was modified to increase overall cleartime. This change was easily accomplished and consisted essentially of moving the 30-foot-diameter rings in towards the pulser to eliminate the biconical line angle change at the end of the continuous conducting section of the bicone. This is illustrated in Figure 84.

Additional output pulse measurements were performed after modification to the bicone. The pulse monitoring system was the same as previously used except that probe position relative to the pulser was altered slightly, but accurate ( $\leq 3$  percent) measurements of probe and pulser position were made. Figure 85 shows the new probe location and Table VIII summarizes wave reflection cleartimes of interest.

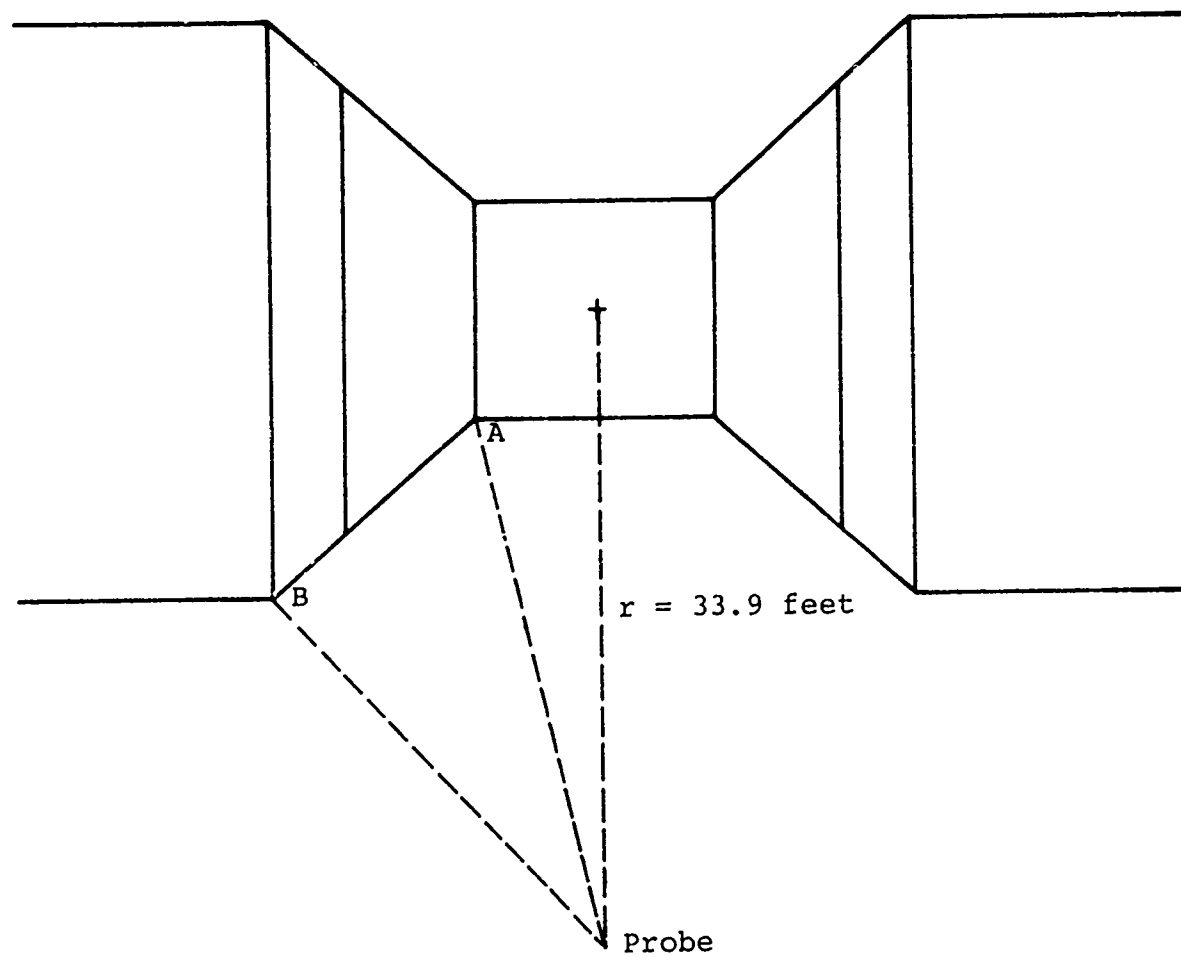


Figure 84 Modified biconical high-frequency transition.



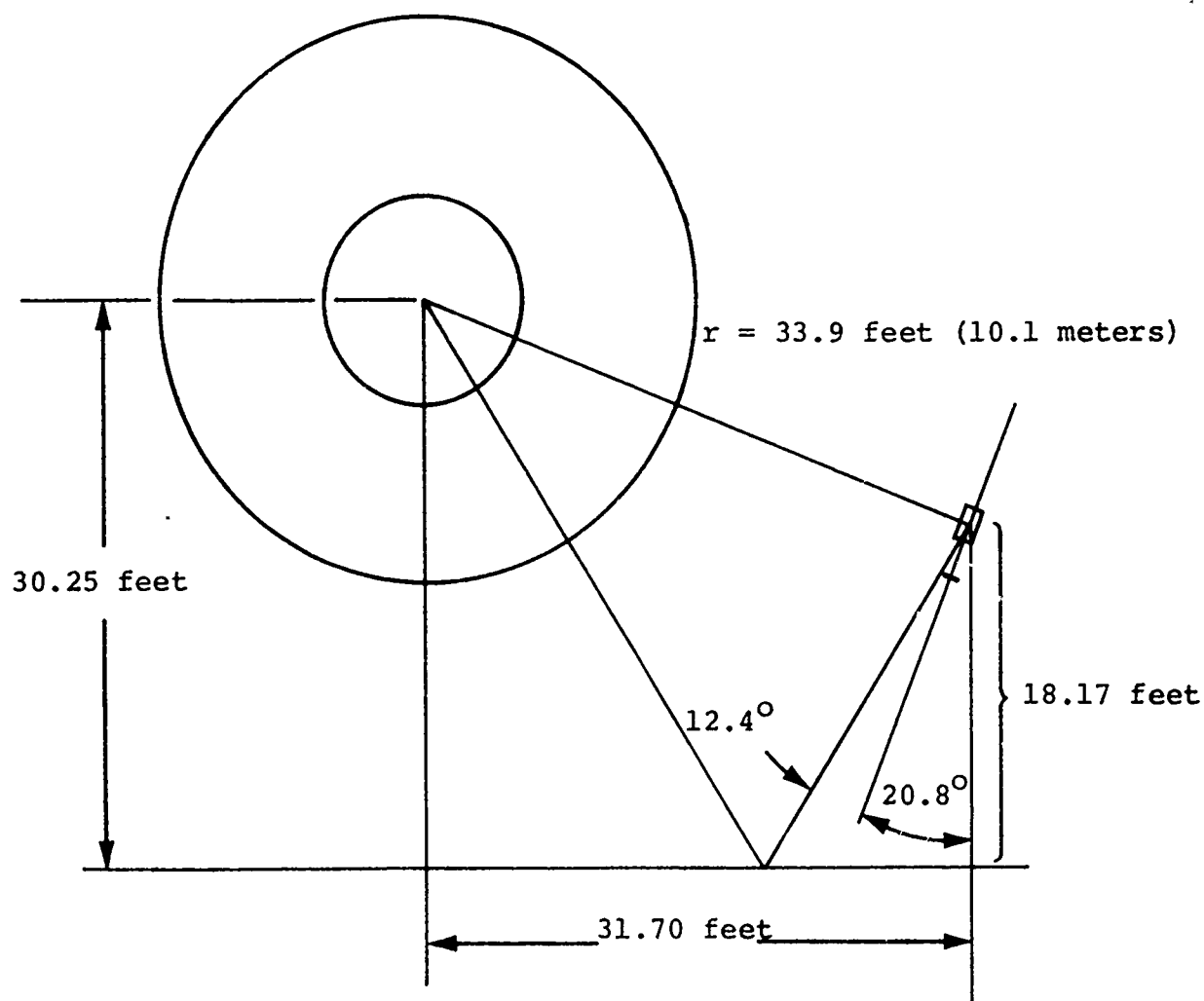


Figure 85 Probe position relative to pulser.

TABLE VIII

## RELATIVE REFLECTED WAVE ARRIVAL TIME

(Probe Position: 31.7 feet horizontal on centerline,  
18 feet 2 inches high pulser/antenna: 30.25 foot centerline)

<u>Location</u>	<u>Source of Reflected Wave</u>	<u>Relative Arrival Time (nsec)</u>
(Figure 84)	Ground reflection	24.3
A	Dielectric cylinder/bicone joint (also end of peakers)	2.2
B	End of bicone transition (start of cylindrical wire cage)	15.3

A typical radiated waveform photograph is illustrated in Figure 86 for the new configuration. (In this example, output voltage is about 5 percent greater than the optimum for the dc charge level and thus the output waveform is slightly more peaked than normal.) Analysis of the waveform (Figure 86) yields the following performance summary (prepulse and recording system correction included).

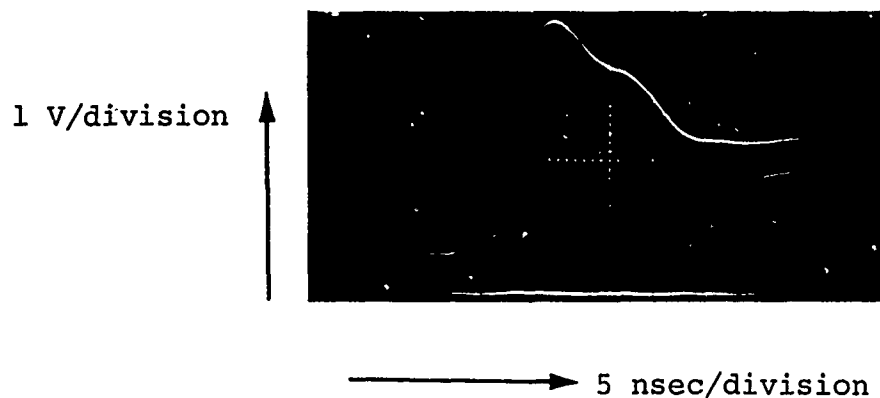
Pulse risetime: (10 to 90 percent)	6.2 nsec
Pulse risetime: (0 to peak)	~ 10 nsec
Peak amplitude:	491 A/m (185 kV/m)
Calculated peak amplitude:	604 A/m (228 kV/m)

The measured value is approximately 19 percent less than the calculated value: almost equal to the difference determined earlier, before modification. Thus, it is unclear, at least for close-in measurements, that the modification had any measurable effect upon system performance.

To date, the maximum output voltage produced by TEMPS is 6.7 MV achieved in the course of system operation at HDL's Woodbridge, Virginia test site. Based upon the analysis performed at Camp Parks, described in the previous paragraphs, projected radiated peak field for this output voltage is 54.3 kV/m at a radial distance of 50 meters from the antenna. The specified monitoring point is actually 50 meters horizontally from

---

\*The 10 percent point determined by extrapolation of the fast pulse front to the baseline.



Integrated  $\dot{B}$  signal

Probe { MGL-2A,  $A_{\text{eff}} = 0.01 \text{ m}^2$   
 Tektronix 454 scope--add mode  
 Integrators: 1  $\mu\text{sec}$  time constant

Pulser {  $V_{\text{dc}} = 75 \text{ kV}$   
 $V_{\text{out}} = 4.7 \text{ MV}$   
 Output switch: 64 psig  $\text{SF}_6$ , 4.0 cm spacing

Figure 86 Typical radiated waveform.

the pulser longitudinal centerline, and for a 20 meter antenna-to-ground spacing, the radial distance from the pulser is 53.85 meters. Scaling the above value of field to the specified location yields 50.4 kV/m. Peak magnetic-field intensity measurements conducted during operation of TEMPS at HDL confirm this level of performance within a probable error of approximately 4 percent rms which includes recording system, probe, and pulser position inaccuracies.

#### 8.6 OUTPUT PREPULSE

As discussed in Reference 1, for a circuit that uses a pulse charged peaking capacitor, stray capacity across the output switch couples a small amount of peaking capacitor pulse charge current into the load impedance, giving rise to a voltage signal (and thus a radiated signal) that precedes output switch closure.

From Reference 1, maximum prepulse voltage occurs at maximum  $dv/dt$  on the pulse charge waveform, which corresponds to nominal output switch closure time in a ideal peaking capacitor circuit. This time  $t_p = \pi/2\omega$ , where  $\omega$  is the angular frequency associated with the pulse charge circuit.

From Reference 1, the ratio of peak prepulse voltage to output voltage for this condition is given approximately by

$$\frac{V_p}{V_o} \cong R\omega C$$

where  $R$  is load resistance (assumed constant) and  $C$  is the stray capacity.

From Reference 1, the estimated value of stray capacity, referred to a one-half generator, was about 80 pF. For the final TEMPS design, the length of a continuous conducting bicone between output switch and peaking capacitors was lengthened slightly to accommodate the peaking capacitors, and this increases the stray estimated capacity to about 97 pF referred to a one-half system.

The measured value of  $\omega$  for TEMPS, determined during Camp Parks testing, is about  $2.35 \times 10^7$  rad/sec and thus the calculated prepulse based upon these parameters is

$$\frac{V_p}{V_o} \cong 60(2.35 \times 10^7)(97 \times 10^{-12}) \cong 14 \text{ percent}$$

This value is in good agreement with the measured value of 16 percent, the difference probably associated with an underestimate of stray capacity.

The final resulting value of prepulse is about twice that originally estimated (Reference 1), about 20 percent of the increase being due to increased stray capacity. The balance of the increase is associated with the low-inductance Marx design. The initial anticipated Marx inductance was about 4.5  $\mu$ H whereas the final value is closer to 2  $\mu$ H. Decreased Marx inductance increases  $\omega$  by about 45 percent compared with the original estimated value and thus system prepulse has increased accordingly.

The TEMPS peaking capacitors are about 1 nF for each one-half system. For the final value of Marx inductance they are oversized by a factor of two. However, this has little effect upon output waveform since the Marx peaking circuits are reasonably well damped. Nonetheless, to more closely satisfy ideal peaking circuit conditions, peaking capacity could either be reduced in keeping with the low value of stray Marx inductance or, alternatively, the Marx inductance could be increased to match the present peaking capacitor value. Of these alternatives, the second is preferred since increasing inductance reduces  $\omega$  and thus reduces system prepulse.

#### 8.7 OUTPUT PULSE AMPLITUDE JITTER

Output-pulse amplitude jitter arises principally from three sources: (a) output switch closure voltage and risetime variations,\* (b) shot-to-shot variation of dc charge level, and (c) variation of relative timing between Marxes. Of these three effects, the first is dominant.

Measurements (Reference 13) have shown that for rapidly charged, highly enhanced self-breaking pressurized gas switches the standard deviation of switch breakdown voltage is a low percentage that decreases with decreasing duration of applied voltage: For a 50-nsec voltage ramp,  $\frac{1}{2}$  percent has been measured; for 2  $\mu$ sec, this increases to 2 percent. Also, as the switch is made less field-enhanced, the jitter increases and approaches that of a slowly charged uniform field switch at moderate gas pressure ( $\sigma \cong 3$  percent).

---

\*Risetime variations do not normally imply pulse amplitude variations. However, in the TEMPS system, pulse amplitude clipping effects associated with the finite length of bicone and cleartime induce an apparent peak amplitude variation for small pulser risetime variations.

This variation taken alone is well within the  $\pm 5$  percent variation specified for TEMPS.

The apparent breakdown field strength of  $SF_6$ , under conditions where the switch is rapidly pulse charged, is substantially greater than the dc or low-frequency breakdown field. This is due to the finite streamer transit time between switch electrodes, and thus, as is the case with higher enhanced self-breaking switches, a rapidly charged near-uniform-field switch displays some time dependence, i.e., its breakdown voltage is proportional to the rate of change of applied voltage albeit weakly for near-uniform-field switches.

Based upon this consideration then, since maximum  $dv/dt$  is in turn proportional to dc charge level, variations of dc charge level induce an apparent variation in output switch closure voltage, assuming that Marx synchronization in a bilateral system is perfect.

A related effect to that described in the previous paragraph is associated with relative Marx timing. The voltage waveform across the output switch is the sum, in time, of the peaking capacitor pulse charge waveforms of each half generator, and as the relative timing between half systems varies, so does the total applied waveform and thus  $dv/dt$ .

The overall effect of switch breakdown, dc charge, and timing variations increases estimated pulse amplitude jitter to as much as 4 to 5 percent rms.



However, in TEMPS, peak amplitude jitter measurements have yielded values less than those quoted above and, in many cases, amplitude jitter less than 2 percent rms has been achieved. A typical example is shown in Table IX. In other instances, full system amplitude jitter has increased to as much as 6 to 7 percent rms and is indicative of an uncontrolled parameter. In this case, it appears that the switch gap spacing varies slightly from shot to shot and is associated with the hydraulic system used to vary gap spacing from the control van. A preliminary assessment of the problem has revealed that  $\text{SF}_6$  gas from the output switch has leaked back into the hydraulic cylinder, yielding a "spongy" adjustment system with associated spacing inaccuracy and potential shot-to-shot variation due to variable gas bubble volume.

Hydraulic cylinder seals have been modified and tested to alleviate the above problem and results indicate that the solution is successful.

#### 8.8 TEMPS TIMING JITTER

As previously discussed, the TEMPS Marx-peaker circuits are synchronized in time to produce the output voltage pulse. Good synchronization is necessary principally to avoid overvoltage of a half generator and to produce an output pulse shape that is reproducible from shot to shot. If the pulse charge waveform of one Marx-peaker circuit precedes in time the other, then its associated peaking capacitors will tend to be overvolted since output switch closure, in the first approximation, depends upon total voltage and not upon synchronization. Unsynchronized operation can lead to voltage breakdown across one set of peaking capacitors if allowed to exceed certain bounds.

TABLE IX

## TEMPS PEAK PULSE AMPLITUDE JITTER

Date data taken: 1/22/73  
 Location: HDL, Woodbridge, Virginia  
 Marx charge level: 70 kV  
 Marx gas and pressure: SF<sub>6</sub> - 0 psig  
 Output switch

Gas: SF<sub>6</sub>  
 Pressure: 70 psig, 4.3 cm

Monitor: MGL-2A loop, 12 feet off ground on centerline, radial  
 distance to pulser  $\approx$  15 meters

<u>Shot Number</u>	<u>Peak Integrated B Signal (mV)</u>
68	140
69	143
70	143
71	143
72	145
73	145
74	145
75	143
76	(photo missed)
77	143
78	144
79	144
80	144
81	145
82	143
83	145
84	143
85	138
86	138

Mean = 143 mV;  $\sigma$  = 1.5 percent

A maximum allowable voltage variation of 10 percent for each Marx-peaker circuit, due to non-synchronous Marx erection and peaking capacitor pulse charge, was established during the TEMPS design phase. Based upon the pulse charge waveform (Figure 73), this implies that both Marxes must erect within a 10 nsec window. Assuming a confidence level of 95 percent, this in turn implies that the timing jitter of each Marx must be less than 3.6 nsec rms.

To achieve this degree of synchronization, a low-timing-jitter trigger system was developed for TEMPS and is discussed in Section 5.4 of this final report.

No command timing jitter requirements was originally placed on TEMPS, but such a requirement did subsequently arise. To satisfy this new requirement, an rf trigger link was designed and fabricated by Philco Ford's WDL Division located in Palo Alto, California. A brief description of the link is contained in Section 8.2.10 of this report.

For completeness then, the following paragraphs address TEMPS system jitter from input to the on-board trigger system to closure of the output switch and subsequent launch of the EM wave. The discussion begins with the Marx trigger system.

#### Marx Trigger System

Trigger Amplifier. The TEMPS trigger amplifier and distribution system is shown schematically in Figure 87.

In this system, closure of a mercury reed switch, initiated by pneumatic command from the ground-based control point, provides the  $t_0$  pulse, a fast-rising pulse ( $\leq 2$  nsec [10 to 90 percent]) of a few volts amplitude. This signal fires the low-voltage trigger amplifiers on each side of the pulser. The signal is carried to the opposite side of the pulser by way of an optical light pipe system.

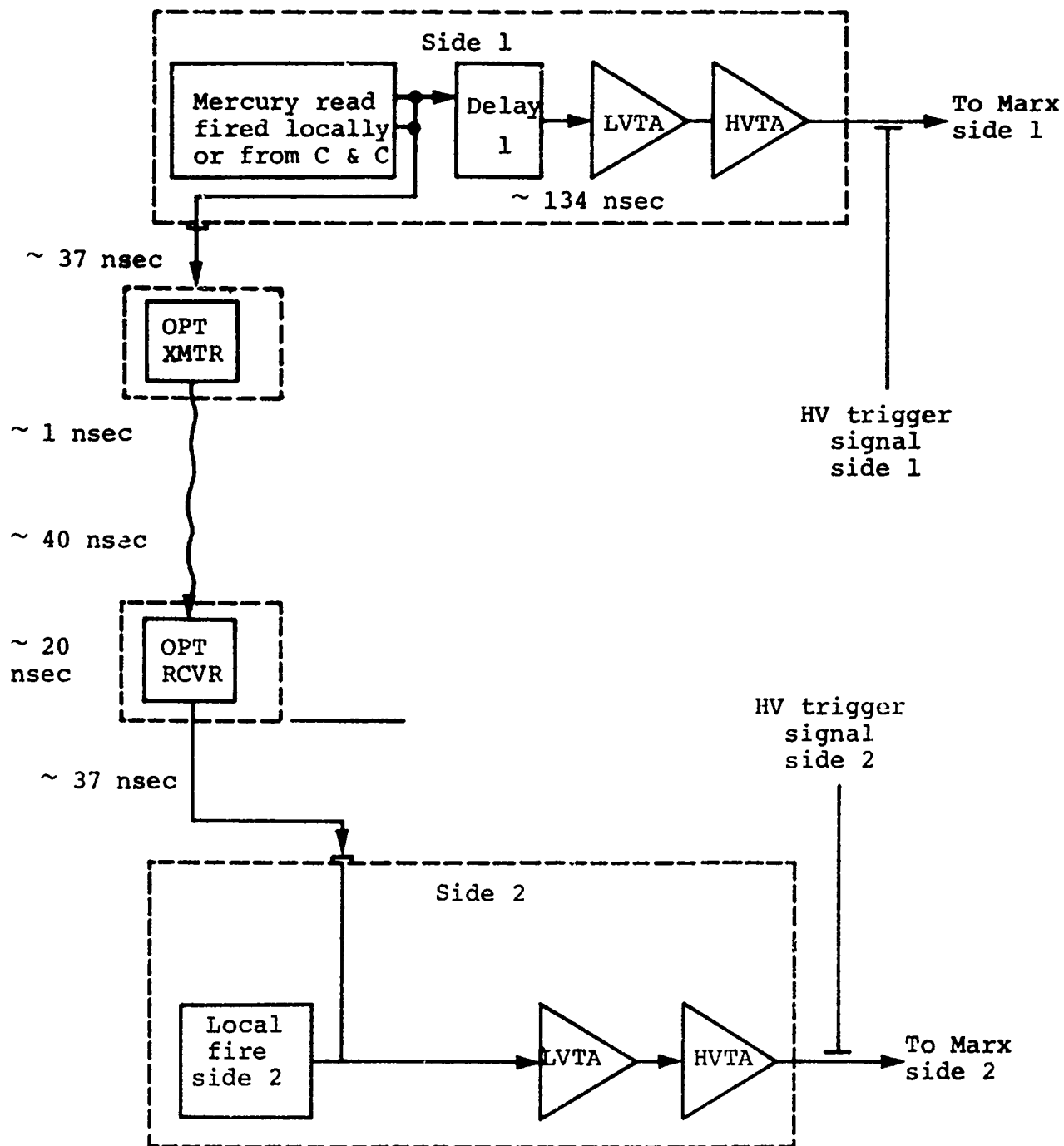


Figure 87 TEMPS trigger system block diagram.

Optical-Link Transmitter. The optical-link transmitter to trigger side 2 of the system takes the form of an avalanche transistor driving an LED, close-coupled to the input of a fiber optic light pipe about 16 feet long. The optical transmitter is contained within a shielded enclosure situated at the input to the dielectric crossover tube shown in Figure 1.

Optical Receiver. The on-board receiver is a 931 photo-multiplier tube and amplifier which drives a 2- to 3-volt fast-rising pulse by means of coaxial cable to the input of the low-voltage trigger amplifier. This component is also contained with a shielded enclosure, and is located at the output of the dielectric crossover tube.

Low-Level Trigger Amplifier. This portion of the trigger system, located on-board the system, is a low-inductance generally coaxial arrangement of three amplifier stages: avalanche transistor and two planar triode stages, the last in a grounded grid configuration. This module accepts a 1-volt trigger and produces a 10-kV, 16- to 18-ampere output pulse that triggers a pressurized gas spark gap. For a typical load capacity of 10 pF or less, a 1.5 to 2 kV/nsec voltage rate of rise can be produced at the trigger gap electrode. The time jitter of this amplifier module, from 1-volt input to the spark-gap trigger electrode, is significantly less than 0.5 nsec rms.

The spark gap, a rail-gap design, short circuits two parallel connected dc-charged cables that are series connected at their far end, forming a cable transformer with a theoretical gain of four. Based upon jitter measurements conducted at PI, gap jitter under conditions of 20-kV charge level, 53 psig N<sub>2</sub> pressure, and 70 percent of self-fire, gap delay was  $27 \pm 1$  nsec with corresponding jitter of  $0.48 \pm 0.15$  nsec.

High-Voltage Trigger Amplifier. The output of the low-level trigger amplifier cable transformer triggers a high-voltage spark gap that short circuits two dc-charged coaxial cables ( $V_{dc} = 80$  kV, cable--RG-19/U). The output of these cables is parallel connected and is coupled resistively to the first four Marx generator spark gaps. Output pulse voltage is about 125 kV rising to this value in less than 9 nsec.

Relative timing jitter measurements (i.e., trigger input arrival time to Marx side 2 relative to trigger input arrival time to Marx side 1) for the TEMPS trigger system have yielded timing jitters consistently less than 2 nsec rms under field environment conditions. A typical illustrative five shot series for jitter measurements taken during Camp Parks testing of TEMPS is shown in Figure 88 along with the measurement circuit diagram.

Marx Generator Erection Delay and Jitter. Marx generator erection is speeded and timing jitter reduced through the use of triggered sparks resistively coupled ( $m = 4$ ) to any preceding stage or to a source of externally applied trigger voltage; (the output of the high-voltage trigger amplifier described in the previous paragraphs).

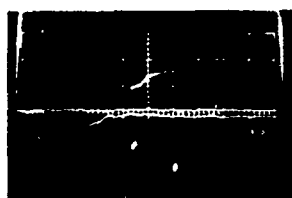
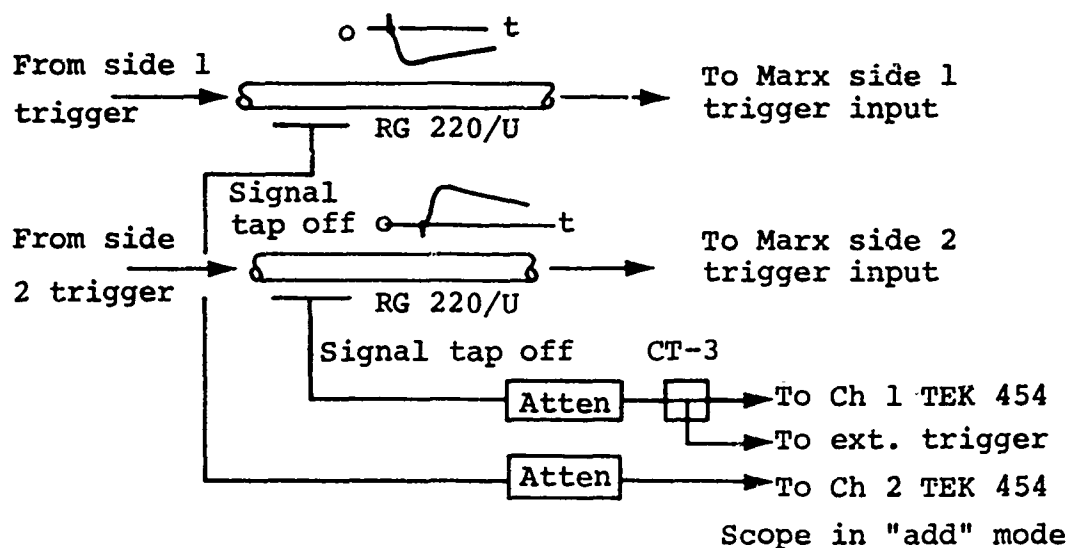
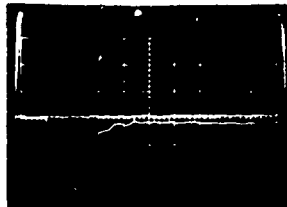
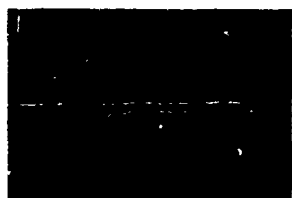
The details of the Marx erection process are complex (Reference 14) and are often experimentally assessed using prototype Marx testing and modification if required.

In TEMPS, Marx erection delay (for a 35 stage Marx) is typically 150 nsec with a corresponding erection delay jitter of less than 3 nsec rms throughout the operating range of 35 kV to 100 kV dc charge. For dc operating voltages greater than about 60 kV, jitter values as low as 1.8 nsec rms are typical.

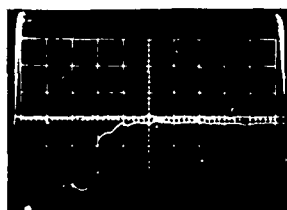
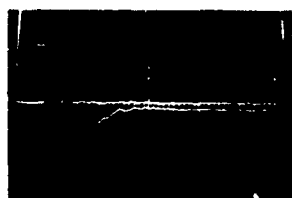
In terms of overall performance, i.e., both Marxes considered together, the total jitter is less than that of each Marx considered alone. This is due to the fact that a single output switch is used and that the Marxes in 50 percent of the firings for a large number of shots tend to be self-compensating. Statistics show that on half the firings, the fact that one Marx is slightly early (late) is offset by the fact that the other is late (early). Thus, the total jitter of the Marxes considered together is likely to be  $3/\sqrt{2}$  nsec or a little over 2 nsec rms. This same consideration applies to the trigger generator system.

## 8.9 OUTPUT SWITCH CLOSURE JITTER

As described in a previous section, peak output pulse amplitude jitter due to output switch closure voltage variations is typically less than 3 percent rms. Assuming perfectly synchronous Marxes, this amplitude variation is directly related to a


 $\Delta = 15.0 \text{ nsec}$ 

 $\Delta = 20.0 \text{ nsec}$ 

 $\Delta = 16.0 \text{ nsec}$ 

Mean delay  
difference = 19.0  
nsec


 $\sigma = 1.6 \text{ nsec}$ 
 $\Delta = 20.5 \text{ nsec}$ 

 $\Delta = 18.5 \text{ nsec}$ 

Scope time base = 10 nsec/div

Figure 88 Relative trigger system jitter.

corresponding time jitter since the pulse charge waveform is of fixed form, i.e., a  $(1 - \cos \omega t)$  waveform. From Figure 73, a 3 percent rms amplitude variation yields a corresponding time variation of less than 2 nsec rms. This is largely independent of actual switching time since  $\partial v/\partial t$  is nearly constant within  $\pm 10$  nsec of optimum output switch closure time.

Assuming normally distributed probability density functions for trigger, Marx, and switch closure timing and assuming mutual independence (although this not strictly valid), the total pulse generator jitter, measured from trigger pulse input to the LV trigger amplifier to launcher of the EM wave, is given approximately by

$$\sigma_T \cong \sqrt{\left(\sigma_t\right)^2 + \left(\frac{\sigma_m}{\sqrt{2}}\right)^2 + \left(\sigma_{sw}\right)^2}$$

where  $\sigma_t$ ,  $\sigma_m$ , and  $\sigma_{sw}$  are trigger, Marx, and switch rms deviations. Thus,

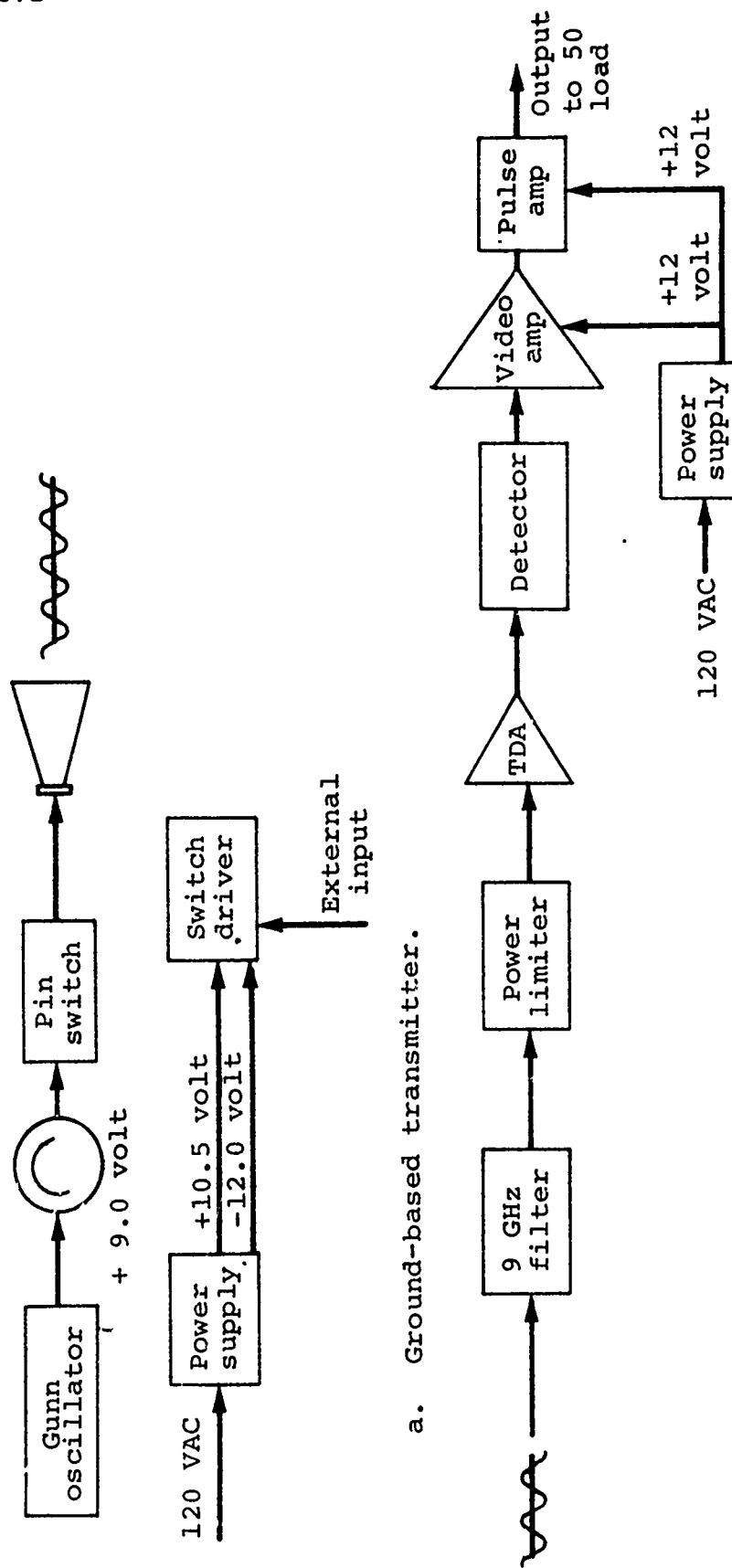
$$\sigma_T \cong \sqrt{(2)^2 + \left(\frac{3}{\sqrt{2}}\right)^2 + (2)^2} = 3.5 \text{ nsec rms}$$

and this value is small compared with the 50 nsec command timing jitter requirement subsequently placed on the TEMPS system.

#### 8.10 COMMAND JITTER

Although not originally proposed, an air path rf trigger link system for TEMPS has been developed and fielded by Philco Ford's WDL (Western Development Laboratories) Division, Palo Alto, California. This system is shown in simplified form in Figure 89.





a. Ground-based transmitter.

b. Pulser-based receiver.

Figure 89 Air path rf trigger link.

The system transmitter accepts a fast-rising 10-volt-maximum positive-going input pulse and produces at the output of the receiver, located at a distance of about 500 feet, a 5-nsec-risetime 10-volt pulser into a 50-ohm load. Overall delay, exclusive of propagation delay, is about 140 nsec and the measured timing jitter (input to output) is approximately 3 nsec or less.

Preliminary checkout and operation of the trigger link system in the field have been satisfactory.

#### 8.11 MARX GENERATOR SELF-FIRE

Pressurized gas, rail type Marx generator switches are employed in the TEMPS system. This type of switch design is particularly well suited to the overall Marx physical configuration and energy storage capacitor design.

At the outset of the TEMPS program, a prototype Marx switch test and evaluation effort was initiated.

A final design TEMPS Marx switch is shown in Figure 11. The main electrodes are formed by 11/16-inch-diameter brass rods about 13 inches long, shaped at their ends to reduce field enhancement. Electrodes are contained with 18-inch-long acrylic plastic envelopes and electrode separation is  $\frac{1}{2}$  inch. Each switch is equipped with a knife-edge, midplane trigger electrode, and every switch is triggered to reduce Marx erection delay and jitter. During dc charge of the Marx generator stages (balanced charging with respect to ground), the midplane trigger electrodes are resistively connected to ground. For this condition, the sharp trigger electrode is physically situated on the appropriate equipotential surface and thus there is ideally no enhancement at its edge. When triggered, however, the electrode is electrically displaced from its midplane position and the electric

fields ending on the knife edge rapidly increase to very large values, breaking down the surrounding gas dielectric with subsequent arc closure to the nearby main electrodes.

The Marx switches are designed for use with two gas dielectrics, nitrogen and sulfur hexafluoride ( $\text{SF}_6$ ), to cover the requisite 3/1 voltage range of the system. Switch self-breakdown voltage as a function of type of gas and gas pressure is shown in Figure 21.

In order to ensure more reliable operation of the TEMPS Marx generators, a Marx switch acceptance test procedure was established. This testing consisted of mechanical inspection to ensure that the assembled switches were within allowable mechanical tolerances and was followed by pulse discharge testing to ensure uniform electrical characteristics in terms of self-breakdown voltage and low self-fire scatter.

Particular attention has been paid to Marx self-fire performance; this is principally the reason switch acceptance test procedures are employed to assure uniform characteristics. These procedures have been instrumental in reducing the TEMPS Marx self-fire rate to a low level. In TEMPS, the Marxes are operated at 80 percent or less of the mean self-fire level. This operating point provides the best compromise between self-fire rate and erection delay and jitter, which are competing effects. In the course of normal TEMPS operation, the self-fire rate has been typically less than once per two hundred firings. However, two effects of importance are worth discussing.

First, with either  $\text{SF}_6$  or  $\text{N}_2$ , self-fire probability at a fixed percentage of mean self-fire voltage, increases with gas pressure. This is balanced, however, by decrease Marx erection

delay and jitter with increasing pressure; (the two effects are probably related). Thus, as Marx voltage and switch pressure is increased, the switches may be operated at reduced percentage of mean self-fire with equal performance.

System output voltage is reduced by lowering both the Marx dc charging voltage and spark gap pressure. This can be performed with the simulator in its operating position off the ground. At some point, with a fixed type of gas, further reduction in voltage leads to excessive Marx erection jitter. Experience with SIEGE II and TEMPS shows that changing from  $\text{SF}_6$  to  $\text{N}_2$  extends the low jitter range of the Marxes to cover the required 3/1 range.

The second effect of importance observed in TEMPS and SIEGE is a noticeable increase of Marx self-fire rate after a period of inactivity (a week or so). This effect is apparently associated with the formation of microscopic hair-like metal projections on the electrode surfaces. The cause of this behavior is largely unknown but may be related to a weakly corrosive action of the surrounding gas at the metal gas boundary. In TEMPS, this problem is solved procedurally by firing the Marxes at low level into a short circuit several dozen times after a period of inactivity on the order of one or more weeks.

## REFERENCES

1. Transportable EMP Simulator (TEMPS), PIP-1022, Physics International Company, San Leandro, CA., May 1971.
2. H. Aslin and W. Scharfman, TEMPS Antenna Concept Review, Pitr-372-1, Physics International Company, San Leandro, CA., October 1971.
3. TEMPS--Antenna and Support Structure, Preliminary Design Review, Pitr-372-3, Physics International Company, San Leandro, CA., January 1972.
4. Schelkunoff and Friis, Antennas--Theory and Practice, J. Wiley and Sons, New York, N.Y., 1952.
5. TEMPS--Generator Preliminary Design Review, Pitr-372-2, Physics International Company, San Leandro, CA., December 1971.
6. TEMPS--Marx Generator Final Design Review, Pitr-372-4, Physics International Company, San Leandro, CA., April 1972.
7. W. Lupton, Waveform Distortion from Peaking Circuit Switch Jitter, NRL Technical Memorandum No. 1829, November 1967.
8. A. Ramrus and P. Woods, RES II Airborne Generator Pulser Design and One-Third-Scale Model Test Results, Phase II, PIFR-168, Physics International Company, San Leandro, CA., October 1969.
9. B. Gasten, Peaking Capacitor Circuit Analysis, TEMPS Design Note No. 8, Physics International Company, San Leandro, CA., October 1971.
10. J. C. Martin, Volume Effect of the Pulser Breakdown Voltage of Plastics, Dielectric Strength Note No. 3, Atomic Weapons Research Establishment, Aldermaston, England, November 1965.
11. R. Gibson, Trigger System, TEMPS Experimental Note No. 3, PIEN-372-3, Physics International Company, San Leandro, CA., October 1971.

13. I. Smith, et al., Design of an Advanced SIEGE II Pulse Generator, Phase II, AFWL TR-69-79, June 1970.
14. R. W. Morrison and A. M. Smith, Overvoltage and Breakdown Patterns of Fast Marx Generators, Department of Physics, Carleton University, Ottawa, Canada.
15. H. Aslin, Current Monitor, TEMPS Design Note No. 3, Physics International Company, San Leandro, CA., September 1971.